The structure, function and specificity of the *Rhodobacter sphaeroides* membrane-associated chemotaxis array



JAMES ROBERT ALLEN

Wadham College
University of Oxford
Trinity Term 2014

A THESIS SUBMITTED FOR THE DEGREE OF

DOCTOR OF PHILOSOPHY

Abstract

THE STRUCTURE, FUNCTION AND SPECIFICITY OF THE *Rhodobacter sphaeroides* MEMBRANE-ASSOCIATED CHEMOTAXIS ARRAY

JAMES ROBERT ALLEN

Wadham College, University of Oxford
Submitted for the degree of Doctor of Philosophy Trinity Term 2014

Bacterial chemotaxis is the movement of bacteria towards or away from chemical stimuli in the surrounding media. Bacteria respond to chemotactic signals through chemoreceptors which bind specific ligands and transduce signals through a modified two-component system. Typical chemoreceptors bind a ligand in the periplasm and signal across the inner membrane to the cytoplasmic chemosensory array through the inner membrane. Bacterial chemoreceptors must integrate multiple signals within an array of different receptor homologues to a single output. Chemoreceptors act cooperatively to allow a rapid signal spread across the array and large signal gain. Chemoreceptors adapt to a signal by chemical modification of their cytoplasmic domains in order respond across a wide range of effector concentrations. How bacterial chemoreceptors transduce signals through the inner membrane, integrate multiple effector responses, signal cooperatively and adapt to result in a single output signal is not currently fully known. In *Rhodobacter sphaeroides*, additional complexity arises from the presence of multiple homologues of various chemotactic components, notably the array scaffold protein CheW. Decoding this signalling mechanism and heterogeneity involved in this system is important in decoding the action of a biological system, with implications for biotechnology and synthetic biology.

This study used the two model systems *Escherichia coli* and *R. sphaeroides* to analyse the mechanism of signalling through bacterial chemoreceptors. Rational design of activity-shifting chemoreceptor mutations was undertaken and these variants were analysed in phenotypic and fluorescence localisation studies. Molecular-dynamics simulations showed an increase in flexibility of chemoreceptors corresponds to a decrease in kinase output activity, which was determined by the computational tracking of bacteria free-swimming in media. Fluorescence recovery after photobleaching was used to show that this increase in flexibility results in a decrease in binding of receptors to their array scaffold proteins. A two-hybrid screen also suggested that inter-receptor affinity is also likely to decrease. These results show that signalling through chemoreceptors is likely through a mechanism involving the selective flexibility of chemoreceptor cytoplasmic domains.

Analysis of *R. sphaeroides* chemoreceptors and CheW scaffold proteins in *E. coli* showed that it should be possible to design, from the bottom-up, a functional bacterial chemotaxis system in order to analyse individual protein specificity. Expression of *R. sphaeroides* MCPs in this *E. coli* system show the reconstitution of a chemotactic array, but not one capable of signalling specifically to proposed attractants. Results gained from this system suggest the *R. sphaeroides* CheW proteins are not homologous and their differential binding affinities may allow array activity 'fine-tuning'.

Declaration

The work in this thesis was undertaken at the University of Oxford; in the Department of Biochemistry. Work was performed from October 2010 to October 2014 under the supervision of Prof. J.P. Armitage. All the work in this thesis is my own unless otherwise stated and has not been submitted for a degree at this or any other university.

Acknowledgements

I would like to thank Prof. Judy Armitage for her supervision during my DPhil, in particular for the freedom to study interesting and exciting research avenues, which developed my abilities and shaped this piece of work.

Throughout my experience in the lab I have been able to draw on the expertise of numerous people. I would especially like to thank Kathryn Scott, George Wadhams, Nicolas Delalez, Nelly Dubarry and Christopher Jones for advice, assistance and whatever else I have required of you. I would also like to thank all present and past members of the lab who have shared my experience.

Through eight years of study at Oxford I have met and been inspired by many people who all deserve thanks, departmental and college friends alike share their part in making my studies enjoyable, challenging and successful. The final four years encompassing my DPhil studies have been a highlight, with particular thanks to the boys of Marlborough Road. My parents have been a constant source of encouragement and grounding throughout and I am grateful that your encouragement has led me to where I am now. Verity, you have been source of immeasurable support and inspiration, thank you.

I would also like to thank the BBSRC and Wadham College for their financial support which has enabled me to undertake this study.

Contents

Abstract.....i

Declaration.....ii

Acknowledgements iii

Contents.....iv

1. Introduction 1

1.1 Bacterial motility 1

1.2 Two-component systems 3

1.2.1 Histidine kinases.....4

1.2.2 Response regulators.....9

1.3 Bacterial chemotaxis.....11

1.4 Bacterial chemoreceptor arrays.....15

1.4.1 Ligand-binding domain 17

1.4.2 Transmembrane domain 19

1.4.3 HAMP domain.....21

1.4.4 Conserved cytoplasmic domain.....23

1.4.5 The scaffold proteins 24

1.4.6 Higher level order of chemoreceptor arrays 27

1.4.7 Cluster signalling.....30

1.5 Signal Diffusion.....34

1.6 Signal Termination 36

1.7 Adaptation....37

1.8 Non-*E. coli* chemotaxis systems....41

1.8.1 Introduction to *R. sphaeroides*....45

1.8.2 *R. sphaeroides* chemotaxis components....46

1.8.3 *R. sphaeroides* chemoreceptors....49

1.8.4 *R. sphaeroides* MCP specificity....50

1.8.5 *R. sphaeroides* MCP classification....50

1.8.6 *R. sphaeroides* scaffold proteins....51

1.8.7 *R. sphaeroides* CheYs....52

1.8.8 *R. sphaeroides* signal termination....53

1.8.9 *R. sphaeroides* adaptation....54

2. Project Aims....55

3. Materials and methods....56

3.1 Strains and Plasmids....56

3.1.1 Strains....56

3.1.2 Plasmids....57

3.2 Growth Conditions....58

3.2.1 Antibiotics....58

3.2.2 *E. coli* liquid cultures....59

3.2.3 *E. coli* agar plates....59

3.2.4 *R. sphaeroides* liquid cultures....59

3.2.5 *R. sphaeroides* agar plates 59

3.2.6 Sucrose selection plates 59

3.3 Genetic techniques 60

3.3.1 Polymerase chain reaction (PCR) 60

3.3.2 Restriction enzyme digests 62

3.3.3 Dephosphorylation 63

3.3.4 Gel electrophoresis 63

3.3.5 Purification of DNA fragments 63

3.3.6 DNA ligation 64

3.3.7 Competent cells 64

3.3.8 Transformation of plasmids into competent cells 65

3.3.9 Plasmid purification 66

3.3.10 DNA sequencing 66

3.3.11 Conjugation of plasmids into *R. sphaeroides* 66

3.3.12 DNA recombination for genomic deletion and replacement in *E. coli* 67

3.4 Phenotypic analysis 68

3.4.1 Swim plates 68

3.4.2 Growth Curves 69

3.4.3 Bacterial two-hybrid 70

3.5 Microscopy 71

3.5.1 Preparation of cells 71

3.5.2 Preparation of slides 71

3.5.3 Microscopes 71

3.5.4 Polar localization analysis 72

3.5.5 Free-swimming capture 73

3.5.6 Free swimming analysis 73

3.5.7 Fluorescence recovery after photobleaching 74

3.6 Computational methods 75

3.6.1 Model building 75

3.6.2 Coarse-grain Molecular dynamics simulations 75

3.6.3 Transmembrane helix simulations 76

4. Signaling through chemoreceptors 77

4.1 *In silico* mutagenesis screen 77

4.2 *In vivo* analysis of variant receptors 82

4.3 Is Growth directly affected by McpB*? 85

4.4 Does McpB signal through the *E. coli* chemosensory network? 88

4.5 Does McpB* also effect chemotaxis in *R. sphaeroides*? 91

4.6 How does McpB* reduce chemotactic efficiency? 93

4.7 Fluorescence microscopy of variant receptors 98

4.7.1 Analysis of native Tsr receptors 99

4.7.2 Analysis of *R. sphaeroides* McpB and McpB* 105

4.8 Localisation of McpB in *R. sphaeroides* 113

4.9 Turnover of scaffold proteins to show interaction strength 119

4.10 Modelling of McpB 128

4.11 Localisation in an adaptation deficient strain 134

4.12 Chapter Discussion 137

5. Defining the specificity of the MCPs and CheWs of *R. sphaeroides* 142

5.1 CheW expression in *E. coli* 142

5.2 Creation of an *R. sphaeroides* MCP plasmid library 145

5.3 Determining the specificity of McpH 146

5.4 Creation of a more native MCP analysis system 149

5.5 Fluorescence localisation of McpH 151

5.5.1 Localisation in *E. coli* 151

5.5.2 Localisation in *R. sphaeroides* 154

5.6 Determining the specificity of McpJ 159

5.7 Fluorescence localisation of McpJ 162

5.8 Determining the specificity of McpG 167

5.9 Direct analysis of chemoreceptor ligands 169

5.9.1 Free swimming analysis 174

5.10 Bacterial two-hybrid to assess heterogeneity 176

5.11 Chapter Discussion 180

6. Discussion 185

6.1 Using computational pipelines to design targeted mutations 185

6.2 A model for signalling 187

6.3 *R. sphaeroides* chemotaxis protein specificity 192

7. Bibliography 194

Appendix A 213

Primers 213

Appendix B 216

Media and reagents 216

1.Introduction

1.1 Bacterial motility

Bacteria must navigate a hostile microscopic environment in order to effectively find nutrients and avoid harmful substances. They have a low Reynolds number and thus feel no inertia, viscosity must be overcome and they must contend with constant battering by molecules moving under Brownian motion (Purcell, 1976). Bacteria have had to evolve specific motility mechanisms in order to swim, both across surfaces and in liquids including twitching motility (Mattick, 2002) (Burrows, 2012), gliding motility (Mignot et al., 2007), utilisation of protein legs to 'pull' bacterium across a surface (Miyata, 2010) and flagellate motility (Miller et al., 2007). Sliding may also be considered a mechanism of motility in which bacteria move by spreading as they grow (Martínez et al., 1999). These mechanisms are shown in Figure 1-1. Many bacteria have the additional complexity inherent in the need to choose between swimming, even selecting the method by which this is achieved or sticking to a surface (McCarter, 2006).

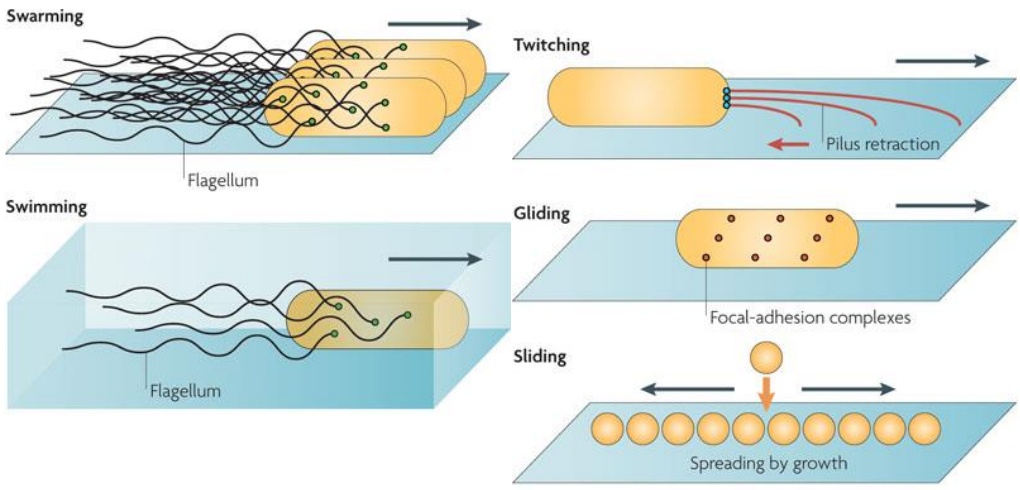

Figure 1-1 The five different types of motility utilised by bacterial species. Taken from (Kearns, 2010).

Flagellate motility is achieved by rotating a helical flagellum or flagella using ion gradients across the membrane as an energy source (Berg, 2003). Motion of chemotactic cells swimming in this way can be divided into two stages: a ‘run’ or a ‘tumble’. Continual rotation of the flagella in the same direction (CCW for *Escherichia coli*, as an example) causes a lateral pushing force which propels the cell. Stopping or reversing the direction of rotation results in a tumbling event which randomly reorients the cell direction upon continuation of the run state (Macnab and Koshland, 1974). This results in random movement in the absence of control as shown in Figure 1-2.

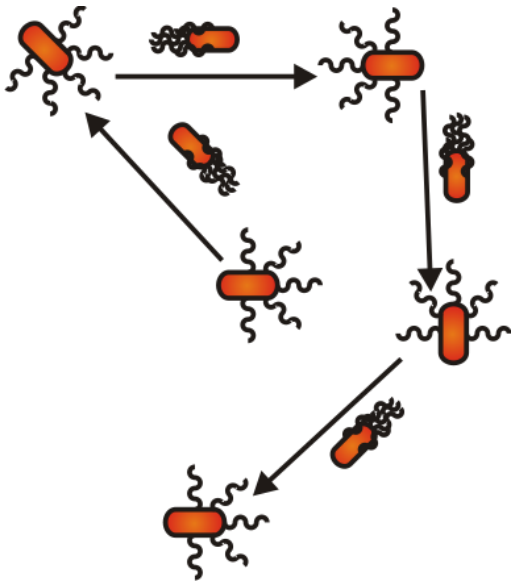

Figure 1-2 Random walk of bacteria showing flagellate motility. This example shows a peritrichous bacteria such as *E. coli* in a series of runs, shown as a rod with bundled multiple flagella. Run phases are separated by tumbling phases in which flagella rotation is reversed causing flagella to splay from the cell. This shifts the direction in which the cell is facing. Without control this process results in random movement through the medium.

Overall control of direction is referred to as a ‘biased random walk’, as the bacteria are able to control tumbling frequency through chemotaxis signalling apparatus (Alt, 1980). This is outlined in Figure 1-3 as the cells swim towards areas of higher attractant concentration.

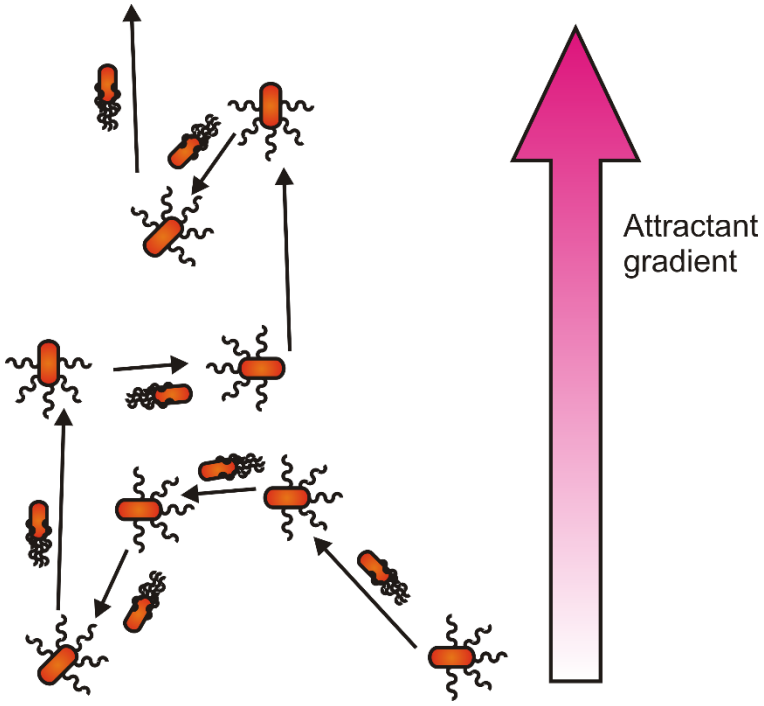

Figure 1-3 Biased random walk. In the presence of a chemotaxis gradient, the random walk is biased by shortening run lengths where no increase in attractant is detected

1.2 Two-component systems

Chemotaxis in bacteria occurs through a specialised two-component system (TCS). TCSs are the predominant signalling mechanisms utilised by bacteria and a typical TCS is composed of a sensor histidine kinase (HK) which senses a specific signal and translates this signal to the desired output by phosphorylating a specific response regulator (RR) (Nixon et al., 1986). Genomic analysis has shown that their presence in bacteria can range from 0 TCS proteins in *Mycoplasma genitalium* to 80 *Synechocystis sp*. and 272 in *Myxococcus xanthus*, in addition, they are fairly ubiquitous among Eubacteria (Mizuno, 1998) (Shi et al., 2008).

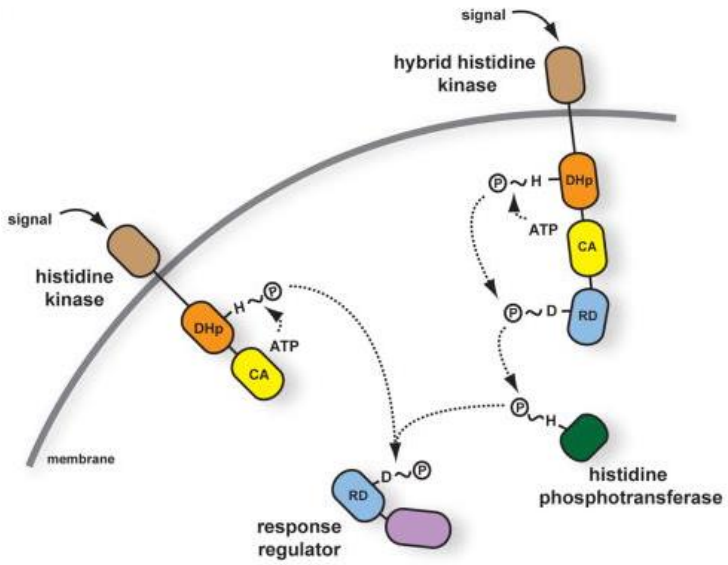

Figure 1-4 Left shows the typical TCS signal transduction pathway. Upon activation, the catalytic and ATPase (CA) domain of the HK transfers a phosporyl group from ATP to the dimerization and histidine phosphotransfer domain (DHp). This then transfers the phosphoryl to the regulatory domain (RD) of the response regulator. On the right is a less typical pathway in which the initial RD is contained on the HK and a histidine phosphotransferase is required to transfer the phosphoryl to the RD on the response regulator. Taken from (Capra and Laub, 2012)

The basic chemistry involved in TCS phosphotransfer typically involves three reactions. These are autophosphorylation, phosphotransfer and dephosphorylation, the first two of these are shown in Figure 1-4. In the first of these, the γ-phosphoryl of ATP is transferred to a conserved histidine side chain on the HK. The RR then catalyses the transfer of the phosphoryl group to a conserved aspartate residue contained on its own regulatory (also termed receiver) domain. In the final step, the phosphoryl group is transferred from the conserved aspartate to water in a hydrolysis reaction.

1.2.1 Histidine kinases

The basic structure of a typical HK is that of a diverse sensing domain coupled to a conserved kinase domain. The modular nature of these domains means that it is possible for individual HKs to be adapted by species to match the needs of a specific pathway. As a result it is

possible to sort HKs into two distinct classes: orthodox and hybrid. Most orthodox HKs, function as periplasmic membrane receptors and have a signal peptide and transmembrane segment(s) that separate the protein into a periplasmic N-terminal sensing domain and a highly conserved cytoplasmic C-terminal kinase core. Members of this family, however, have an integral membrane sensor domain. Hybrid kinases contain multiple phosphodonor and phosphoacceptor sites and use multi-step phospho-relay schemes instead of promoting a single phosphoryl transfer. In addition to the sensor domain and kinase core, they contain a CheY-like receiver domain and a His-containing phosphotransfer (HPt) domain. *E. coli*, as an example, contains 30 different HKs and 32 RRs, 5 of the former are termed hybrid kinases (Mizuno, 1997). The organisation of domains of both typical and atypical HKs are outlined in Figure 1-5.

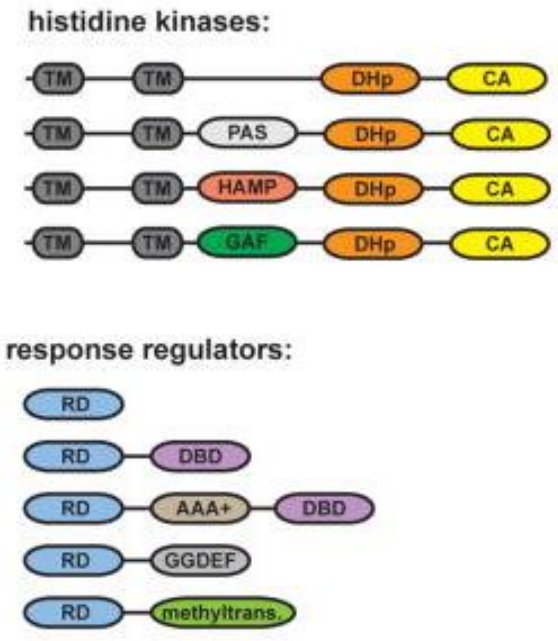

Figure 1-5 Common domains of histidine kinases and response regulators. The common HK organisation is shown first with two transmembrane regions (TM), the catalytic and ATPase (CA) domain, a dimerization and histidine phosphotransfer domain (DHp). This is followed by those containing common additional domains: the heme- and flavin-binding PAS domain, a HAMP domain, the cGMP-binding GAF domain. The conserved receiver domain is shown alone or with the common additional output domains: a DNA-binding domain (DBD), a AAA+ ATPase in tandem with a DBD, a cyclic-di-GMP synthesis GGDEF domain and a methyltransferase domain. Taken from (Capra and Laub, 2012)

Typical HKs function as periplasmic membrane receptors, as an example, the EnvZ sensor kinase has two transmembrane helices, anchoring it in the membrane and creating a periplasmic domain. More complex membrane interactions are also known in HKs, such as UhpB which is involved in *E. coli* sugar transport and contains 8 TM helices (Island et al., 1992). In addition, not all HKs are membrane bound, the nitrogen regulatory kinase NtrC and the chemotaxis kinase CheA are both soluble proteins (MacFarlane and Merrick, 1985) (Stock et al., 1988).

All HKs contain a common kinase catalytic core which consists of a dimerization and histidine phosphotransferase (DHp) domain and the catalytic and ATPase (CA) domain

(Stock, 1999). Structures exist of these domains from both NMR and crystallographic studies. The former of the typical EnvZ kinase and the latter of the atypical soluble kinase CheA, for example: (Tomomori et al., 1999) (Tanaka et al., 1998) (Bilwes et al., 1999). These structures show defined separate domains of the core kinase and their arrangement with respect to each other (Figure 1-6).

The core of HKs in eukaryotes and prokaryotes consists of five conserved motifs (Alex and Simon, 1994). The H-box contains the phosphoryl-acceptor histidine and in typical HKs is contained on the dimerisation domain. However, this is not always the case and in the example of CheA it is contained on the N-terminus of the protein on a separate histidine phosphotransfer (Hpt) domain. The other four conserved motifs, the N, G1, F and G2 boxes are contained on the catalytic domain and are responsible for nucleotide binding. The main body of the catalytic domain is unlike that of previously studied Ser/Thr kinases and is therefore likely to act through a different mechanism (Robinson and Stock, 1999). 5 antiparallel β-strands and 3 α-helices make up an α/β-sandwich fold, creating a highly flexible domain orienting the conserved motifs towards the nucleotide binding site. In analogous protein domains this flexibility is thought to relate nucleotide binding to interactions with other proteins (Ban et al., 1999). The dimerisation domain forms an antiparallel four-helix bundle which, as discussed, contains the H box and conserved phosphorylatable histidine. Notable in the overall arrangement of these domains is that if the CheA structure is analogous to that of typical HKs, the H box would be placed too far away from the kinase active site for phosphotransfer to occur efficiently and so either another arrangement must be present or large structural reorientations must be allowed.

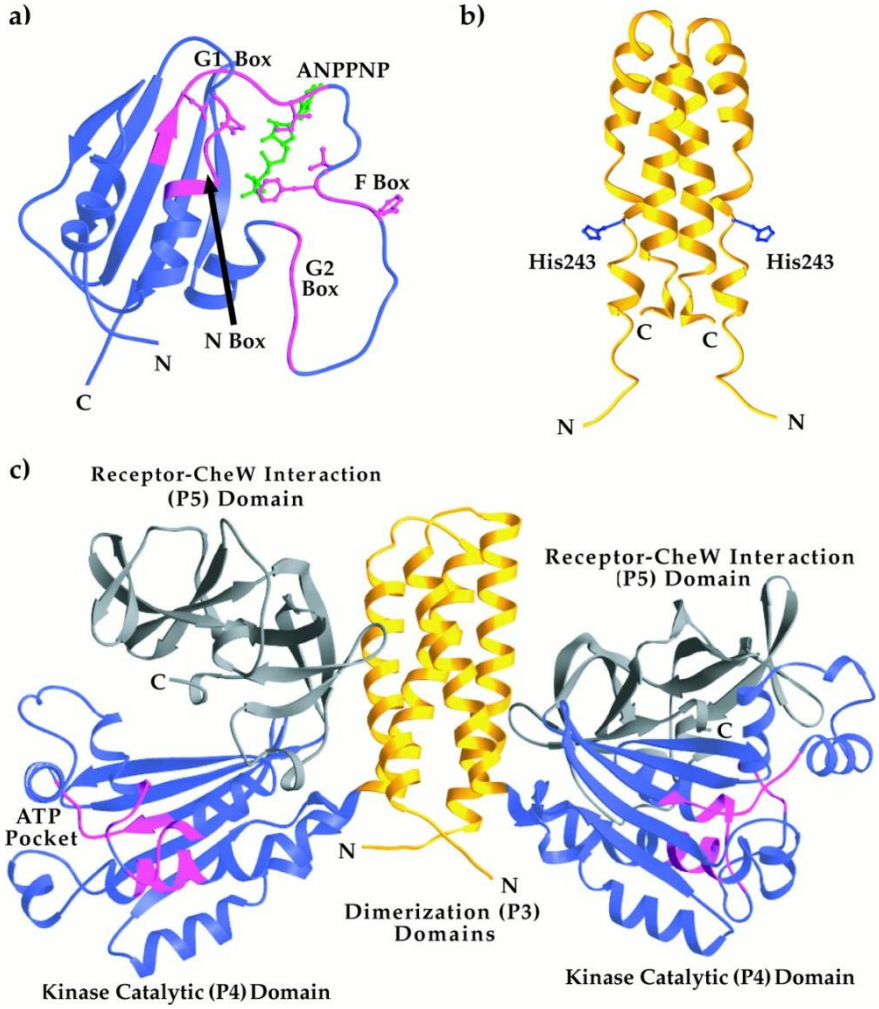

Figure 1-6 The kinase core of EnvZ. a) The catalytic domain of EnvZ as determined by NMR spectroscopy. Labelled in magenta are the conserved regions that make up the ATP-binding core with a bound analogue labelled in green. The various box regions responsible for the nucleotide binding cleft are labelled also. b) The dimerization domain of EnvZ as determined by NMR spectroscopy, labelled is the phosphoryl acceptor histidine 243 (blue). c) The kinase core of *Thermatoga maritima* CheA as determined by x-ray crystallography. The folds are conserved here but the phosphoryl-accepting histidine is contained on a separate acceptor domain, not shown. Taken from (Stock et al., 2000).

The sensing domains of HKs directly or indirectly respond to environmental stimuli. They are very diverse and share very little sequence identity. In addition, sensing is not always from the periplasm and in the case of the oxygen sensor FixL, among others, a PAS domain is located at the N-terminus in the cytoplasm and regulates kinase activity through its heme coordination state (Lukat-Rodgers and Rodgers, 1997). Recent structural evidence of the dimeric PhoQ sensory domain shows that a dimer contact salt bridge is important for

signalling in this case (Cheung et al., 2008). The linker domain between the sensing and kinase domains is known to be important in transducing signals to the catalytic core (Park and Inouye, 1997). Proposed to consist of a coiled coil motif, these linkers are of variable length and directly precede what is typically the H box-containing dimerisation domain (Singh et al., 1998). However, the lack of similarities between sensing domains has prevented detailed analysis of how signals are transduced to the kinase core.

1.2.2 Response regulators

Response regulators typically enact a role as the terminal signal acceptors and once activated perform the resultant response of the TCS. As discussed, RRs catalyse the transfer of a phosphoryl group from the HK phospho-histidine to their own conserved aspartate residue. Most consist of two separate domains, the phosphoryl-accepting regulatory domain and a variable effector domain. Of the 32 *E. coli* RRs, it has been shown that 25 of these are DNA-binding effectors; DNA binding domains are the predominant outputs domains of typical RRs (Mizuno, 1997). Examples of none-DNA binding RRs include the enzymatic chemotaxis methylesterase CheB and the cAMP phosphodiesterase RegA (Simms et al., 1985). Spo0F and CheY are two RRs that lack a second domain altogether, the former is used for shuttling phosphoryl groups between a separate Hpt protein and the original HK and the latter directly binds to its effector FliM at the flagellar motor (Burbulys et al., 1991) (Welch et al., 1993). As a result of this simplicity, CheY has proved to be a good representative of the regulatory domains of RRs.

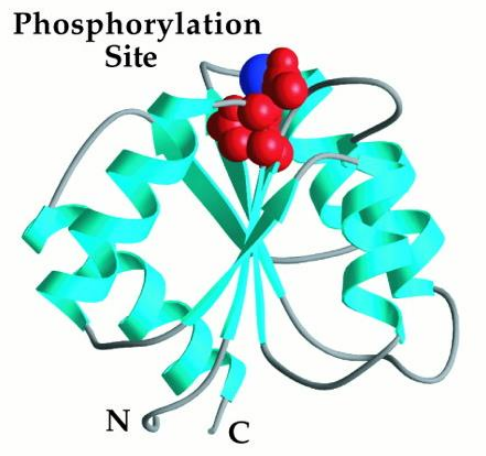

Figure 1-7 A typical response regulator regulatory domain. Shown is the crystal structure of *Salmonella typhimurium* CheY with the conserved aspartate atoms labelled (red balls) and a bound magnesium (blue ball). Taken from (Stock et al., 2000)

The typical RR regulatory domain consists of a 5 stranded parallel β-sheet core surrounded by 5 α-helices (Stock et al., 1989). The phosphorylation site is a conserved aspartate located on an exposed loop between β3 and αC (Sanders et al., 1989). This is surrounded by two further acidic residues (both are also aspartates in CheY), a conserved threonine and a conserved serine. The acidic pocket serves to coordinate a magnesium ion as shown in Figure 1-7, this magnesium ion is essential for phosphoryl transfer and subsequent dephosphorylation (Lukat et al., 1990). Structures from other RR regulatory domains have shown that the central core and binding pocket seems conserved and differences seem to occur in the surface loops and outer helix orientation (Djordjevic et al., 1998) (Feher et al., 1997).

As discussed, effector domains can be very varied with different structures and functions altogether. As an example, OmpR is a typical RR that binds DNA upon activation by the regulatory domain and affects expression of genes involved in outer membrane porin production. Through a winged-helix interaction, OmpR binds DNA and activates *ompC* and represses *ompR* expression through an interaction with the α subunit of RNA polymerase (Aiba et al., 1989) (Kondo et al., 1997). This example highlights differences even between

similar RR effector domains as PhoB, a RR and transcription factor involved in the phosphate starvation response in *E. coli,* affects transcription of its target genes by binding to the σ70 protein (Makino et al., 1993). Given the diversity of effector domains, a common activation mechanism could be discounted. However, evidence is mounting that the shifting between active and inactive states of RR regulatory domains affects the effector domains analogously. A 'release of inhibition' mechanism has been proposed based on deletion studies (Grimsley et al., 1994) (Huala et al., 1992). Crystal structures of some complete RRs have supported this mechanism and yet some structural data also proposes evidence that oligomerisation is achieved by the regulatory domain and that this is important for signalling of the effector domains (Fiedler and Weiss, 1995) (McCleary, 1996). Further difficulty determining mechanisms of action has arisen from the very low half-life of the phosphorylated states and hence an inability to determine structural information of both active and inactive conformations. NMR studies have shown some ability to distinguish large motions undertaken as a result of a shift in state but the few crystal structures that have been obtained have not shown such motions (Lowry et al., 1994) (Jiang et al., 1997). The structure of a non-hydrolysable analogue of phospho-cheY disagrees with these early crystallographic studies and supports the NMR data that long-range shifts of the outer α-helices do occur are likely to be the mechanism through which RRs change their interactions with the effector domains, other RR monomers or external protein effectors (Lee et al., 2001).

1.3 Bacterial chemotaxis

Swimming can be regulated to respond to chemical stimuli in the process known as chemotaxis and is the 'biasing of movement towards regions that contain higher concentrations of beneficial, or lower concentrations of toxic, chemicals' (Wadhams and Armitage, 2004). Bacteria use an atypical two-component signalling system in order to

respond to environmental changes (Stock et al., 2000). As one of the most extensively studied bacterial systems, it has therefore become an important model for the study of atypical TCSs and the transfer of this knowledge to more typical TCS pathways and components.

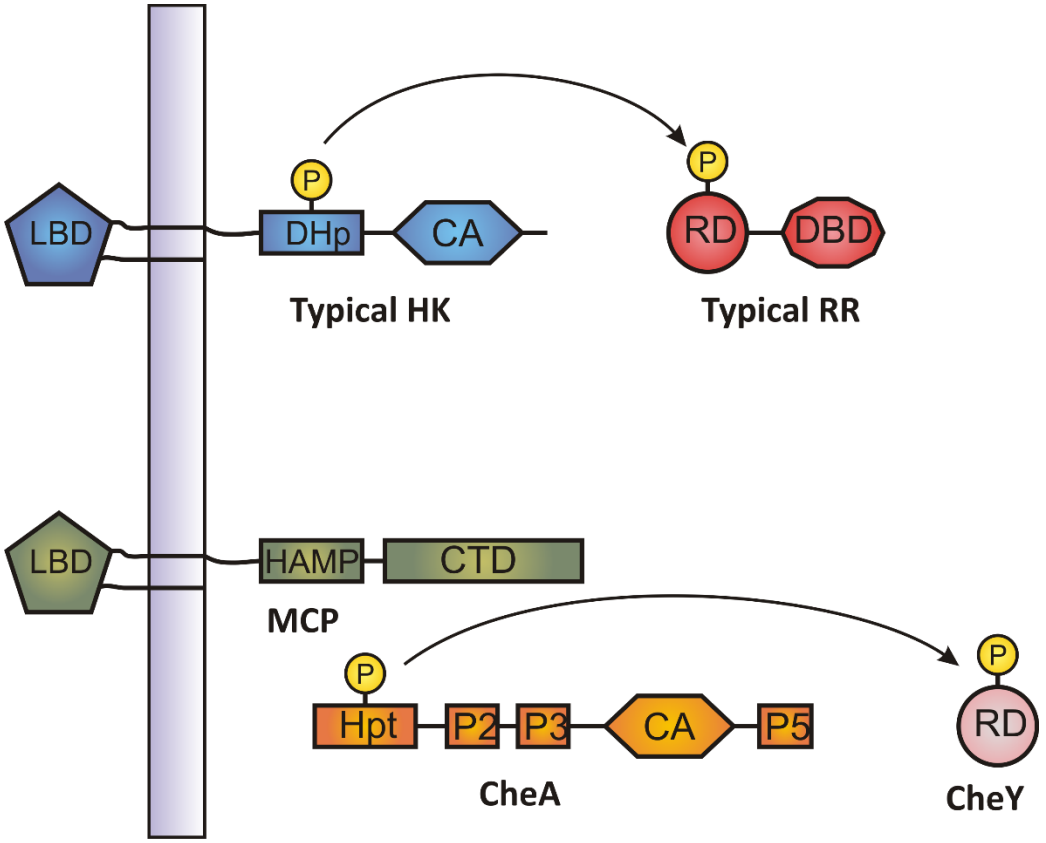

Figure 1-8 Comparison between a typical TCS and the chemotaxis pathway. A typical TCS HK binds extra-cellular signals directly using a ligand binding domain (LBD), shown are the catalytic and ATPase (CA) domain and dimerization and histidine phosphotransfer domain (DHp). Binding activates the phosphoryltransferase activity which transfers a phosphoryl group to the regulatory domain (RD) of a DNA-binding domain (DBD)-containing RR. Chemotaxis requires MCPs to bind ligands at the LBD which then signals through its C-terminal domain (CTD) to CheA, a hybrid kinase. The Hpt domain on CheA (also known as P1 domain) phosphorylates the single domain CheY protein. The atypical CheA contains a separate dimerisation domain (P3), a RR binding domain (P2), and a regulatory MCP binding domain P5.

As discussed in chapter 1.2, a typical two-component system consists of a Histidine Kinase (HK) which binds an extra-cellular stimulus and a Response Regulator (RR) which has an effector domain to create an intra-cellular response to this stimulus. In chemotaxis the extra-

cellular stimulus does not interact directly with the HK, a chemoreceptor is required to sense chemoeffectors and then signal to the HK; these receptors are termed methyl-accepting chemotaxis proteins (MCPs). These differences are outlined in Figure 1-8.

E. coli chemotaxis is the model chemotactic system, owing largely to the length of time it has been under study as well as its comparative simplicity. There is a single atypical HPK, termed CheA, which phosphorylates the RRs CheY and CheB (Figure 1-9). CheA is described fully in chapter 1.4.5 and the domain arrangement and atypical features are outlined in Figure 1-8. MCPs binds their cognate ligands in the periplasm when attractant levels are high (Hazelbauer et al., 2008). A drop in attractant levels causes MCPs to shift conformation in some way which is proposed to cause a conformational shift in CheA, thus activating the HPK in turn (Falke et al., 1997). The exact mechanisms for the activity shifts of MCPs and CheA are still under study and the current models are outlined in chapter 1.4.7 and 1.4.5 respectively. Upon activation of CheA its autophosphorylation activity is increased, resulting in the transfer of the terminal phosphoryl group from ATP to its conserved histidine. Phosphorylated CheA then transfers the phosphoryl group onto the CheY conserved aspartate residue. CheY-P has reduced affinity for CheA and so dissociates and diffuses through the cytoplasm to the flagellar motor where it binds FliM and induces a switch in motor direction (Sourjik and Berg, 2002a) (Dyer et al., 2009) (Sarkar et al., 2010).

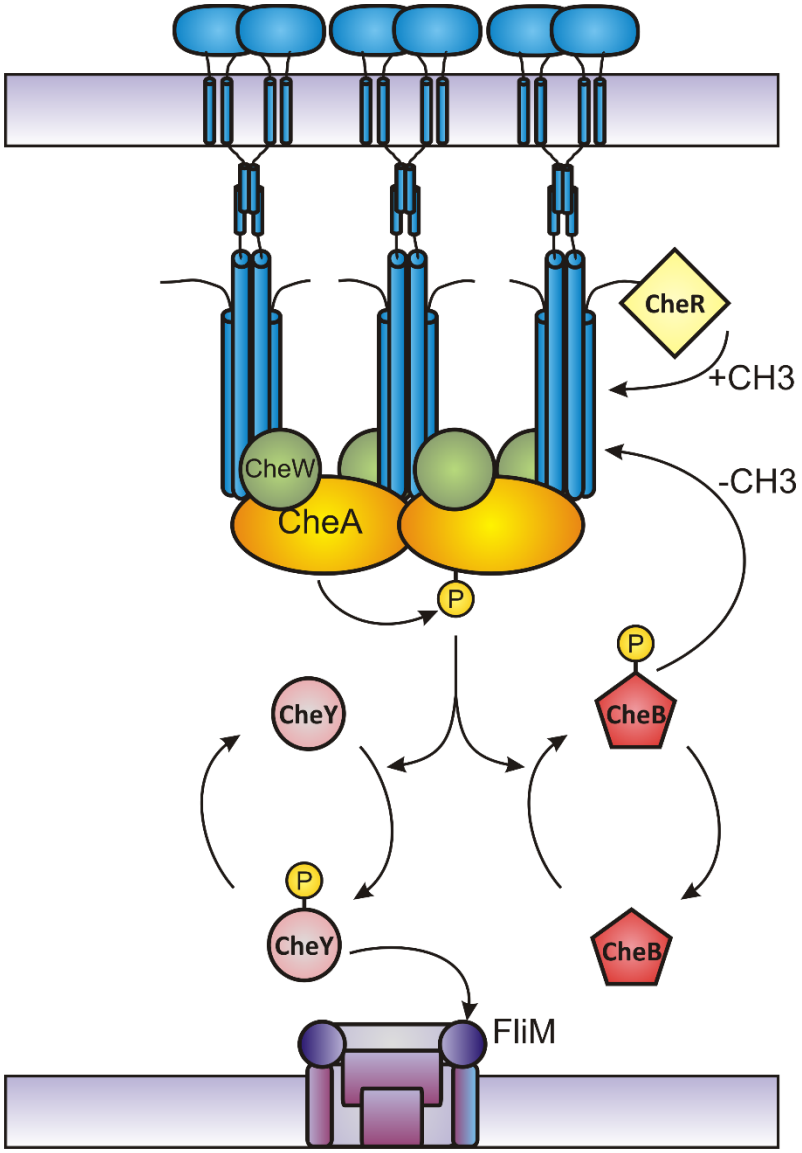

Figure 1-9 The components and reactivity of the *E. coli* chemotaxis system. Trimer of MCPs is bound by CheA dimer and CheW scaffold. One CheA monomer phosphorylates opposing monomer. CheA then phosphorylates CheY and CheB. CheY-P can bind FliM at the motor to initiate a tumble and CheB-P can remove methyl groups from MCPs that are added by the constitutively active CheR. Fewer methyl groups results in higher sensitivity to attractant concentration increases.

CheY-P is auto-dephosphorylated as well as dephosphorylated by CheZ in order to remove the signal from the system (Zhao et al., 2002). CheA phosphorylates the methylesterase CheB at a slower rate than CheY. This allows the CheB-P levels to increase after motor switching, increasing the methylesterase activity of CheB (Anand and Stock, 2002). MCPs can be methylated on certain exposed glutamate residues and a higher number of methylated

glutamates corresponds to a lower sensitivity of a receptor to a change in attractant concentration (Engström and Hazelbauer, 1980). CheB activity counteracts the methytransferase activity from the constitutively active CheR. CheR continually adds methyl groups to the MCP adaptation domain which, in the absence of CheB-P, results in a net decrease in sensitivity of the MCP to attractants.

1.4 Bacterial chemoreceptor arrays

Chemotactic sensing in bacteria is achieved using chemoreceptor signalling proteins, which vary greatly between species. *Methanococcoides burtonii* has a single MCP whereas species such as *Mesorhizobium loti* contain 65 putative chemoreceptors encoded in the genome (Alexander and Zhulin, 2007). The archetypal chemotaxis model *E. coli* codes for 5 known chemoreceptors: Tar, Tsr, Tap, Trg and Aer (Reader et al., 1979) (Rebbapragada et al., 1997). These are named after their predominant interacting ligands aspartate, serine, dipeptides, ribose and galactose, and cellular redox state respectively. The *in vivo* expression levels of these MCPs is different for each with Tar and Tsr being much more highly expressed than the others, in addition, the NWETF binding motif for the CheR adaptation protein is present only in these two MCPs. This has led to models suggesting that these are the dominant responders (Sourjik, 2004).

MCPs are transmembrane receptors, inserted into the membrane as functional homodimers. They are approximately 350 Å in length with a unique ligand binding domain (LBD) situated in the bacterial periplasm linked through to the cytoplasmic region through the second Transmembrane helix (TM2). The cytoplasmic domain contains at least one HAMP (present in Histidine kinases, Adenyl cyclases, Methyl-accepting proteins and Phosphatases) domain followed by a coiled coil domain (Figure 1-10). The coiled-coil domain consists of

methylation regions important in adaptation and typically a glycine hinge thought to be important for flexibility of this region which, in turn, is predicted to be involved in the signalling mechanism. The coiled coil domain is also responsible for forming the interactions required to form the functional trimer of dimers unit as well as being responsible for kinase binding.

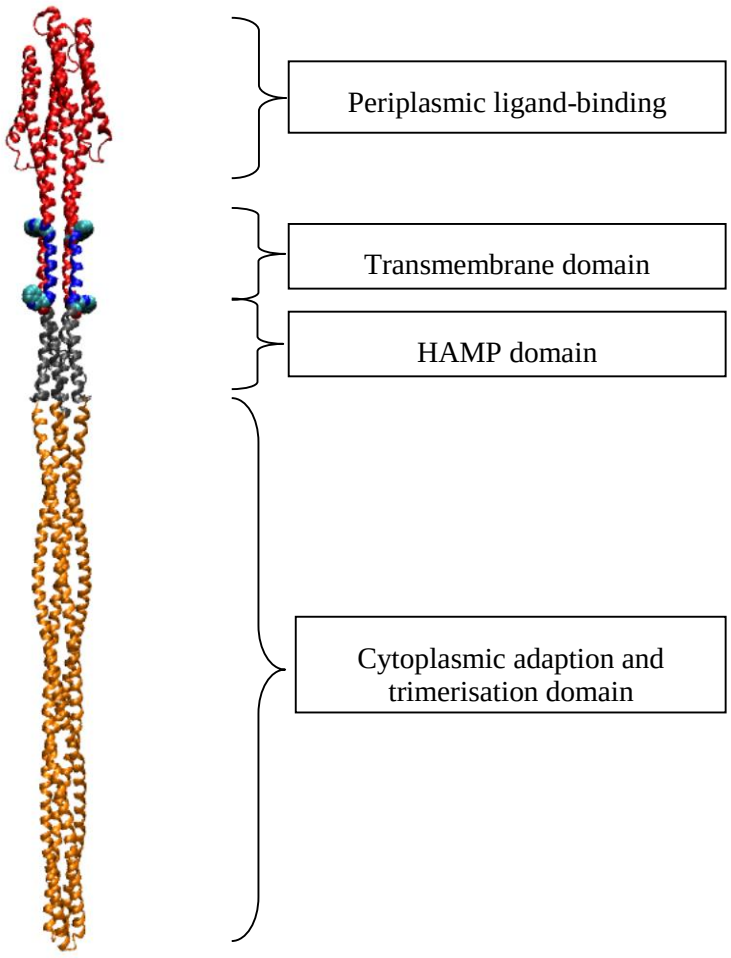

Figure 1-10 Full length *E. coli* serine receptor dimer, Tsr. The domains are labelled in different colours: LBD in red, TM2 in blue, HAMP domain in green and the coiled-coil in yellow. The membrane interfacial tryptophan and tyrosine residues are modelled as balls to outline the positions of the inner membrane leaflet interface. Model taken from (Hall et al., 2012) and adapted here for clarity.

MCPs can be classed by the number of heptad repeats that make up the coiled coil region as shown in Figure 1-11. *E. coli* receptors, for example, are all 36H and multiple classes can

be present in the same organism (Alexander and Zhulin, 2007). At the tip of the cytoplasmic domain, there is a glycine-rich region which allows the protein to turn back on itself and continue the coiled coil. The C-terminus of MCPs contains a predicted unstructured segment that houses a conserved motif (NWETF in *E. coli*) responsible for CheR binding.

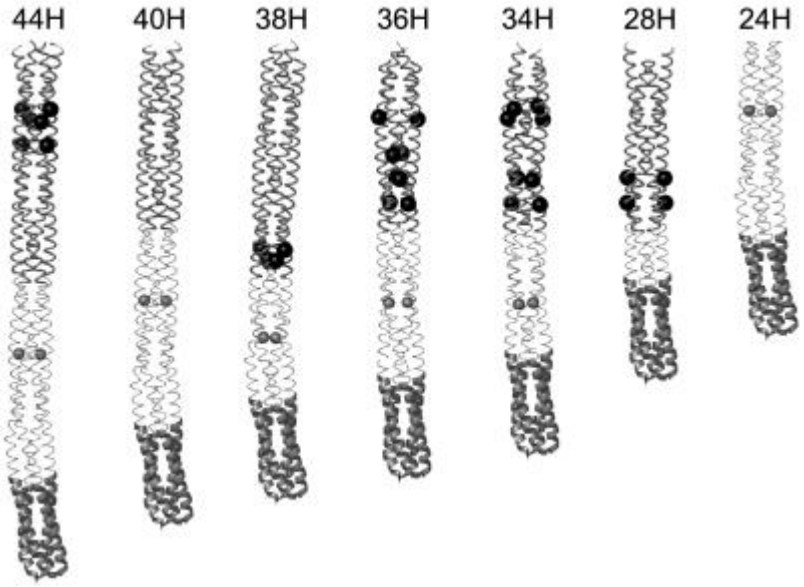

Figure 1-11 Homology models of the cytoplasmic domain of known classes of MCPs outlining the different lengths of receptor. The numbers above each model indicates the number of heptad repeats within a receptor of that class. The positions of the proposed methylation residues are shown as dark grey spheres, light grey spheres show the position of the glycine hinge. Taken from (Alexander and Zhulin, 2007).

1.4.1 Ligand-binding domain

The periplasmic domain of *E. coli* and *S. typhimurium* MCPs have been studied at length, particularly using crystallography as the LBD alone is, compared to the full length protein, easily crystallised (Jeffery and Koshland, 1993) (Yeh et al., 1993) (Milburn et al., 1991). Multiple mutagenesis studies have also yielded important information with regards to the chemotactic ability and specificity of these LBDs (Reader et al., 1979). In the case of *E. coli* the four well characterized LBDs (all except Aer) have similar structures and most likely arose via gene duplication. The LBD is typically a four-helical bundle monomer which

forms hydrogen bonds to create a dimeric signalling unit (Scott et al., 1993). The structure of a typical LBD (*E. coli* Tar) is shown in Figure 1-12.

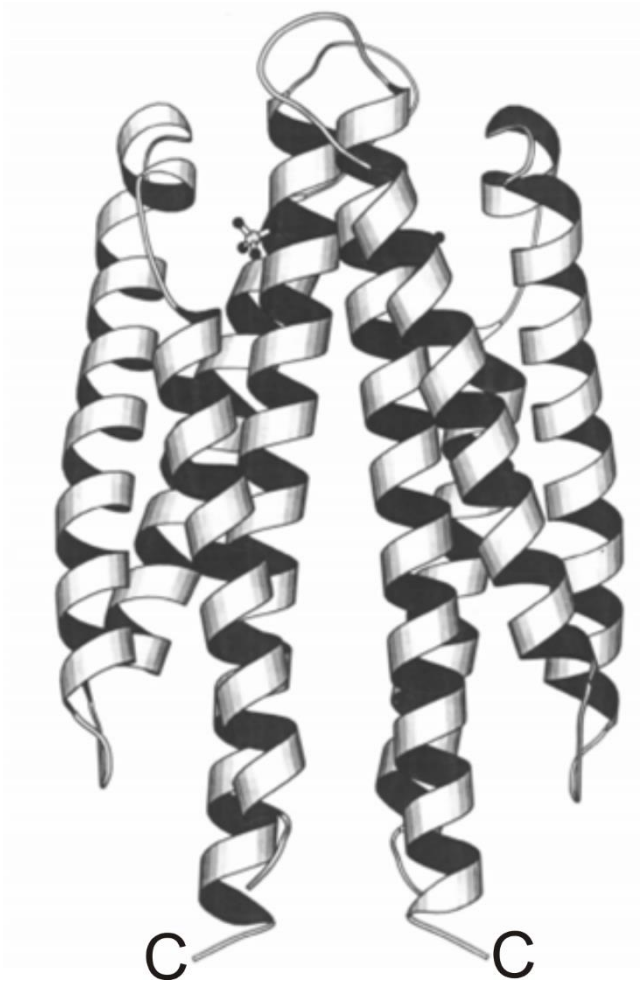

Figure 1-12 The dimeric ligand-binding domain (LBD) of the Tar aspartate receptor from *E. coli*. A sulphate molecule is shown crystallised at the aspartate binding sites as a ball and stick model. The C-terminus of each monomer that would continue to the TM2 helix have been labelled. Taken from (Bowie et al., 1995)

Very different LBD structures can be present in MCPs. For example, the PAS-domain (found in Period clock protein, Aryl hydrocarbon receptor and Single-minded protein) of the aerotaxis protein, Aer, must accommodate an FAD cofactor and is situated in the cytoplasm, N-terminal to the first transmembrane helix (Xie et al., 2010). In addition, many MCPs that have not had their LBDs crystallised can be analysed for potential structural similarities based on sequence alone. In *Rhodobacter sphaeroides*, McpA and McpM are both MCPs

not of the standard 34H class of *R. sphaeroides* (they are predicted to be 36H and 38H respectively). In addition, the aligned sequences of their proposed LBDs are predicted to be approximately 60 amino acids longer than typical *R. sphaeroides* and *E. coli* LBDs (Porter et al., 2011a). The specificity of the similar LBD structures has been proposed to be due to the individual residue differences of the surface rather than gross structural changes (Bowie et al., 1995). As a result of this binding mechanism, MCPs are potentially powerful tools for the sensing of various ligands. Recent uses in the field of synthetic biology have shown that the rational design of chemoreceptors to specific ligands is possible (Bi et al., 2013). It is proposed from crystal structures that the dimeric LBD structure contains two non-equal binding sites and binding at one may produce a small, rigid-body rotation between the subunits within a dimer (Yeh et al., 1996) (Yu and Koshland, 2001). This unequal structural change may be the signalling mechanism through to the transmembrane signalling helix, TM2.

1.4.2 Transmembrane domain

LBDs can vary extensively, however, C-terminal to this domain they are generally well conserved. Typical MCPs contain two transmembrane (TM) helices. TM1 is N-terminal to the LBD and is not currently thought to have any specific role in signalling, although it has been suggested that an interface with TM2 is important (Baumgartner and Hazelbauer, 1996) (Barnakov et al., 2002). TM2 is the linker helix between the LBD and the HAMP domain and as such is the transmission helix for any signal created by ligand binding. Multiple mechanisms for the transduction of a signal have been proposed that largely relate to three potential motions undertaken by TM2: a piston shift, a helix tilt or a helix axial rotation (Kitanovic et al., 2011) (Draheim et al., 2005) (Falke and Hazelbauer, 2001) (Szurmant et al., 2004a) (Hulko et al., 2006). Mutational analysis and more recent computational models

have shown strong support for the piston shift model, in which a ~2 Å shift in the helix z-position in the membrane causes a change in MCP activation state (Miller and Falke, 2004) (Hall et al., 2011). Comparison of the ligand bound and empty LBD structures also supports the piston-shift model (Chervitz and Falke, 1996). Cysteine reporters in the TM segments show formation of disulphide binds in concurrence with this model and a 1.6 Å shift was also reported from NMR studies (Hughson and Hazelbauer, 1996) (Falke and Hazelbauer, 2001) (Isaac et al., 2002). In addition, the free energy change required to drive such a motion is considered to be small if ~2 Å and this has been shown to fit with the free energy provided by small molecule binding (Cheung and Hendrickson, 2009) (Falke and Erbse, 2009). Mutations that mimic such a shift have been extensively studied and do indeed produce proteins with shifted activity profiles (Draheim et al., 2005) (Draheim et al., 2006).

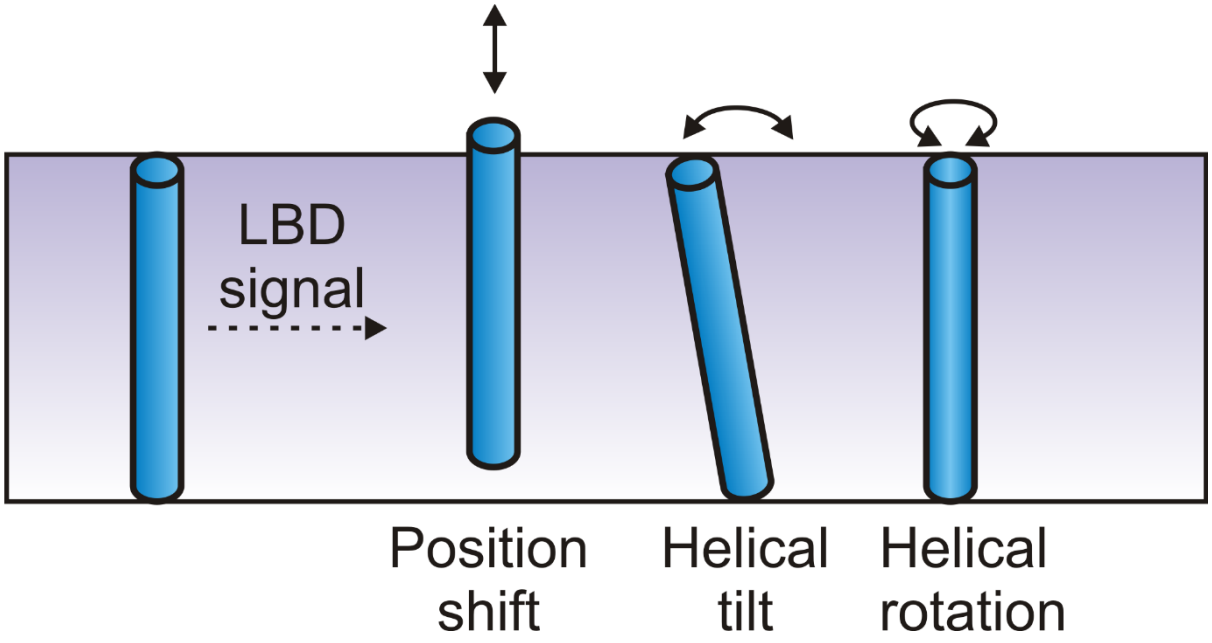

Figure 1-13 Potential motions of TM2 caused by binding events to the LBD. Helix can shift up or down in the bilayer, tilt with respect to helix axis or rotate on its own axis. The former motion is thought to be most important for signalling to the cytoplasmic domain

Mutations that result in a shift of the TM2 helix toward the periplasm have been shown to enhance clockwise (CW) motor output activity in *E. coli* whereas shifts that pull the helix

away from the periplasm induce greater counter-clockwise (CCW) motor output bias. Further study of proteins with shifted profiles should produce more accurate models of how signalling proceeds downstream (Hall et al., 2012).

1.4.3 HAMP domain

Central to many signalling proteins in bacterial cells, including many HKs and MCPs, is the HAMP domain which acts to couple sensing in the LBD of these proteins to an output signal in the signalling domain. The HAMP domain is proposed to be the signal transmitting domain which transfers the piston shift motion into the conformational change which alters the MCP activation state (Ferris et al., 2012). Two 16 residue amphiphilic helices make up an individual monomer of a HAMP domain, two of which pack together to form a functional dimer (Hulko et al., 2006). The proposed HAMP structure has been recently confirmed through crystallographic studies and is outlined in Figure 1-14, showing one proposed orientation of the four HAMP helices.(Airola et al., 2010).

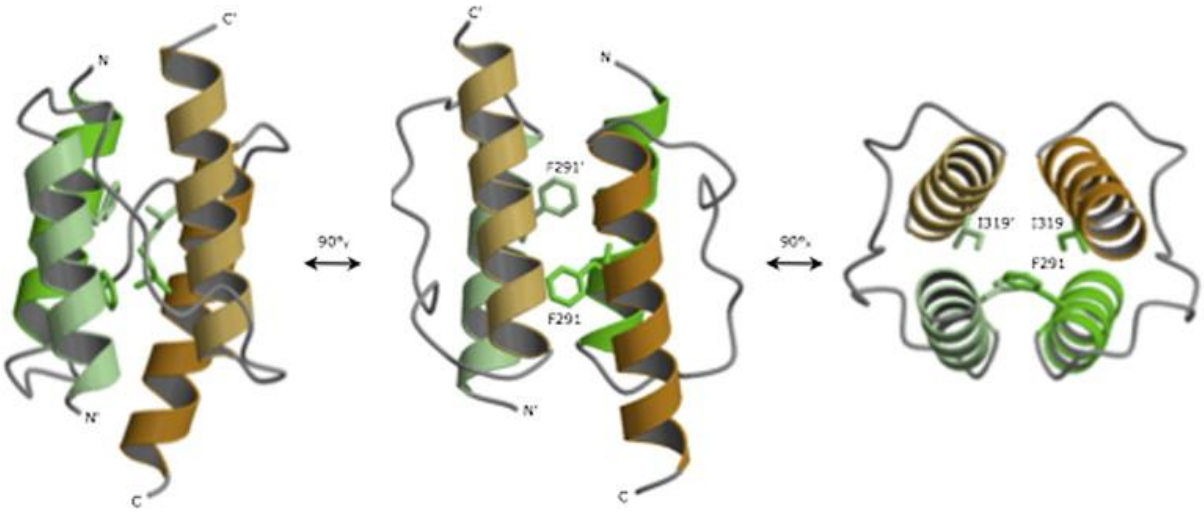

Figure 1-14 The structure of a HAMP domain in a parallel organisation shown from three different angles. Labelled are the central phenylalanine and isoleucine residues that overlap at the interface of the 4 helices. Taken from (Ferris et al., 2011)

As a typical coiled coil structure, HAMP domains contain a ‘heptad repeat’ arrangement, consisting of a seven residue repeat pattern. The residues of this repeat are labelled a-g and hydrophobic residues occupy positions a and d. Initial structures showed an atypical coiled-coil packing mode termed complementary x-da packing (Hulko et al., 2006). The arrangement of this packing is outlined in the left of Figure 1-15 which also shows the proposed method of signalling through HAMP domains as a result. Structures now exist of HAMP domains in two different arrangements which has led to the proposed mechanism of action (Airola et al., 2010). In addition, mutagenesis of the unusually small coiled coil core residue, alanine, at the centre of the HAMP to more typical larger hydrophobic residues suggests that the switching of packing modes to the more typical ‘knobs-into-holes’ is possible and results in a shift of HAMP output bias (Ferris et al., 2011). This is shown in Figure 1-15.

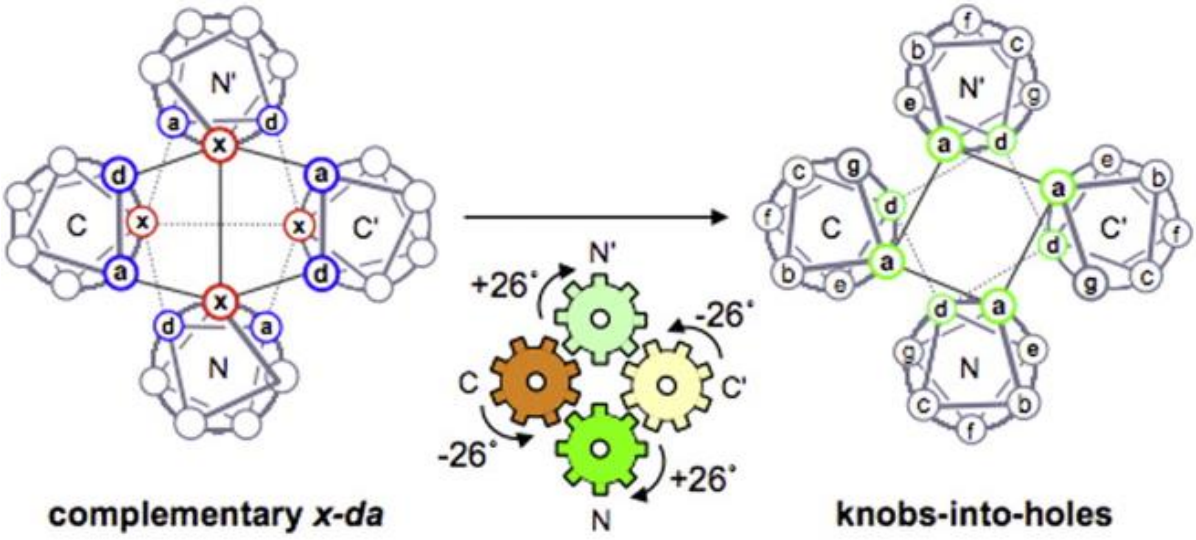

Figure 1-15 The packing modes outlining the gearbox model of HAMP signalling. The a and d position hydrophobic residues are labelled and their motion between the two states outlined. A 26° rotation of individual helices should switch the packing state and destabilise the output helices. Taken from (Ferris et al., 2011)

As a result, piston shift of the ‘control cable’ helix that links TM2 is proposed to cause a switch from one HAMP arrangement to the other, a mechanism well explained in a recent review (Parkinson, 2010). Shifts in packing favourability between these two states has been suggested to shift the packing between the two output helices which may alter the stability, this is supported by mutational data (Zhou et al., 2009) (Stewart and Chen, 2010) (Ferris et al., 2011). Rational design of HAMP domains based on these principals has involved the mutation of key residues predicted from these models to have a defined effect on packing. The activity of resultant downstream signalling domains was shifted as predicted and was even able to be reversed thus suggesting that rational engineering of these vital gearbox domains is possible to shift the output of signalling proteins (Airola et al., 2013).

1.4.4 Conserved cytoplasmic domain

Initial genomic studies of MCPs showed a conserve motif of 7 amino acids repeated within the cytoplasmic domain, within which the first and fourth residues were predominantly hydrophobic (Le Moual and Koshland, 1996). These 7 residues corresponded to two turns of the coiled coil domain and analysis of over 300 prokaryotic genomes for homologues of the MCP cytoplasmic domain have revealed the presence of 7 classes of MCPS, defined by the number of heptad repeats located in this region (Alexander and Zhulin, 2007). In the same study, the cytoplasmic domain was defined further into separate methylation and signalling domains along with the glycine turn at the tip (outlined in Figure 1-11). The result of this structure is a four-helical bundle at the cytoplasmic tip (Kim et al., 1999). The cytoplasmic domain ends in an unstructured C-terminal flexible domain (Bartelli and Hazelbauer, 2011). At the tip of this region there exists in *E. coli* a NWETF pentapeptide motif responsible for CheR binding (Wu et al., 1996). This binding region has not been definitely identified outside of *E. coli* and *S. typhimurium* and in some cases, removal of the

flexible region completely has been shown to have limited effect on the ability of MCPs to undergo efficient methylation (Perez and Stock, 2007). Packing in this region has been suggested as a mechanism through which signals are transduced to the kinase, with strong packing in the adaptation region enabling a kinase-on state and strong packing in the protein interaction region favouring the 'off' state of the kinase (Swain et al., 2009).

1.4.5 The scaffold proteins

CheW

CheW is a soluble linker protein of approximately 15 kDa in size. It contains two β sheet domains, each consisting of a 5-stranded β barrel, similar to the CheA P5 domain (discussed in detail in the following paragraphs), the structure of which has been analysed by both NMR and X-ray crystallography (Griswold et al., 2002) (Park et al., 2006) (Li et al., 2007). Notable in recent studies is that CheW often has little sequence homology between species, however, complementation has been demonstrated (Shah et al., 2000). The reason allowing for such complementation was shown to be due to strong structural homology despite often little sequence homology (Alexandre and Zhulin, 2003). This has led to the ability to easily model CheW structures but often to miss their presence in genomes (Cashman et al., 2013).

The conserved CheW structure is shown in Figure 1-16 as well as its proposed interaction to the homologous P5 CheA subunit. It has been shown that the role of CheW is to bind to the cytoplasmic domain of MCPs near the tip region (Vu et al., 2012), the same study, however, showed that MCP trimerisation residues are likely to be the same and as a result there is a potential for competition between tight trimeric structures and CheW scaffold binding. Over-expression of CheW results in array disruption and yet mutations in CheW that abolish binding to chemoreceptors prevent chemotaxis (Cardozo et al., 2010)

(Boukhvalova et al., 2002). It appears a trade-off between activity and competition is required.

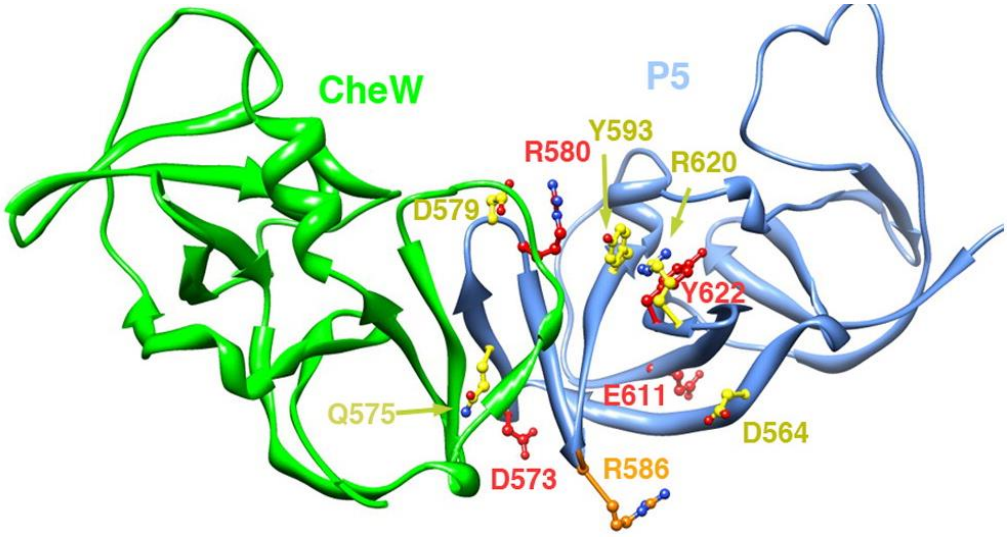

Figure 1-16 The structure of CheW (green) and a proposed interaction with the homologous P5 subunit of CheA (Cyan). Also labelled are CheA residues that, when mutated, are proposed to disrupt chemotaxis (red), CheW binding (orange), or kinase activity (yellow). Adapted from (Li et al., 2013).

The chemotaxis HK CheA requires CheW binding to the receptor in order to complete the chemosensory ternary complex, however, polar clustering of chemoreceptors is not dependent on CheA but is merely enhanced in fully chemotactically able cells (Gegner et al., 1992) (Boukhvalova et al., 2002) (Skidmore et al., 2000).

CheA

CheA is a soluble HK containing 5 distinct domains and existing as a functional dimer. In response to decreased attractant binding to MCPs, CheA autophosphorylation activity is increased. Phosphorylated CheA can then transfer this phosphoryl group to its cognate response regulators resulting in an increase in soluble levels of the activated RR CheY-P and thus increases tumbling of the cell (Borkovich and Simon, 1990). The roles of each domain of CheA are fairly well understood, P2 binds the response regulators CheY and

CheB; P3 is the dimerization domain; P4 is the kinase domain that binds ATP and phosphorylates the histidine residue (His48) in the P1 domain (also known as the Hpt (histidine phosphotransfer) domain); and P5 is the regulatory domain that controls kinase activity and contains the interaction surface for CheW and the chemoreceptors (Miller et al., 2006) (McEvoy et al., 1996).

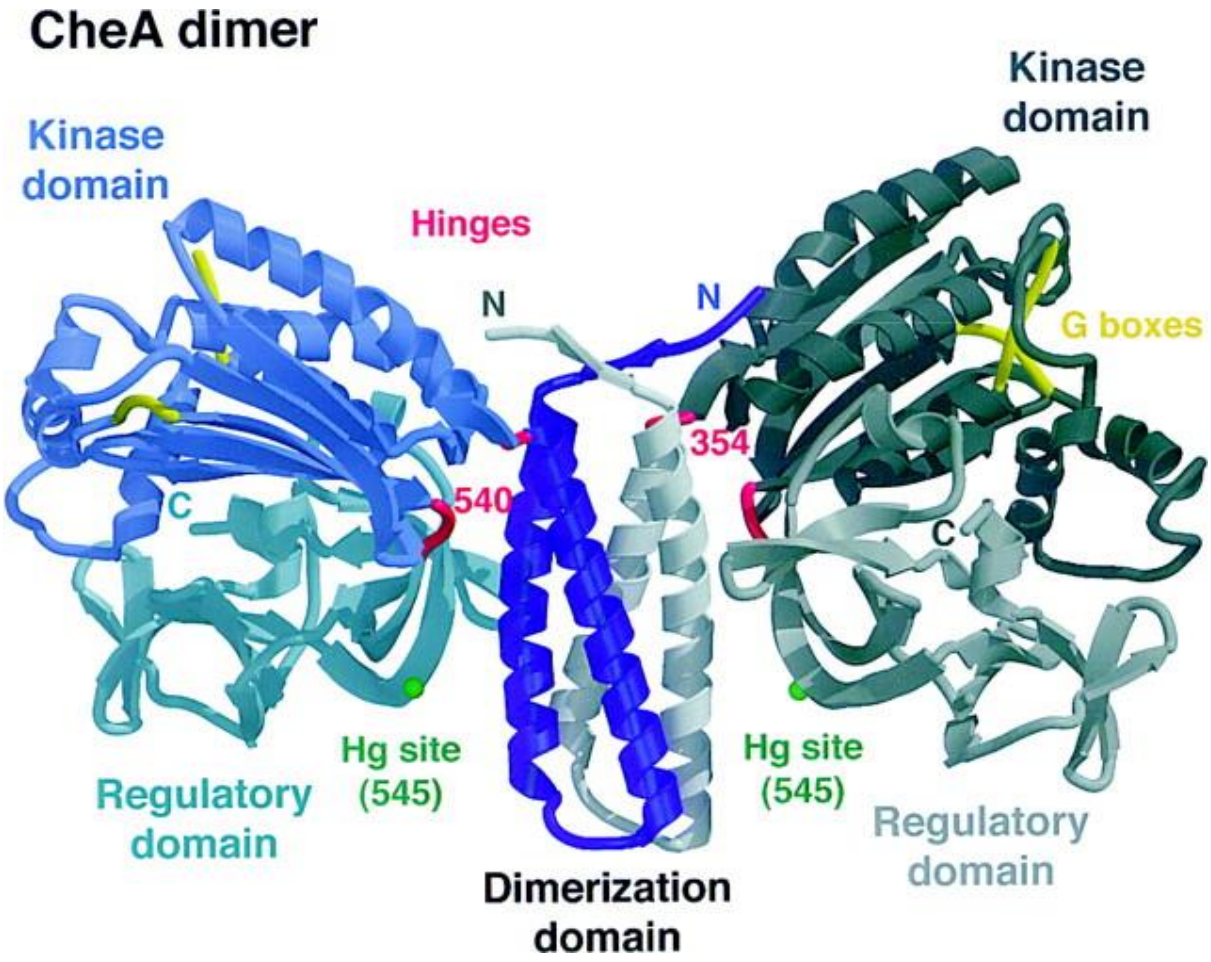

Figure 1-17 The dimeric structure of CheA domains P3-P5. Two monomers are coloured separately (blue and grey) and labelled are the dimerisation (P3), kinase (P4) and regulatory (P5) domains of each. The hinge linkers that connect these domains, arginine 354 and threonine 540, are also labelled. Also shown is the site of the mutation used to allow heavy metal modification in order to determine the crystal structure (Q545C). The ATP binding regions (labelled G-boxes) are also shown. Taken from (Bilwes et al., 1999)

The mechanism of signal transduction to the kinase domain is beginning to be understood in more detail and it is believed that the P4-P5 linker controls the activation of CheA and the P3-P4 linker controls both the basal autophosphorylation activity and the activation of

CheA. The ternary chemosensing complex has been studied extensively using electron microscopy (EM) to analyse the overall arrangement (Francis et al., 2002) (Francis et al., 2004) (Wang et al., 2012). More recently, crystallography has shed further light on how the 3 cluster proteins combine *in vivo* (Briegel et al., 2012) (Li et al., 2013). The CheA/W binding site at the cytoplasmic tip has been suggested from these structures among others and biochemical evidence has now narrowed down precisely the interactions involved (Piasta et al., 2013). Notable are residues at the MCP tip and the CheW hydrophobic groove shown to form interactions vital for efficient chemotaxis (Ortega et al., 2013a). The current model suggests that sequential CheA P5 domains and CheW form a ring structure with pseudo hexagonal symmetry around receptors, which is conclusive with lower resolution EM data (Briegel et al., 2012).

1.4.6 Higher level order of chemoreceptor arrays

Individual chemoreceptor dimers form functional receptor trimer units with the cytoplasmic four-helix bundle tip important for the binding interaction (Kim et al., 1999) (Boldog et al., 2006). MCPs have been shown to act as dimers and require a trimeric arrangement to enable full binding and activation of downstream signalling components (Boldog et al., 2006). This trimeric arrangement is supported by cross-linking studies *in vivo* (Ames et al., 2002). Trimers have been shown to self-assemble in bilayers into higher order arrays (Greenfield et al., 2009). These clusters are naturally excluded from lateral cell regions due to an affinity for membrane curvature (Endres, 2009) (Rudner and Losick, 2010). Full, tight packing of a functional array, however, requires the addition of CheA and CheW (Zhang et al., 2007). As discussed in 1.4.5, the scaffold proteins form a ring around receptor tips with pseudo hexagonal packing (Figure 1-19). This forms a hexagonal array of chemoreceptors bound to

their signal transducing partners at the tip distal to the membrane (Briegel et al., 2008) (Khursigara et al., 2008a) (Briegel et al., 2012). This is now the accepted model, replacing previous models suggested from structural data of MCPs and the scaffold proteins in less-native states (Weis et al., 2003).

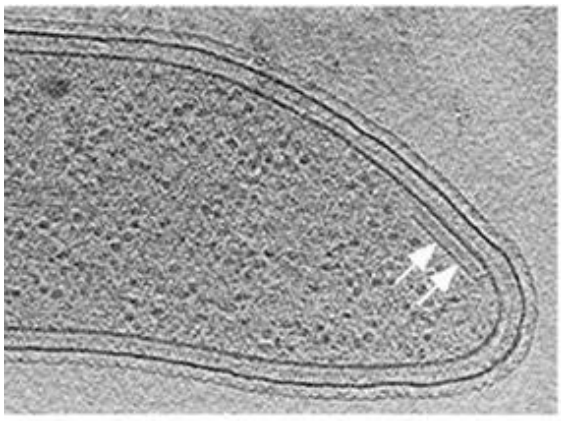

Figure 1-18 Cryo-EM image showing the scaffold proteins at the base of a polar cluster in *Caluobacter crescentus*.

Clusters form predominantly at the poles of cells in the majority of species. However, there is much evidence that clusters can form elsewhere around the membrane (Zhang et al., 2007) (Briegel et al., 2008). Recent super-resolution images of various array components have proven this *in vivo* and support the notion of stochastic self-assembly of arrays along the bilayer (Greenfield et al., 2009) (Thiem and Sourjik, 2008). The presence of a rigid array has been visualised directly using cryo-electron microscopy (EM) tomography to view thin cell slices (Figure 1-18). Slices such as these have been averaged in three-dimensions to form an image of the average density of an array, which helped determine the topology model shown in Figure 1-19. This model suggests that MCP:CheW:CheA stoichiometry should be 6:2:1 to fit correctly into the density. However, due to the lower density of the CheW/CheA ring this may not be accurate. This lower density might, however, give evidence to the average occupancy of these components and how they may turnover.

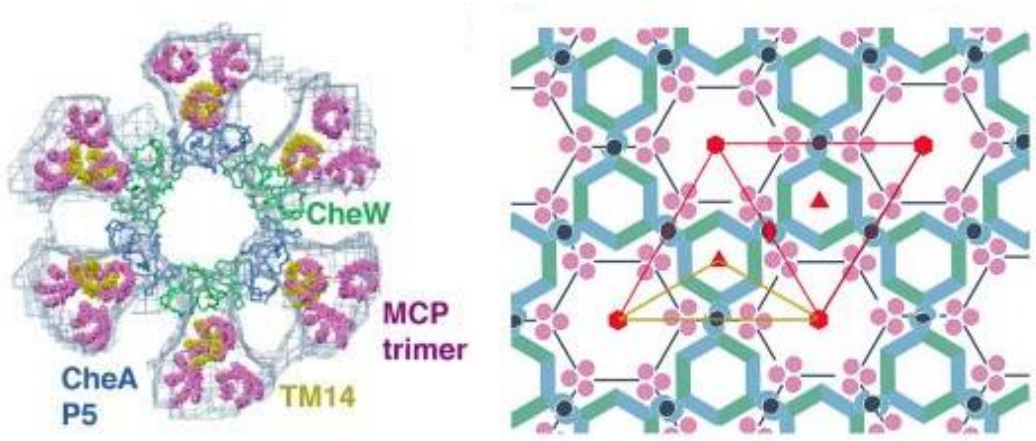

Figure 1-19 The proposed arrangement and symmetry of CheA and CheW proteins in the tight chemotaxis array. **Left** shows the model of one ring of the crystal structure of CheA-P5 and CheW proteins with the bound six receptor dimer tips (labelled TM14). The rest of the functional trimer unit is also shown as modelled into the density shown from EM images. The density of the CheA/W ring from this EM study is lower, suggesting lower occupancy or increased flexibility. **Right** shows a schematic of this symmetry with the MCP trimers labelled as pink circles, CheW and CheA-P5 as green and blue sides of the hexagonal lattice respectively. Taken from (Briegel et al., 2012)

Turnover of the individual proteins of the *E. coli* cluster has been measured using fluorescence recovery after photobleaching (FRAP) to determine how tightly each is held in place. The different polar cluster components do not turnover from the cluster at the same rates. The chemoreceptors are held tightly within the cluster, whereas the scaffold proteins CheA and CheW do appear to turnover ($t_{1/2}$ ≈30min for MCPs and ≈12min for CheA and CheW) (Schulmeister et al., 2008). CheA and CheW are therefore not held tightly to the lattice and the interaction to the MCPs can be transient. However, fluorescence resonance energy transfer (FRET) analysis, which determines the distance between two fluorophores by measuring the ability to exchange photons between them, has shown a signalling independent interaction network between these proteins (Kentner and Sourjik, 2009). This shows that the array proteins are in close proximity to one another regardless of signalling state, however, it does not show whether the interactions between these proteins is stronger or weaker during signalling and turnover of these proteins with respect to activation state has not previously been studied.

1.4.7 Cluster signalling

Despite mounting strong evidence as to what the signalling array looks like, there is still a strong debate as to precisely how signalling occurs both through chemoreceptors and through the array. Another important aspect of signalling is whether, and how, cooperativity contributes and how cooperativity is created within the system. The chemosensory network is a very sensitive signalling pathway, able to respond to as little as 3 nM aspartate and only a 0.2 % change in ligand occupancy can result in a 23 % change in motor rotation bias (Mao et al., 2003) (Sourjik and Berg, 2002b). This shows that the chemosensory signal is able to amplify by 100 fold. This amplification within the cells occurs at two distinct places: MCP cooperativity and cooperativity of CheY-P binding to FliM (discussed in chapter 1.5).

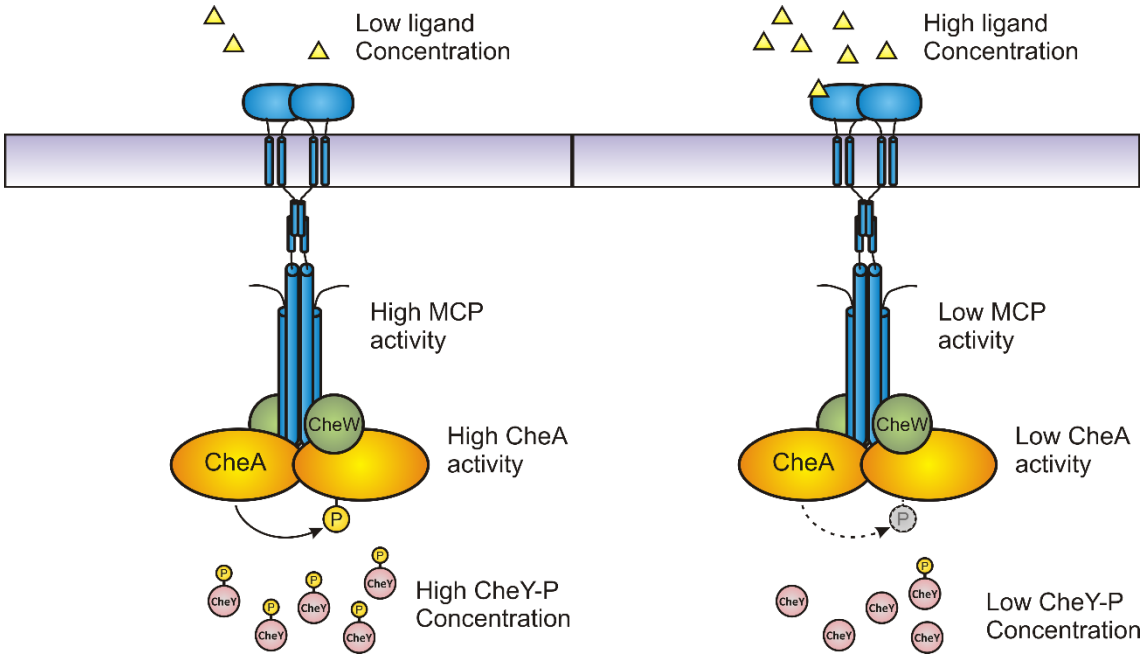

Figure 1-20 Simple allosteric model for MCP activation. **Left**: low ligand concentration causes low LBD occupancy which results in high MCP activation and thus high CheA activity. As a result, CheY-P is increased resulting in more motor reversal events. **Right**: high ligand concentration causes high occupancy of LBD which results in low MCP activation and thus low cheA activity. As a result, CheY-P concentration is low and no motor reversals occur.

Traditional models of signalling through membranes occurs through a standard allosteric change mechanism with binding causing structural shifts at the interaction with the signalling partner leading to activation (Figure 1-20). Figure 1-20 shows that a structural shift is difficult to reconcile with the known arrangement of the array: in the case of MCPs, this simple model is not sufficient. As discussed (1.4.2), the free energy gained from ligand binding is insufficient to drive gross structural change. In addition to this, MCPs do not form single signalling units (chapter 1.4.6), they form signalling trimers which then oligomerise further into an array (Figure 1-22).

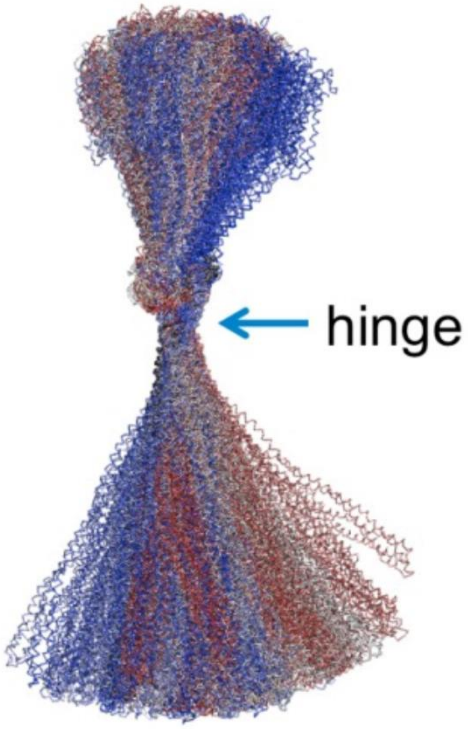

Figure 1-21 A schematic showing the sampling of an MCP over time when modelled and simulated in solution. Structures from individual time points through the simulation are shown and coloured red to blue. Labelled is the glycine hinge region around which flexibility occurs. Taken from (Hall et al., 2012).

When analysing the signalling through trimeric units it is also important to note that MCPs are not rigid, immobile structures (Figure 1-21). *In silico* studies to determine MCP structural sampling in solution have shown that MCPs are inherently flexible, this flexibility

must be accounted for when modelling how chemosensing occurs at a molecular level (Hall et al., 2012). Studies on the chemoreceptors, particularly recent *in silico* work, have shown that MCPs can adopt two stable conformations at the scaffold binding tip (Ortega et al., 2013b). However, this study still relates individual dimer motion to interactions at the trimeric interface.

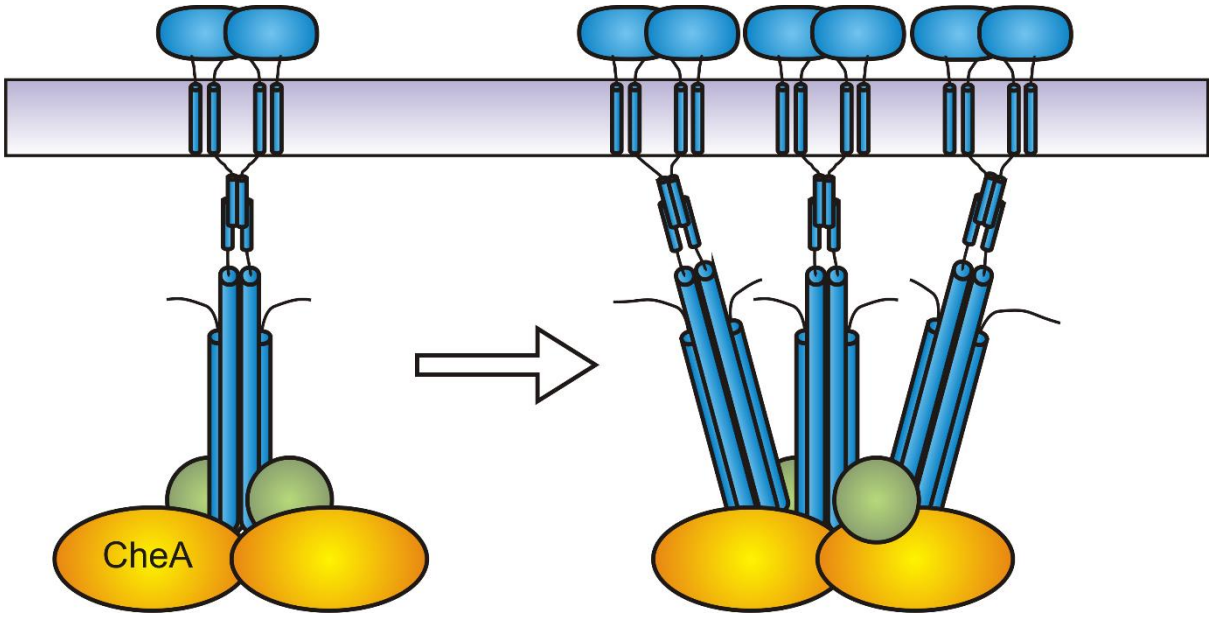

Figure 1-22 MCPs do not exist as functional dimers but rather as trimers of dimers bound at the tip by the CheW/CheA scaffold. Shown here is a schematic of trimeric bundle bound by dimeric CheA and dimeric CheW. For ease of drawing, MCPs are shown to kink above the HAMP region rather than at the proposed glycine hinge in order to meet at the trimeric contact point at the receptor tips.

To date, the most successful method used to directly show receptor output and activation, is a FRET method. This analyses the reaction between CheY-P and CheZ that is dependent on CheY-P production resulting from CheA activity (Sourjik and Berg, 2004). This experiment has been used to show that responses from one receptor are dependent on presence and levels of other receptors in the system (Vaknin and Berg, 2007). Some analysis has been undertaken on isolated receptors in artificial nanodiscs. These are lipid discs surrounded by stabilising proteins that allows a membrane-like environment and single-molecule study. This study suggests that, based on receptor methylation levels, a single receptor dimer is the

core component of signalling (Amin and Hazelbauer, 2010). In contrast however, similar experiments have shown that full kinase activation requires higher level order of chemoreceptors than a single dimer (Boldog et al., 2006). Initial EM analyses showed strong hexagonal packing across the array that does not support signal-induced packing changes (Briegel et al., 2008). However, local disordering of the cluster has been seen in different studies suggesting the use of structural shifts in response to stimuli (Khursigara et al., 2008b). The latter study suggests that the strict hexagonal packing is as a result of cluster-wide averaging and in fact local disorder is intrinsic to the system and potentially useful in signalling. Fluorescence anisotropy measurements also appear to show that there are large scale shifts in receptor packing in response to a change in stimulus and that dimer separation within trimers is important in signal transduction (Vaknin and Berg, 2007) (Vaknin and Berg, 2008). These results suggest that attractant occupancy favours an ‘expanded state’ of the receptor complex in which individual receptors dimers have a higher average distance from their nearest neighbour. The exact mechanism for this, however is still not fully understood, neither is how this change will result in a shift of kinase activity. Recent cross-linking studies have been undertaken to analyse CheW interactions proposed from NMR experiments (Vu et al., 2012). The cross-linking analysis shows that there is a dynamic binding site for CheW at the MCP hairpin tip and that the residues involved in binding change with respect to CheA presence, MCP signalling state (which is locked using mutagenesis) and attractant concentration (Pedetta et al., 2014). These data, along with the previous studies could suggest a potential model for scaffold binding in response to signalling (Figure 1-23).

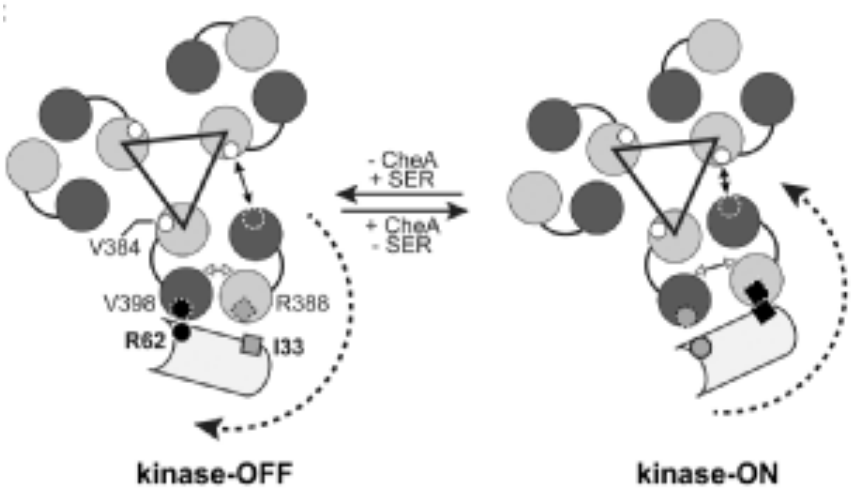

Figure 1-23 A proposed model of CheW binding shifts on Tsr hairpin loop in response to signalling. The Tsr N- and C- helices are depicted in grey and dark grey circles respectively. The centre triangle depicts trimeric symmetry between single central helices. The grey cylinder depicts a single CheW binding at the proposed interface. The depicted motion of CheW reflects the cross-link efficiencies in both the kinase on and kinase off states respectively. These efficiencies lead to the proposed model of CheW (and thus potentially CheA) binding shifts with changes in receptor state. Adapted from (Pedetta et al., 2014)

1.5 Signal Diffusion

From the polar chemotaxis array, a signal to elicit a tumble must then be passed to the flagella motor to either reverse or stop the motor (Toker and Macnab, 1997). This is achieved using the soluble RR CheY. CheY is a small, compact globular protein whose structure has been solved to good resolution using crystallographic methods (Volz and Matsumura, 1991) (Stock et al., 1993). It is typically present at around 8,000 copies/cell and as such is second only to MCPs in copy number of the chemotaxis proteins (Li and Hazelbauer, 2004). A single phosphoryl group is transferred from an activated CheA P1 domain histidine to the active site aspartate in CheY. Structural analysis of this complex has also enabled analysis of specificity and cross-talk between CheA and CheY homologues (Bell et al., 2010). Such decoding is of particular interest in organisms such as *R. sphaeroides* that contain multiple chemotaxis protein homologues and must integrate signals across them all. Structures of the

activated CheY also exist which show minimal gross structural changes. This has led to a current theory that activation merely results in stabilisation of a particular state that is in equilibrium with the inactive form without addition of a phosphoryl group (Lee et al., 2001).



Figure 1-24 The crystal structure of *E. coli* CheY activated by BeF. Structure shows 5 β-strands and 5 outer α-helices as well as the BeF binding residues Asp^{57}, Thr^{87} and Tyr^{106} labelled as balls and sticks. Taken from (Lee et al., 2001)

Another theory proposed from structural data, however, suggests that CheY specificity for its target protein at the motor, FliM, is shifted by amino acid side chain rotations away from the binding site, which ordinarily prevent binding by causing steric clashes (Cho et al., 2000). Once phosphorylated by CheA, CheY-P diffuses through the cytosol to the motor where switching can be induced (Segall et al., 1985) (Terasawa et al., 2011). Binding of CheY-P to the flagella motor occurs at FliM (Toker and Macnab, 1997). This protein is a flagellar motor component responsible for motor switching as a result of CheY-P binding. In *E. coli*,

CheY-P binds to FliM at the flagellar motor which causes a change in motor rotation direction (CCW to CW) and results in the cell tumbling. Crystal structures have been used to determine the interactions involved and to show CheY-P binding to the N-terminal portion of FliM, supporting the model that suggests a CheY loop region connecting two of the outer helices and a conserved threonine are important for the binding specificity (Dyer and Dahlquist, 2006). As discussed in chapter 1.4.7, CheY-P binding to FliM is a cooperative process thus small numbers of cellular CheY-P are likely not effective in inducing motor switching but in the event of a sudden large increase in CheY-P at the motor, switching will occur rapidly (Cluzel et al., 2000).

1.6 Signal Termination

CheY-P must be removed from the system in order to return to a chemotactic-neutral state and continue a run. It has been determined that it typically takes around 100ms for CheY-P to diffuse from the polar cluster to the flagellar motor (Lipkow et al., 2005). Once the motor direction has been switched, CheY-P must be removed from the system within 1 second in order to allow the following run event to occur. This can occur by auto-dephosphorylation in which the phosphoryl group is released as a phosphate as the product of hydrolysis, a reaction with a half-life of ~14 s in *E. coli* (Appleby and Bourret, 1998) (Lukat et al., 1991). This time frame is obviously not consistent with the ~1 second limit. *E. coli* contains the phosphatase CheZ which is able to remove phosphoryl groups from CheY-P directly and decrease the half-life approximately 100 fold (Silversmith et al., 2008). The presence of a phosphatase and the resultant decrease in half-life of the phosphoryl CheY species means that once the MCP cluster reverts to a kinase-OFF state, CheY-P is quickly removed from the system, returning the bacteria to a run state.

1.7 Adaptation

As discussed, micrometer scale environments prevent the use of direct distance sensing mechanisms to determine chemotactic gradients and as such bacteria must sense temporally. In order to achieve this sensing, they retain a primitive form of 'memory' through which MCP clusters are adapted to continual stimuli (Vladimirov and Sourjik, 2009). This same mechanism allows bacteria to respond to ligand concentrations in the range of 5 orders of magnitude (Bourret et al., 1991). The signalling states of bacterial chemoreceptors are influenced by two distinct processes: ligand occupancy and receptor methylation levels. MCPs are methylated on specific conserved glutamate residues situated within the cytoplasmic coiled-coil domain (as shown in Figure 1-11). These are located in *E. coli* at a conserved E-**E**-X-X-S/T motif where the X residues can be any amino acid and the bold glutamate is the methylated residue (Terwilliger et al., 1986a). *E. coli* Tar receptor contains four of these methylation sites, two are coded in the genome as glutamines and two as glutamates and all four have different methylation kinetics (Terwilliger et al., 1986b). In addition, the rates of methylation at one site are dependent on receptor methylation levels of the site C-terminal to it. (Shapiro et al., 1995). In *E. coli*, the protein methyltransferase CheR constitutively methylates receptors on four glutamate residues in the cytoplasmic domain (Springer et al., 1979). Methylation of chemoreceptors lowers CheA activity and thus decreases tumbling bias (Borkovich et al., 1992). As a result, a continual and constant signal will not continue to bias towards a run as the receptors are methylated and CheA activity is increased. This ensures gradients are continually sought out. Methylation of receptors also causes a reduction of attractant affinity, providing bi-directional adaptation (Borkovich et al., 1992) (Li and Weis, 2000) (Levit and Stock, 2002). Crystal structures of CheR have given insight into its method of action (Djordjevic and Stock, 1997). CheR is composed of

a C-terminal modified Rossman fold domain, which is characteristic of class I methyltransferases, and a smaller N-terminal domain. The former is a characteristic nucleotide-binding fold and is the major contributor to the binding of S-adenosylmethionine (AdoMet), which it uses as the methyl donor. The N-terminal domain contributes to ligand binding to a lesser extent and also contains the major recognition helix (helix α2) responsible for receptor interactions (Shiomi et al., 2002). This helix is highly positively charged and therefore is thought to interact at the negatively charged glutamate sites on the receptor.

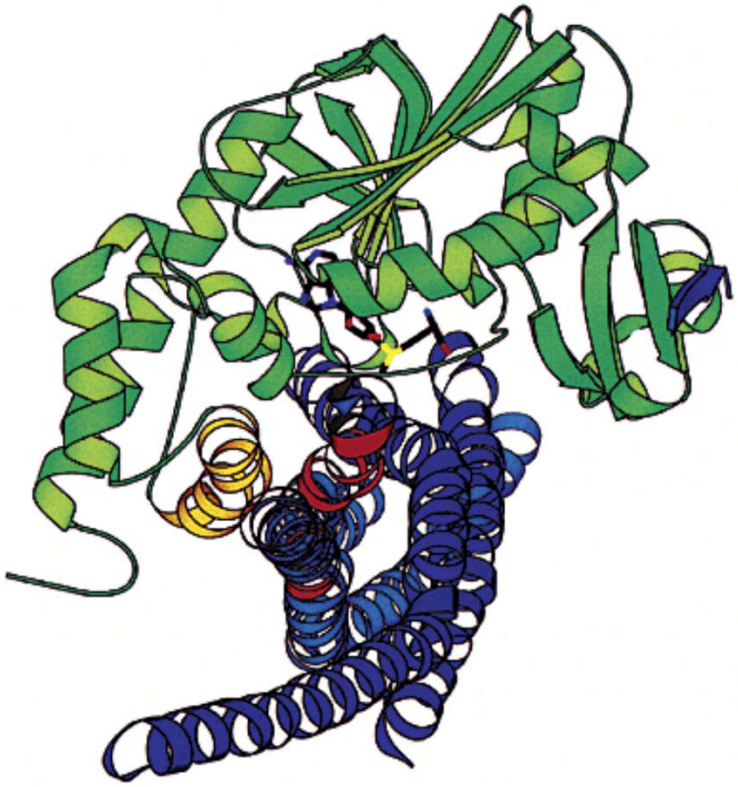

Figure 1-25 Computationally-derived model for CheR interaction with the MCP cytoplasmic domain at a methylation site. CheR is shown (green) with its α2 helix (gold) in contact with a penta-peptide corresponding to the receptor (blue). An AdoMet molecule has been modelled at the binding site as a ball and stick. The methylation sites in this image are also coloured (red). Taken from (Perez et al., 2004)

CheB is the second response regulator target of the HK CheA, along with CheY. It is a methylesterase enzyme that works in opposition to CheR to remove methyl groups added to glutamate adaptation residues and deamidate specific glutamines (Hess et al., 1988) (Wylie

et al., 1988). Upon phosphorylation by CheA, CheB activity increases and receptor methylation levels are decreased. CheB has a typical RR domain architecture consisting of an N-terminal regulatory domain and a distinct C-terminal effector domain. Removal of the regulatory domain allows constituent activity of the methylesterase domain suggesting a negative regulatory role for the regulatory domain (Simms et al., 1985).

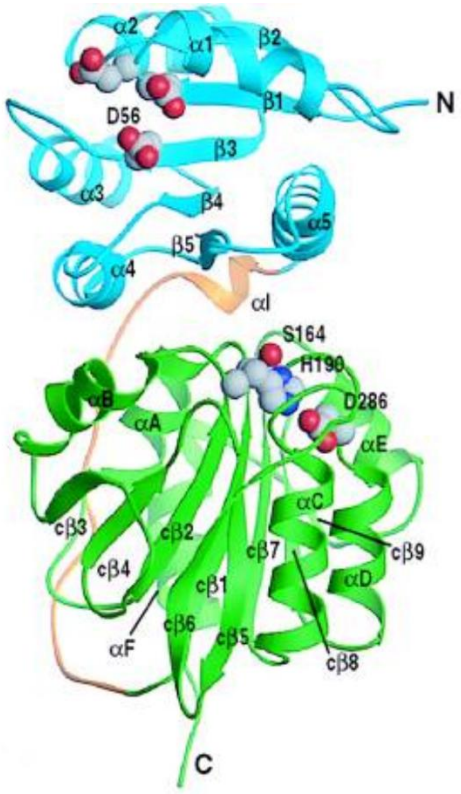

Figure 1-26 The crystal structure of CheB. The N-terminal regulatory domain is labelled in blue, the linker helix in gold and the C-terminal catalytic domain is shown in green. The N-terminal phosphorylation site consisting of the three aspartates: 11, 12 and 56 is labelled as spheres as are the catalytic triad residues of the catalytic domain: Ser164, His190 and Asp286. The β-sheets and α-helices are numbered conventionally with those of catalytic domain containing a 'c' prefix. Taken from (Djordjevic et al., 1998)

Structures have been determined of both the distinct domains and the full length CheB protein from crystallography and homology modelling studies (West et al., 1995) (Djordjevic et al., 1998) (Volz, 1993). These show a typical regulatory domain (see chapters 1.2.2 and 1.5) best characterised by the CheY studies and an N-terminal serine hydrolase domain consisting of a modified doubly wound α/β protein containing a long antiparallel β-

hairpin insertion and the catalytic serine, histidine and aspartate residues. Notable from the structure of the regulatory domain is an active site glutamate that when deleted decreases the relatively fast rate of dephosphorylation. As a result, it is thought that this residue is responsible for maintaining fast turnover rate of the phosphoryl site. Phosphorylation causes a conformational change that is proposed to reorientate the two domains, freeing up the substrate binding site (Anand et al., 2000). The full length structure of CheB has given some suggestion as to how this occurs (Figure 1-26). There exists a large interfacial surface between the two domains that buries two hydrophobic residues that are conserved among RRs. In CheY, the N-terminal residue is a tyrosine which has been shown to become buried upon activation (Zhu et al., 1997). This may allow release of the regulatory domain, freeing up the methylesterase domain. The MCP binding site is partially occluded by the regulatory domain and as a result, the chemoreceptor dimer substrate is unable to bind until this domain separation occurs (Djordjevic et al., 1998). Upon binding to the receptor, catalysis is performed through a standard serine hydrolase catalytic triad mechanism to remove a methyl group from the γ-methyl glutamate residues (West et al., 1995). Models of adaptation have elegantly demonstrated how precise adaptation can occur and how allosteric coupling effects receptor modification (Barkai and Leibler, 1997) (Endres and Wingreen, 2006). The latter study describes receptor ‘assistance neighbourhoods’ which includes cooperativity into the adaptation model and thus limits large heterogeneity in methylation levels. Neither studies, however, link this to structural changes in the receptor complex and therefore do not suggest how such ‘neighbourhoods’ would undergo such cooperativity and how this would affect the interaction with the kinase.

1.8 Non-*E. coli* chemotaxis systems

The *E. coli* system is a model organism for chemotaxis due to its simplicity, allowing for easy manipulation and study of individual components. A recent study showed that 30% of tested species contained multiple copies of at least one of the core chemotaxis proteins and nearly 70% of these contained the cytoplasmic clustering protein PpfA (Hamer et al., 2010). This shows that the *E. coli* paradigm does not hold for all bacteria and in fact, a significant portion are much more complex and require integration of signals through multiple homologues (Porter et al., 2011b). In some cases, the chemotaxis components have been co-opted for new roles within cells, such as the flagellar expression and cist formation control pathways in *Rhodospirillum centrum* (Berleman and Bauer, 2005a) (Berleman and Bauer, 2005b).

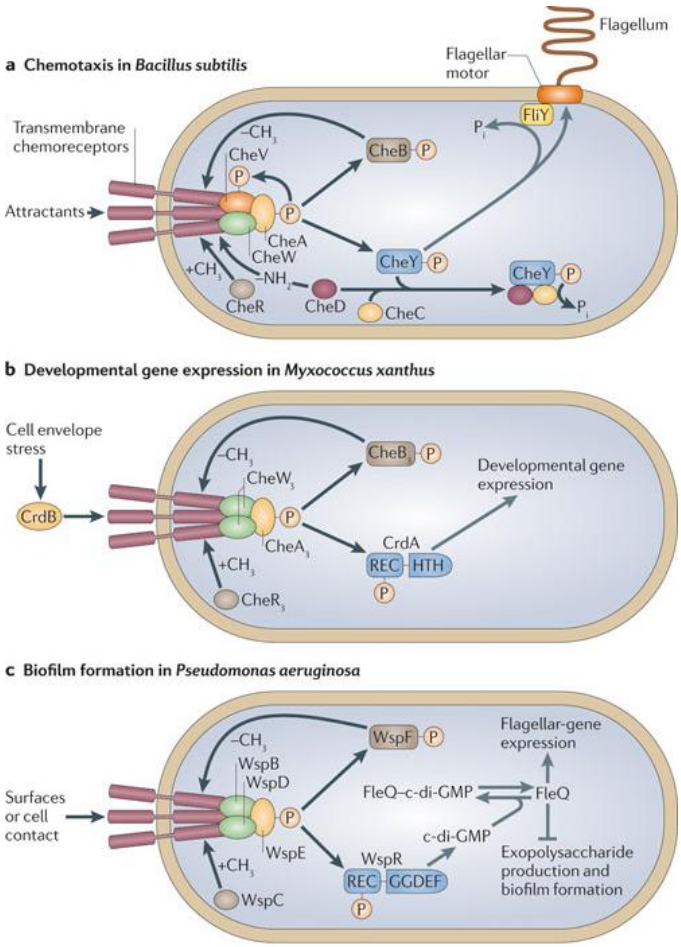

Figure 1-27 **a** The chemotaxis and chemotaxis-like systems of 3 bacteria that utilise proteins different to the *E. coli* system. *B. subtilis* has an inverted response, requiring attractant binding to chemoreceptors in order to activate CheA and produce CheY-P to bind the motor and cause smooth swimming. Its three distinct adaptation systems are shown: the CheB/CheR, CheC/CheD and the CheV systems. **b** The chemotaxis-like pathway of developmental gene expression of *M. xanthus*. The periplasmic lipoprotein CrdB detects changes in cell envelope stress and signals to $CheA_3$. This phosphorylates its two RRs: CheB as part of a CheB/CheR adaptation pathway and the transcription factor CrdA (shown are its helix-turn-helix (HTH) DNA binding and its regulatory (REC) domains). **c** The biofilm formation pathway of *P. aeruginosa*. Contains hmoologues of the major chemotaxis scaffold proteins as well as CheB/CheR homologues (WspF and WspC). The RR in this case has di-guanylyl cyclase activity once activated. Taken from (Porter et al., 2011b).

The *B. subtilis* has an *E. coli*-like chemotaxis system with some specific differences, notably the adaptation system. *B. subtilis* has 3 adaptation systems: an *E. coli*-like CheB/CheR system, a CheC/CheD system and a CheV system (Rao et al., 2008). The methylation system employing CheB and CheR proteins is different to *E. coli*, with the receptors being rapidly

demethylated in response to attractant and then slowly remethylated if attractant levels are maintained. Methylation level in steady state environments is constant and does not shift like the *E. coli* system. As a result, methanol, the by-product of demethylation, is released on addition and removal of attractant, unlike *E. coli* where only the latter is true (Kirby et al., 1999). It is predicted, therefore that certain methylation sites activate the kinase whereas others serve to repress it (Zimmer et al., 2000).

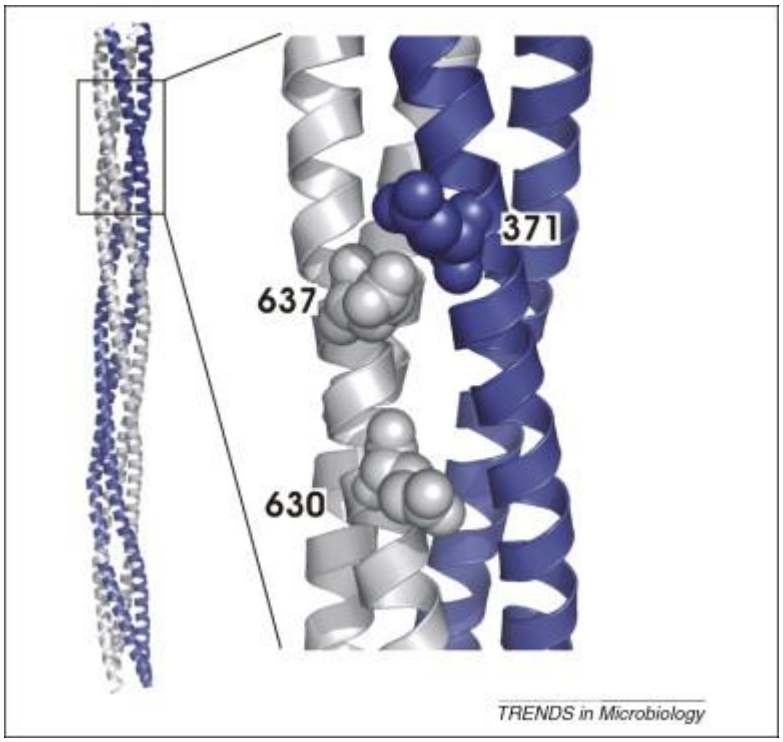

Figure 1-28 The receptor methylation sites of *B. subtilis*. The cytoplasmic domain of McpB of *B. subtilis* modelled onto the crystal structure of a *Thermatoga maritima* MCP. Separate monomers of the dimer are coloured blue and white respectively and glutamate side chains are modelled as balls. Taken from (Rao et al., 2008)

Modelling the glutamate methylation residues onto a structure of the MCP cytoplasmic domain from *T. maritima* has given on insight on how the methylation affects the signalling state of *B. subtilis* MCPs (Rao et al., 2008). The three methylation sites form a tight cluster on the outer face of the receptor (Figure 1-28). Repulsion between these glutamates is likely to result in destabilisation of the cytoplasmic domain. Selective methylation of these

glutamates could therefore result in either a stabilising inward rotation or destabilising outward rotation of the helices within the dimer. Destabilisation will reduce the interaction to the kinase and lower output, whereas stabilisation will have the reverse effect.

CheC is a CheY phosphatase that removes phosphoryl groups from activated CheY and thus terminates the chemotactic signal. However, CheC deletion does not drastically decrease the hydrolysis levels of CheY-P and it has been shown that CheC plays a role in chemotactic adaptation and not just in signal termination (Kirby et al., 2001). CheD is a receptor deamidase and as such removes amine groups from MCP glutamine residues. In addition, CheD has been shown to bind chemoreceptors and activate the kinase. However, it has also been shown to bind CheC and in doing so increase its phosphatase activity by a factor of 5 (Szurmant et al., 2004b). It has been proposed, therefore, that CheC/CheY-P and the chemoreceptors compete for CheD binding, and so when CheY-P is high, less CheD is bound at the receptors and CheA activity is lowered with the reverse true when CheY-P is low (Rao et al., 2008).

CheV consists of an N-terminal CheW domain and a C-terminal RR regulatory domain. As a result, CheV acts analogously to a CheW scaffold protein until phosphorylation by CheA. The phosphorylated form inhibits kinase activity and thus acts as a negative feedback loop, presumably by inhibiting receptor-kinase interaction when phosphorylated (Rao et al., 2008). Some species have been shown to lack *E. coli*-like adaptation systems altogether and appear to rely solely on CheV negative feedback, one such being the ε-proteobacter *Helicobacter pylori* (Alexander et al., 2010)

In addition to species having varying components involved in their chemotaxis systems, many species use chemotaxis-like pathways to perform other tasks. The expression of developmental genes in *M. xanthus* is controlled by a chemotaxis-like system in which

changes in cell envelope stress are detected by a periplasmic lipoprotein, CrdB, that then signals through MCPs (Kirby and Zusman, 2003). The resultant RR, CrdA, has a DNA binding domain that up-regulates expression of the required genes (see Figure 1-27b). Biofilm formation in *Pseudomonas aeruginosa* is controlled by a similar chemotaxis-like pathway. The resultant RR from this pathway is a di-guanylyl cyclase and results in an increase in the secondary messenger cyclic di-GMP (Figure 1-27). The use of a chemotaxis-like pathway in these cases is likely due to the ability of these pathways to adapt to a signal, which allows a degree of time resolution to signalling. The prevention or inclusion of cross-talk between these pathways is important to understand in order to fully understand cellular function. This is not easily studied in simple models such as *E. coli* and as a result a different model organism is needed to study signalling through more complex chemotaxis systems.

1.8.1 Introduction to *R. sphaeroides*

R. sphaeroides is a Gram-negative, purple non-sulphur α-proteobacteria mostly found in water and ponds, often in the sediment layers. It was first characterized in 1944 and has since been used extensively as a model organism for photosynthesis (van Niel, 1944). This work has focused largely on the strain 2. 4. 1. for which, the full genome was the first *R. sphaeroides* genome sequenced. However, this strain is inefficient at chemotaxis and chemotactic analysis has focused on the strain WS8N, a spontaneous Nalidixic acid mutant of WS8 (Mackenzie et al., 2001) (Sistrom, 1977) (Airola et al., 2010). The genome of WS8N has also recently been sequenced showing it contains two chromosomes, one of which is 3.1 Mbps and the other 0.9 Mbps, and 2 plasmids (Porter et al., 2011a). WS8N responds to a wide variety of chemoattractants, however, it responds comparatively strongly to its two preferred growth nutrients propionate and succinate (Kojadinovic et al., 2011).

1.8.2 *R. sphaeroides* chemotaxis components

R. sphaeroides contains multiple homologues of many chemotaxis genes, shown in recent genomic sequencing of various strains (Mackenzie et al., 2001) (Lim et al., 2009) (Porter et al., 2011a). These gene homologues are located largely across 3 operons with the protein products of two of these operons localizing to two distinct cellular regions Localisation of the protein products of the third operon has not been demonstrated (Porter et al., 2008a).

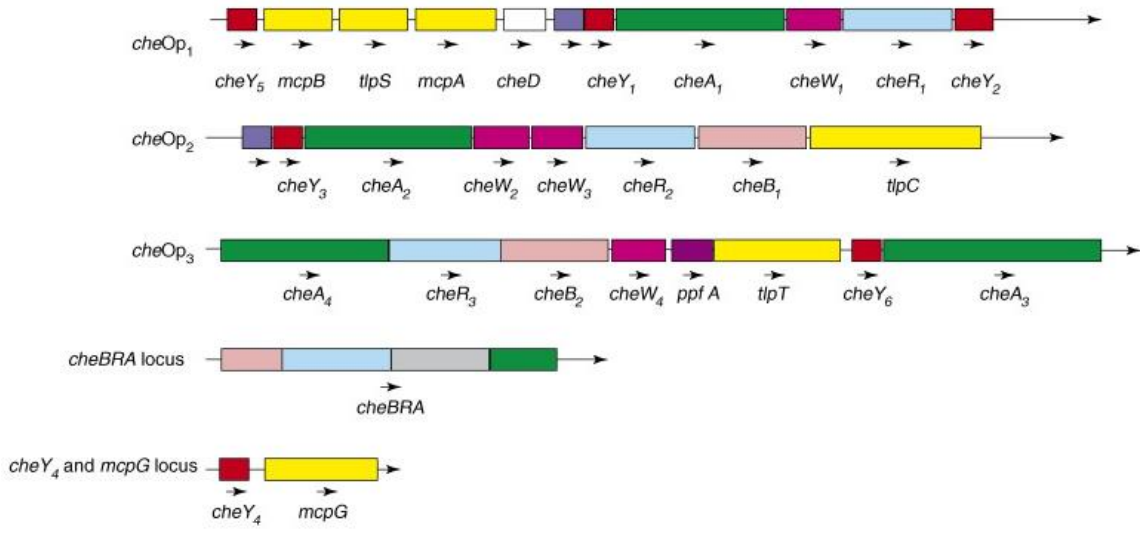

Figure 1-29 The chemotaxis genetic loci of *R. sphaeroides*. Gene product types are labelled by colour: red (CheYs), yellow (chemoreceptors), white (CheDs), green (CheAs), pink (CheWs), light blue (CheRs), purple (ppfA): involved in *cheOp3* protein product localisation), dark blue (unkown function). Adapted from (Porter et al., 2008a).

R. sphaeroides contains two separate flagella systems coded for on its genome. The Fla1 system is constitutively expressed under normal laboratory conditions and has been studied previously (Pilizota et al., 2009). The Fla2 system is not expressed under normal laboratory conditions and as a result has not been studied extensively. This flagellal system, however, is thought to be controlled by the *cheOp1* gene products, also similarly not expressed (del Campo et al., 2007). The arrangement of chemotaxis genes in *R. sphaeroides* is shown in

Figure 1-29 which includes the genes of *cheOp1* as well as the two well-studied operons *cheOp2* and *cheOp3* and two other loci containing chemotaxis genes.

Notable in the chemotaxis system of *R. sphaeroides* is the presence in of 6 CheYs, with each Fla system coding for 3. The Fla1 system and its associated chemotaxis genes code for the proteins $CheY_3$, $CheY_4$ and $CheY_6$ and precisely how the bacterium integrates a chemotactic signal through these is unknown. It has been shown that only $CheY_6$-P can stop the motor, whereas $CheY_3$ and $CheY_4$ can interact but not elicit a stop event and as a result are thought to tune the activity of $CheY_6$ (Porter et al., 2006). $CheY_6$-P binding at the motor has been shown to cause motor stopping, unlike *E. coli* where it causes direction reversal (Pilizota et al., 2009). Products of chemotaxis operon 2 (*cheOp2*), are known to localise predominantly to the polar cluster, much like the *E. coli* chemotaxis system (Porter et al., 2007). The protein products of chemotaxis operon 3 (*cheOp3*), however, localize to a discreet cytoplasmic cluster that is not present in *E. coli* (Wadhams et al., 2005). The precise role of this cluster in *R. sphaeroides* is unknown but it is believed to sense the metabolic state of the cell, potentially as a means of integrating the ability to photosynthesize (Wadhams et al., 2002). Despite its unknown role, the presence of the cytoplasmic cluster has been shown to be essential for efficient chemotaxis (Porter et al., 2002). The cytoplasmic cluster contains its own, specific $CheW_4$ protein, an atypical $CheA_{3/4}$ dimer and unique specificity for the CheY homologues (outlined in Figure 1-30). Chemotaxis operon 1 (*cheOp1*) is not expressed under laboratory conditions and its reason for conservation is unknown, however, it is proposed to control the second flagellar system Fla2 (Martin et al., 2006) (Martínez-del Campo et al., 2011).

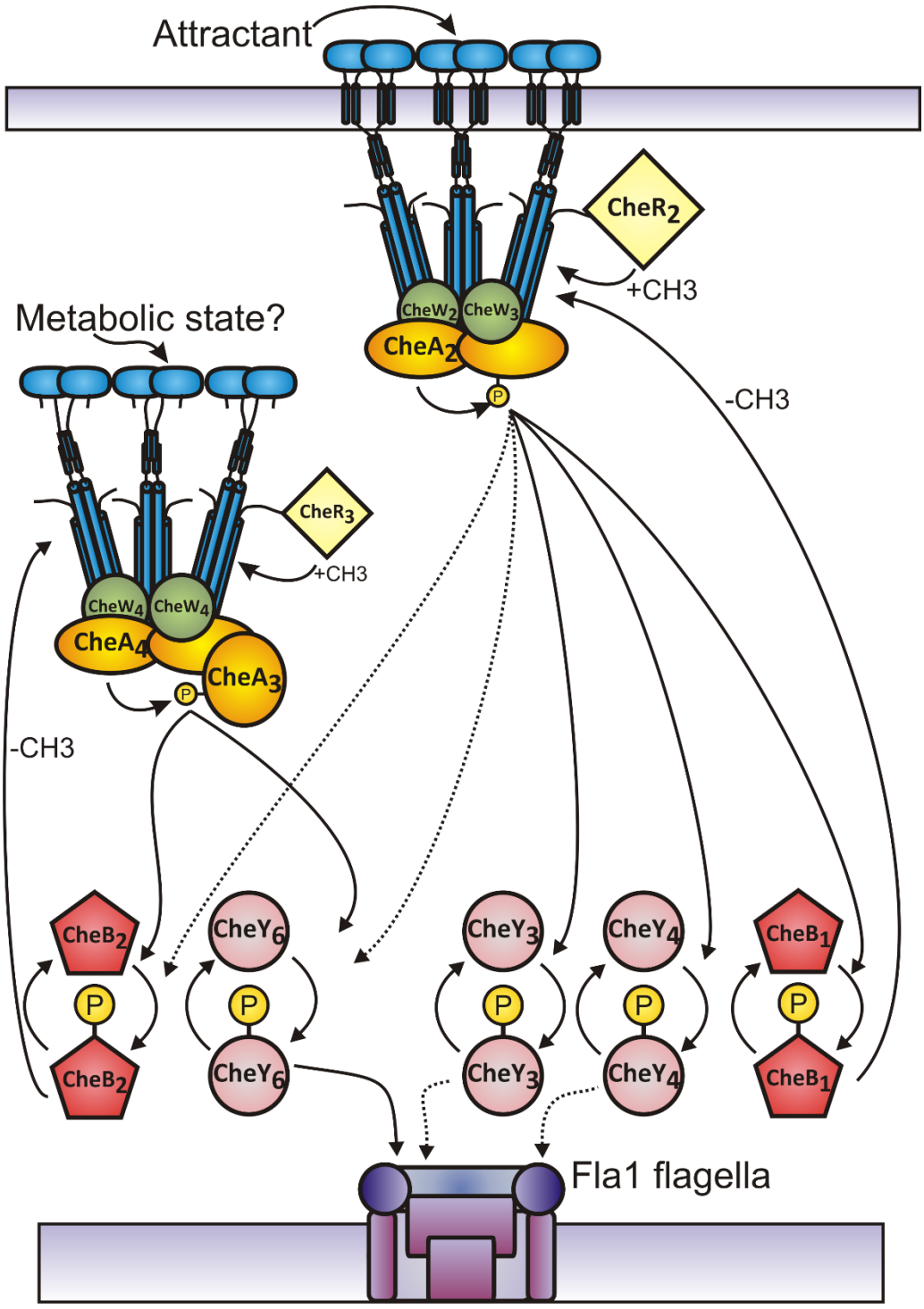

Figure 1-30 The Fla1 chemotaxis system of *R. sphaeroides*. MCPs at the polar cluster signal attractant level through to the *cheOp2* system HK, $CheA_2$, which then phosphorylates the cheOp2 RRs. The cytoplasmic system is mainly expressed form *cheOp3* and is thought to sense cellular metabolic state. Transducer-like proteins (TLPs) from this cluster signal to the atypical $CheA_{3/4}$ which then phosphorylates the *cheOp3* RRs. Known interactions are shown as thick black lines, dotted lines outline unknown in vivo interactions: $CheA_2$ to $CheY_6$ and $CheB_2$ are slow in vitro and only $CheY_6$ is capable of stopping the motor.

1.8.3 *R. sphaeroides* chemoreceptors

R. sphaeroides encodes 13 putative chemoreceptor genes, with 9 of these containing predicted TM helices. The remaining four contain no predicted TM segments and thus are proposed to localize to the cytoplasmic chemoreceptor array and are classified as Transducer-like proteins (Tlps) (Mackenzie et al., 2001). Table 1 describes the known and predicted characteristics of *R. sphaeroides* chemoreceptors.

Name	TM helices	Localisation	Chromosome	Class
McpA	2	Polar*	1	36H
McpB	2	Polar*	1	34H
TlpC	0	Cytoplasm	2	†
McpE	2	Polar	2	34H
McpG	2	Polar	2	34H
McpH	2	Polar	2	34H
McpJ	2	Polar	2	34H
TlpL	0	Cytoplasm	1	†
McpM	2	Polar	1	38H
McpR	2	Polar	2	34H
TlpS	0	Cytoplasm	1	†
TlpT	0	Cytoplasm	1	36H
McpV	2	Polar	2	34H

Table 1 The chemoreceptors of *R. sphaeroides*, the number of predicted helices, their localisation or predicted localisation, their chromosomal gene locations and their predicted heptad class. * indicates localisation that is predicted but not previously seen directly. † indicates currently unknown data and not accurately predicted.

Chemoreceptors expressed from chromosome 1 (McpA, McpB, McpM and TlpS) have not been detected in laboratory conditions and are thought, along with *cheOp1* components to not be normally expressed. As a result, very little is known about these chemoreceptors,

including their localisation pattern and their associated ligands. As described in Table 1, the chemoreceptors from *R. sphaeroides* have been shown to localise to two distinct cellular locations, forming a polar cluster similar to that found in *E. coli* and a separate, cytoplasmic cluster (Wadhams et al., 2000) (Wadhams et al., 2002) (Wadhams et al., 2003). Both of these clusters are required for full chemotactic signalling in *R. sphaeroides* (Porter et al., 2002).

1.8.4 *R. sphaeroides* MCP specificity

As discussed, *R. sphaeroides* responds to a wide variety of attractants, however, the exact specificity of these interactions are not yet known. Deletion of McpH is known to abolish chemotaxis, whereas deletion of the other polar chemoreceptors causes merely a decrease (Thompson, 2005). This suggests that, not only is McpH a dominant MCP in this system, but the latter result also suggests that there is a complex network of interactions that contributes to full chemotaxis efficiency. The same study suggested that McpH responded to the attractant that causes the largest response, propionate, but this was only indirectly shown through its deletion and so could be a result of indirect loss of receptor array integrity. The study showed that sequential deletion of MCPs resulted in complete loss of chemotaxis and so it is believed that a minimum subset may be required to elicit a response. As a result, MCPs and their corresponding ligands in *R. sphaeroides* are yet to be studied directly as sole chemoreceptors as has been the case for *E. coli* (Zhou et al., 2011). Thus, in order to study sole receptors and assess their potential ligands a new method is needed that does not require sequential *R. sphaeroides* deletion.

1.8.5 *R. sphaeroides* MCP classification

Classification of the *R. sphaeroides* MCPs and a single Tlp (TlpC) was achieved along with the *E. coli* MCPs and were defined as predominantly 34H (Alexander and Zhulin, 2007).

However, unlike *E. coli*, different length classes do exist, with McpA classed as 36H (the same class as *E. coli* receptors) and McpM classed as the longer 38H. No previous analysis of these two chemoreceptors has been directly undertaken in *R. sphaeroides*. Integration of signals of these different lengths into a single output is a complication that is not understood. Recent studies, however, have shown that mixed trimers of different lengths do not seem to form within arrays (Herrera Seitz et al., 2014). This adds evidence to a current theory that MCPs are likely to form 'rafts' of different classes in the cluster if expressed together. One result of these rafts would be a lack of cooperativity between these clusters and may suggest a reason for their evolution and retention in preventing unwanted cross-talk.

1.8.6 *R. sphaeroides* scaffold proteins

The polar cluster of *R. sphaeroides* contains two homologues of CheW ($CheW_2$ and $CheW_3$) and a single CheA ($CheA_2$). Deletion of $CheW_2$ abolishes $CheA_2$ recruitment and thus prevents cluster formation, whereas $CheW_3$ deletion results in only a decrease but not complete loss (Wadhams et al., 2005). The two homologues are therefore not redundant, however, their individual roles are unknown. Previous analysis of their ability to support chemotaxis in *E. coli* also suggests that they have differing affinities for other chemotaxis components with $CheW_3$ able and $CheW_2$ unable to restore an *E. coli* CheW deletion (Shah et al., 2000). In order to understand the control of cross-talk in these complex networks, the precise roles for these homologues must be studied further to determine why they are retained in the bacterial genomes. At the cytoplasmic cluster, the scaffold proteins form an atypical complex of $CheW_4$, $CheA_3$ and $CheA_4$. $CheA_{3/4}$ do not individually contain all five domains usual retained by CheA monomers but in fact each contain a subset. $CheA_3$ contains only the P1 and P5 domains with a 794 amino acid sequence linking the two that has

currently unknown function. $CheA_4$ contains the P2, P3 and P4 domains and is thought to dimerise and phosphorylate the P1 domain of a single $CheA_3$ monomer.

1.8.7 *R. sphaeroides* CheYs

The complexity of *R. sphaeroides* CheYs has been studied in some detail using phosphotransfer experiments to assess the affinities of the CheYs for the CheAs (Porter et al., 2006). The resultant specificity is outlined in Figure 1-31 but briefly, $CheA_2$ at the poles is able to phosphorylate all 6 CheY proteins that are encoded across the *R. sphaeroides* chemotaxis and so it is likely that $CheY_3$, $CheY_4$ and $CheY_6$ are *in vivo* targets. $CheA_{3/4}$ is able to phosphorylate only $CheY_6$ *in vivo* and is shown in its predicted, atypical arrangement of a $CheA_4$ dimer and a single $CheA_3$ monomer. Deletion studies show that $CheY_6$ is absolutely required for chemotaxis, along with either $CheY_3$ or $CheY_4$ (Porter et al., 2006). This suggests some redundancy in the system with either $CheY_3$ or $CheY_4$ enabling full chemotaxis in the absence of the other. All CheYs have been shown to bind FliM *in vitro*, however, only $CheY_6$ is able to cause a motor stopping event (Ferré et al., 2004). This leads to the current model of signalling that suggests $CheY_6$ is the RR responsible for binding to the motor and causing a stop event and $CheY_3$ and $CheY_4$ act as 'phosphate sinks' to regulate this process. This would also show how signals are integrated between the two clusters without the need for additional cross-talk.

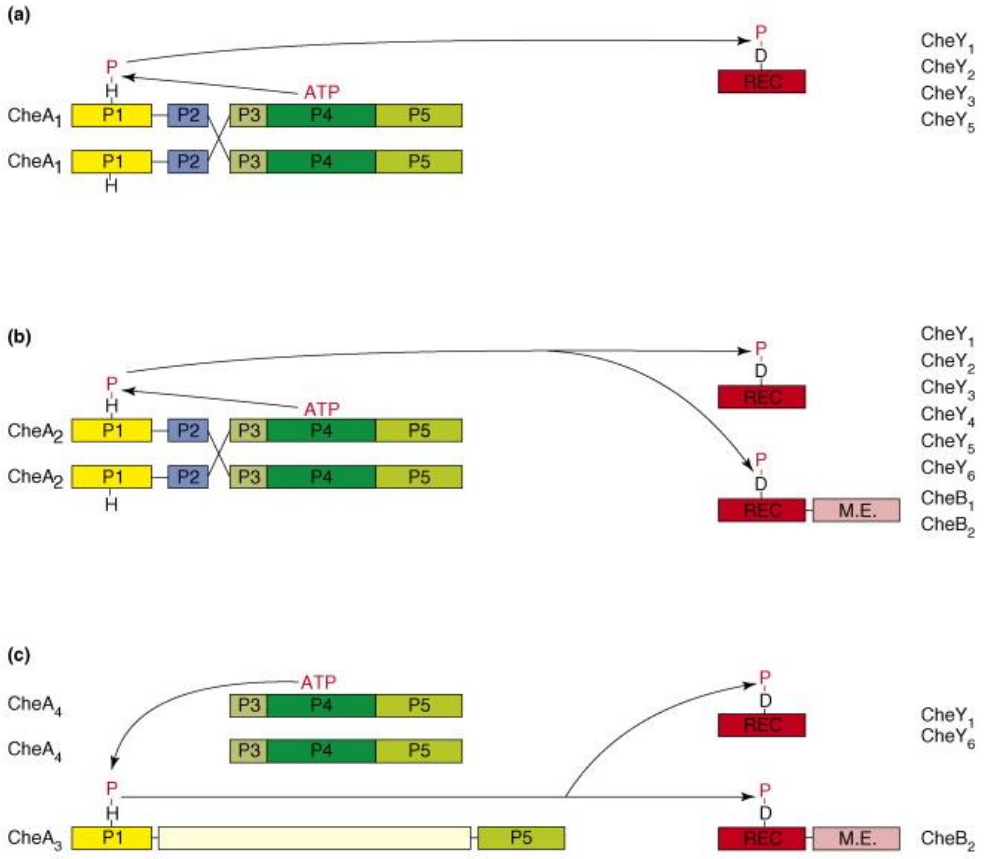

Figure 1-31 The specificity of CheAs in *R. sphaeroides* showing *cheOp1* specificity (a), polar cluster (b) and cytoplasmic cluster specificity (c) determined from phosphotransfer. Taken from (Porter et al., 2008a).

1.8.8 *R. sphaeroides* signal termination

Unlike the *E. coli* model, *R. sphaeroides* does not encode a *cheZ* gene. As a result, it does not contain a homologous phosphatase. $CheY_6$-P has been shown to have a faster dephosphorylation rate than its *E. coli* homologue (4 s compared with 14 s) which could negate the need for a CheZ. However, it has been shown that $CheA_3$ can increase the dephosphorylation of $CheY_6$ and therefore could be the phosphatase in this system (Porter et al., 2008b). The model of signalling to the motor described in chapter 1.8.7 goes some way to explaining the lack of a phosphatase as the presence of phosphate sinks in $CheY_3$ and $CheY_4$ mean that levels of $CheY_6$-P can be controlled by trans-phosphorylation (Porter et al., 2008a).

1.8.9 *R. sphaeroides* adaptation

Direct evidence for *R. sphaeroides* methylated adaptation has been recently analysed, however, its mechanism was previously assumed to be analogous to *E. coli* due to the presence of CheR and CheB homologues (DeBeyer, 2013). Again, deletion of the *cheOp1* $CheR_1$ has no effect on chemotaxis under the conditions tested, nor does it compliment an *E. coli* CheR deletion. $CheR_2$ is able to compliment this *E. coli* deletion and the deletion of $CheR_2$ in *R. sphaeroides* results in loss of chemotaxis, presumably resulting from the inability to respond correctly to a drop in attractant (Martin et al., 2001). The third CheR present in *R. sphaeroides*, $CheR_3$, does not complement *E. coli* deletions and its loss again abolishes chemotaxis. It also localises to the cytoplasmic cluster supporting the notion that *cheOp3* gene products are associated with this cluster (Porter et al., 2002).

There are multiple homologues of the methylesterase CheB in *R. sphaeroides*: $CheB_1$, $CheB_2$. Both are found diffuse in the cytoplasm and both have been shown to be phosphorylated by the polar HK $CheA_2$, however, only the latter is phosphorylated by $CheA_{3/4}$ (Porter and Armitage, 2002). $CheB_1$ and $CheB_2$ can both compliment an *E. coli* deletion, the latter only partially, and both disrupt chemotaxis when deleted in *R. sphaeroides*, again the latter only partially (Martin et al., 2001) (Porter et al., 2002). Interestingly, cheOp1 does not encode its own CheB homologue despite coding for a CheR homologue, suggesting either $CheB_1$ or $CheB_2$ can perform this role. This also suggests that either CheB was lost from this system as either $CheB_1$ or $CheB_2$ could perform at least as well, or it was never present in what is thought to be the original *R. sphaeroides* chemotaxis system (del Campo et al., 2007). If the former is true it suggests that redundancy, where present, is lost from these systems which follows that the homologues present in this system are indeed performing specific, individual roles.

2. Project Aims

The aim of this project was to investigate the mechanism of signalling through chemoreceptors using a mixture of *R. sphaeroides* and *E. coli* model systems. Using the same model systems, this project also investigated the heterogeneity of *R. sphaeroides* chemotaxis components in order to determine why *R. sphaeroides* retains multiple copies of individual components. Specifically, this involved:

- Use of computational modelling to determine possible activation mutants of MCPs.
- Analysis of the designed mutants to determine chemotactic ability
- Use of any locked mutants of MCPs to determine whether localisation and structure of the polar cluster is effected by signalling state
- Determine how this signalling state effects interactions with the cluster and whether this is likely to reflect a signalling mechanism
- Propose a model for signalling based on these conclusions
- Create a minimal functioning chemotactic unit in order to analyse the specificity of the *R. sphaeroides* MCPs
- Analyse the heterogeneity of the *R. sphaeroides* scaffold protein homologues and their specificity for individual chemotactic components
- Determine individual roles for chemotaxis array homologues

3.Materials and methods

3.1 Strains and Plasmids

3.1.1 Strains

Strain	Species	Genotype	Source
XL-1-Blue	*E. coli*	*recA1 endA1 gyrA96 thi-1 hsdR17 supE44 relA1 lac* [F´ *proAB lacIq ZΔM15 Tn10* (Tet^r)]	Stratagene
S-17-λ-pir	*E. coli*	*thi rspL* (Str^r) *endA sbcB15 sbcC hsdR* (rk- mk-) Δ (*lac-proAB*) [F' *traD36 lacI*q Δ(*lacZ*)*M15 proA+B+*]	(Simon et al., 1983)
BW25142	*E. coli*	F- *lacI*q*rrnB3* Δ*lacZ4787 hsdR514* DE(*araBAD*)*567* DE*(rhaBA D*)*568* Δ*phoBR580 rph-1 galU95* Δ*endA9 uidA*(Δ*MluI*)::*pir-116*	(Haldimann and Wanner, 2001)
DMH1	*E. coli*	F− *glnV44*(AS) *recA1 endA gyrA96 thi-1 hsdR17 spoT1 rfbD1 cya-854*	(Karimova et al., 2005)
RP437	*E. coli*	F- *thi thr leu his met eda* rpsL	(Parkinson, 1978)
UU2612	*E. coli*	Δ*aer*-1 Δ(*tar-tap*)*4530* Δ*tsr-5547* Δ*trg-4543*	(Zhou et al., 2011)
UU2836	*E. coli*	Δ*aer*-1 Δ(*tar-tap*)*4530* Δ*tsr-5547* Δ*trg-4543* Δ*cheW*	(J. S. Parkinson, personal communication)
JPA3000	*E. coli*	Δ*aer*-1 Δ(*tar-tap*)*4530* Δ*tsr-5547* Δ*trg-4543 cheW::cheW2*$_{rs}$	This study
JPA3001	*E. coli*	Δ*aer*-1 Δ(*tar-tap*)*4530* Δ*tsr-5547* Δ*trg-4543 cheW::cheW3*$_{rs}$	This study
JPA910	*R. sphaeroides*	Δ*cheOp2* McpJ::McpJ-GFP	G. Wadhams
JPA1415	*R. sphaeroides*	CheW$_3$::CheW$_3$-CFP	G. Wadhams
JPA1497	*R. sphaeroides*	CheA$_2$::CheA$_2$ -CFP	G. Wadhams
WS8N	*R. sphaeroides*	Nal^r	(Sockett et al., 1990)

Table 3-1 : Bacterial strains used or created in this study

3.1.2 Plasmids

Plasmid Name	Description	Source
pIND4	$Km^{r.}$ IPTG inducible plasmid for gene expression in *R. sphaeroides*.	(Ind et al., 2009)
pIND4B	pIND4 containing the *mcpB* gene	This study
pIND4B*	pIND4 containing the *mcpB** gene	This study
pIND4G	pIND4 containing the *mcpG* gene	This study
pIND4H	pIND4 containing the *mcpH* gene	This study
pIND4J	pIND4 containing the *mcpJ* gene	This study
pIND4cRFP	pIND4 containing a RFP fusion C-terminal to the multiple cloning site	This study
pIND4BR	pIND4R containing the *mcpB* gene	This study
pIND4B*R	pIND4R containing the *mcpB** gene	This study
pIND4HR	pIND4R containing the *mcpH* gene	This study
pBAD33	Cm^{r}. Arabinose-inducible plasmid for gene expression in *E. coli*	(Guzman et al., 1995)
pBADA2	pBAD33 containing the $cheA_2$ gene and a shine-dalgano sequence	This study
pDS132	*sacB*, Cm^{r}. Suicide plasmid for allelic exchange	(Philippe et al., 2004)
pDS132W2ex	pDS132 containing an insert for genomic exchange of the $cheW_2$ gene	This study
pDS132W3ex	pDS132 containing an insert for genomic exchange of the $cheW_3$ gene	This study

Plasmid Name	Description	Source
pKT18	Amp^r. BATCH expression vector containing T18 fragment of Adyenylate cyclase gene *cyaA* encoded C-terminal to the MCS	(Karimova et al., 2005)
pKT18C	Amp^r. BATCH expression vector containing T18 fragment of Adyenylate cyclase gene *cyaA* encoded N-terminal to the MCS	(Karimova et al., 2005)
pKT25	Km^r. BATCH expression vector containing T25 fragment of Adyenylate cyclase gene *cyaA* encoded N-terminal to the MCS	(Karimova et al., 2005)
pKNT25	Km^r. BATCH expression vector containing T25 fragment of Adyenylate cyclase gene *cyaA* encoded C-terminal to the MCS	(Karimova et al., 2005)

Table 3-2 : Plasmids used in this study. Bacterial two-hybrid (BATCH) derivatives are described in full in chapter 5.10.

3.2 Growth Conditions

3.2.1 Antibiotics

Antibiotic	Concentration for RS	Concentration for EC
Ampicillin	-	100 µg/ml
Chloramphenicol	-	30 µg/ml
Kannamycin	25 µg/ml	25 µg/ml
Nalidixic Acid	25 µg/ml	25 µg/ml

Table 3-3 : Antibiotic concentrations.

3.2.2 *E. coli* liquid cultures

Liquid cultures of *E. coli* were grown in Lysogeny Broth (LB) (Appendix B) containing the appropriate antibiotic at 37°C with shaking.

3.2.3 *E. coli* agar plates

E. coli was grown on solid plates containing LB (Appendix B) with 2% agar and the appropriate antibiotic. Plates were incubated at 37 °C, unless the strain contains *R. sphaeroides* proteins in which case 30 °C was used to prevent mis-folding.

3.2.4 *R. sphaeroides* liquid cultures

Aerobic liquid cultures of *R. sphaeroides* were grown in succinate media (Appendix B) containing the appropriate antibiotic at 30 °C with shaking.

Photoheterotrophic liquid cultures were grown in succinate media (Appendix B) containing the appropriate antibiotic in sealed bottles or tubes with minimal airspace under white light at 30 °C

3.2.5 *R. sphaeroides* agar plates

R. sphaeroides was grown on solid plates as described in section 3.2.3 and incubated at 30 °C.

3.2.6 Sucrose selection plates

Sucrose selection was performed on plates containing LBA with 5 % sucrose, incubated at 37 °C

3.3 Genetic techniques

3.3.1 Polymerase chain reaction (PCR)

Standard *R. sphaeroides* PCR

PCR was performed using the reaction mixture as described in Table 3-4. Reactions were then placed in a thermocycler and set in the cycle as described in Table 3-5. Annealing temperature was altered to reflect the melting temperature (Tm) for the individual primers used in each reaction.

Component	Amount
Primer 1	1 µl
Primer 2	1 µl
Phusion 5x GC Buffer	5 µl
dNTPs (2.5mM stock)	5 µl
DMSO	0 µl for 0% 2.5 µl for 5% 5 µl for 10%
MilliQ water	Make up to total volume of 50 µl

Table 3-4 : Standard R. sphaeroides PCR composition

Stage	Number of Cycles	Temperature	Time
Initial Denaturation	1	98 °C	10 min
Denaturation	30	98 °C	30 s
Annealing		55 °C – 65 °C	30 s
Extension		72 °C	30 s/kb
Final Extension	1	72 °C	10 min

Table 3-5 : Standard PCR reaction program

Overlap extension PCR

Overlap extension PCR was used to create constructs for genomic insertions and other such compound DNA molecules. A schematic for this is shown in Figure 3-1. An additional step is required for insertions that fuses the required gene to either the up- or downstream region prior to the final PCR round.

Colony PCR

Colonies were picked into 100 µl MilliQ water and boiled for 10 minutes. 1-10 µl of this was then used as the template mixture in a standard reaction as above.

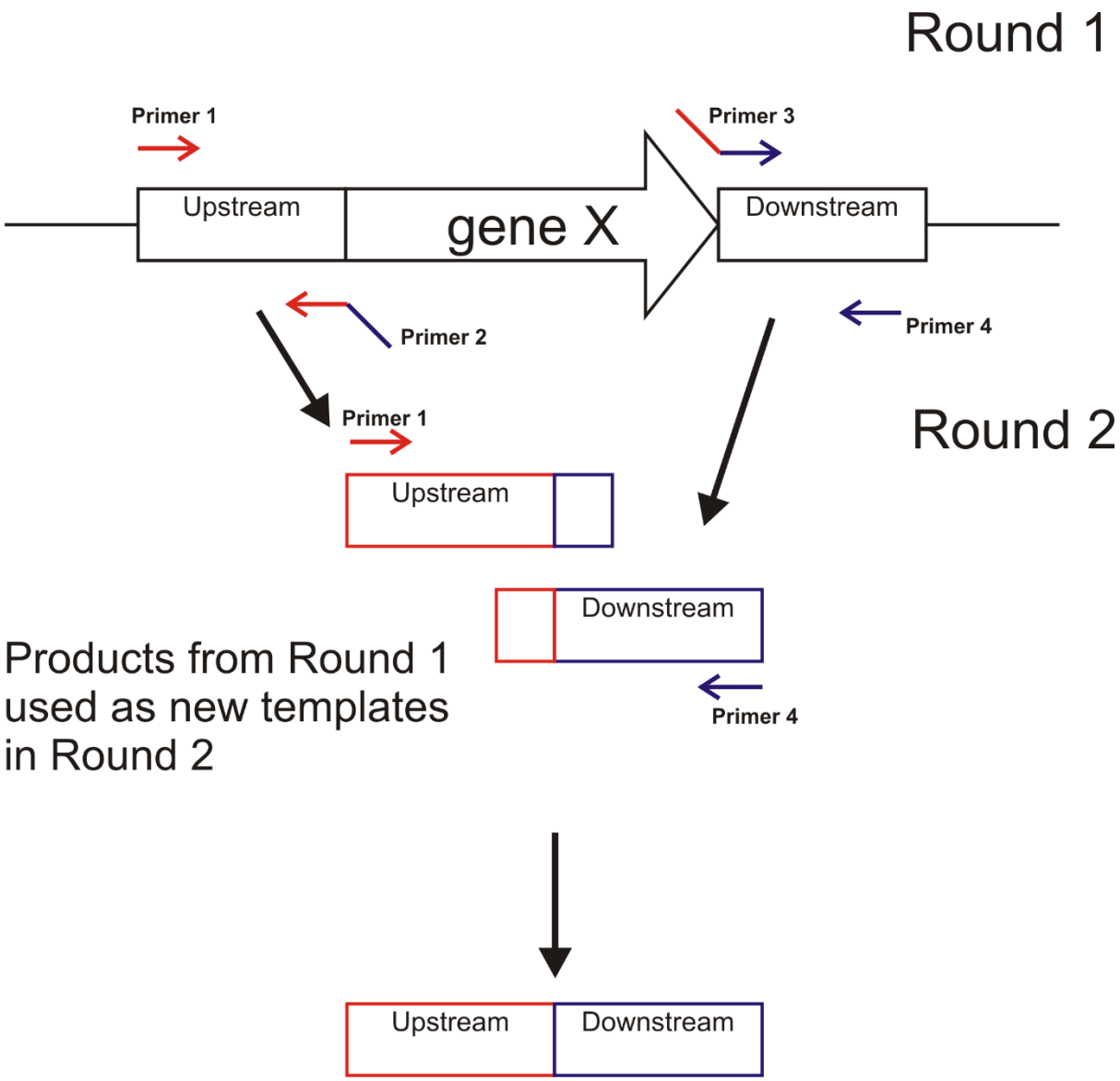

Figure 3-1: Overlap extension PCR to create a construct for deletion of gene X. In Round 1 two separate reactions are run to amplify the up- and downstream DNA of gene X. Primers 2 and 3 are complementary in order to leave a homologous overlap of DNA on each of the products. In Round 2 the products from Round 1 are used as new templates and only primers 1 and 4 are added. The complementary regions act as primers themselves resulting in elongation to a single fused DNA strand lacking gene X.

3.3.2 Restriction enzyme digests

Restriction digests were performed using a typical reaction mixture as described in Table 3-6. These reactions were then incubated at 37 °C for 2 hours (or appropriate temperature for enzymes used).

Componenet	Quantity
DNA	50 µl
10x NEBuffer X	10 µl
BSA (if required)	0.5 µl
Enzyme	1 µl each
MilliQ water	Make up to total volume of 50 µl

Table 3-6: Typical restriction digest composition. Specific NEBuffer was chosen based on reactivity of enzyme used (New England Biolabs).

3.3.3 Dephosphorylation

Restriction digests of plasmids were stopped by heating to 80 °C for 20 minutes. Calf intestinal alkaline phosphatase (CIP) (New England Biolabs) was added and then the reactions incubated at 37 °C for 1 hour in order to dephosphorylate vectors and prevent self-ligation.

3.3.4 Gel electrophoresis

DNA fragments were separated in an agarose gel matrix using gel electrophoresis. 0.8-2% w/v Agarose was added to 0.5% TBE, see Appendix B, depending on the fragment sizes that required separation. Fragments were separated under 80-140V until appropriate distance had been travelled through the matrix. Visualisation of DNA bands was achieved by soaking in 1 ng/ml Ethidium Bromide solution for 30 minutes and viewing with a UV transilluminator.

3.3.5 Purification of DNA fragments

DNA fragments were excised from gels and extracted from the agarose matrix using the Gel Extraction Kit (QIAGEN), following the protocol provided.

3.3.6 DNA ligation

DNA ligation reactions were set up typically as described by Table 3-7. Concentrations of vector and insert DNA were checked using a Nanodrop 1000 UV-Vis spectrophotometer (Thermo Scientific) and then volumes added corresponding to a 3:1 molar ratio of insert:vector.

Component	Quantity
Vector	10 µl
Insert	30 µl
10x T4 DNA ligase Buffer (NEB)	1 µl
T4 DNA ligase (NEB)	5 µl
MilliQ water	4 µl

Table 3-7: Typical DNA ligation reaction to insert a DNA strand into a plasmid vector.

3.3.7 Competent cells

Chemical competency

E. coli cells were made chemically competent to plasmid uptake using the rubidium chloride method. 50 ml of LB media (Appendix B) was inoculated with 1 ml of stationary phase *E. coli* and incubated at 37 °C to OD_{600nm} of 0.4. The culture is then incubated on ice for 30 minutes and centrifuged at 1000 x g for 10 minutes at 4 °C. Cells were then resuspended in 16 ml ice cold TFB-I (Appendix B) and incubated on ice for 30 minutes. Cells were centrifuged again at 1000 x g for 10 minutes at 4 °C and resuspended in 4 ml TFB-II (Appendix B). 200 µl aliquots were flash frozen in liquid nitrogen and stored at -80 °C.

Electrocompetency

Transformation of DNA by electroporation was used to insert pDS132 plasmid derivatives into *E. coli* cells. Cells were made competent to electroporation and plasmid uptake using the method described in (Sambrook and W Russell, 2001) and flash frozen into 20 µl aliquots.

3.3.8 Transformation of plasmids into competent cells.

Transformation into chemically competent cells

100 µl competent *E. coli* XL-1 blue cells (3.3.7) were defrosted on ice and then inoculated with the required plasmid. For new ligation mixtures, 20 µl of the ligation mixture was used for inoculation; for purified plasmids, only 1 µl was used. Cells were incubated with the plasmid solution on ice for 1 hour and then heated to 45 °C for 2 minutes. Cells were then immediately returned to ice for a further 2 minutes after which 1 ml LB (Appendix B) was added and the cells were incubated at 37 °C for 1 hour. Cells were then plated onto LB agar (Appendix B) containing the selection antibiotic and incubated overnight.

Transformation into electrocompetent cells

20 µl of electrocompetent cells were defrosted on ice and then incubated on ice with 5 µl of the required plasmid for 5 minutes. Cells were then transferred to a pre-chilled electroporation cuvette (Geneflow). An electrical pulse of 2400V, 25 µF and 200 Ω was applied to the cells and 1 ml SOC medium (Appendix B) was immediately added. The cells were then incubated at 37 °C for 2 hours after which they were pelleted at 1000 x g,

resuspended in 100 µl LB (Appendix B) and plated onto LBA (Appendix B) containing the appropriate antibiotic. Plates were then incubated at 37 °C for 36-48 hours.

3.3.9 Plasmid purification

Colonies successfully grown on the selective media were picked from the agar plate into 5 ml LB (Appendix B) containing the appropriate antibiotic and incubated overnight at 37 °C. Plasmid DNA was then extracted from these cultures using the QIAfilter plasmid mini or midi prep kits (QIAGEN) according to the manufacturer's instructions.

3.3.10 DNA sequencing

DNA sequencing was performed by the automated sequencing service form SourceBioscience. Sequences were assembled and analysed using the Clone Manager Professional version 9.0 software (Sci Ed Central).

3.3.11 Conjugation of plasmids into *R. sphaeroides*

R. sphaeroides cannot be made chemically competent and therefore, plasmids must be transferred via conjugation with S-17-λ-pir cells. This was achieved using the standard protocol as described in (Sambrook and W Russell, 2001) but briefly: S-17-λ-pir cells were made chemically competent as described in 3.3.7 and plasmids transformed into these as described in 3.3.8. 1ml of mid-log phase transformed S-17-λ-pir cells and 1ml of photoheterotrophic, stationary *R. sphaeroides* cells were pelleted by centrifugation at 1000 x g for 3 minutes. Pellets were washed in 1 ml LB (Appendix B), pelleted in the same manner and finally resuspended in 100 µl LB (Appendix B). Special care was taken

resuspending S-17-λ-pir cells to prevent damage to the pili caused by shear forces. 10 µl of S-17-λ-pir cells were mixed, gently, with 100 µl *R. sphaeroides* and the whole mixture pipetted onto a sterile nitrocellulose filter on LBA (Appendix B). This was incubated at 30 °C overnight, the filter was then washed with 800 µl to remove the cells and 200 µl plated onto LBA (Appendix B) containing the appropriate antibiotics (Nalidixic acid and that of the resistance coded on the plasmid).

3.3.12 DNA recombination for genomic deletion and replacement in *E. coli*

Recombinant DNA was prepared as described in 3.3.1 and ligated into the pDS132 plasmid (3.3.6). pDS132 plasmids were transformed by electroporation (3.3.8) into the strain BW25142, which is capable of replicating plasmids containing the R6K origin of replication. Purified plasmid could then be transformed into parental strains using the same electroporation method. After electroporation, cells were plated onto chloramphenicol LBA (Appendix B) and grown for 36-48 hours. Resultant colonies were then grown in 5 ml chloramphenicol overnight, both of these steps ensure selection of integration of plasmid pDS132 derivatives into the host genome as replication and propagation of resistance would not occur otherwise. 5 µl of this culture was then grown in LB-sucrose medium (Appendix B) overnight to stationary phase and this step was repeated 3 times. This ensures selection for the second cross-over event resulting in plasmid loss from the genome and thus loss of the *sacB* suicide gene encoded on it which encodes the levansucrase protein, lethal for *E. coli* in the presence of sucrose. 100 µl of the final culture was serial diluted in 10 mM $MgSO_4$, plated onto LBA-sucrose (Appendix B) and incubated at 37 °C overnight. 50 colonies from this plate were then replica-plated onto LBA (Appendix B) with and without

chloramphenicol to select again for vector excision. Gene replacement was tested for using colony PCR (3.3.1). A schematic for this is given in Figure 3-2.

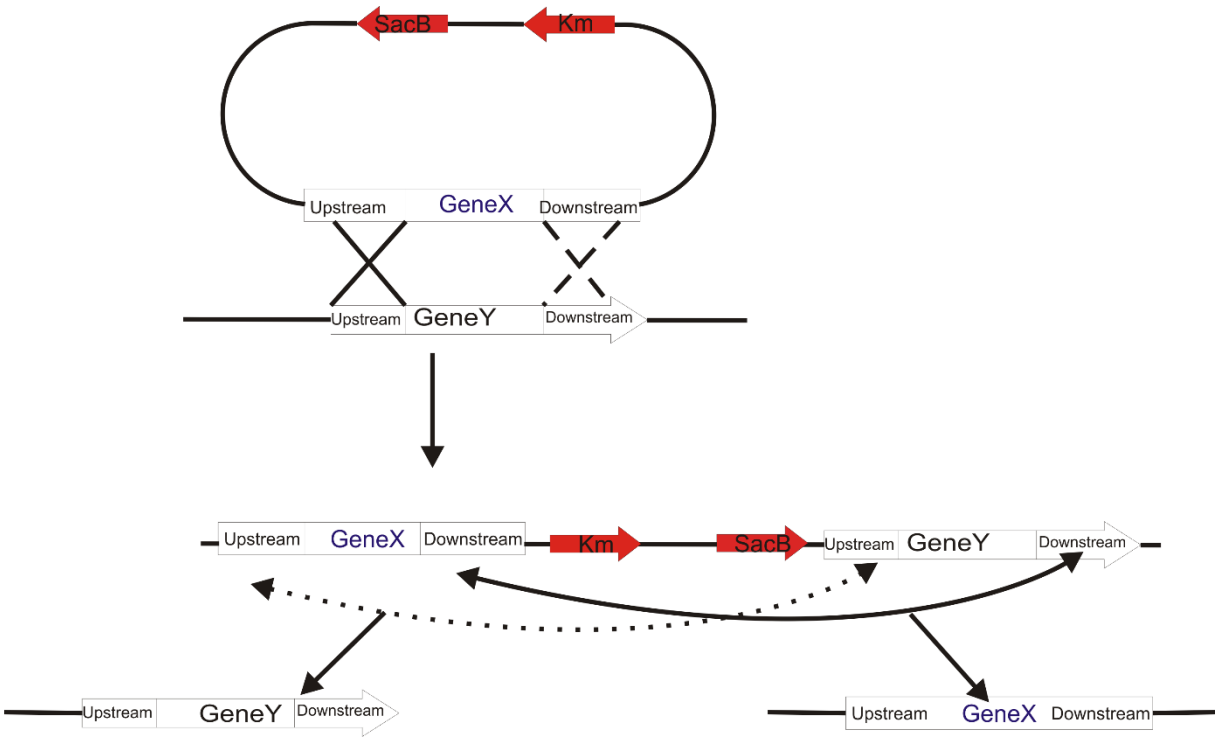

Figure 3-2: Gene replacement using homologous recombination. There are two, theoretically equal, outcomes: the DNA reverts back to its original genotype, or the intended insertion is replaced onto the genome instead.

3.4 Phenotypic analysis

3.4.1 Swim plates

Swim plates are used to assess the chemotactic ability of bacterial strains. As attractants are taken up and metabolised around the plated bacteria, a chemoattractant gradient is created causing a chemotactic bacteria to move away from its original position up the gradient. Distance travelled can thus determine chemotaxis efficiency.

R. sphaeroides swim plates

Semi-solid agar plates were made using 0.25% agar (BiTek) in M22 minimal media (Appendix B) containing the appropriate antibiotics (Nalidixic acid and any conferred by plasmid resistance). A chemoattractant was also included as the only carbon source (typically for *R. sphaeroides* this is propionate). 5 µl of stationary photoheterotrophic cells were plated onto the agar and incubated for 48 hours at 30 °C. The swarm ring diameter was then measured to determine chemotactic ability and analysed relative to control strains (typically WS8N).

E. coli swim plates

E. coli swim plates were set up as above with some differences. TB (Appendix B) rich media was used unless otherwise stated instead of M22 + attractant. Plates were incubated for 12 hours at 30 °C, unless otherwise stated, due to the faster swimming and thus larger rings created by *E. coli*.

3.4.2 Growth Curves

Analysis of growth was determined by measuring the OD_{600nm} of cells at set intervals. Cell cultures were grown overnight to stationary phase in 5ml LB containing the appropriate antibiotic(s). 1 µl of this stationary culture was then used to inoculate a Corning 3603 96-well black microplate containing wells with 100 µl LB and the appropriate antibiotic(s) and inducer(s). Measurements were taken every 30 minutes for 24 hours on a TECAN infinite 200 PRO plate reader at 30 °C with orbital shaking of 2 mm diameter. Fluorescence readings were also taken for RFP during the growth curves to determine RFP stoichiometry between strains. Samples were excited with light of wavelength 555 nm and emission was detected at wavelength 584 nm and the gain value was set to 100.

3.4.3 Bacterial two-hybrid

Target proteins were cloned onto the four bacterial adenylate cyclase two-hybrid system (BATCH) plasmids: pKT25, pKNT25, pUT18, pUT18C. All pKT25 and pKNT25 plasmids were then transformed with all other pUT18 and pUT18C plasmids to create a library of transformants. This was achieved in 96-well plates for ease. 20 µl of DMH1 cells was inoculated with 0.5 µl of each plasmid and incubated on ice for 1 hour. Cells were incubated at 42 °C for 2 minutes and then returned to ice for 2 minutes more. 100 µl of LB was added to each well and then the plates were incubated at 30 °C for 1 hour. 30 µl from each well was then transformed onto an array on square LBA plates containing ampicillin and kanamycin and incubated at 30 °C overnight. Single colonies were then picked into sterile 2.2 ml storage 96-well plates, 1 ml LB with ampicillin and kanamycin added and the plates incubated at 30 °C overnight. 10 µl of each double transformation was then spotted onto a large assay plate of LBA, containing kanamycin, ampicillin 50 µM IPTG and 40 µM 5-bromo-4-chloro-3-indolyl-β-d-galactoside (X-Gal). The plates were incubated at 30 °C overnight and then imaged immediately or left at room temperature for a further 24 hours for colour to develop fully. The presence of a blue colour in the spots indicates cAMP production deriving from activity of the adenylate cyclase (CyaA) enzyme reconstituted due to close interaction of the two proteins fused to each half of the full protein.

3.5 Microscopy

3.5.1 Preparation of cells

E. coli

Cells were grown as described in 3.2.2 to OD_{600nm} 0.5-0.6 unless otherwise stated. 1 ml of cells were pelleted at 3000 rpm in a desktop centrifuge and washed in 1ml M9 minimal media (Appendix B) to remove any autofluorescent LB (Appendix B) and resuspended in 100 µl M9 minimal media

R. sphaeroides

Cells were grown aerobically as described in 3.2.4 to OD_{700nm} 0.4-0.6 unless otherwise stated. 1ml of cells was then resuspended in 100 µl Sux media (Appendix B).

3.5.2 Preparation of slides

Agarose pad slides

The center well of a Gene Frame (Thermo Fisher Scientific) mount was filled with 1% Agarose in MilliQ water and pressed with a coverslip. Once set, 5 µl of cells are pipetted onto the agarose pad and the mount is sealed on top with a coverslip.

3.5.3 Microscopes

Nikon Eclipse TE2000-E

A Nikon Eclipse TE2000-E inverted epifluorescence microscope was used to capture fluorescent images, 60x oil objectives (Nikon) were used. Samples were illuminated with a

mercury lamp with the appropriate excitation and emission filters. Brightfield images were captured using a halogen lamp for illumination and contrast was enhanced using a DIC set up. Image capture was achieved with an Andor iXON CCD camera. Microscope control was achieved with the NIS Elements software (Nikon).

3.5.4 Polar localization analysis

Line profiles across each cell were drawn manually using imageJ from the brighter pole to the other. These profiles were then normalised and averaged in MATLAB as follows: Profiles of each cell were individually normalised by determining total fluorescence of each cell and determining then percentage fluorescence present at each point. These percentages were then summed into 20 separate bins across the cell length to create a fully normalised profile in both length of cell and fluorescence intensity. Profiles for all cells of each strain and condition were then averaged to determine the average normalised fluorescence intensity in each case. In order to determine the average fluorescence contained in the poles of the cell, fluorescence intensities of the first and last 20% of the cell profile were summed. These positions were chosen as the wild type Tsr profiles show sharp, distinct peaks that cover the first and last 20% of the cell profile, which shows that in wild type *E. coli* cells, this is the localisation region for tight polar clustering. Statistical analysis between data sets was achieved using the ttest2() function in MATLAB which automatically performed student t-test analysis across the two data sets to reject or accept the null hypothesis that they are identical.

3.5.5 Free-swimming capture

E. coli cells were grown aerobically to OD_{600nm} 0.4-0.6 and then 100 µl of cells is spun down at 1500 g for 1 min to pellet. Pellet is washed in M9 buffer (Appendix B) and gently resuspended in 100 µl containing chloramphenicol. Cells were then incubated for 15-30 minutes at room temperature to ensure motility has returned. Cells were then drawn into a flat capillary tube and the ends were sealed with silicon grease to prevent evaporation creating flow. Although this prevents unwanted flow, it also prevents oxygen from accessing the cells and so videos must be taken quickly to ensure cells do not become anaerobic. The sealed tube is laid on a glass slide and imaged with a phase contrast microscopic using 20x magnification.

3.5.6 Free swimming analysis

The Tracker program was used to detect the cells and form the tracks of their progress through the video (Wood et al., 2012). This detected the cells by differences in pixel intensity using the Niblack algorithm with a moving window size of 15 pixels and objects defined as larger than 2 pixels. Objects were then tracked between frames by determining the probability distributions of where the objects in the preceding frame could be compared with all the objects in the current frame. The swimming speed of *E. coli* was used to form these probabilities. Tracks were censored to remove are non-motile (cells that do not exit a set circle during their length), tracks that make non-native motions and are therefore unlikely to be real (tracks that appear to move faster than the maximum speed determined for *R. sphaeroides*, for example) and tracks that have torsion angles that suggest non-native motions and are therefore likely to disrupt any analysis due to the nature of the programme (those tracks whose angles shifts between frames are too small and thus tortuous).

A non-motile and a smooth swimming phenotype are required by the RunStopAnalysis programme and KDE functions for frame-wise speed distributions are built for both of these controls. The programme then classifies every frame-wise transition into either a run or a stop event. Statistical analyses can then be used to determine differences between the lengths of stop events in the total tracks of different strains.

3.5.7 Fluorescence recovery after photobleaching

Fluorescence recovery after photobleaching (FRAP) was used to determine motion of fluorescent molecules, or fluorescently tagged molecules *in vivo*.

FRAP using custom-built TIRF microscope

In order to reduce background cellular fluorescence and increase signal-noise ratio, TIRF microscopy was used. A custom-built multi-colour fluorescence microscope was used which allows photobleaching of one fluorescent spot within the cell using slim-field while simultaneously monitoring the fluorescence emission using conventional wide-field epifluorescence (Leake et al., 2006) (Plank et al., 2009). Bacteria were grown as in 3.2.2 and slides made as in 3.5.2. Fluorescence was excited using a 440 nm laser and fluorescence emission was imaged at 50 nm/pixel in frame-transfer mode at 25 Hz by a 128 × 128-pixel, cooled, back-thinned electron-multiplying charge-coupled device camera (Andor Technology iXon DV860-BI). 5 pre-bleach 40ms exposures were taken at 1 second intervals followed by bleaching with a focused laser spot for 150ms. 40 ms exposures were then taken at 1 minute intervals. Analysis was achieved using easyFRAP and the method suggested by its authors (Rapsomaniki et al., 2012). ImageJ was used to determine mean

pixel intensities of the three regions of interest (ROIs) over time, as required by easyFRAP (Hu et al., 2011).

3.6 Computational methods

3.6.1 Model building

Protein models were generated using the Modeller program version 9v7 (Sali and Blundell, 1993). This uses spatial restraints from a template structure to model a homologous sequence. Model was based on Tsr model produced (Hall et al., 2012) and alignment to this was performed using ClustalW2 (Larkin et al., 2007).

Molpdf scores were used to crudely distinguish between models and by eye analysis was used to determine initial viability of chosen models. Models were energy minimised using gromacs in a box containing water and ions using the GROMOS96 forcefield (Lindahl et al., 2001).

RMSD calculations were performed using the GROMACS tool *g_rms*. This first overlays the structures and then performs the RMSD calculation.

3.6.2 Coarse-grain Molecular dynamics simulations

Protein simulations were carried out using molecular dynamics of proteins modelled in coarse-grain particles. This uses the MARTINI forcefield which, briefly, maps four heavy atoms to coarse-grain interaction centre (Monticelli et al., 2008). Four main interaction sites are considered: polar, nonpolar, apolar, and charged. As a result, a coarse-grain protein structure was produced from the amino acid sequence and atomic structure of a given

protein. The resultant model was then simulated using the GROMACS software which models the physical constraints and process undertaken by the particles through the time-course of the simulation. For MCP modelling, proteins were placed in a theoretical simulation box which was then filled with water, counter ions and lipids and then a short simulation run in order for the bilayer to assemble around the protein. This prevents bias for where the bilayer forms on the protein structure. The MCP simulation was then run using the md_run GROMACS program to simulate motion within a formed bilayer.

3.6.3 Transmembrane helix simulations

TM simulations were run on the Sidekick submission server developed by Benjamin Hall (Hall et al., 2014). Briefly, the submitted sequence is rendered as a typical Course-Grain (CG) helix representation and inserted into a lipid bilayer. The resultant CG representation of a helix was placed in a simulation box ($90Å^3$) along with randomly positioned lipids, waters, and counter-ions. A 1000 step steepest-descent energy minimization was performed to remove any steric clashes. Self-assembly simulations of the system were performed to form a bilayer around the peptide while minimizing the potential sources of bias arising from the use of a preformed bilayer. Independence of each run is achieved by randomly altering the starting particle velocities in each simulation. Molecular dynamics simulations were then run using the GROMACS tool mdrun for 100 ns and 100 repeats for each sample were submitted (Van Der Spoel et al., 2005).

4. Signaling through chemoreceptors

4.1 *In silico* mutagenesis screen

MCP mutations that lock or shift the activity of chemoreceptors have been studied previously, largely in *E. coli* (Draheim et al., 2005) (Draheim et al., 2006). These studies have shown that MCP signalling occurs through what is currently accepted to be a piston shift of the TM2 helix. Despite these studies however, it is still debated precisely how signals are cooperatively transferred through the chemotaxis array and subsequently to the motor.

Analogous activity shifts have never been studied in *R. sphaeroides* and so it is unknown whether the proposed models fit with this system. Of particular interest is whether additional heterogeneity in *R. sphaeroides* affects how signals are transferred through to the soluble response regulators. This heterogeneity is manifested in two places important to this signaling: does a heptad class length different from the studied 36H in *E. coli* behave differently and how do multiple heptad class lengths effect the proposed signaling model. In addition, does the presence of multiple scaffold protein homologues affect how the array responds to these structural shifts.

McpB was chosen as the chemoreceptor to initially analyse for two reasons. It is not believed to be expressed, along with the rest of *cheOp1*, under normal laboratory conditions. As a result, the presence of a native receptor will not affect any experiments undertaken in *R. sphaeroides*. In addition, as McpB is not expressed, even less is known about it than other *R. sphaeroides* chemoreceptors and finding a route to determine its potential ligands may reveal why *R. sphaeroides* retains *cheOp1* and what this operon's role may be.

In order to analyse the signal processing through *R. sphaeroides* MCPs, mutations in the signal transduction transmembrane helix 2 (TM2) were screened *in silico* (Chapter 3.6.3). All proposed mutations are based on a variety of previously tested analogous mutations in *E. coli* chemoreceptors TM2 helices which have also been analysed *in silico* (Draheim et al., 2005) (Draheim et al., 2006) (Miller and Falke, 2004) (Hall et al., 2011). These mutations resulted in either a baseline shift in clockwise (CW)- or counterclockwise (CCW)-bias of the motor or full locking of the motor in either CW or CCW states. Chemoreceptor protein sequences were aligned to the *E. coli* receptor sequences using ClustalW2 (Larkin et al., 2007). Once the alignments of the TM helices were determined the sequences were altered to represent the mutations required and are shown in Table 4-1. The locations of the mutations undertaken on TM2 and examples of the motion undertaken are shown in Table 4-1. These helix sequences were fed into the Sidekick pipeline (Chapter 3.6.3) which converts them to coarse-grain molecular dynamics representation, positions them in a bilayer based on the helix centre and then runs the simulation (Hall et al., 2014).

Name	Sequence (184-211)	Orignal effect on bias
WI+3	RLTVLGAFLANILLVAAAGSAGS**WI**LST	CW locked
WI+2	RLTVLGAFLANILLVAAAGSAG**WI**TLST	CW locked
WI+1	RLTVLGAFLANILLVAAAGSA**WI**VTLST	Increased CW bias
W/R	RLTVLGAFLANILLVAAAGS**R**IVVTLST	CW locked
Wild type (WT)	R**L**TV**L**GAFLANILLVAAAGS**WI**VVTLST	
WI-2 **(MCPB*)**	RLTVLGAFLANILLVAAA**WI**GSVVTLST	Increased CCW
WI-3	RLTVLGAFLANILLVAA**WI**AGSVVTLST	CCW locked
L5R	RLTV**R**GAFLANILLVAAAGSWIVVTLST	CCW locked
L2R	R**R**TVLGAFLANILLVAAAGSWIVVTLST	CCW locked

Table 4-1 The names and sequences of the mutations of the TM2 helix in McpB simulated through the Sidekick pipeline. In bold are the residues in the wild type altered in the various mutants and the particular residues effected in each individual case. The final column depicts the resultant activity change determined from the original analogous biochemical studies described in the text.

The conversion of atomistic simulations to coarse-grain representation means that there are fewer particles present in the system. This allows either greater numbers of simulations or longer simulations to be run, both for the same computational cost. The coarse-grained peptide helix was placed into the centre of a simulation box and Coarse-Grain (CG) water and lipids randomly positioned around it. Self-assembly simulations were then performed to allow lipid bilayer assembly and avoid any bias created by placing the helix directly into a preformed layer. 100 simulations of 100 ns each were then run to analyse the motion of the helix within the bilayer.

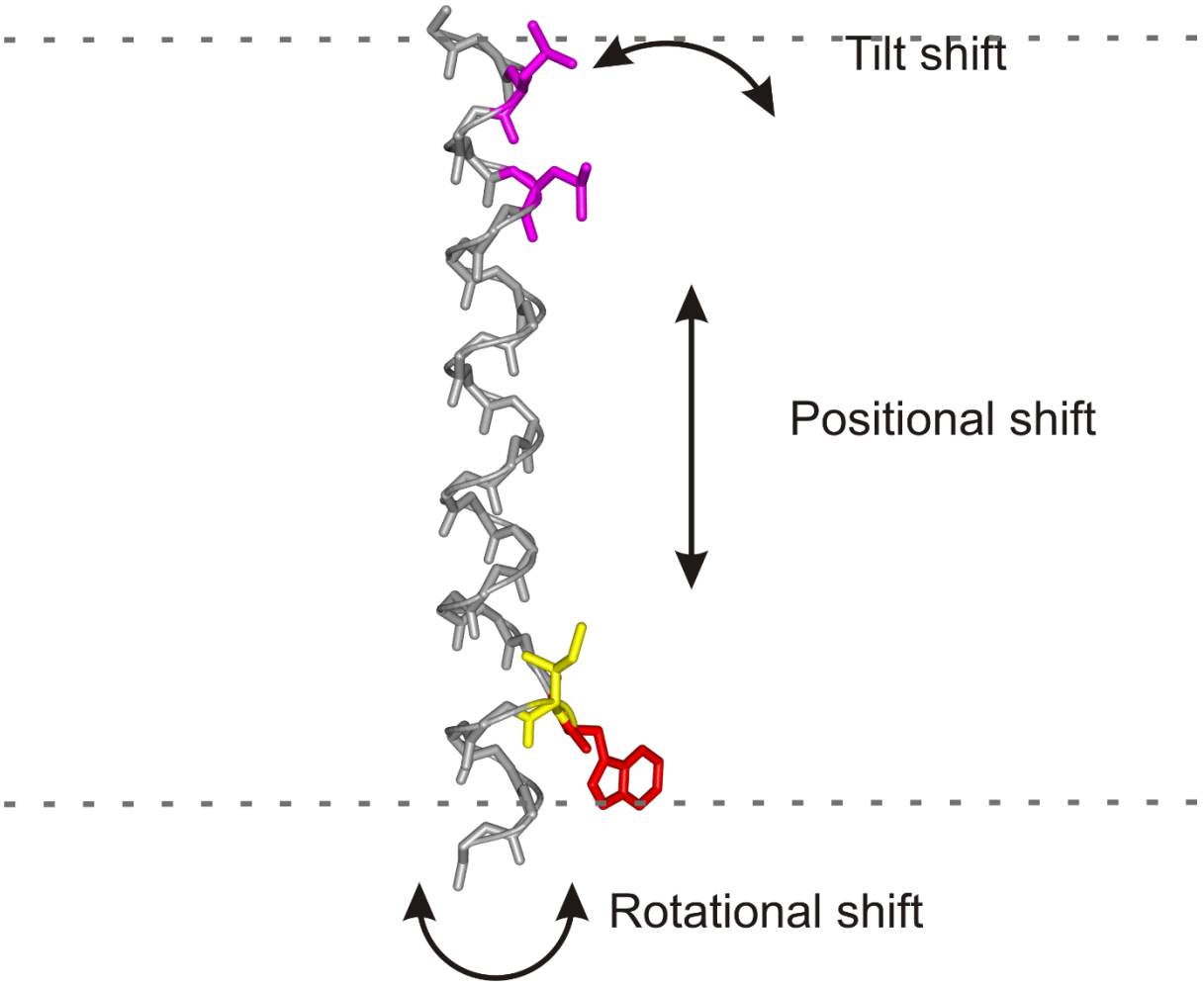

Figure 4-1 The TM2 helix of MCPB and the three proposed motions it could undergo to result in a shift in activity. Leucine 185 and leucine 187 are labelled in magenta, tryptophan 204 is labelled in red and isoleucine 205 is labelled in yellow. The dotted line represents the proposed bilayer/solution interface.

The results of the computational pipeline can be analysed for various properties including helix tilt, rotation and z-position relative to the membrane and the helix centre. Both tilt and rotation were found to be poor parameters to test in this case. This is most likely due to the unfavorable placing of small volumes of amino acid into solution. Small volumes of protein placed outside the bilayer can cause a loss of energy as the water has fewer potential hydrogen bonds available. This is clearly unfavorable in free energy terms and in addition is not a physiological state seen in stable proteins. In order to maximize favorable free energy changes in the system during the simulation, the helices were seen to tilt to maintain residue

contact with the bilayer. This effected the tilt and rotation measurements and were thus determined to be non-native artifacts in these cases. As a result these two measurements have not been included. However, z-position was found to give definite, interpretable result, particularly in cases where the helix stability in the bilayer was not disrupted as described.

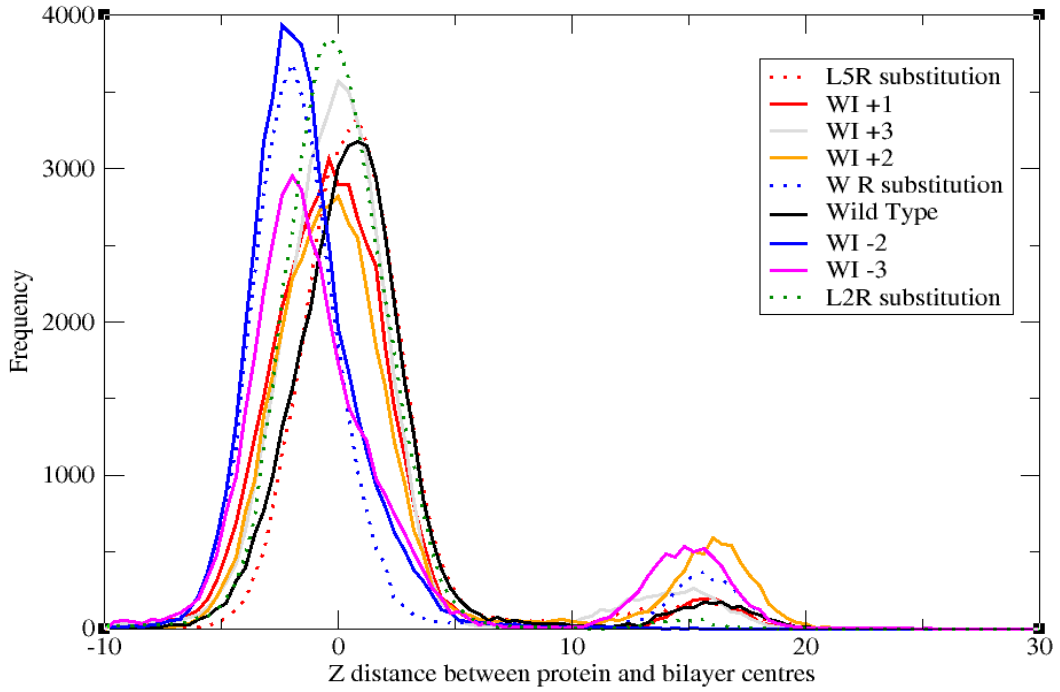

Figure 4-2 The change in Z-distance positions of the centre of the TM2 helix relative to the centre of the bilayer in Sidekick simulations.

The z-position shift for each of the mutants is shown in Figure 4-2. Negative Z shifts correspond to the helix, as shown in Figure 4-1, shifting downwards in the bilayer (towards the cytoplasm). Most show very little shift form the wild type position, however, WI-2, WI-3 and W/R all show a shit of around -4 Å. This has been postulated to be the motion involved in signal transduction through TM2 (Draheim et al., 2005). The WI-2 mutation showed very little rotational or tilt distortion and as a result is likely to be a real and interpretable shift. This mutation also caused the expected 4 Å shift and in analysis of *E. coli* receptors causes a CCW shift of flagella rotation bias but does not lock the signalling to this state (Draheim

et al., 2005). Thus, it appears that by shifting the position of the interfacial residues in the sequence of the TM2 N-terminus and thus towards the periplasm, the TM2 helix has moved in the opposite direction in order to complement this shift and return the interfacial residues to the bilayer solution interface. This is in accordance with previously studied shifts whose *in vivo* activity changes have been determined (Hall et al., 2011). As a result, WI-2 was investigated further by *in vivo* analysis to determine whether the *in silico*-determined mutation does indeed disrupt signalling efficiency.

4.2 *In vivo* analysis of variant receptors

In vivo analysis of individual chemoreceptors has proved difficult due to the inability to create a strain that will respond to an individual effector. Sequential deletion strains eventually lose the ability to respond chemotactically and show a strong decrease in response to all chemoeffectors (Thompson, 2005). As a result, a receptor-less strain of *E. coli*, UU2612, was used to analyse the *R. sphaeroides* McpB mutation *in vivo* (Zhou et al., 2011). Phenotypic analysis of chemotaxis efficiency is typically achieved on soft agar swim plates. These are agar plates containing a sufficiently low quantity of agar (typically 0.25%) to allow bacteria to swim across the surface. By adding a metabolisable chemoattractant to the agar, the bacteria are able to set up their own chemotaxis gradient. Once spotted onto the agar they grow and metabolise the attractant, the local attractant levels will decrease causing a gradient to be set up. As a result, the bacteria can then move away from the original spot up the chemoattractant gradient. The movement away from the original point is thus based on chemotactic ability towards the specific attractants present and the size of the swim ring will directly correlate to the cells ability to sense attractant.

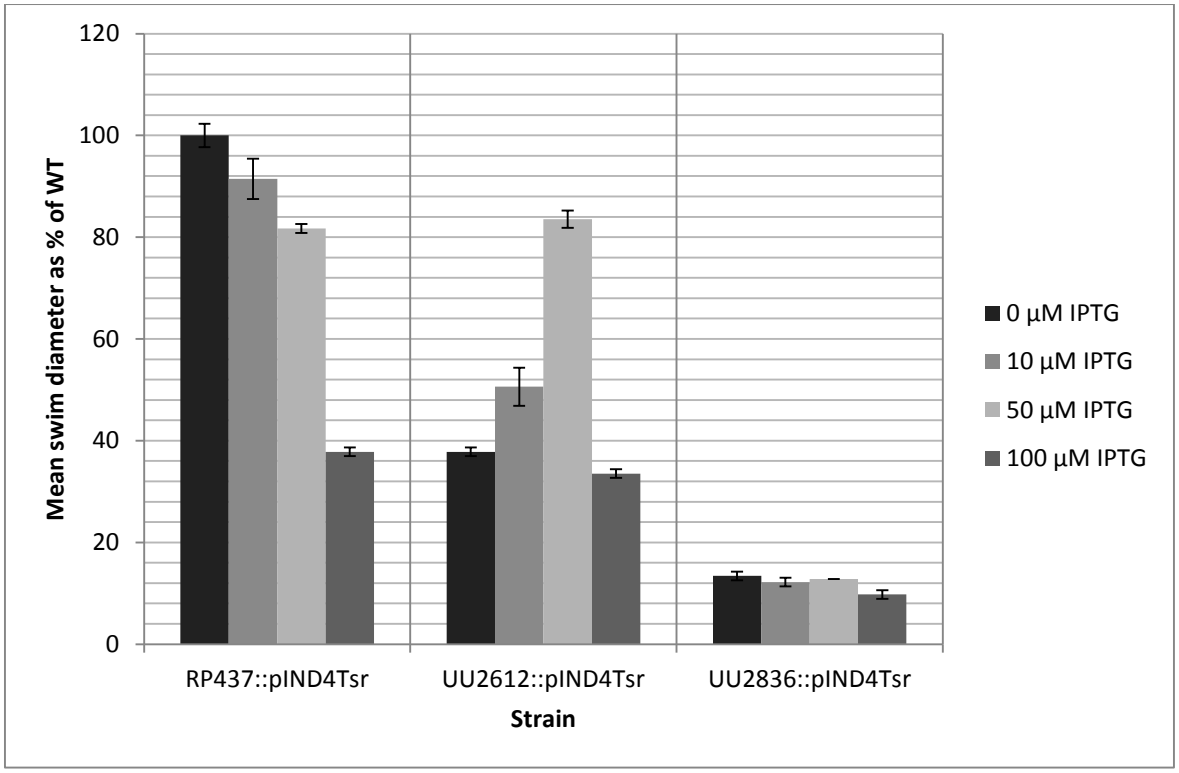

Figure 4-3 Mean swim diameter measurements from tryptone broth (TB) soft agar swim plates showing re-introduction of Tsr into the receptor-less strain UU2612 from the plasmid pIND4 at various induction levels. Mean swim diameter after 12 hours growth is shown as a percentage of the mean wild type swim diameter

The pIND4 plasmid was chosen as it was created for lac inducible expression in α-proteobacter and as *R. sphaeroides* MCPs have proven difficult to clone both in this study and previously, a single plasmid allowing expression in both platforms would be more versatile (Ind et al., 2009). Prior to analysing the mutant chemoreceptors, the pIND4 vector was analysed for controlled induction of chemoreceptors in this system (Figure 4-3). The pIND4 plasmid has not been extensively characterised in *E. coli* previously and therefore, the ability to control expression of chemoreceptors in this system must be analysed. Tsr was expressed from the plasmid pIND4 in strain UU2612. Using rich-media soft agar swim plates to analyse chemotactic ability, greater than 80% of wild type chemotaxis was seen after 12 hours growth in 50 µM IPTG. Notably, chemotaxis was reduced in levels of IPTG that caused over-expression. This shows that Tsr-controlled chemotaxis can be reconstituted

in UU2612 using the plasmid pIND4 and that the chemotactic ability is dependent on levels of induction with IPTG.

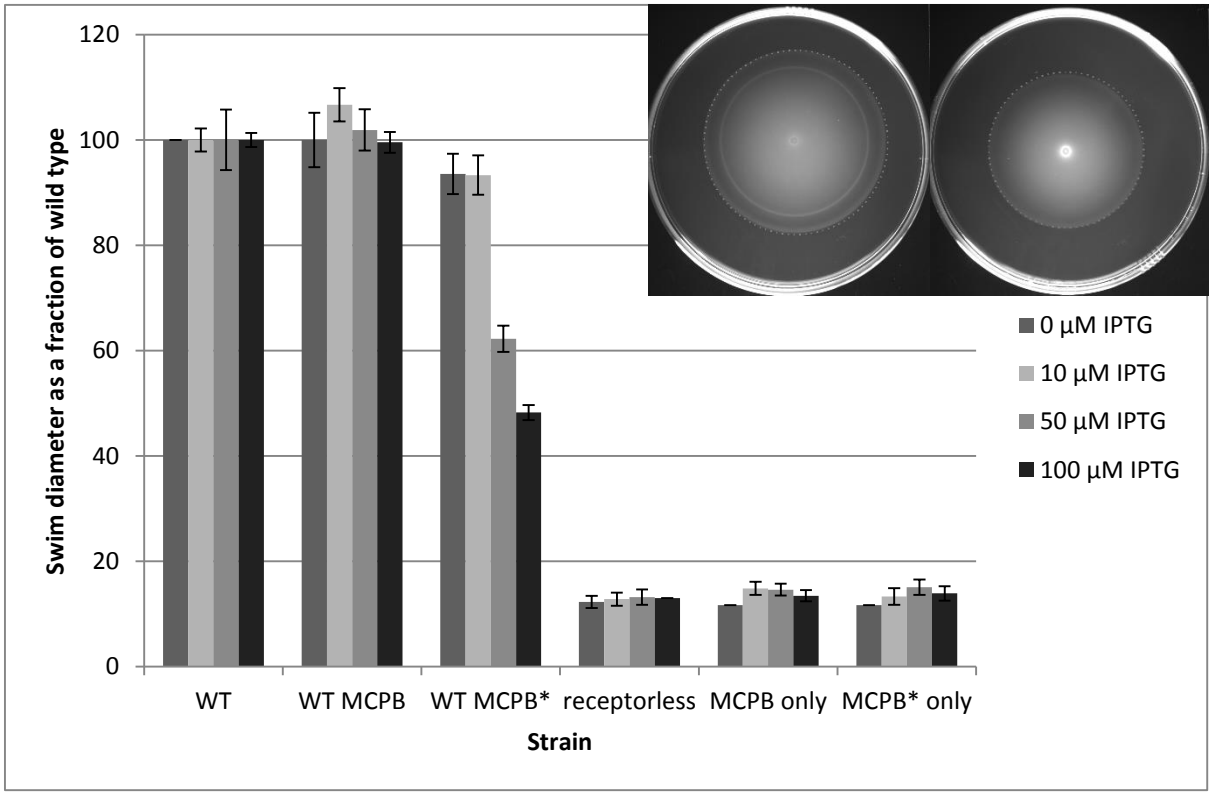

Figure 4-4 Mean swim diameter measurements from tryptone broth soft agar swim plates showing induction of wild type and variant McpB in wild type and receptor-less *E. coli* strains from the plasmid pIND4 at various induction levels. Mean swim diameter after 12 hours growth is shown as a percentage of the mean wild type swim diameter with no induction. **Inset**: left is an example swim ring of RP437 wild type *E. coli* expressing McpB under 50 µM IPTG. Right is an example swarm ring of RP437 wild type *E. coli* expressing MCPB* under 50 µM IPTG. Both swarm rings are outlined with dotted grey for clarity.

The effect of the WI-2 mutation on chemotactic ability was then assessed using this *in vivo* analysis method. The gene for *mcpB* was mutated as described for WI-2 (Table 4-1) and the resultant gene named *mcpB**. The wild type and mutated versions were cloned into the pIND4 vector to allow expression in both *E. coli* and *R. sphaeroides*. These vectors were then expressed in wild type and receptor-less *E. coli* backgrounds. The chemotactic efficiency of these strains was analysed using soft agar swim plates (Chapter 3.4.1) and the results shown in Figure 4-4. No chemotaxis was seen for the receptor-less strain UU2612

containing either McpB or variant McpB*. This shows that either McpB is unable to signal through the *E. coli* signal transduction pathway or that it does not respond positively to components of TB agar used. Induction of McpB in a wild type background has no effect. However, induction of variant McpB* in wild type *E. coli* results in a reduction of chemotactic efficiency. This suggests the following:

- McpB can signal through the *E. coli* chemotaxis system
- McpB does not therefore respond to any component of TB
- McpB* locks the activity and hence allows response through system without binding any component of TB

OR

- McpB does not signal through the *E. coli* chemotaxis system
- McpB* locks the activity and effects the surrounding chemoreceptors in a negatively-cooperative manner thus shifting the global activity of the whole array

OR

- McpB* affects growth of *E. coli* strains and is therefore reducing swarm sizes indirectly

4.3 Is Growth directly affected by McpB*?

Growth of strains is easily tested over time by measuring the absorbance at $\lambda = 600$nm of the growth medium. This can be done in a plate reader to allow many strains to be tested in tandem and it also allows fluorescence to be measured to determine protein expression is consistent.

RP437 cells expressing McpB-RFP or McpB*-RFP were grown to stationary overnight and then 1 µl of this culture was used to inoculate 1 ml of LB containing 50 µM IPTG in a 24 well growth plate. This allowed multiple repeats per plate in order to calculate mean and standard deviation measurements. OD_{600nm} measurements were taken every 30 minutes for 24 hours to determine growth.

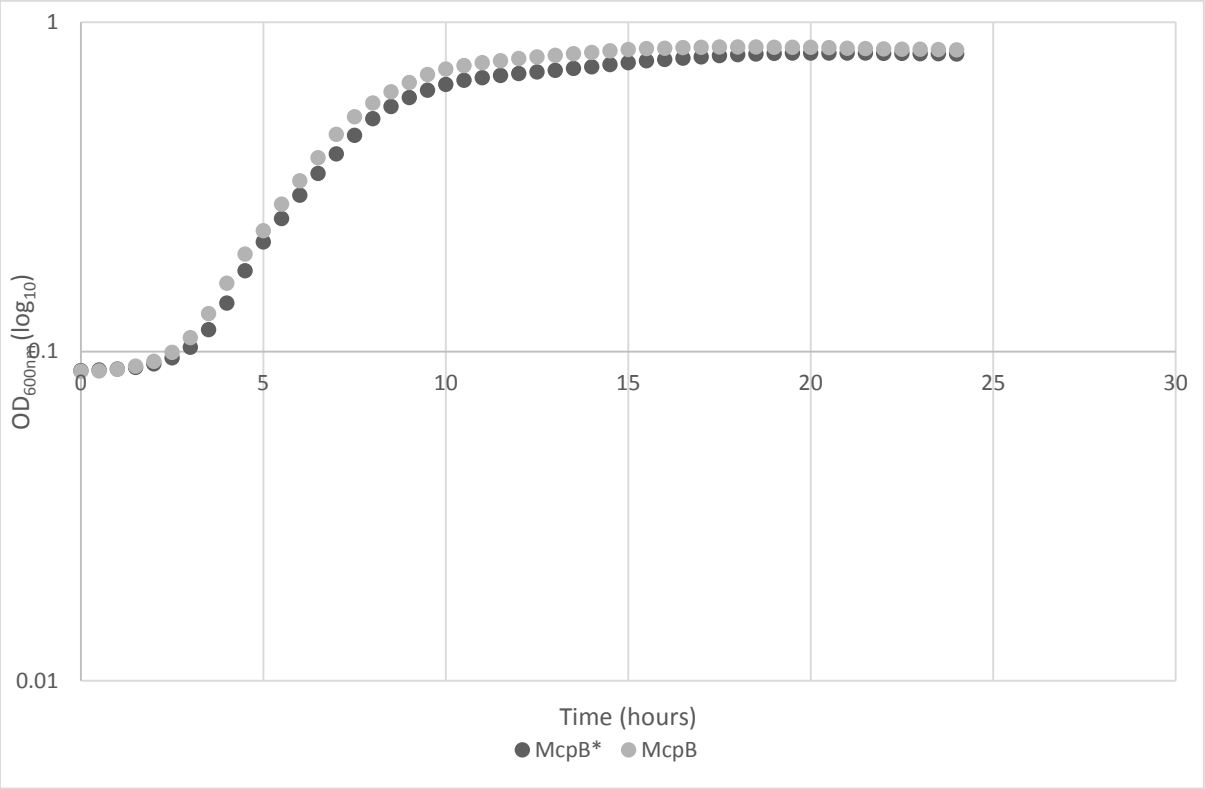

Figure 4-5 Semi-log plot of the mean OD_{600nm} measurements over time of RP437 wild type *E. coli* cells expressing McpB (light grey) or McpB* (dark grey) from the pIND4 plasmid using 50 µM IPTG.

Analysis of the growth over time of R437 cells expressing either McpB or McpB* shows that both strains grow at similar rates and any differences in these should not account for the large difference seen in chemotaxis efficiency on swim plates (Figure 4-5).

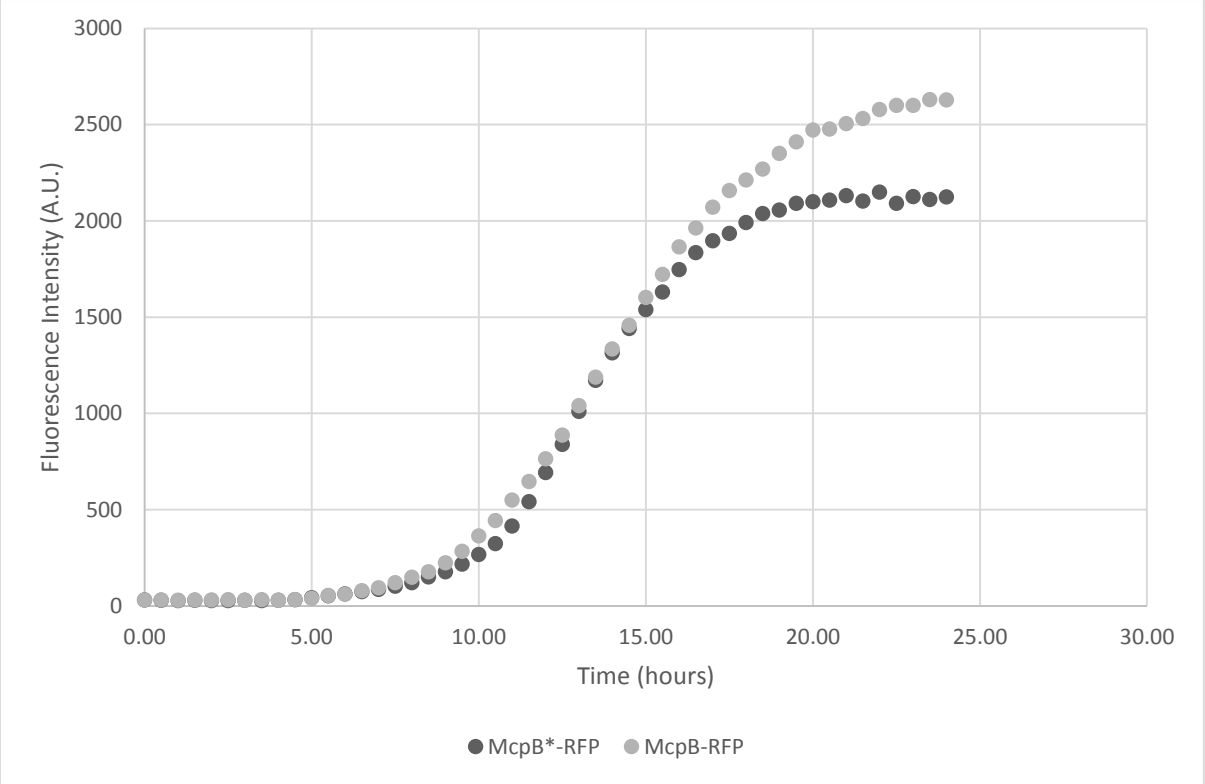

Figure 4-6 Fluorescence intensity, in arbitrary units (A.U.) of McpB or McpB* expressed from pIND4 with 50 µM IPTG in RP437 cells. Time course of 24 hours used to ensure stationary phase reached.

The analysis of fluorescence intensity in wild type *E. coli* cells of the RFP fusions of McpB and the variant McpB* show that in log phase, expression is very similar. When the cells reach stationary phase, expression of McpB* becomes constant before that of McpB. However, this will not affect any results obtained from microscopy images at they are undertaken during log phase. This may affect results from swim plates to a small extent but it is unlikely that this would create the change seen in RP437 chemotaxis efficiency previously.

4.4 Does McpB signal through the *E. coli* chemosensory network?

The swim plate data alone is insufficient to determine which of the above scenarios is correct. Components of the chemotaxis array have been used to complement deletions in *E. coli* strains previously (Hamblin et al., 1997) (Shah et al., 2000). As a result, reconstitution of a more *R. sphaeroides*-like signal transduction pathway should allow determination between these two theories.

UU2836 is an *E. coli* strain containing deletions for all chemoreceptors and the native c*heW* and hence contains no native chemoreceptors or scaffold CheW proteins. This strain, therefore contains only the *E. coli* CheA and therefore allows *R. sphaeroides* CheW proteins to be tested to determine whether they link *R. sphaeroides* McpB to *E. coli* CheA. Using the standard genomic replacement protocol (Chapter 3.3.12) *R. sphaeroides cheW2* and *cheW3* genes were separately introduced into the *E. coli* genome at the position of the original *E. coli cheW* gene. These strains were respectively named JPA3000 and JPA3001. This allows expression of wild-type levels of a *R. sphaeroides* CheW scaffold protein in tandem with inducible expression of a selected MCP.

If McpB was able to signal through *E. coli* CheA, the inclusion of a native CheW scaffold should enable this to occur. $CheW_3$ has been shown to be able to recover chemotaxis in an *E. coli* CheW deletion and so it was expected that this should allow a complete signalling complex to form and then signal to the *E. coli* CheY (Shah et al., 2000).

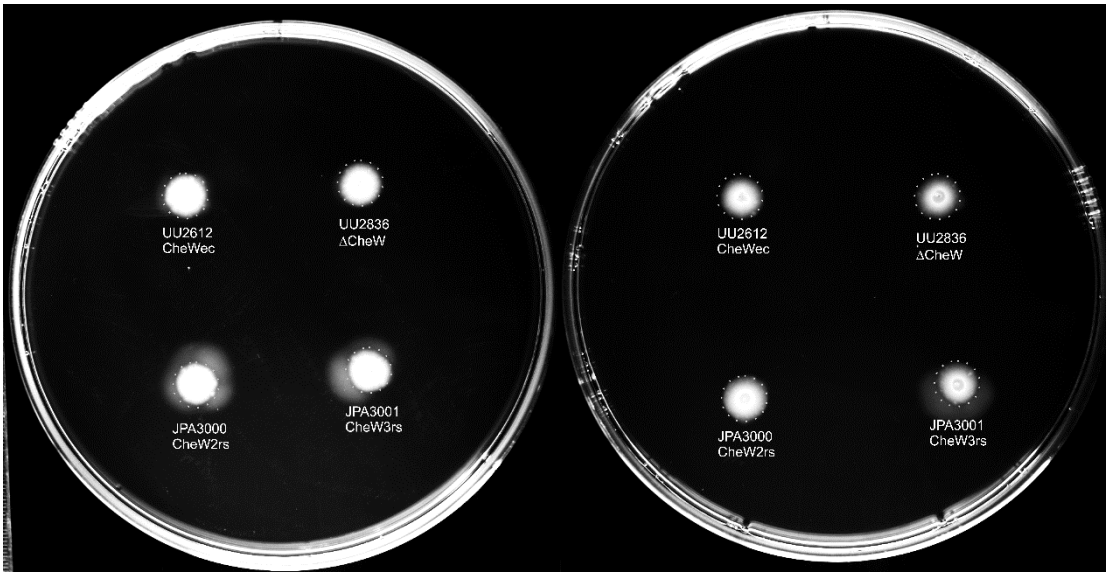

Figure 4-7 Example soft agar swim plate of *E. coli*::McpB (left) and *E. coli*::McpB* (right) in various CheW backgrounds. UU2612 contains native *E. coli* CheW, UU2836 does not express a CheW protein, JPA3000 expresses *R. sphaeroides* $CheW_2$ and JPA3001 expresses *R. sphaeroides* $CheW_3$. Slight visible flaring was inconsistent, suggesting random mutagenesis that has restored chemotaxis, most likely by allowing interactions that form a functioning array. Due to the inconsistency of this flaring, measurements were taken from solid, complete swim rings only. Plasmid expression was induced with 50 µM IPTG. Swim rings are labelled with a grey hashed circle for clarity.

Figure 4-7 shows that MCPB is unable to elicit a consistent chemotactic response through native $CheW_{ec}$, $CheW2_{rs}$ or $CheW3_{rs}$. The presence of flaring in JPA3000 and JPA3001 expressing McpB suggests that random mutagenesis is able to recover a chemotactic phenotype. This is most likely due to new interactions arising that allow formation of a functioning and signalling array. The lack of such strong flaring in other cases shows that these strains are particularly susceptible to this. This is a potential method for future work to analyse the specificity of these proteins at a molecular level further. It is likely that the lack of chemotactic signalling initially in these cells is due to lacking interactions that are easily recovered by small changes to the proteins involved.

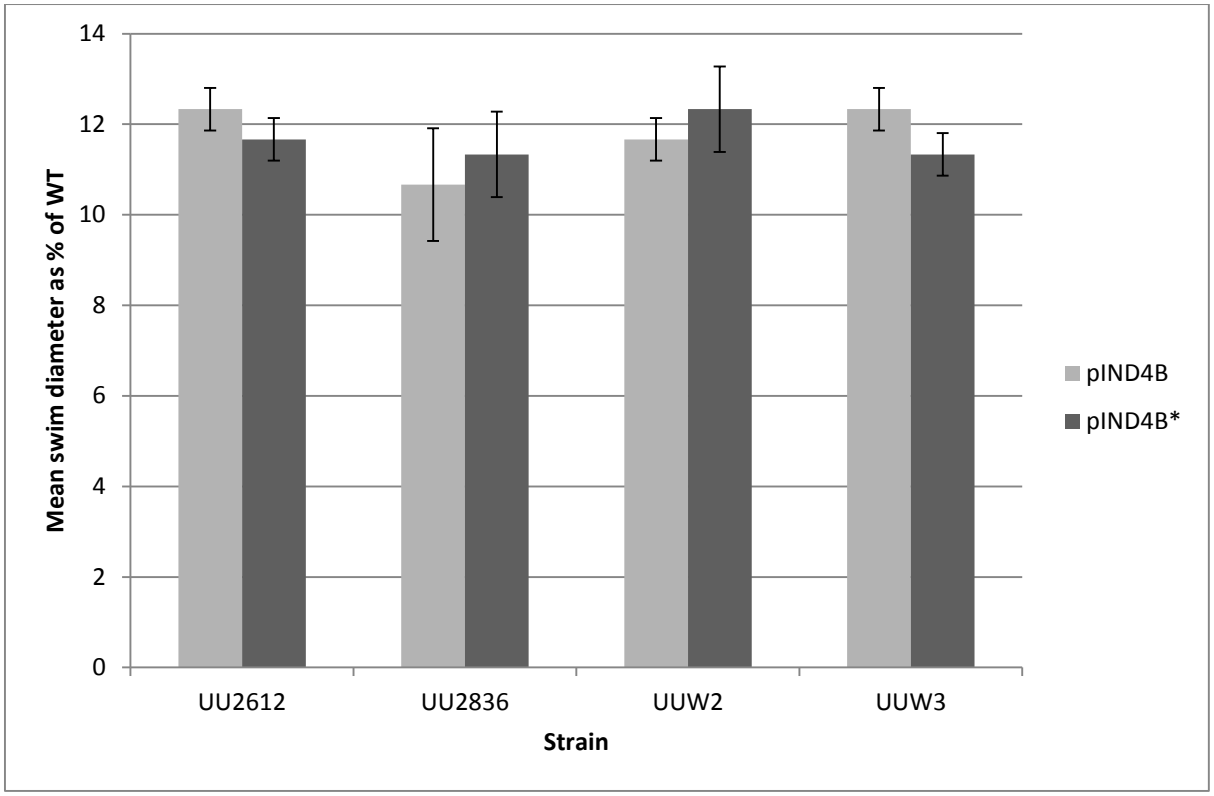

Figure 4-8 The swim diameters of cells expressing McpB (light grey) and McpB*(dark grey) as the sole receptor. UU2612 contains native *E. coli* CheW, UU2836 does not express a CheW protein, UUW2 expresses *R. sphaeroides* $CheW_2$ and UUW3 expresses *R. sphaeroides* $CheW_3$. Plasmids were induced with 50 µM IPTG.

The lack of swarm rings for cells expressing any of the tested CheW proteins with either McpB or the variant McpB* present shows that these strains are not chemotactically competent. This shows that no cells containing McpB in tandem with *E. coli* or *R. sphaeroides* CheW proteins can elicit a chemotactic response and in these cases, it appears McpB cannot signal through the *E. coli* chemotaxis pathway. (Figure 4-8). Shown graphically it is clear that no background has chemotactic ability above the non-chemotactic CheW deletion background UU2836 (Figure 4-8) Therefore the second hypothesis appears correct and McpB* shifts chemotaxis efficiency by altering the state of the surrounding chemoreceptors.

4.5 Does McpB* also effect chemotaxis in *R. sphaeroides*?

As these experiments have been undertaken in *E. coli*, it is possible that the reduction in chemotaxis seen is an artefact of working in a non-native system. In order to test this, the two plasmids were also expressed in *R. sphaeroides* strain WS8N and their chemotactic abilities analysed on soft agar swim plates. Examples of these plates are shown in Figure 4-9.

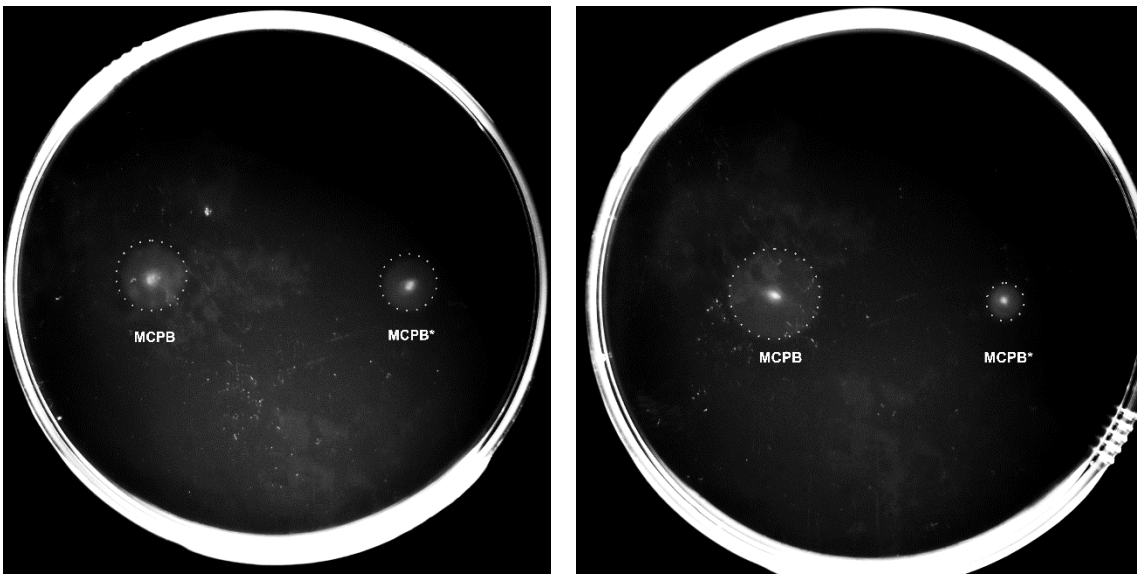

Figure 4-9 Soft agar swim plates of wild type and variant McpB expressed in *R. sphaeroides* WS8N cells. Left shows the two strains (labelled) without IPTG induction. Right shows both strains induced with 50 µM IPTG. Swim rings are labelled with a grey hashed circle for clarity.

These swim plates show that McpB* also reduces swim diameter in its native *R. sphaeroides* background, in comparison to the wild type McpB. Figure 4-10 shows that as IPTG induction is increased, the swim diameters of cells expressing variant McpB* decreases to approximately 50% wild type levels. The same effect is not seen for cells expressing wild type MCPB and in fact swim diameters were increased at higher levels of induction to

approximately 120% wild type levels. This is interesting as it suggests that the presence of wild type McpB increases chemotactic efficiency to propionate. The mechanism for this could be either a direct response to propionate through McpB or a secondary effect with McpB presence merely somehow increasing the effective output of the chemotactic array. These models cannot be further analysed through these results alone and suggest further questions about the specificity of McpB that are not within the scope of this study. As a result, it is possible to conclude that the effect seen on *E. coli* swim plates is a real shift and not as a result of the change to a foreign system.

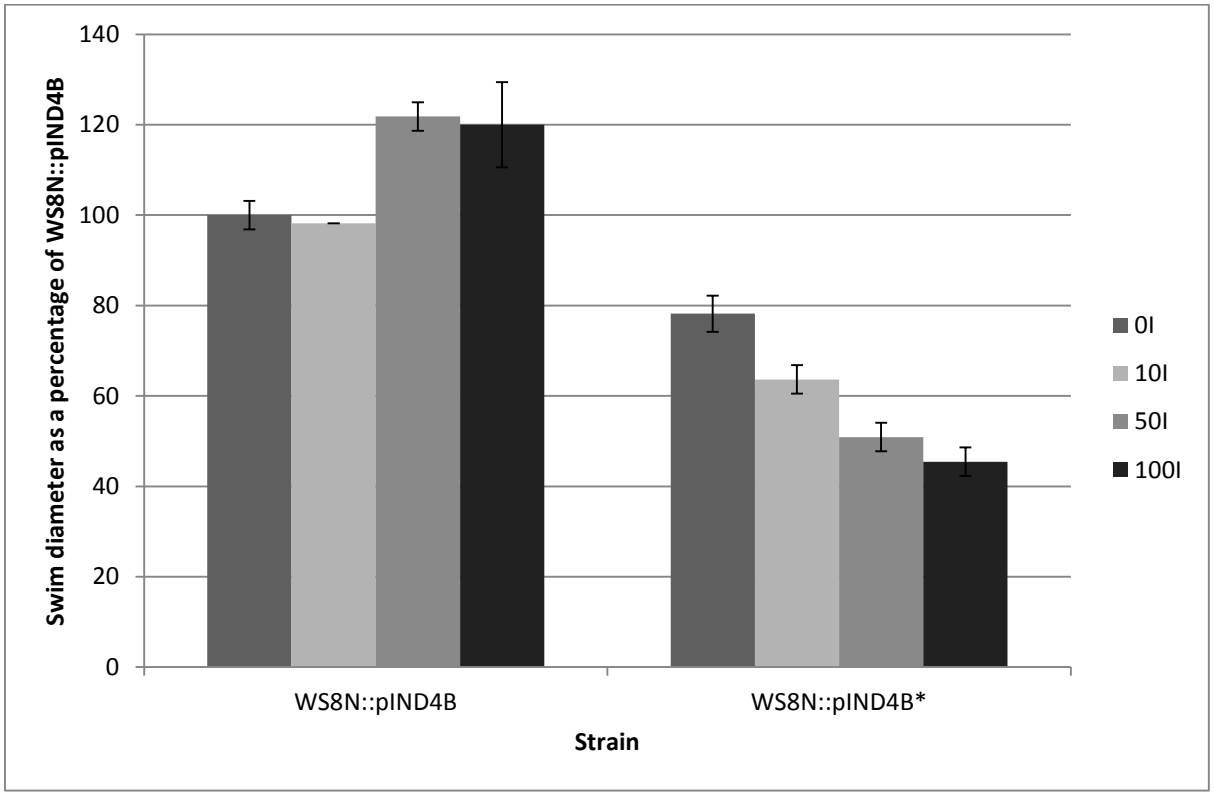

Figure 4-10 Swim diameters of WS8N cells expressing either wild type or variant McpB in minimal media with 100 µM propionate. Cells were expressed with increasing [IPTG] and diameter is displayed as a percentage of WS8N containing pIND4B with no IPTG added. Errors bars show the standard deviation of the sample.

4.6 How does McpB* reduce chemotactic efficiency?

Figure 4-8 shows that McpB* reduces the efficiency of the *E. coli* chemosensory system, likely by shifting the responses of the native chemoreceptors present in the RP437 strain. However, it cannot inform us of what happens to the signal at the molecular level. There are multiple ways that chemosensing in bacteria can be altered, this is due to the multiple nodes present within the chemosensory signalling cascade. In addition, swim plates do not give us specific data on how chemotaxis is affected. Motility defects could cause a reduced swarming phenotype as well as increased or decreased tumbling frequency. The latter of these hypotheses can be analysed by examining the swimming behaviour of free bacteria in solution. If the native level of signalling through the chemosensory apparatus is shifted to allow increased activity of CheA, more CheY-P will be present at basal levels without stimulus. This will result in more motor switching events and will thus result in an increase in tumbling frequency. By tracking the swimming of cells in minimal media, the frequency of tumbling can then be determined and differences tested for significance.

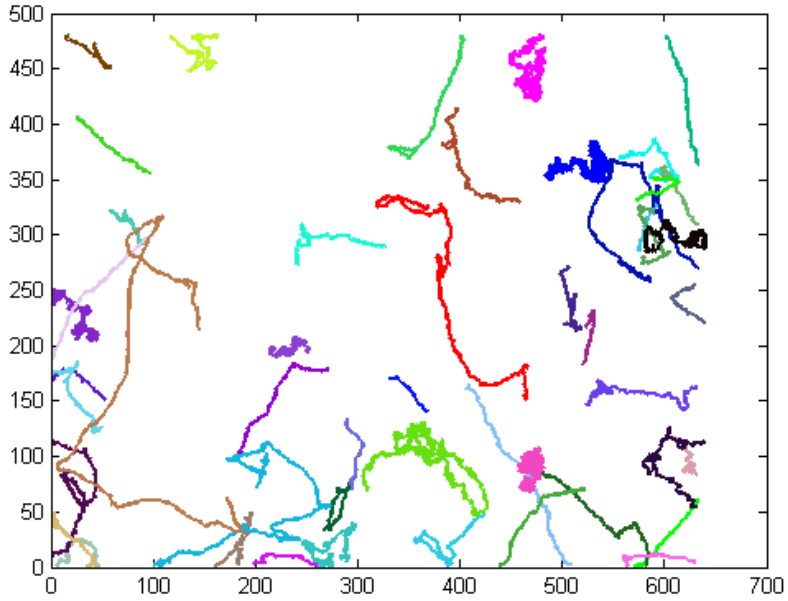

Figure 4-11 Example tracks from free swimming analysis of *E. coli* wild type RP437 containing empty pIND4 plasmid in 50 µM IPTG. A selection of the tracks can be seen to undergo both run and reorientation events, whereas a subset displays anomalous swimming and has not been able to be removed by the censoring process.

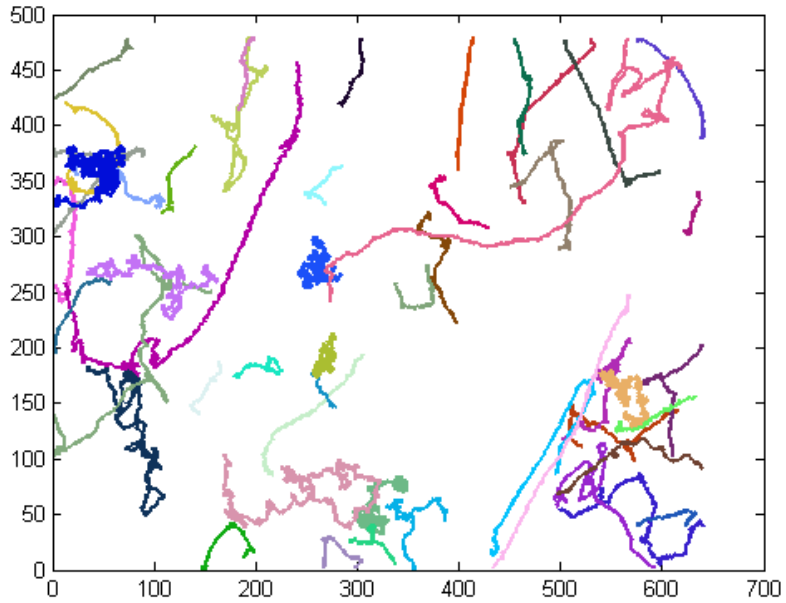

Figure 4-12 Example tracks from free swimming analysis of wild type *E. coli* RP437 cells expressing McpB from the pIND4 plasmid in 50 µM IPTG.

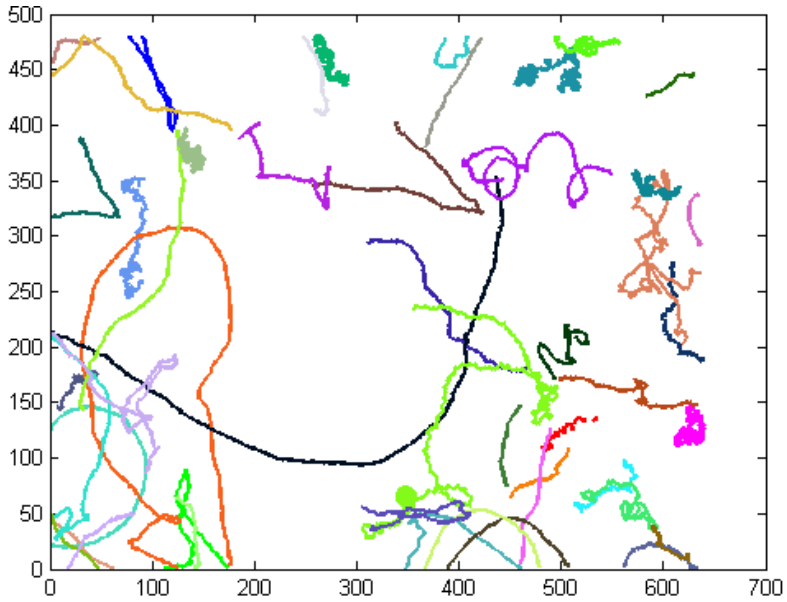

Figure 4-13 Example tracks from free swimming analysis of wild type *E. coli* RP437 expressing McpB* from the plasmid pIND4 in 50 µM IPTG.

Tracking and censoring of resultant tracks in *R. sphaeroides* has been studied previously using novel software (Rosser et al., 2013) (DeBeyer, 2013). This software was used in this study to track the swimming behaviour of *E. coli* strains in order to indirectly determine the levels of chemosensory signalling in absence of stimulus. Free swimming capture and analysis was achieved as described in Chapter 3.5.5. Briefly, cells were grown aerobically to OD_{600nm} 0.4-0.6 and then imaged inside sealed capillary tubes to prevent external flow. Two-minute videos were obtained and then threshold values were used to determine objects in each frame. Objects were then tracked between frames to create full length tracks for each cell that exists within the field of view during the video. Tracks are censored for cells that are non-motile (cells that do not exit a set circle during their length), tracks that make non-native motions (tracks that appear to move faster than the maximum for *R. sphaeroides*) and tracks that have torsion angles that suggest non-native motions (those tracks whose angles shifts between frames are too small and thus tortuous). Three sets of example tracks are shown for RP437 expressing empty pIND4 plasmid, McpB and McpB* (Figure 4-11, Figure

4-12, Figure 4-13 respectively). By eye the original videos captured of the strains show little difference between them and as a result are inconclusive. However, once tracks have been made of individual cells, numerous pieces of information can be extracted from these. Tracks can be segmented into perceived 'stop' phases and perceived 'run' phases. This essentially allows the relative amount of time each cell spends stopped to be calculated for each track. These values can be then analysed statistically to determine differences between data sets.

The analysis of the fraction of time stopped by each cell tracked during the video shows that on average, wild type RP437 spends approximately 40% of its time in a 'tumble' state (Figure 4-14). This number is likely influenced by some cells during the course of the simulation not entering a defined 'run' phase and therefore being recorded as 100% stopped. As a result it is likely that this is an overestimate of the average fully motile cell stopped percentage, however, a similar proportion of cells recorded as 100% stopped should be present in each data set and so results should be influenced equally by this. RP437 expressing McpB appears to show a similar percentage of time stopped to the wild type RP437, this suggests that in minimal medium, wild type *R. sphaeroides* McpB has no detectable effect on tumbling frequency or length. RP437 expressing variant McpB* spends a greater fraction of time in a tumble phase as opposed to a run phase (Figure 4-14). This is exhibited as an increased mean fraction of time spent stopped in cells containing the variant receptor. Increased total tumble time can be caused by either an increased frequency of tumbles or an increased length of tumbles. In the former, the chemotaxis array is activated more often and therefore cells tumble more often, however, the signal termination and adaptation mechanisms are unchanged and CheY-P is removed at the same rate as wild type, causing tumble lengths to remain the same. In the latter case, the array is not necessarily activated more often but the CheY-P signal is not removed at the same rate and cells are not adapting

to the signal. This will increase the length of a single tumbling event and not the number of these that occur. These two cannot be distinguished by this method but given the nature of the mutation tested it is more likely to be a change in signalling frequency rather than a secondary effect from adaptation or termination.

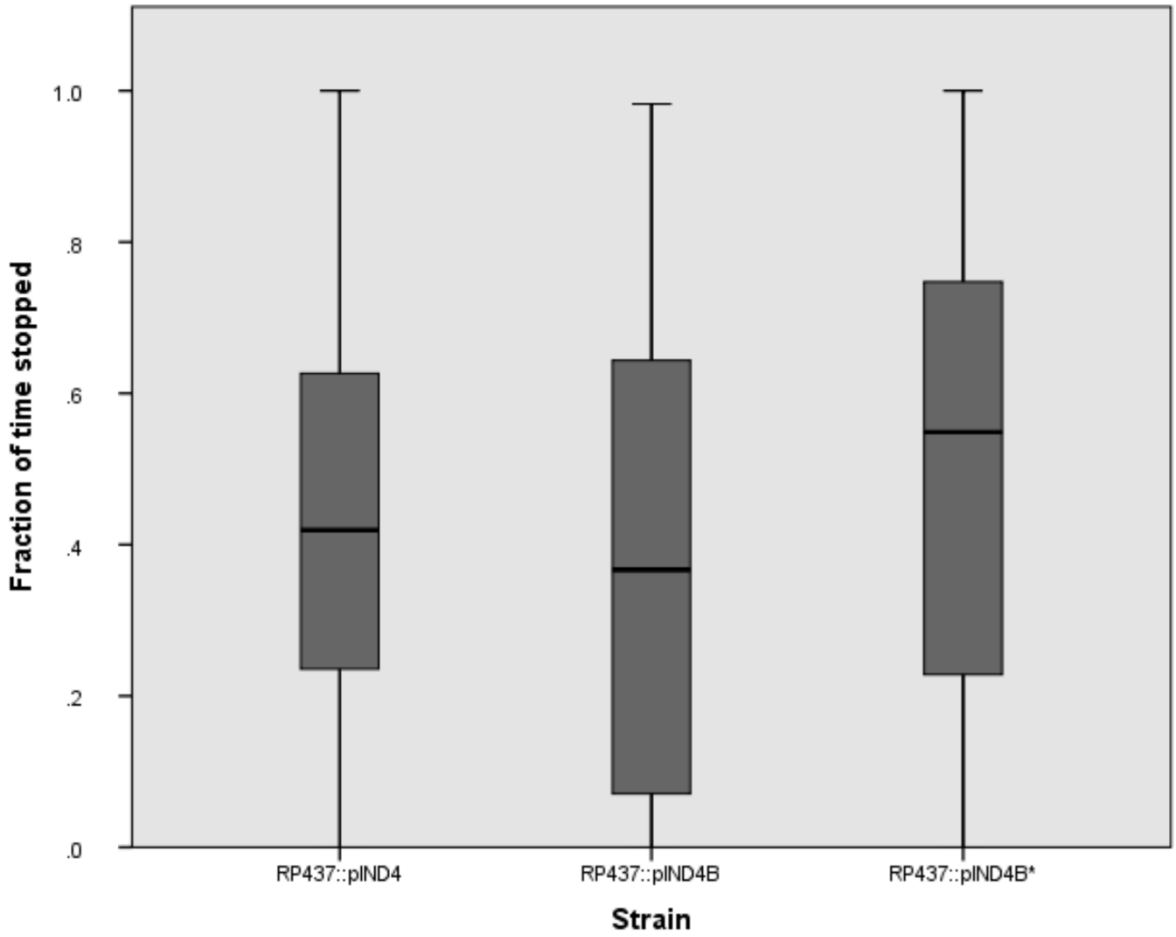

Figure 4-14 The fraction of time stopped of wild type RP437 and RP437 expressing wild type or variant McpB. Boxplot edges indicate first and third quartiles, box centre indicates median and whiskers indicate the total range.

A Shapiro-Wilk test for normality of the data shows a significance value of 0.00 and hence the data is not distributed normally. Therefore, a Kruskal-Wallace test for non-parametric data was used to determine significance of similarity between independent data sets. A Kruskal-Wallace test with the null hypothesis that RP437::pIND4B and RP437::pIND4B* have the same fraction of time spent stopped shows an adjusted significance of 0.044. Values

less than 0.05 can reject the null hypothesis with 95% confidence, therefore, the two data sets do not significantly overlap.

The variant McpB* protein, therefore causes an increase in the tumbling frequency or length of RP437 cells. This increased tumbling is likely to have a significant effect on the chemotactic efficiency of cells, which has been shown to be true in both *E. coli* RP437 cells (Chapter 4.2) and *R. sphaeroides* WS8N cells (Chapter 4.5). An increase in tumbling frequency in this case is likely to be caused by higher levels of CheY-P in the system. Therefore, McpB* is increasing the activity of the native CheA and this is a potentially marginal shift which results in only a slight change in the tuning of basal activity of CheA, not the full locking of one state over the other. As shown in chapter 4.4, this must be due to the activity of the surrounding MCPs acting upon the native CheA. So McpB* exhibits a cooperative effect and indirectly increases the signalling output of CheA compared to McpB.

4.7 Fluorescence microscopy of variant receptors

Chapter 4.6 shows that the variant McpB* reduces chemotactic efficiency by increased tumbling as a result of increased CheA output. However, this does not show how the mutation of McpB causes a change in signalling. There is evidence that shifts in the activation states of receptors cause global changes in the array (Khursigara et al., 2008b) (Vaknin and Berg, 2007). These arguments are good models for the initiation of cooperativity within the system as activation state changes affects global structure and thus whole-array signalling. However, due to the adaptation of receptors in the array through CheB and CheR systems in *E. coli* and *R. sphaeroides* these structural shifts are difficult to prove experimentally and are hence debated. In a system where the activity of one receptor

is locked, any change in the global array structure should be visible by whole-array fluorescence microscopy. However, as discussed (chapter 4.2) it is difficult to analyse single MCP proteins in the native *R. sphaeroides* system. As a result, analysis of fluorescence in UU2612 was used to determine if any effects of shifted signalling could be seen in the whole array.

4.7.1 Analysis of native Tsr receptors

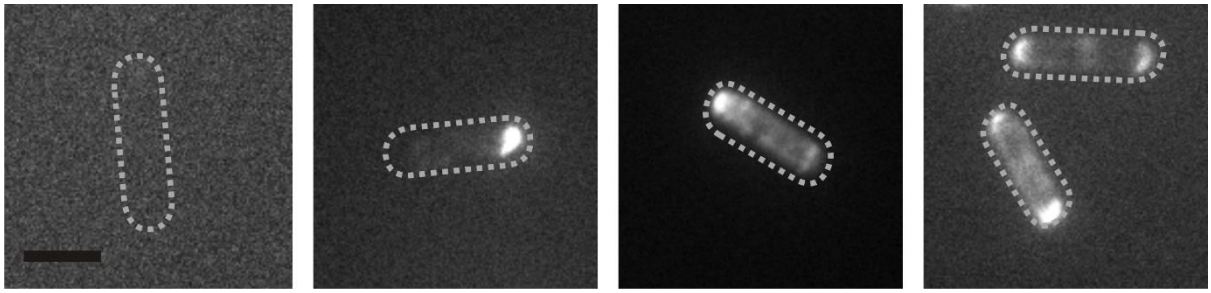

Figure 4-15 Localisation of wild type Tsr receptors expressed in wild type *E. coli* RP437 cells. Shown is increasing induction levels from left to right: 0 µM, 10 µM, 50 µM and 100 µM IPTG. In all images, contrast has been enhanced for maximum clarity. Cell outlines are drawn from the DIC images and shown here as a grey dotted line. Scale is consistent and scale bar in left image indicates 1 µm.

In order to analyse the localisation of McpB and McpB* in *R. sphaeroides* it was first necessary to characterise the localisation of Tsr, a native *E. coli* MCP, expressed from the same plasmid in this system. As it is a native, polar MCP, expression from pIND4 should create distinct, tight polar spots with little lateral fluorescence intensity detectable. This is precisely what is seen when expressed in this system (Figure 4-15). Tsr-RFP is shown to localise predominantly to the poles. Very little fluorescence is seen when cells are not induced by IPTG showing there is not significant leakage from pIND4 in this system. Induction with 10 µM IPTG does show fluorescence signal which is localised to the poles of the cell. There is very little fluorescent signal localised to lateral cellular regions showing strong bias for Tsr receptor to the poles, as expected. Induction with higher levels of IPTG

(50 µM and 100 µM) increases the levels of Tsr-RFP present as expected, and in these cases the levels appear more like previously studied localisation patterns, suggesting that more wild type levels of protein are being expressed. A slight increase in lateral fluorescence is seen in the highest induction level tested. This shows that when levels of Tsr increase too high, MCPs can localise to non-polar regions, presumably due to overcrowding. These results suggest that fluorescence analysis of *R. sphaeroides* MCPs in this system is possible and expression is titratable using pIND4 as an expression system. Induction of MCPs from this system is likely to yield most accurate results using 50-100 µM IPTG as these values appear to show the most native levels of MCP expression.

Localisation of fluorescence was analysed by recording the profile of fluorescence intensities across each cell and then normalising the lengths to one. Profiles of each cell were normalised by determining total fluorescence of each cell and determining percentage fluorescence present at each point. These percentages were then summed into 20 separate bins to create a fully normalised profile for each cell. Profiles for all cells of each strain and condition could then be averaged to determine the average normalised fluorescence intensity across the cell as shown in Figure 4-16. Percentage of fluorescence that was localised to the poles was then summed as the total of the first and last 20% of the cell. These positions were chosen as the profiles show sharp, distinct peaks that cover the first and last 20% of the cell profile. This shows that in wild type cells, spots are contained within these bounds and the remainder is cellular autofluorescence or partially delocalised receptors not currently formed at the cluster. Determining the fluorescence between these bounds should determine the levels of receptor localising specifically to the polar cluster compared with the levels diffuse around the rest of the cell membrane.

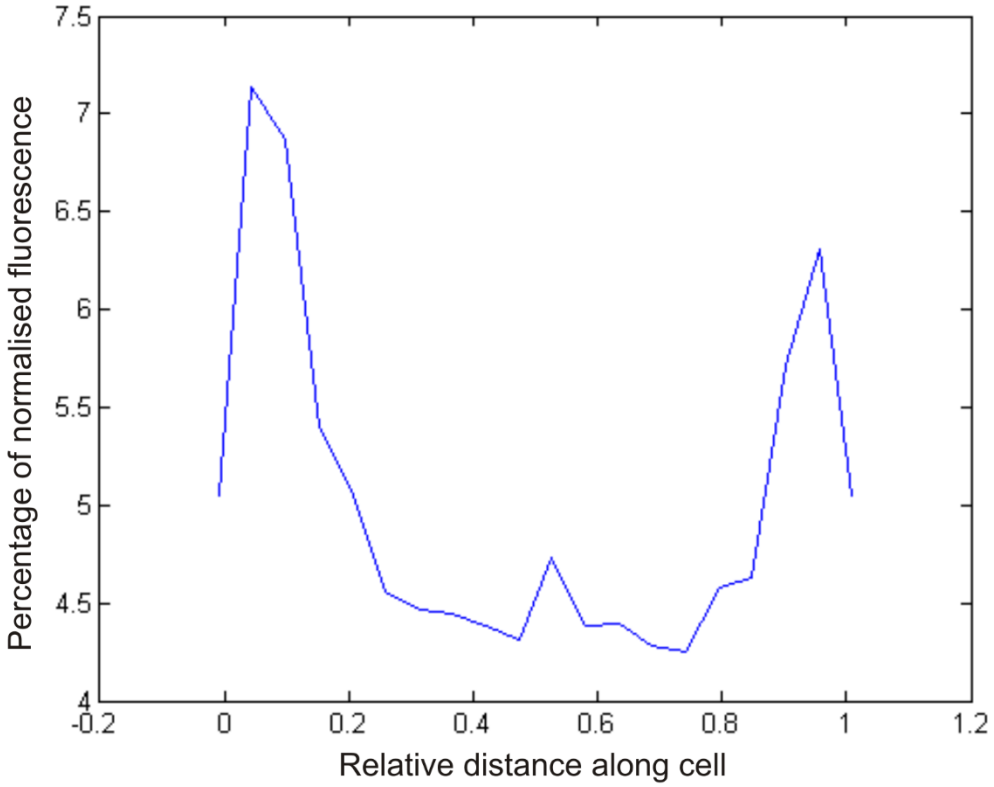

Figure 4-16 The normalised average fluorescence intensity of Tsr-RFP across the length of wild type *E. coli* RP437 cells. Cells were induced with 50 µM IPTG and plots were generated as described in the text.

Average localisation of Tsr-RFP across the cell is shown in Figure 4-16. This profile clearly shows predominantly polar localisation of RFP fluorescence showing that Tsr does indeed localise to the poles in wild type *E. coli* as previously shown. This localisation is asymmetrical as profiles were determined from the brightest pole first showing that one pole is on average brighter for wild type cells. Percentage of fluorescence at the poles of these cells totalled 51% of total fluorescence intensity.

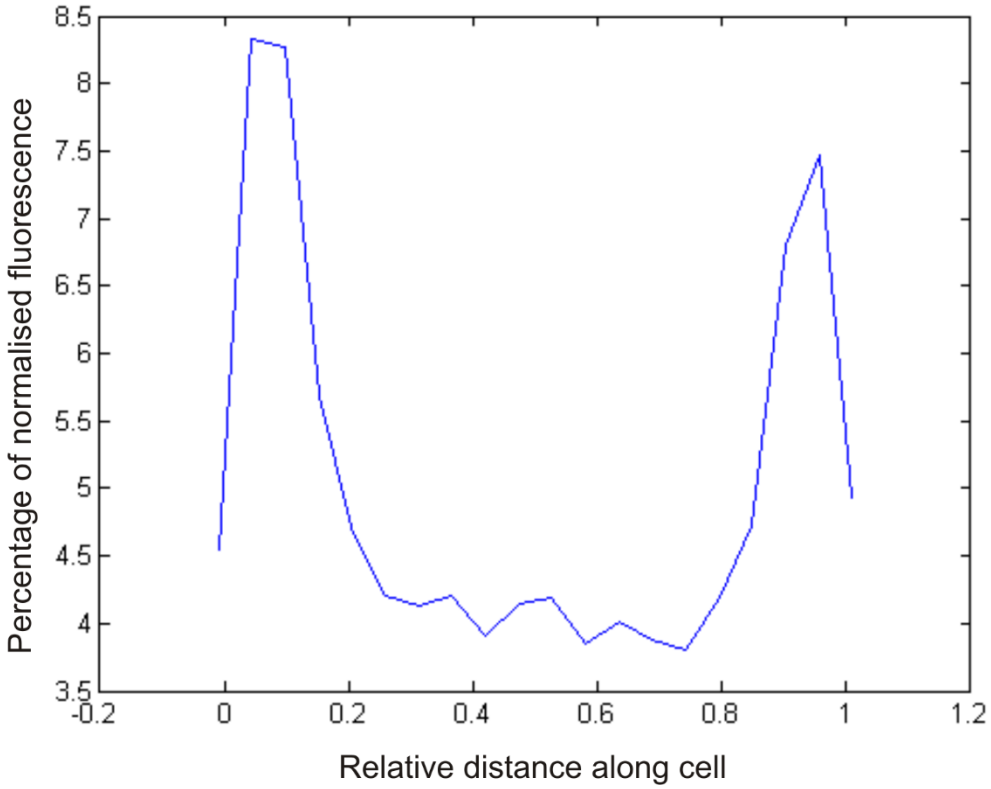

Figure 4-17 The normalised average fluorescence intensity of Tsr-RFP across the length of *E. coli* cells lacking all other chemoreceptors (UU2612). Cells were induced with 50 µM IPTG.

The normalised fluorescence profile of UU2612 cells expressing Tsr-RFP shows a similar localisation to wild type cells (Figure 4-17). This strain has been deleted for all native *E. coli* chemoreceptors and so allows expression and analysis of single receptors in the *E. coli* system. The percentage of fluorescence localised to the poles when induced with 50 µM IPTG, in this case is 55±5%. This is higher than wild type cells and suggests that some overcrowding of the polar cluster may occur in RP437 cells that are expressing normal levels of all other receptors as well as those induced. This overcrowding may result in some Tsr-RFP delocalisation to the lateral regions of the cell. As a result it is likely that UU2612 is a better parental strain for analysing localisation of chemoreceptors as it prevents such overcrowding effects.

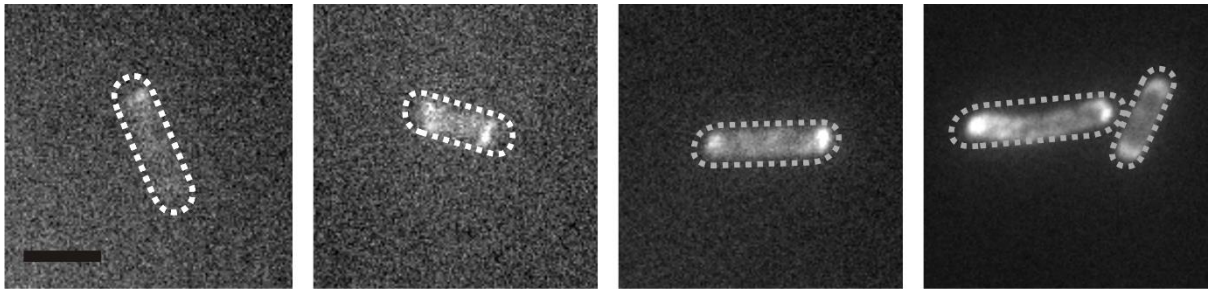

Figure 4-18 Localisation of wild type Tsr receptors expressed in cells lacking all other receptors and deleted for the native CheW scaffold protein (UU2836). Shown is increasing induction levels from left to right: 0 µM, 10 µM, 50 µM and 100 µM IPTG. In all images, contrast has been enhanced for maximum clarity. Cell outlines are drawn from the DIC images and shown here as a grey dotted line. Scale is consistent and scale bar in left image indicates 1 µm.

By determining the localisation pattern of Tsr-RFP in cells lacking any scaffold proteins, it was possible to show the phenotype of a delocalised array. Without the native CheW scaffold protein, stable arrays will not form and fluorescence intensity should increase in lateral regions of the cell. Figure 4-18 clearly shows that lateral fluorescence intensity increases when CheW is not present and a stable array is unable to form. Notable also, is the presence of strong foci still in the cell poles, showing that Tsr still retains strong affinity for polar regions of the cell without stable array formation.

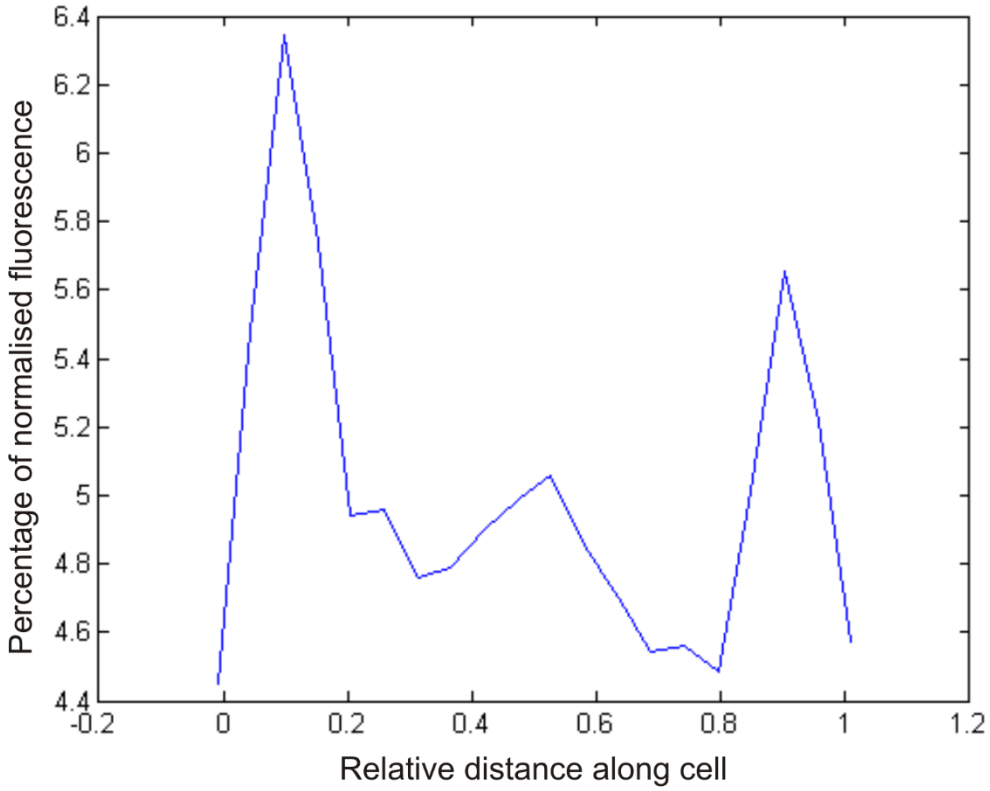

Figure 4-19 The normalised average fluorescence intensity of Tsr-RFP across the length of cells lacking all other receptors and deleted for the native CheW scaffold protein (UU2836). Cells were induced with 50 µM IPTG.

The average cell profile of Tsr-RFP fluorescence in cells not expressing a CheW scaffold protein is shown in Figure 4-19. By eye, this profile looks similar to that of the wild type (Figure 4-16) and it appears that removal of the scaffold CheW results in only a slight increase in lateral fluorescence, visualised by a higher normalised fluorescence value in the middle of the plot. The total fluorescence of the polar regions of the cells is calculated to be 47±2%, agreeing with the conclusion that there is only a slight increase in fluorescence intensity in the lateral regions upon cluster delocalisation. It is notable, that the difference in polar intensity between delocalised and localised cells appears to be very small. As a result, the two data sets were compared for similarity using a student t test. This determines whether the two sets of data are indeed different and can therefore be distinguished. In this case, the null hypothesis that the data sets are the same was rejected with a p-value of $1.9e^{-006}$. This

shows that there is a significant and detectable difference between localised and delocalised polar clusters using this method, despite the absolute differences in value seeming small.

4.7.2 Analysis of *R. sphaeroides* McpB and McpB*

Validation of this method using the Tsr receptor allowed analysis of the McpB protein and McpB* variant in the *E. coli* systems. Expression of fluorescent fusions of these proteins in the UU2612 background will allow analysis of amount of cellular fluorescence present at the polar regions compared to lateral regions. The use of a strain lacking its native receptors in this case is beneficial due to the prevention of uncontrollable amounts of native receptors preventing localisation to the cluster as well as the prevention of interactions with native receptors which may result in anomalous results.

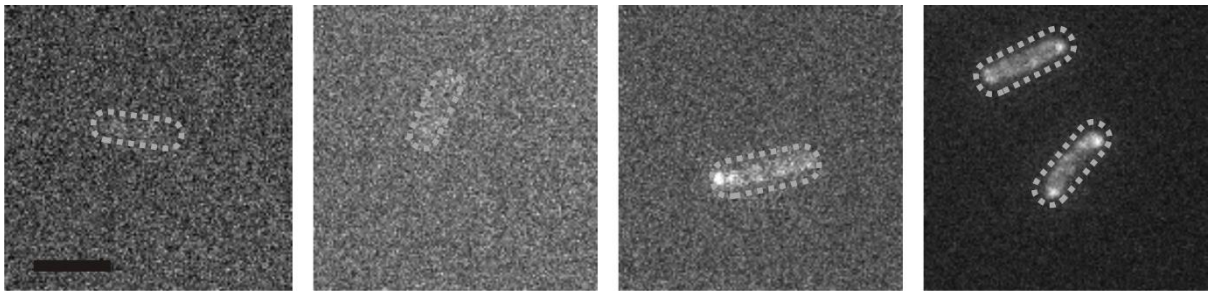

Figure 4-20 Localisation of McpB receptors expressed in cells lacking all other receptors (UU2612). Shown is increasing induction levels from left to right: 0 µM, 10 µM, 50 µM and 100 µM IPTG. In all images, contrast has been enhanced for maximum clarity. Cell outlines are drawn from the DIC images and shown here as a grey dotted line. Scale is consistent and scale bar in left image indicates 2 µm.

McpB localises predominantly to the poles, as would be expected from a typical MCP. However, unlike Tsr in this system, there is significant lateral fluorescence. This suggests that although McpB still has affinity for polar membrane regions, it may not be able to form tight polar clusters with the *E. coli* scaffold protein CheW.

The average fluorescence intensity profile shows that at lower induction levels, polar localisation is relatively strong, however, at higher induction levels, fluorescence becomes localised to the lateral regions much more strongly and much of the bias for polar fluorescence appears lost (Figure 4-21). At 50 µM IPTG, only 47±3% of fluorescence is localised to the poles of the cell. This is lower than wild type Tsr-RFP in a wild type background and is in fact the same value as that seen for Tsr-RFP localisation without the presence of a CheW scaffold. This was confirmed in the t test where the null hypothesis was accepted that the two data sets are identical with a p-value of 0.44. At 100 µM IPTG, this level decreases further to 45±3%.

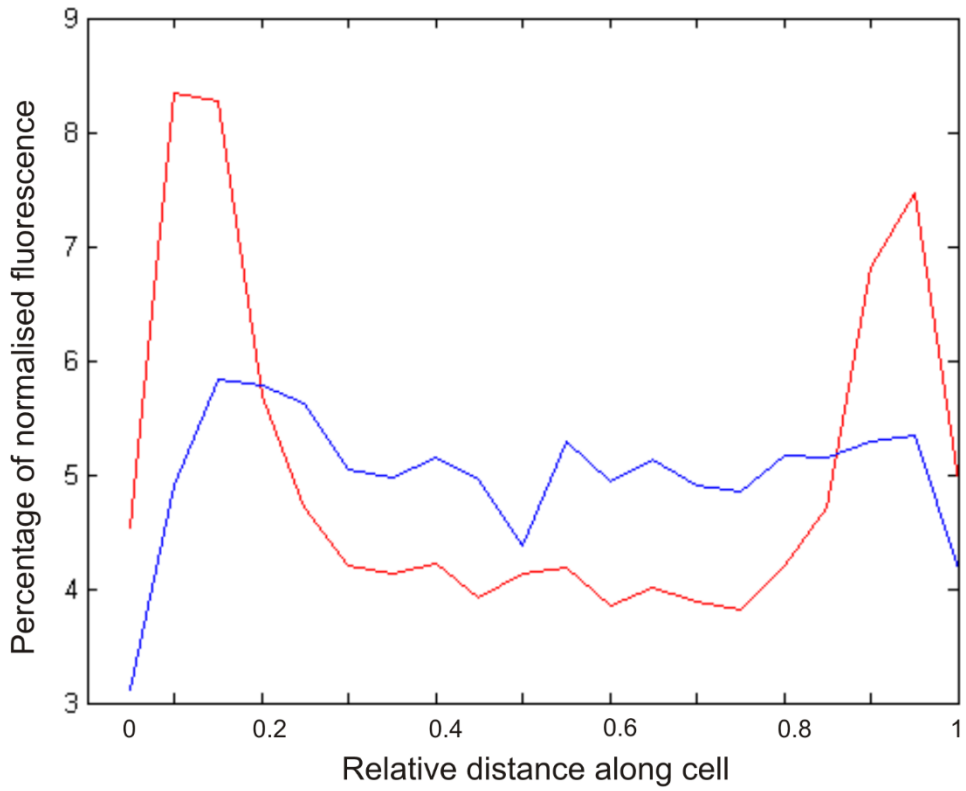

Figure 4-21 The normalised average fluorescence intensity of McpB-RFP across the length of cells lacking all other receptors (UU2612). Cells were induced with 50 µM IPTG (red) and 100 µM (blue).

This is below that seen for delocalised Tsr receptors and may suggest that McpB from *R. sphaeroides* has a lower native affinity for membranes at the cell poles over lateral membranes. Statistically, this is an accepted conclusion with the data set for 100I induction shown to be different to that of delocalised Tsr profiles with a p-value of 2.1410e-004. This shows that McpB does not appear to form tight polar clusters with the native *E. coli* CheW despite some preference for polar membrane regions.

McpB*-RFP localises predominantly to the poles as has been seen in other cases, however, it appears from the images that less lateral fluorescence is present (Figure 4-22). This suggests that McpB* has increased affinity for the cell poles over its wild type form.

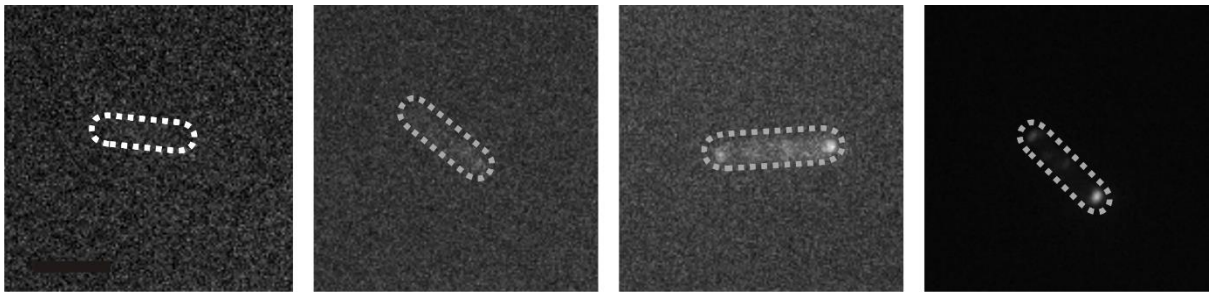

Figure 4-22 Localisation of McpB* variant receptors expressed in cells lacking all other (UU2612). Shown is increasing induction levels from left to right: 0 µM, 10 µM, 50 µM and 100 µM IPTG. In all images, contrast has been enhanced for maximum clarity. Cell outlines are drawn from the DIC images and shown here as a grey dotted line. Scale is consistent and scale bar in left image indicates 2 µm.

The profile of fluorescence across these cell is shown in Figure 4-23. This suggests that, unlike wild type McpB, increase of the induction levels actually results in increased localisation at the cell poles, presumably due to an increased ability to form stable homomeric interactions due to higher levels. The total polar fluorescence in this case is 47±5% and 54±6% for 50 µM and 100 µM IPTG respectively. The latter value matches that of Tsr receptors in this background, suggesting that polar localisation of McpB* is as wild type *E. coli* receptors. Statistical analysis shows that McpB* expressed with 100 µM IPTG does indeed show the same percentage polar localisation as Tsr with a p-value of 0.56. The

variant data set also differs statistically from McpB wild type. The null hypothesis that the two are the same was rejected with a p-value of $2.1e^{-016}$. This shows that variant McpB* is indeed localised at the poles significantly more than the wild type form showing that it has a higher propensity to form clusters. It is unlikely that McpB is able to interact with the native CheW scaffold due to the delocalisation of fluorescence seen in Figure 4-21. As a result, the increased polar fluorescence of McpB* seen here must be due to one of two possibilities. Either the mutation in this case has caused a structural change that allows greater interactions between MCP dimers and multimers independently of CheW, or, a low affinity interaction with CheW that is insufficient to form clusters with McpB has been somehow enhanced to allow clusters in this case.

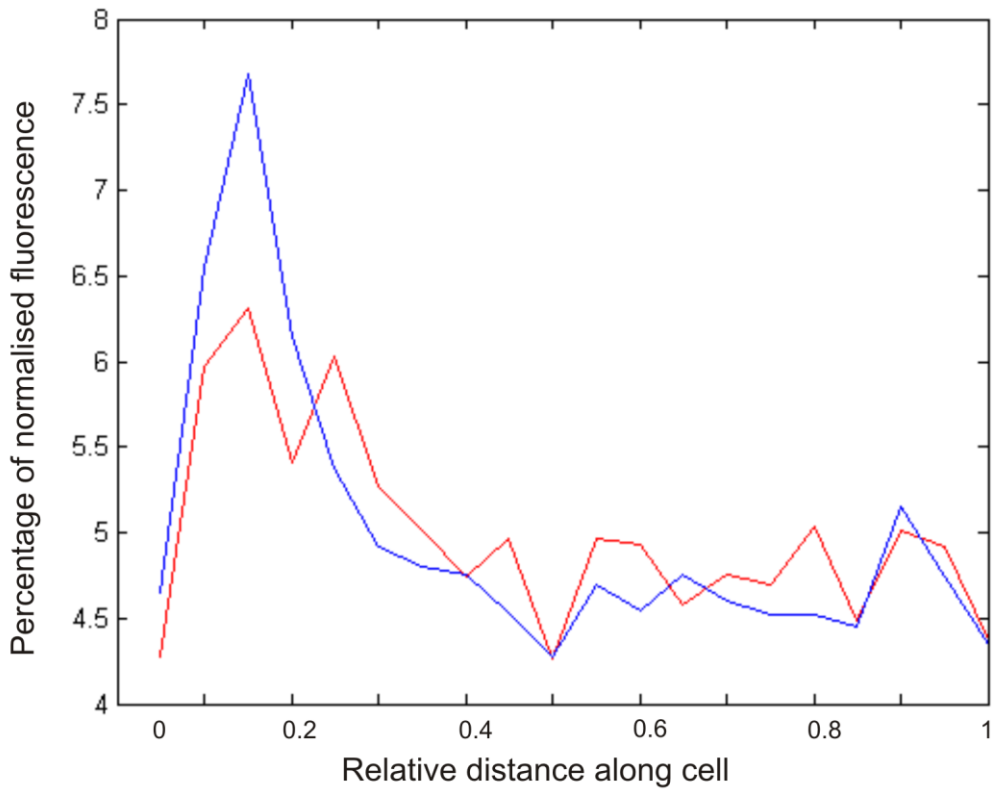

Figure 4-23 The normalised average fluorescence intensity of McpB*-RFP across the length of cells lacking all other receptors (UU2612). Cells were induced with 50 µM IPTG (red) and 100 µM (blue).

To determine which of these possibilities is more likely, clustering of McpB and variant McpB* was analysed in *E. coli* cells lacking other chemoreceptors and deleted for the native *cheW* gene. If a similar localisation pattern is seen without a CheW scaffold present then the tighter packing is independent of CheW. If the variant McpB* receptors remain diffuse, a CheW interaction is required for tight clustering.

McpB-RFP appears to have far less affinity for the polar membrane regions without the presence of a native CheW (Figure 4-24). This suggests that *R. sphaeroides* McpB may require an interaction with the native *E. coli* CheW in order to create the weak polar affinity seen previously (Figure 4-20). Plots of the fluorescence profile agree with this and show a lack of enrichment of fluorescence at the poles (Figure 4-25).

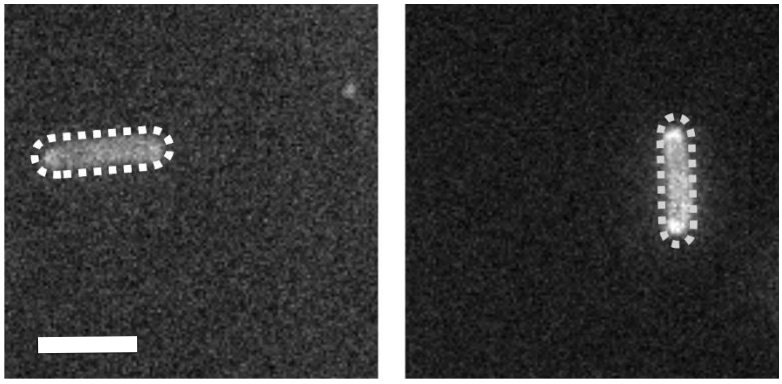

Figure 4-24 Localisation of McpB receptors expressed in cells lacking all other receptors and deleted for the native CheW scaffold (UU2836). Shown is induction with 50 µM (left) and 100 µM (right) IPTG. In all images, contrast has been enhanced for maximum clarity. Cell outlines are drawn from the DIC images and shown here as a grey dotted line. Scale is consistent and scale bar in left image indicates 2 µm.

Analysis of the fluorescence profile shows that induction of McpB-RFP with 50 µM IPTG causes 42±2% of fluorescence localised to the polar region. This rises to only 44±2% when induced with higher levels (100 µM) of IPTG. Both of these values are lower than that seen for McpB-RFP expressed in a strain containing native *E. coli* CheW. This agrees with the

suggestion that McpB may bind weakly to CheW in these strains but insufficiently to cause full localisation as is seen for Tsr.

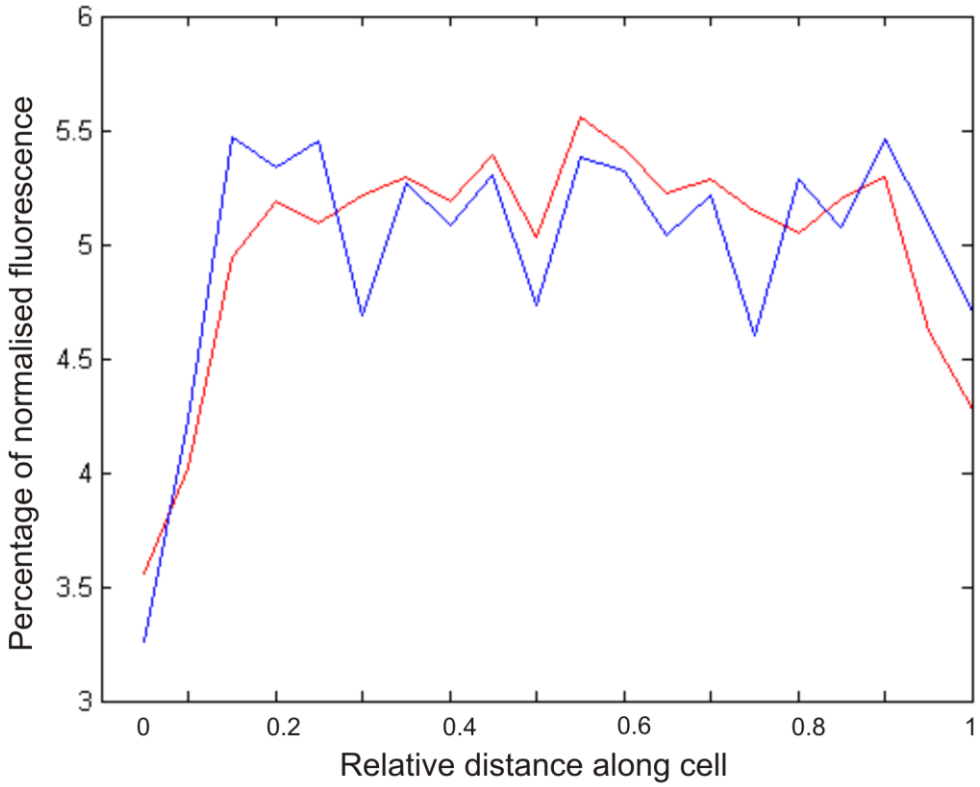

Figure 4-25 The normalised average fluorescence intensity of McpB-RFP across the length of cells lacking all other receptors and deleted for the native CheW scaffold (UU2836). Cells were induced with 50 µM IPTG (red) and 100 µM (blue).

McpB* appears to localise tightly in *E. coli* cells lacking a native CheW scaffold protein (Figure 4-26). This suggests that CheW is not required for the polar localisation seen previously and McpB* forms tight clusters in its absence. This suggests that McpB* has increased affinity for cluster formation and as there are no other chemoreceptors or CheW scaffold proteins, the tighter clustering seen here is likely to be due to an increased interaction to other receptor dimers.

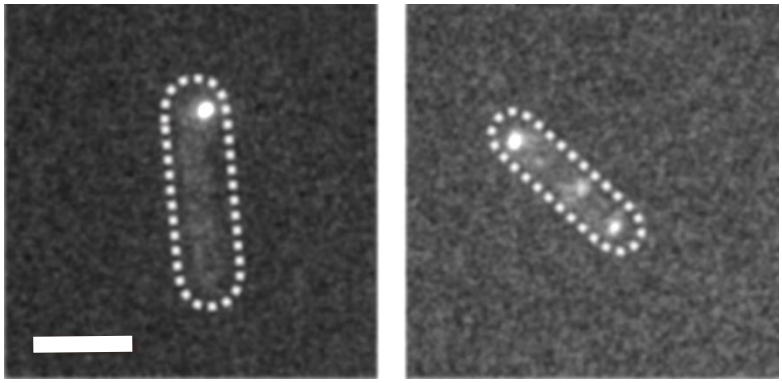

Figure 4-26 Localisation of McpB* receptors expressed in cells lacking all other receptors and deleted for the native CheW scaffold (UU2836). Shown is induction with 50 µM (left) and 100 µM (right) IPTG. In all images, contrast has been enhanced for maximum clarity. Cell outlines are drawn from the DIC images and shown here as a grey dotted line. Scale is consistent and scale bar in left image indicates 2 µm.

Analysis of fluorescence profile plots of these strains, as has been done previously does not show the increase in clustering seen from the microscopy images (Figure 4-27). A sharp peak is seen at one pole, particularly under higher induction levels (Figure 4-27 blue line). This result matches the microscopy images, however, analysis of polar localisation of fluorescence in this strain shows that only 46±4% and 48±4%, for 50 µM and 100 µM IPTG induction respectively, of fluorescence was localised to the poles. This is statistically, significantly different from the wild type Tsr protein localisation with a p-value of 5.6384e-010, showing that the localisation is not similar to that seen for *E. coli* Tsr receptors. These values, however, reflect a value closer to the 47% polar fluorescence exhibited by Tsr lacking the native CheW scaffold. This discrepancy is explicable through analysis of the images by eye. As can be seen in Figure 4-26, the fluorescence is localised to a very tight spot at one pole. This results in a comparatively low relative average fluorescence at the poles during the analysis due to the small region of the cell occupied by the polar spot. It may be the case that in the absence of CheW, the McpB* variant protein is able to localise to an even tighter region than when *E. coli* CheW is present, however, this conclusion is unable to be statistically verified with these methods.

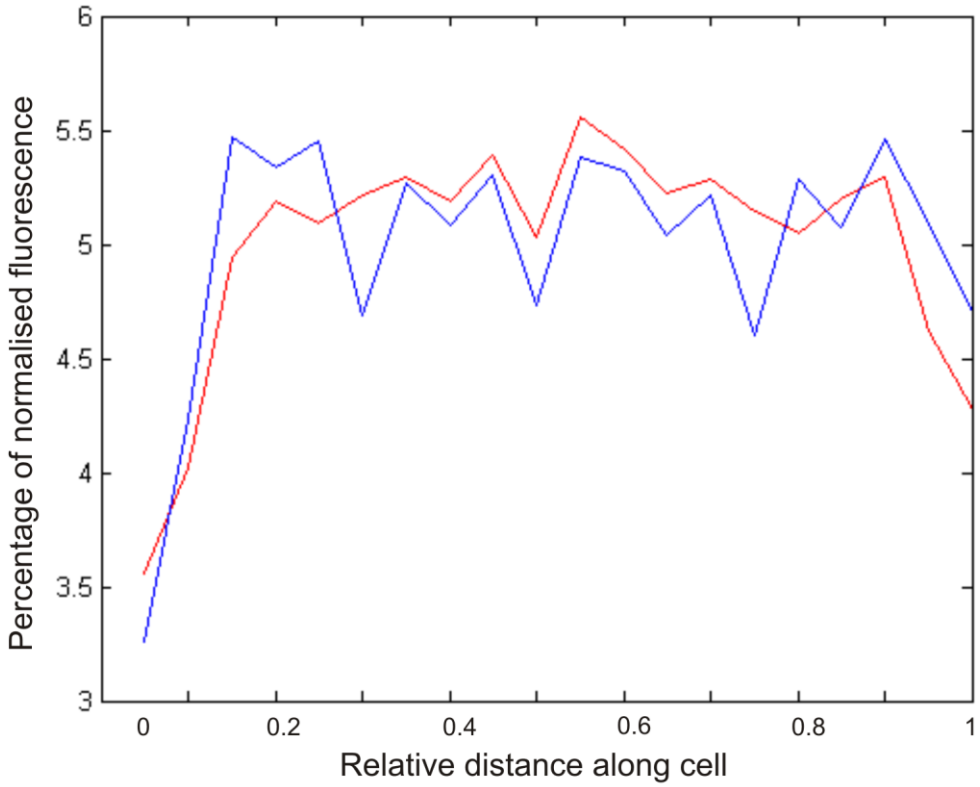

Figure 4-27 The normalised average fluorescence intensity of McpB*-RFP across the length of cells lacking all other receptors and deleted for the native CheW scaffold (UU2836). Cells were induced with 50 µM IPTG (red) and 100 µM (blue).

These data together suggest that variant McpB* causes a signalling shift in *E. coli* cells by increasing density of the cluster in some way. One possibility for the cause of this change in density is an increase in MCP flexibility, resulting in a larger average volume occupied by individual receptors. An increased flexibility would also lower the favourability of any interactions created, such as MCP:MCP and MCP:scaffold, both of which appear affected here. These results suggest that an increased cluster stability occurs through either a slight increase in interaction with the scaffold proteins, which then allows signalling to occur, or through causing a higher affinity for array formation overall by allowing closer contacts to other receptors in the array. The data thus far suggests that an interaction with the scaffold protein does occur and so may be important in the change seen, but it also appears that an increase in clustering occurs in the absence of CheW. This suggests that array formation is

more favourable for the variant protein even in the absence of scaffold proteins. Tighter clustering of the chemoreceptors therefore, could in turn result in increased scaffold protein binding.

4.8 Localisation of McpB in *R. sphaeroides*

In order to determine whether this effect is not an artefact of non-native expression it is necessary to analyse the localisation of McpB and its variant form in native *R. sphaeroides* arrays. McpB-RFP and McpB*-RFP were expressed from the same pIND4 vector used for the *E. coli* studies in a wild type WS8N *R. sphaeroides* background. The fluorescence localisation in these strains was then analysed to determine whether McpB localises to the polar cluster as has been seen previously in *R. sphaeroides* for other MCPs (Wadhams et al., 2000). The localisation of fluorescence was also analysed to determine whether localisation changes for the variant McpB* protein, as has been seen in the *E. coli* system.

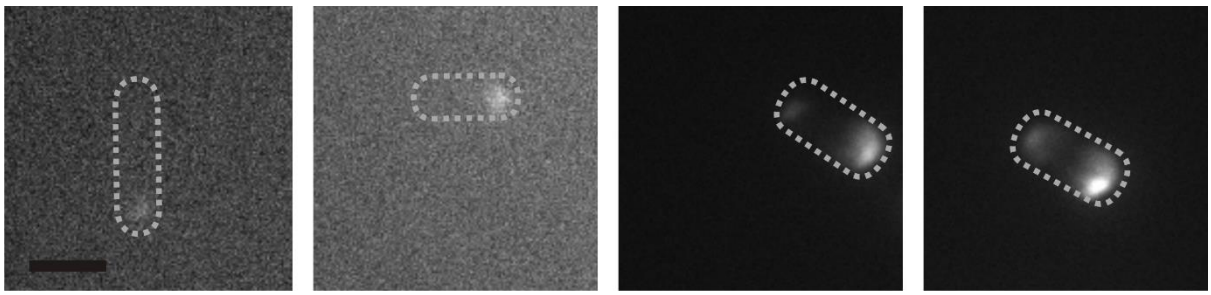

Figure 4-28 Localisation of McpB-RFP in wild type *R. sphaeroides* cells (WS8N). Shown is increasing induction levels from left to right: 0 µM, 10 µM, 50 µM and 100 µM IPTG. In all images, contrast has been enhanced for maximum clarity. Cell outlines are drawn from the DIC images and shown here as a grey dotted line. Scale is consistent and scale bar in left image indicates 1 µm.

McpB-RFP localises preferentially to the polar regions of the cell in *R. sphaeroides* with some lateral fluorescence discernible in what is a similar localisation pattern to that seen for other native *R. sphaeroides* MCPs (Figure 4-28) (Wadhams et al., 2000). This is the first time, localisation of McpB has been analysed in *R. sphaeroides*. Notable is that the gene for

McpB is located on *cheOp1*, the locus not expressed under normal laboratory conditions. This operon codes its own CheW scaffold protein $CheW_1$. It is therefore interesting that McpB-RFP is localised normally in WS8N cells in these conditions and suggests that there is redundancy between the *R. sphaeroides* CheW proteins. Alternatively, there may be a further role of $CheW_1$ that is not merely enabling scaffold formation. This role cannot be analysed through these localisation studies but may be interesting to study in future.

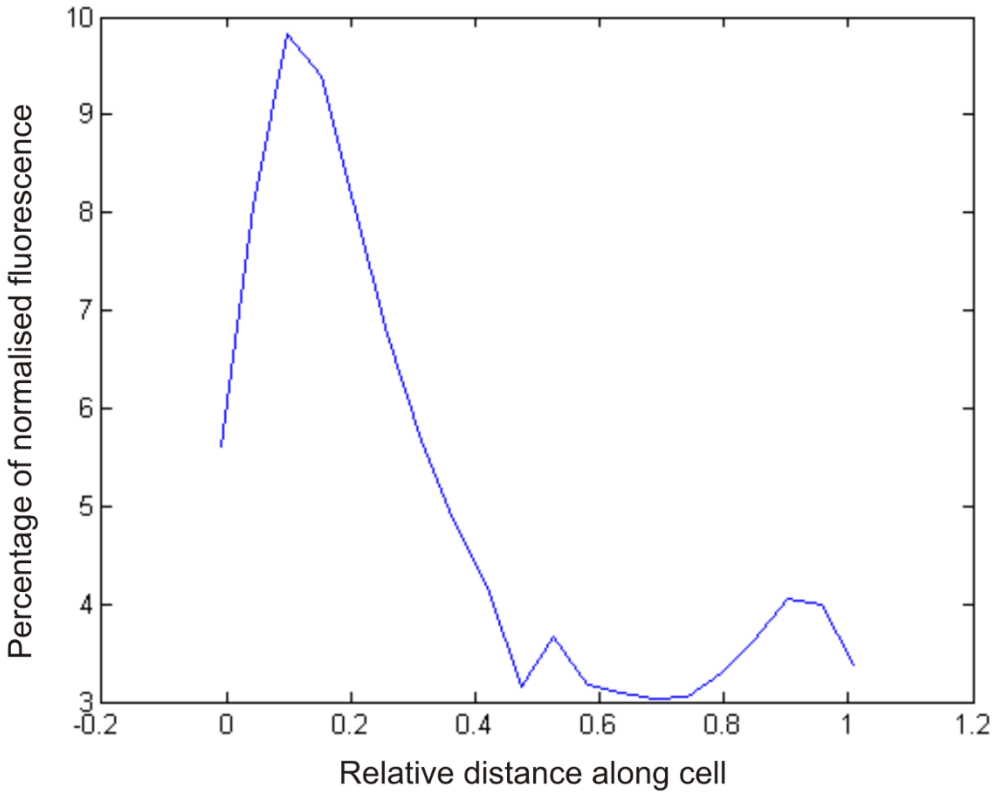

Figure 4-29 The normalised average fluorescence intensity of McpB-RFP across the length of wild type *R. sphaeroides* cells (WS8N). Cells were induced with 50 µM IPTG.

Analysis of the fluorescence profiles of these cells shows a single large peak corresponding to fluorescence density localised to a single pole of the cell. A smaller peak is present at the other pole location. This shows that *R. sphaeroides* MCPs have a much stronger bias for one pole over the other which may merely be due to the smaller cell volume making it more

stable for a single large cluster. This would prevent stable additional clusters forming until the cell becomes larger during replication.

The total polar fluorescence in this case is 51±6%, however, 33% of this is from a single polar region. Given that *cheOp1* in *R. sphaeroides* contains the genes for both McpB and CheW1, it could be assumed that McpB would need $CheW_1$ expressed in order to localise to the cluster. But, *cheOp1* is not expressed under normal laboratory conditions and therefore this result suggests that McpB is localised to a stable array at the poles via the *cheOp2* scaffold proteins $CheW_2$ and $CheW_3$. This has not been shown previously and is somewhat unexpected. If this is the case, then why does *R. sphaeroides* retain $CheW_1$?

Analysis of the localisation of the variant McpB*-RFP protein also shows discreet polar fluorescence localisation (Figure 4-30). In this case, very little lateral fluorescence can be seen, suggesting that tight clusters do form at the poles of the cell and that they may be held in a more stable arrangement than the wild type McpB. This would support the data seen for the *E. coli* studies suggesting that tighter clustering is caused by the variant McpB* (chapter 4.7.2).

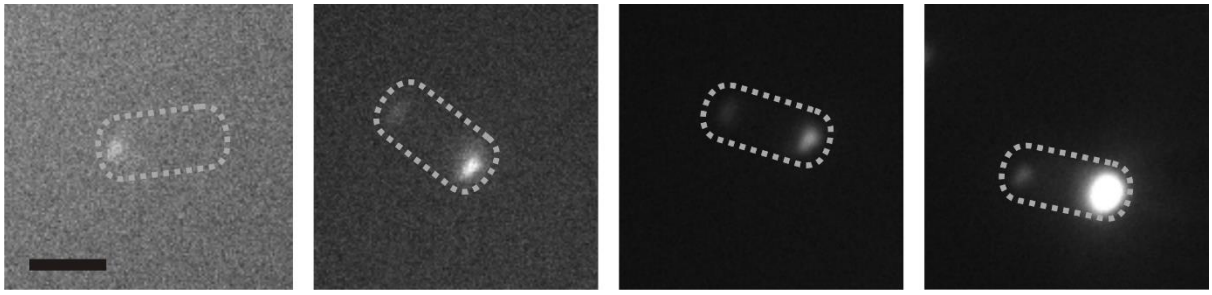

Figure 4-30 Localisation of variant McpB*-RFP in wild type *R. sphaeroides* cells (WS8N). Shown is increasing induction levels from left to right: 0 µM, 10 µM, 50 µM and 100 µM IPTG. In all images, contrast has been enhanced for maximum clarity. Cell outlines are drawn from the DIC images and shown here as a grey dotted line. Scale is consistent and scale bar in left image indicates 1 µm.

Analysis of the fluorescence profile of these cells agrees with this suggestion also. A similar large peak exists at one pole of the cell with, again, a smaller peak at the other pole. In this case, however, the large peak appears sharper with 36% of cellular fluorescence localised to this region and 54±6% localised to the poles in total. This also suggests a slight increase in clustering at the poles upon mutation of the McpB gene. Again, this conclusion is shown to be statistically correct with the t-test showing that the null hypothesis that the two data sets are the same is rejected with a p-value of 0.015. Taken together with the *E. coli* data it agrees with the conclusion that the signalling state of the polar cluster is shifted by increasing its stability.

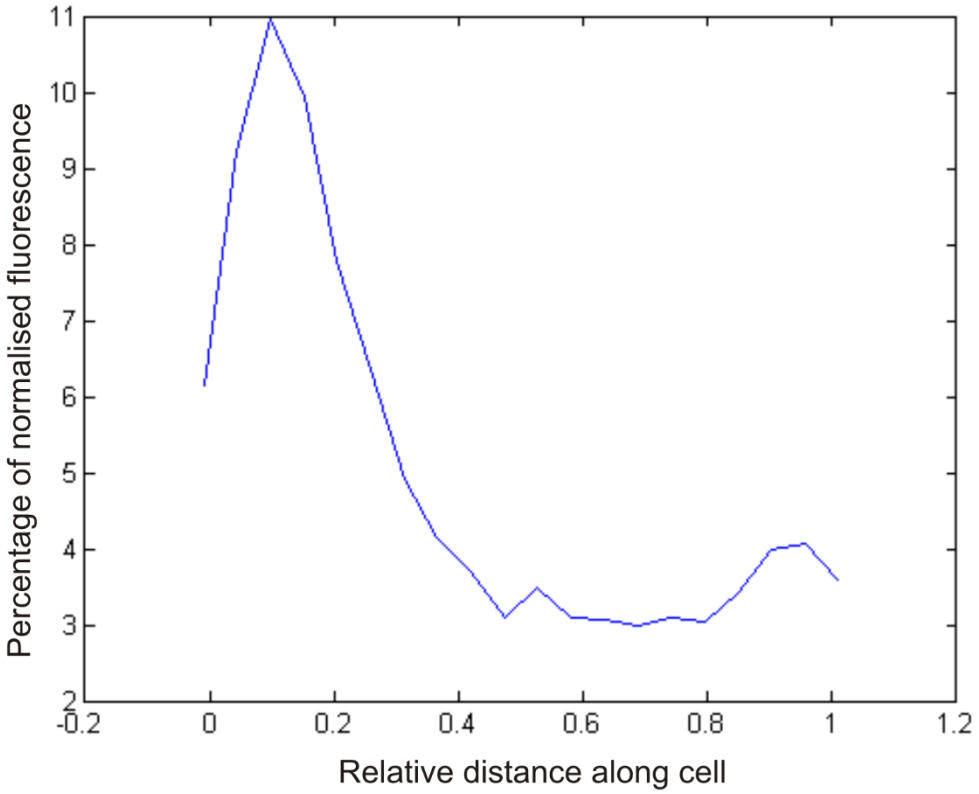

Figure 4-31 The normalised average fluorescence intensity of McpB*-RFP across the length of wild type *R. sphaeroides* cells (WS8N). Cells were induced with 50 µM IPTG.

Deletion of CheOp2 from WS8N cells removes the scaffold proteins $CheW_2$ and $CheW_3$ and also the kinase $CheA_2$ that should together contribute to the formation of a stable polar

cluster. This should enable analysis of whether the McpB* variant causes increased interactions between other MCP dimers independently of the scaffold in its native system. 50 µM IPTG expression was chosen for each case as cellular fluorescence levels appeared similar in most cells across the data sets and previous fluorescence analysis at this expression level showed similar fluorescence levels (Chapter 4.3). Figure 4-32 (left) shows that in the absence of a scaffold, McpB-RFP still localises preferentially to the polar membrane regions. It loses bias for one pole over another, however, and appears to form loose clusters at both poles. McpB*-RFP, however, retains tight localisation at one pole and appears still to form a tight cluster independently of the scaffold proteins. This supports the conclusion that in *E. coli* and *R. sphaeroides*, the McpB* variant causes tighter clustering by allowing closer interaction with other MCP dimers independently of the scaffold proteins. This does not however, rule out a role for a weak interaction of *E. coli* CheW with McpB.

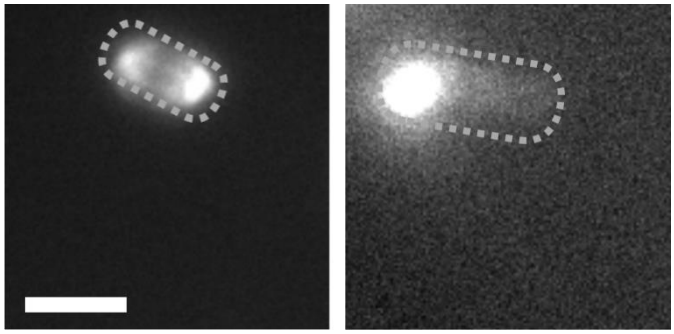

Figure 4-32 Localisation of McpB-RFP (left) and McpB*-RFP receptors in a background deleted for second chemotaxis operon (*cheOp2*) which contains the necessary scaffold proteins for polar cluster chemoreceptor localisation (JPA910). McpB-RFP expressed from pIND4 with 50 µM IPTG. In all images, contrast has been enhanced for maximum clarity. Cell outlines are drawn from the DIC images and shown here as a grey dotted line. Scale is consistent and scale bar in left image indicates 1 µm.

Data shown in this chapter supports the conclusion that locking the signalling state of the receptor to a ‘kinase-on’ conformation causes a tighter cluster formation than the native unlocked receptor. There are two explanations for the tighter cluster formation:

- Locking the receptor in the ‘kinase-on’ state allows greater interaction with the scaffold protein and thus in wild type *E. coli* allows tight cluster formation. This may be important if the interaction to *E. coli* CheW is of low affinity but may still form. This new interaction with CheW allows signalling through to CheA and thus the increased tumbling
- Locking the receptor causes a tighter MCP array by enabling closer interactions between trimers yet does not increase *E. coli* CheW affinity for McpB. This would allow for the cooperative effect on signalling which is hypothesised in chapter 4.7.

Based on the information gathered previously on the ability of McpB to signal through the *E. coli* chemotaxis system, it is unlikely that the former hypothesis is correct. As a result it is likely that tighter receptor clustering within the array is important in the mechanism by which McpB* causes an increase in kinase output. Thus, a model of signalling through the array that includes this change in clustering and its effect on CheA output is likely to be more accurate than a standard allosteric signalling model. It is possible that only a weak interaction between *E. coli* CheW and McpB exists and that by shifting the native activity, additional stability allows this weak interaction to form. Either of these scenarios would account for the increased clustering seen in some recent studies as well as the two separate states of receptor seen in some tomography studies (Khursigara et al., 2008b) (Vaknin and Berg, 2008). Determining whether CheW binding is altered by the mutation should be possible by analysing the affinity of CheW proteins to the chemoreceptor array.

4.9 Turnover of scaffold proteins to show interaction strength

One possibility for the mechanism of signalling through the array is that activation causes a tighter interaction of the chemoreceptor array to the scaffold and kinase proteins. A closer interaction would result in a greater chance of the specific interactions forming that cause kinase activity to increase. This mechanism would support what is seen when variant McpB is expressed in RP437 cells. It is possible that McpB* forms a tighter cluster than McpB. if this is the case, flexibility will be more limited and thus interactions with the kinase would be more favourable, which in turn increases the chance of the kinase being activated. This mechanism prevents the need for large structural shifts in the cytoplasmic domain which have been shown to be unlikely due to the small free energy change provided by ligand binding (Cheung and Hendrickson, 2009).

If the variant protein McpB* causes tighter binding to the scaffold, it would be possible to view this change in interaction affinity through fluorescence recovery after photobleaching (FRAP). This technique measures the recovery of fluorescence in a bleached region and thus determines turnover in and out of that region. When the fluorescence originated from a tag affixed to a protein that is bound within that region the recovery corresponds to the ability of that bound protein to dissociate. As a result it gives a measure of binding affinity for the tagged protein to its scaffold at the bleached region. As the receptors bind more tightly, turnover of the scaffold components will decrease and thus recovery of a bleached spot will decrease also. The turnover of scaffold proteins has been analysed previously and shows that CheW and CheA exchange within both a short and long time scale (Schulmeister et al.,

2008). The short time-scale recovery is proposed to correspond to turnover within the cluster and the longer recovery to turnover to and from the whole cluster.

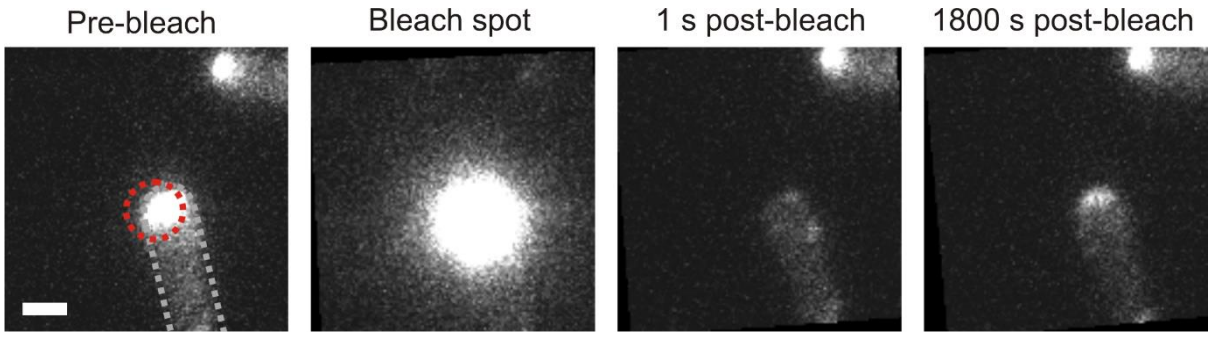

Figure 4-33 FRAP images showing $CheW_3$-CFP in wild type *R. sphaeroides* cells (JPA1415) expressing McpB from the pIND4 plasmid at selected time points during the sequence. Shown are the initial fluorescence, the bleaching event, 1 second post bleach and the final image of a 30 minute image sequence showing the fluorescence recovery. Plasmid expression was induced with 50 µM IPTG and cells kept in chloramphenicol during time course. In the initial frame the bleach spot is outlined with red dotted line and the cell outlined with a grey dotted line, contrast has been enhanced for clarity. Scale bar is 1 µm.

Wild type McpB was expressed in JPA1415, a strain expressing $CheW_3$ with a C-terminal CFP fusion from its native promoter. This allowed the visualisation and bleaching of the $CheW_3$ protein. The advantage of using McpB expression in these cells is that this receptor is not normally present, therefore, its expression can be controlled without the need for further genetic manipulation of the host. Cells were imaged in a custom-built microscope that allows simultaneous FRAP and epi-fluorescent laser excitation. Cells were grown to mid-log phase and then spun down and resuspended in M22 minimal media containing chloramphenicol. This was to prevent new protein being created and so limiting the turnover seen to that within the cluster itself. Images were initially taken to line up the bleach spot and then 5 pre-bleach images were taken at 1 s intervals. The polar cluster was then partially bleached to allow analysis of diffusion of CheW molecules within the cluster. 30 images were then taken immediately after bleaching at 60 s intervals to measure recovery of the bleached region (selected frames in Figure 4-33). Recovery of fluorescence was analysed

using the MATLAB plugin easyFRAP (Rapsomaniki et al., 2012). This program allows correction for background fluorescence and whole-cell bleaching by defining additional regions of interest (ROIs). Curves are then normalized between 0 and 1 for immediately post bleach and the pre-bleach maximum respectively. The total recovery of $CheW_3$ can then be analysed by drawing the horizontal asymptote of the recovery line. This allows the value of $t_{1/2}$ (the time taken to reach half maximal recovery) to be analysed which gives a value relating to the diffusion of molecules in and out of the bleached spot. This in turn relates in this case to the affinity of CheW proteins for the cluster as slower diffusion into the bleached spot denotes slower turnover of the bleached CheW molecules bound within the bleached spot.

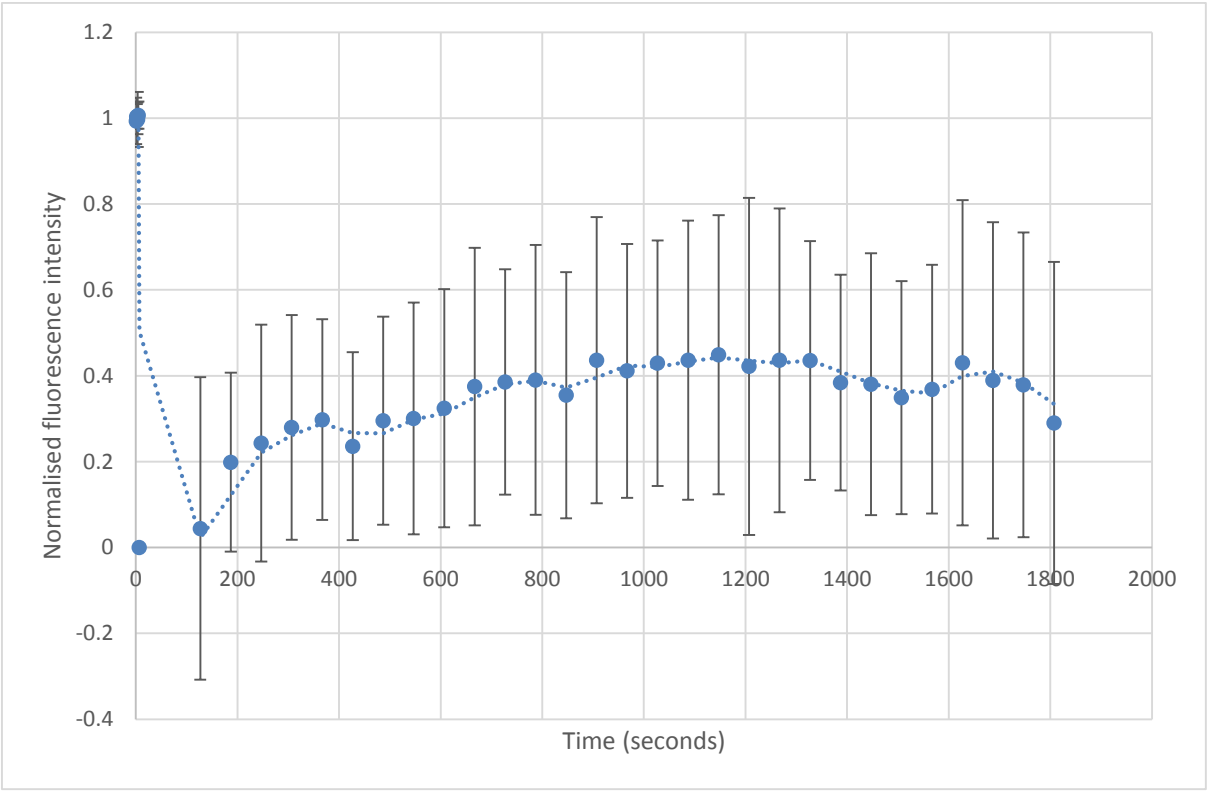

Figure 4-34 Normalised recovery of $CheW_3$-CFP fluorescence after bleaching in cells expressing McpB. Fluorescence intensity was normalised to 1 and 0 at maximum (initial) and minimal (immediately post-bleach) levels. Error bars are standard deviation around the mean.

Analysis of $CheW_3$-CFP in JPA1415 cells shows that after 30 minutes only 40% maximal fluorescence intensity is reached (Figure 4-34). The half time for diffusional recovery ($t_{1/2}$) can be defined as the time taken for cells to reach half their maximal recovery value (in this case 40% of its original). For the case of JPA1415::pIND4B, this is approximately 250 s. This shows that $CheW_3$ does indeed turnover within the polar cluster, however full recovery does not occur. This may be due to most of the cellular fluorescence intensity being present at the polar cluster to begin with and therefore there is relatively little diffuse $CheW_3$ in the cytoplasm. With the presence of chloramphenicol, no new $CheW_3$-CFP is created and so there is very little is free to fully recover the fluorescence. If ~100% of $CheW_3$ exists at the poles and 50% is bleached, even if the whole array turns over within 30 minutes, only 50% of fluorescence intensity will be recovered at the bleached spot.

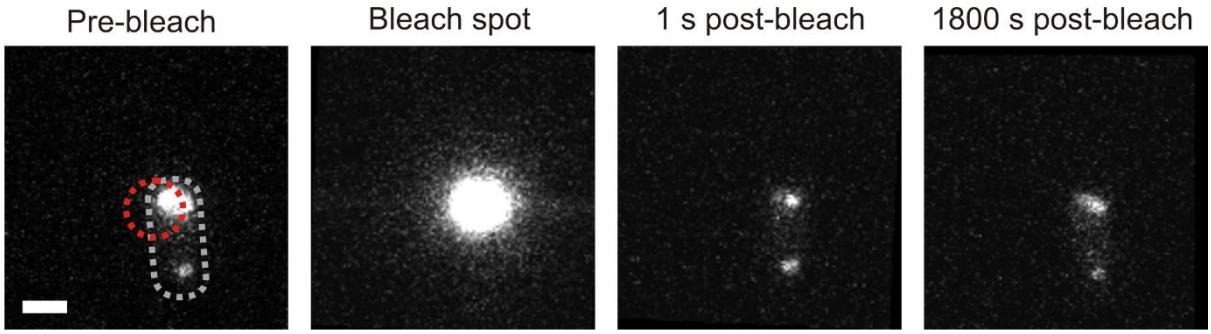

Figure 4-35 FRAP images showing $CheW_3$-CFP in wild type *R. sphaeroides* cells (JPA1415) expressing McpB* from the pIND4 plasmid at selected time points during the sequence. Shown are the initial fluorescence, the bleaching event, 1 second post bleach and the final image of a 30 minute image sequence showing the fluorescence recovery. Plasmid expression was induced with 50 µM IPTG and cells kept in chloramphenicol during time course. In the initial frame the bleach spot is outlined with red dotted line and the cell outlined with a grey dotted line contrast has been enhanced for clarity. Scale bar is 1 µm.

Expression of McpB* in JPA1415 also shows recovery of the cluster, seen Figure 4-35. Plotting the average normalized fluorescence time course shows that this recovery does not appear to be complete within the experimental time limit, as seen by the graph not reaching a plateau (Figure 4-36). Time frames longer than 30 minutes are not accurate with this

experimental set-up as cellular bleaching becomes a problem with greater exposure to light and this increases the error. However, extrapolation of the line, to a plateau, suggests a similar recovery maximum of 40%. This shows that the pool of $CheW_3$ available to exchange with the polar cluster does not change, as would be expected. However, in the case of JPA1415::pIND4B*, the $t_{1/2}$ is approximately 800 s or longer.

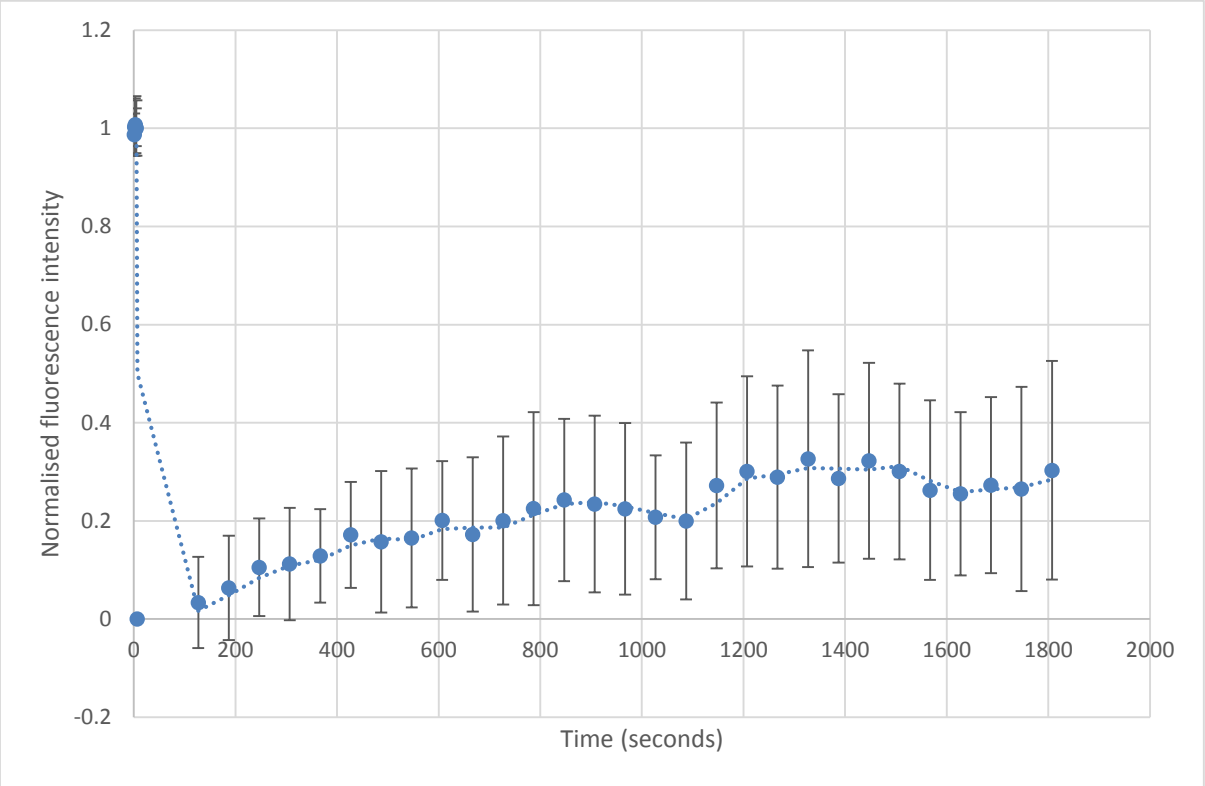

Figure 4-36 Normalised recovery of $CheW_3$-CFP fluorescence after bleaching in cells expressing McpB*. Fluorescence intensity was normalised to 1 and 0 at maximum (initial) and minimal (immediately post-bleach) levels. Error bars are standard deviation around the mean.

These recovery rates shows that $CheW_3$ exchanges into the bleached ROI at a much slower rate when the 'kinase-on' shifted variant McpB* is present compared to its wild type form. This reasons that the 'kinase-on' state binds the $CheW_3$ protein more strongly than the wild type. This suggests that the 'kinase-on' McpB* causes an increase in CheA activity due to an increased interaction with the scaffold caused by a more densely packed array. This is

the first comprehensive evidence supporting this model for signalling through the chemotaxis pathway.

If the CheW scaffold protein is bound more strongly by the chemoreceptors when in the 'kinase-on' state, it is reasonable to assume that CheA will also associate more strongly. The two proteins bind at the same region of the MCP and models have suggested that some residues may be important for interactions with both CheW and CheA (Piasta et al., 2013). As a result, assaying CheA binding by similar means should be able to determine whether this assumption is true.

Wild type McpB was expressed in JPA1497, an otherwise wild type *R. sphaeroides* strain that has CheA C-terminal CFP fusion expressed from its native promoter. The turnover of fluorescence at the cluster was then analysed in order to determine the stability of CheA binding at the polar cluster.

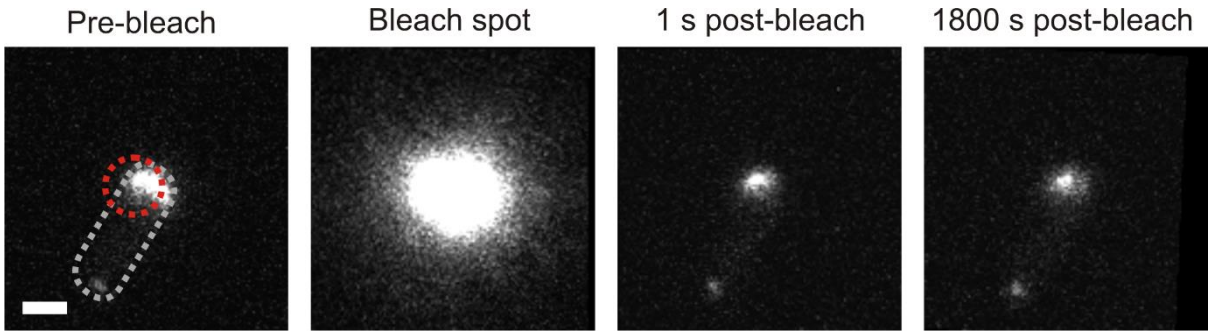

Figure 4-37 FRAP images showing $CheA_2$-CFP in wild type *R. sphaeroides* cells (JPA1497) expressing McpB from the pIND4 plasmid at selected time points during the sequence. Shown are the initial fluorescence, the bleaching event, 1 second post bleach and the final image of a 30 minute image sequence showing the fluorescence recovery. Plasmid expression was induced with 50 µM IPTG and cells kept in chloramphenicol during time course. In the initial frame the bleach spot is outlined with red dotted line and the cell outlined with a grey dotted line contrast has been enhanced for clarity. Scale bar is 1 µm

Analysis of the bleached CheA-CFP spot showed very little recovery of fluorescence at the polar cluster (Figure 4-37). As discussed, longer time frames using this experimental set-up increased error further and are therefore not possible. This suggests that $CheA_2$ is tightly

associated to the polar cluster in *R. sphaeroides*. The lack of $CheA_2$-CFP recovery at the polar bleach spot can clearly be seen in the plot of normalised fluorescence recovery (Figure 4-38). This shows that CheA is held more tightly than CheW at the cluster and therefore exhibits less turnover.

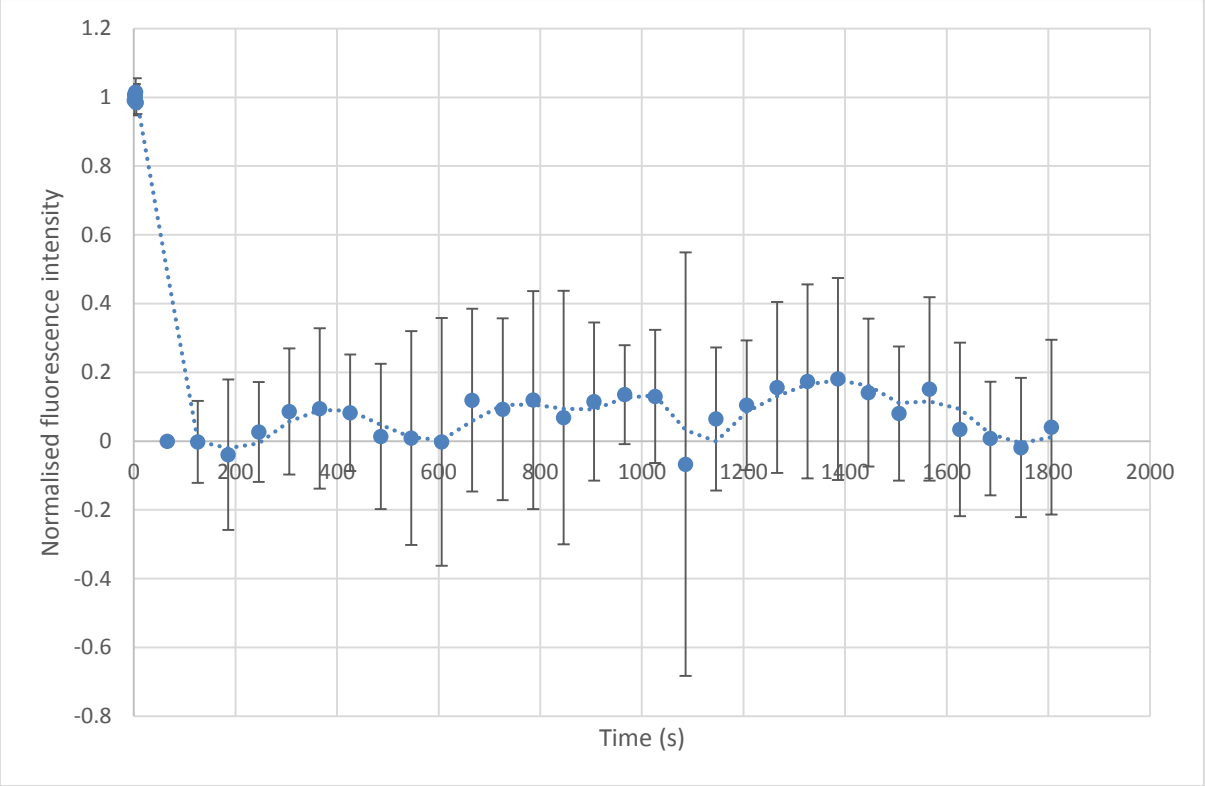

Figure 4-38 Normalised recovery of $CheA_2$-CFP fluorescence after bleaching in cells (JPA1497) expressing McpB. Fluorescence intensity was normalised to 1 and 0 at maximum (initial) and minimal (immediately post-bleach) levels. Error bars are standard deviation around the mean.

The analysis of CheW suggests that McpB* causes a tighter association to the polar array. However, as CheA does not exhibit any turnover in the presence of wild type McpB, it is unlikely that McpB* will show any change. Figure 4-39 shows that this is in fact the case.

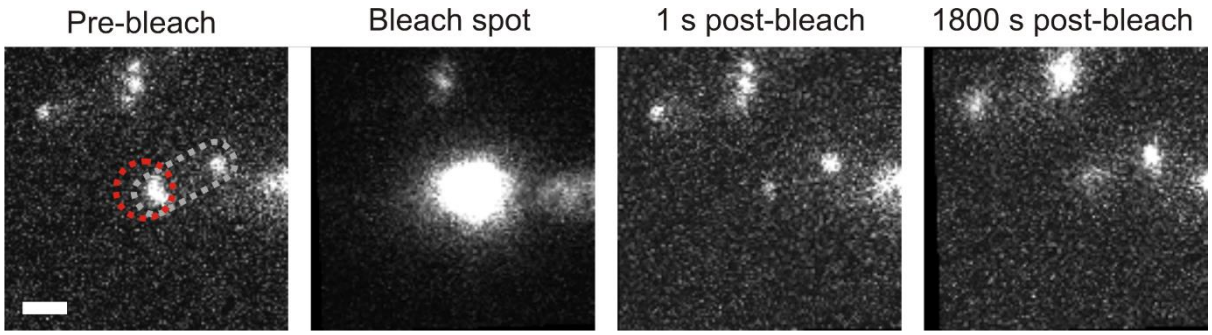

Figure 4-39 FRAP images showing $CheA_2$-CFP in wild type *R. sphaeroides* cells (JPA1497) expressing McpB* from the pIND4 plasmid at selected time points during the sequence. Shown are the initial fluorescence, the bleaching event, 1 second post bleach and the final image of a 30 minute image sequence showing the fluorescence recovery. Plasmid expression was induced with 50 µM IPTG and cells kept in chloramphenicol during time course. In initial frame the bleach spot is outlined with red dotted line and the cell outlined with a grey dotted line contrast has been enhanced for clarity Scale bar is 1 µm.

The normalised fluorescence recovery plot shows that CheA fluorescence does not recover during the course of the experiment. In addition, no enrichment of CheA at the bleached spot can be seen at all by the end of the time course. This suggests that CheA does not turnover at all during 30 minutes, suggesting that the $t_{1/2}$ could be very large indeed.

The lack of turnover during the 30 minute time course of this experiment is inconsistent with previous data (Schulmeister et al., 2008). This may reflect differences between species. It is possible *R. sphaeroides* $CheA_2$ binds McpB chemoreceptors much more strongly than *E. coli* CheA does to its own. This may explain why $CheA_2$ is unable to fully restore chemotaxis in an *E. coli* CheA deletion (Shah et al., 2000). It may also be the case that in the previous study, chloramphenicol was not used and only a 1 hr incubation at 4 °C was implemented to stop protein production. This may enable more diffuse protein to be present to recover the cluster but is unlikely to account for the whole effect.

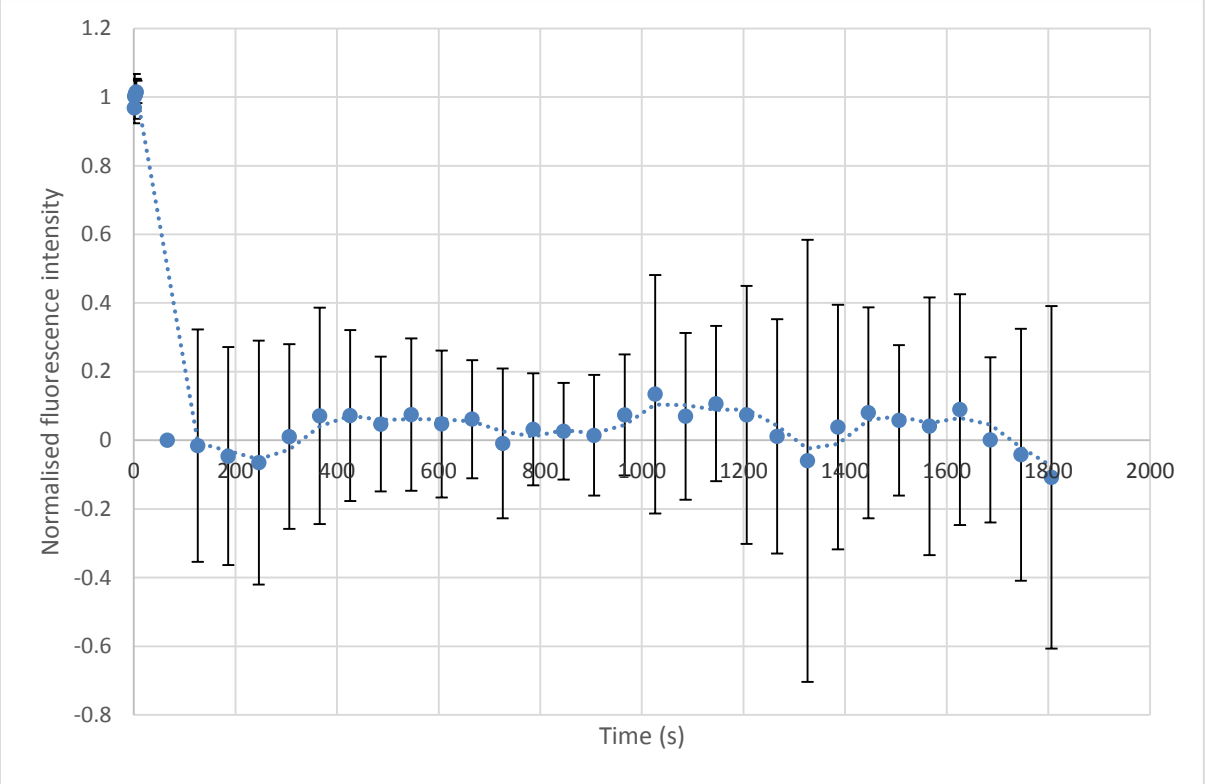

Figure 4-40 Normalised recovery of $CheA_2$-CFP fluorescence after bleaching in cells (JPA1497) expressing McpB. Fluorescence intensity was normalised to 1 and 0 at maximum (initial) and minimal (immediately post-bleach) levels. Error bars are standard deviation around the mean.

The FRAP data shows that CheW turnover is decreased by the variant McpB* protein, however, CheA turnover is not. This supports the first hypothesis suggested in the previous chapter that increased receptor interaction with the scaffold causes a change in signalling state of CheA. Taken with the fluorescence data, it is likely that McpB* both causes a change in affinity to CheW which may, in *E. coli,* enable a normally weak interaction to occur and increases MCP stability which increases inter-chemoreceptor interactions promoting a tight and stable signalling cluster. Both of these could be caused by decreased flexibility of the cytoplasmic domain. A highly flexible domain would be unlikely to associate to CheW if the interaction was ordinarily a weak one. In addition, it is unlikely to form stable interactions with other MCPs. If the MCP is made less flexible by the mutation of the TM2 helix (or by activation, in the native system), then a weak affinity for CheW may be

sufficient to form an association. In addition, decreased flexibility would allow tighter packing between MCP dimers due to the smaller average volume occupied by the receptor. As a result MCPs may signal by shifting between a flexible state that is unable to strongly bind the scaffold and thus activate the kinase and an inflexible stable state that is able to strongly bind the scaffold and thus activate the kinase. Flexibility of one dimer may affect its neighbouring receptors by an inability to complex with and thus stabilise them in turn. Adaptation of receptors is therefore likely to either stabilise or destabilise the cytoplasmic domain packing and thus favour a less or more flexible state.

4.10 Modelling of McpB

MCPs are flexible in their cytoplasmic region below the HAMP signal processing domain (Hall et al., 2012). This flexibility may decrease effective binding to a scaffold by lowering the average availability of the tip for interaction with CheA and CheW proteins. As a result, in an active state, the MCP should be less flexible and thus allow a stronger interaction with the downstream array proteins. If the mutation causing McpB* creates tighter clusters, it may be that inherently lower flexibility of the chemoreceptor allows tighter packing and possibly increased CheW interaction.

In order to analyse the flexibility of McpB, it was modelled both as its wild type and variant forms *in silico* to allow simulations of the motions undertaken in solution. This was achieved using the Modeller programme (Sali and Blundell, 1993). Alignments were made of McpB against the Tsr receptor and then the structure was threaded onto the model of Tsr previously built (Hall et al., 2012). These models were then inserted into a simulation box which is filled with water, ions and lipids. Models were then converted to coarse-grain representation which converts every 4 atoms to a single particle of similar overall properties and thus uses

less computational power for the same atomistic simulation. An initial simulation was run to allow lipid layer assembly which forms a bilayer around the MCP in the most favourable region. After this structure was checked to determine correct bilayer assembly, a 1 μs simulation was run to analyse solution flexibility.

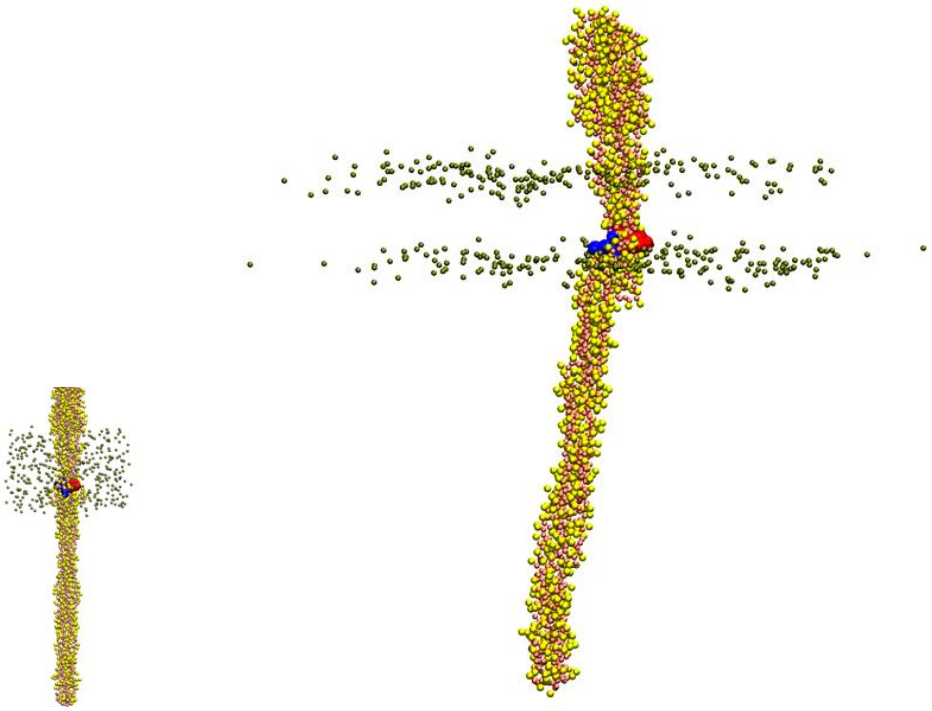

Figure 4-41 Final frame and, inset, the initial frame of the simulation of 1 μs CG simulation of McpB modelled into a phosphatidylglycerol (PG) bilayer. Lipid head groups are shown in dark green and the MCP particles are shown in yellow. Labelled as red and blue spheres are the tryptophan residues from each chain of the dimer that form the bilayer interface. The tryptophan was one of the residues mutated to form McpB*. Water molecules, ions and lipid tails have been omitted for clarity.

Figure 4-41 shows the final frame of the simulation of McpB and shows that the model indeed resembles a predicted MCP structure and the bilayer has assembled around the predicted TM region. The interfacial tryptophan residues sit at the predicted interface between solution and lipid head groups anchoring the position of the TM portion. A small kink is present around the HAMP domain but the cytoplasmic domain overall is straight and the simulation shows that this domain undergoes small motions with no major

conformational shifts throughout the simulation, suggesting flexibility. The lack of major, non-native distortions, no abnormal bilayer interactions, and no evidence of lack of stability within the bilayer suggests that this structure is also a stable arrangement.

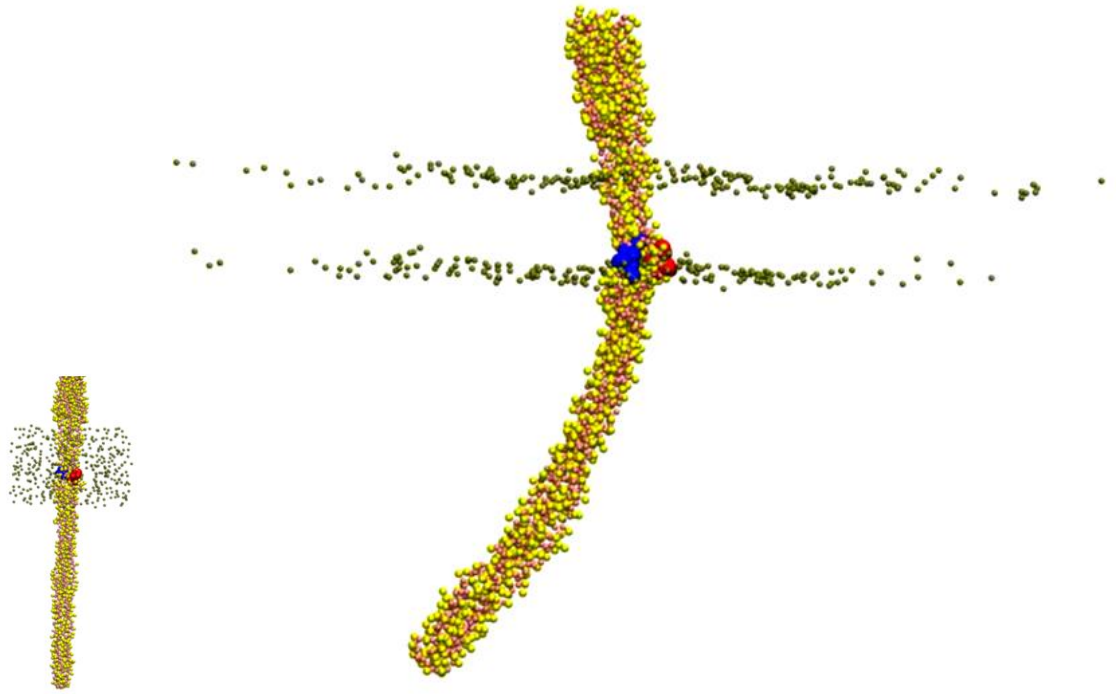

Figure 4-42 Final frame and, inset, the initial frame of 1 μs CG simulation of McpB* modelled into a PG bilayer. Lipid head groups are shown in dark green and the MCP particles are shown in yellow. Labelled as red and blue spheres are the tryptophan residues from each chain of the dimer that form the bilayer interface. The tryptophan was one of the residues mutated. Water molecules, ions and lipid tails have been omitted for clarity.

Figure 4-42 shows that the variant McpB* protein kinks around the same region but is much more curved overall in the cytoplasmic region. This does not directly fit with the model proposed by the fluorescence imaging data. However, when thought of in terms of the global MCP organisation it does comply with the proposed signalling model. MCPs exist in structural trimers of dimers (Endres, 2009) (Briegel et al., 2012). As such, each monomer requires a kink at the HAMP domain in order to come together with the trimer at the tip region. If the variant McpB* is less flexible and more kinked then it is more likely to form

a stable complex at the trimer interface and thus more likely to interact with the scaffold proteins and thus promote signalling.

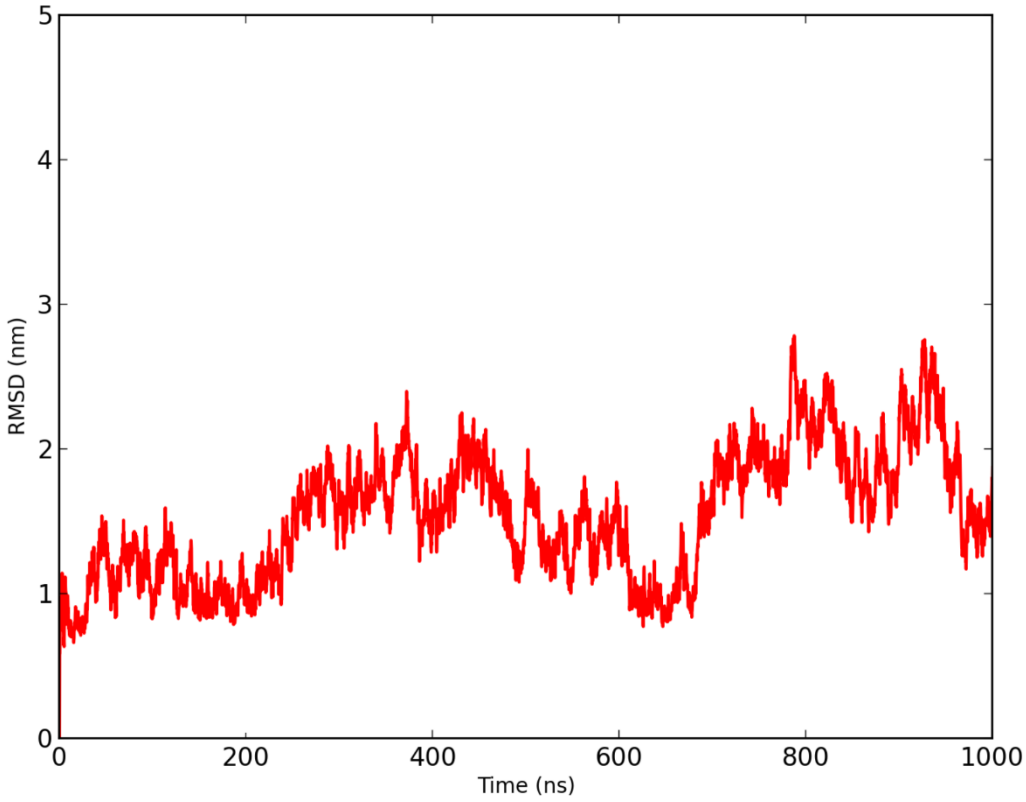

Figure 4-43 RMSD profile of McpB showing the change of position of each atom, in nm, between each frame through the 1 μs simulation. Higher values give an indication of higher average flexibility of the atoms analysed.

The RMSD profile gives a measure of disorder in the system. It measures the average change in position of each atom relative to the previous frame and so by measuring only the atoms of the protein through the simulation it is possible to determine how much its atoms move frame to frame. This gives a measure of the flexibility of the protein throughout the simulation. The RMSD of McpB shows an average motion of 1-2 nm between frames during the simulation showing that there is indeed some flexibility but that it is not likely to be due to protein instability.

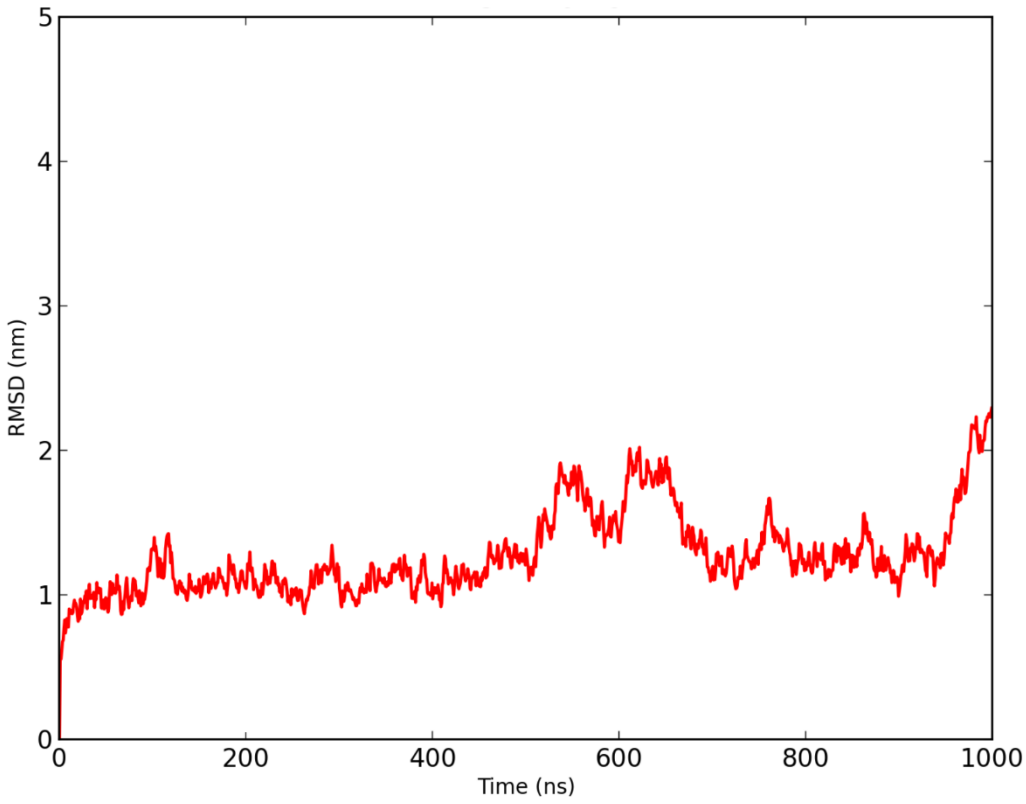

Figure 4-44 RMSD profile of McpB* showing the change of position of each atom, in nm, between each frame through the 1 μs simulation. Higher values give an indication of higher average flexibility of the atoms analysed.

The RMSD plot of the variant MCPB* protein shows a consistent average movement of approximately 1 nm between frames. In addition, there is far less noise in the system, visualised by a relatively straight line with fewer jumps. This is consistent with a more stable and therefore less flexible structure and supports the conclusion that the variant McpB* is indeed less flexible.

Analysis of the motion of the TM2 helix should confirm the predicted motion from the initial computation study (Figure 4-2). By analysing the centre of mass of the TM2 helix vs the average centre of mass of the lipids in the system it should be possible to determine the relative position of the TM2 helix in the bilayer between the wild type and variant McpB proteins.

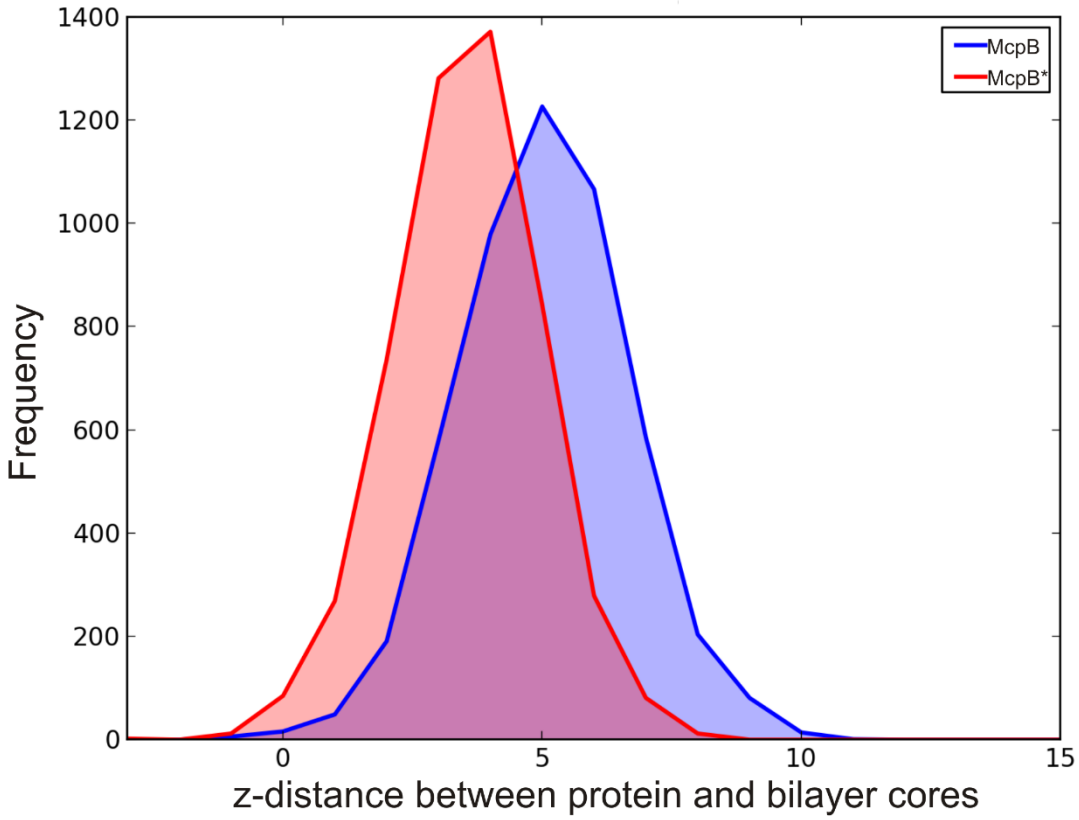

Figure 4-45 The relative distance in z-position, in angstroms, between the TM2 helix and bilayer cores throughout the simulation. Positions were placed into bins to give an account of the modal arrangement of between bilayer and helix through the simulation.

Analysis of this z-distance shift shows that variant McpB* TM2 sits approximately 1-2 Å closer to the cytoplasm than the TM2 in the wild type protein. This is as predicted by the computational modelling initially. As the interfacial residues are moved closer to the periplasm, the TM helix should move closer to the cytoplasm to prevent instability. Interestingly, the helix doesn't appear to shift as far towards the cytoplasm as the interfacial residues were moved (2-4 Å). This may account for the change in stability of the protein, the helix may initially be slightly too long to be fully stable in the bilayer, creating initial instability. The mutation may relax this instability, allowing more stability to be continued through to the HAMP and cytoplasmic domains which would account for the measured increase in scaffold interaction and kinase signalling seen.

4.11 Localisation in an adaptation deficient strain

As receptor clustering seems to be affected by the signal locking mutation on McpB, it should be possible to detect a similar change in response to signalling. This is difficult to test in wild type *R. sphaeroides* and *E. coli* cells as the adaptation pathways will quickly revert the receptors back to a non-signalling state in response to prolonged stimuli. However, if the cells are deleted for the adaptation system, then the array will be unable to adjust the sensitivity in response to stimuli and the effect should be retained. As a result, there should be a detectable difference between adaptation deficient clusters in minimal media and rich media.

In order to analyse this, an *R. sphaeroides* background was used that was deleted for the four cheB and cheR genes that are expressed under normal laboratory conditions: $cheB_1$, $cheB_2$, $cheR_2$, $cheR_3$ (Elayne Byles). In this background, wild type McpB and variant McpB* RFP c-terminal fusions were expressed from the pIND4 plasmid as in the previous chapter. Cells were grown to OD_{600nm} 0.4-0.6 and then 1 ml of cells was centrifuged at 1.5 x g for 1 minute. Cells were then washed in M22 minimal media (Appendix B) before being resuspended in 100 µL of either LB, Sux, or M22 media. A separate 100 µL of cells was resuspended in M22 to which the known *R. sphaeroides* attractant propionate was added to a final concentration of 100 µM. Localisation of RFP fluorescence was then analysed as previously to determine any differences in localisation between the conditions.

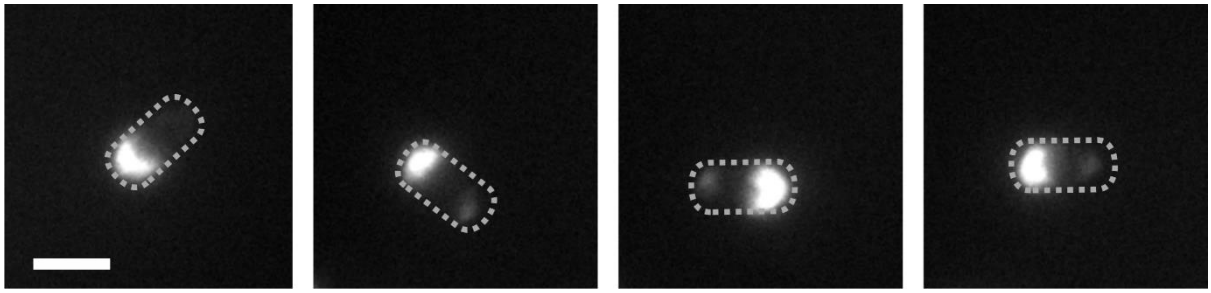

Figure 4-46 Localisation of McpB-RFP in adaptation deficient *R. sphaeroides* cells. Shown are example cell RFP fluorescence from (left to right) LB, Sux, M22+propionate and M22 media. In all images, contrast has been enhanced for maximum clarity. Cell outlines are drawn from the DIC images and shown here as a grey dotted line. Scale is consistent and indicates 1 μm.

In the case of the wild type protein McpB, it appears that the localisation patterns vary very little between conditions. In rich media, RFP fluorescence was localised to a tight cluster at, predominantly, a single pole of the cell (Figure 4-1). In minimal media, where a change in cluster affinity would be expected, a similar pattern of localisation was seen.

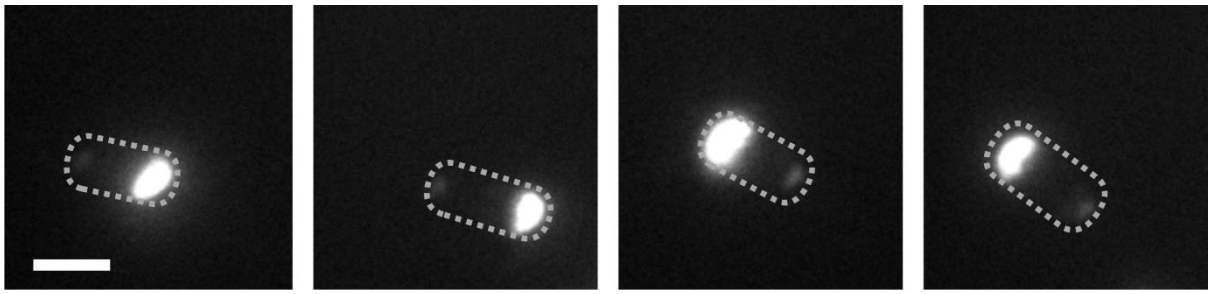

Figure 4-47 Localisation of McpB*-RFP in adaptation deficient *R. sphaeroides* cells. Shown are example cell RFP fluorescence from (left to right) LB, Sux, M22+propionate and M22 media. In all images, contrast has been enhanced for maximum clarity. Cell outlines are drawn from the DIC images and shown here as a grey dotted line. Scale is consistent and indicates 1 μm.

The McpB*-RFP fusion protein shows a similar pattern of localisation in the different media. It appears to be consistently localised to the poles of the cell with one pole being significantly favoured.

Protein	LB	Sux	M22+propionate	M22(minimal)
McpB	49±5(31)	50±5(31)	47±6(30)	48±5(30)
McpB*	47±6(29)	50±7(32)	50±6(33)	48±6(32)

Table 4-2 The percentage of normalised fluorescence intensity localised to the poles of *R. sphaeroides* cells lacking expression of a CheR/CheB adaptation system. Shown is the sum of the average normalised fluorescence located in the first and last 20% of the cell length with the standard deviation of each value. In brackets is the percentage localised to the brighter pole in each case.

Shown in Table 4-2 are the percentage of fluorescence localised to the poles in each condition for both the variant and wild type McpB-RFP chemoreceptor fusions. The total localised fluorescence in each case seems similar. Statistically, localisation in propionate only is significantly less than Sux for wild type McpB, with a p-value of 0.0036. The model of signalling previously suggested would predict tighter clustering for this condition as strong attractant occupancy of MCPs at the cluster should cause decreased scaffold binding. However, despite the change being statistically significant it is slight and is not statistically different from the localisation in minimal media. In the latter, the cluster should be locked in a 'kinase-on' state due to the lack of MCP ligand occupancy and should therefore be significantly more localised than when in the presence of a strong attractant. The same change is not seen in the variant protein in this case. In minimal media with propionate, the data sets are statistically the same as all other media tested for that protein.

This suggests that the localisation of McpB to the poles is not greatly affected by signalling or that we are unable to determine a large change using this method. If the latter is the case, it may be because all other MCPs are currently present in the polar cluster and this causes overcrowding with the addition of McpB. As a result it may be that the cluster already appears less tightly bound together and the change is masked by this. If it is the case that a change does not occur under the conditions of the experiment, it may be that in this system,

the scaffold proteins are bound tightly to the MCPs in all conditions and the effect on localisation of signalling is resultantly much smaller.

4.12 Chapter Discussion

Mutation and subsequent analysis of *R. sphaeroides* chemoreceptor McpB was undertaken in order to not only validate the Sidekick computational pipeline as a method for designing transmembrane helix mutations but to determine whether activity, localisation and clustering of the chemoreceptors are affected by signalling state. The result of such analysis should be to suggest a model for chemotactic signalling in bacteria that is able to integrate periplasmic signals, adaptation signals and cooperative signals into a single output.

Sidekick can accurately model protein mutations and predict resultant behavior

The Sidekick simulation pipeline has shown itself to be a useful tool in designing mutations in transmembrane helices when used in tandem with previous biochemical data. Mutations in the second transmembrane helix of *E. coli* chemoreceptors known to shift the activity of the output kinase were predicted by Sidekick to have similar effects on *R. sphaeroides* chemoreceptors by aligning the sequences and screening the analogous mutations *in silico*. Greater use of this tool should help to determine its limitations and streamline its use for specific, site-directed alterations in protein sequence. In future, it may be possible to predict the behaviour of membrane protein variants without the need for prior biochemical study.

Expression of variant protein McpB*, designed through the Sidekick study, was shown in swim plates to effect the chemotactic efficiency of the wild type *E. coli* strain RP437. As a result, an activity shifted *R. sphaeroides* MCP has been created for the first time. However, determination of precisely how this mutation affects signalling, and whether this fits with

the predicted activity from the Sidekick simulation required use of techniques capable of determining how the output of the chemotactic array shifted. The tracking of cells swimming in solution has been shown here to be a useful method in determining specifically how chemotactic efficiency is altered. This a metric which is not determined by simple phenotypic techniques such as soft agar swim plate analysis and yet is important in decoding the effect shown by these. The decrease in chemotactic efficiency exhibited by McpB* in the *E. coli* wild type strain RP437, was caused by an increase in tumbling frequency and therefore an increase in basal activity of the kinase (Figure 4-14). Previous studies have used complicated FRET assays to accurately analyse this shift (Khursigara et al., 2011). This increase in tumbling frequency matches the prediction by Sidekick based on previous biochemical data and suggests that Sidekick can successfully model protein variants and their resultant behaviour based on previous biochemical study.

McpB* increases bias for receptor clustering

The results presented here suggest that McpB is unable to respond to attractant in rich media through the *E. coli* chemotaxis pathway, even with the presence of *R. sphaeroides* scaffold proteins (Figure 4-8). As a result of this, any shift in signal is presumably occurring due to a cooperativity effect on the surrounding chemoreceptors. The effect on cooperativity is interesting as McpB is predicted to be of the 34H class of receptor, whereas *E. coli* chemoreceptors are all of the 36H class. This means that the scaffold binding sites should be at different distances from the bilayer. Different receptor lengths have recently been shown to cause separate signalling 'rafts' of receptors in the array due to inability to mix receptors (Herrera Seitz et al., 2014). Together, this suggests that there could be a long range cooperativity effect within the chemotaxis array. Alternatively, there is ordinarily a low affinity interaction between *R. sphaeroides* chemotactic components and the *E. coli* counterparts. Such a low affinity interaction would not allow sufficient interaction for

effective signalling to occur. Variant McpB* may have increased affinity for the *E. coli* components and thus promote an interaction. The presence of an interaction would then allow a functioning chemotactic complex to form and a signal from the CheA kinase to be created.

Analysis of the clustering by fluorescence microscopy showed that in *E. coli* McpB* has greater affinity for cluster formation at the poles than the wild type McpB. The increased affinity for polar cluster localisation exhibited by the McpB* variant over its wild type form suggests that the formation of a cluster over free diffusion of the protein within the cytoplasmic membrane is more favourable in the case of the variant form. From this data, it cannot be determined whether increased scaffold binding causes the higher affinity for cluster formation or whether higher affinity for cluster formation is independent of scaffold binding and is caused by increased interaction between receptors. The fluorescence microscopy data however, does agree with some recent studies of the array that suggest the cluster has a relaxed state and a tight state and that these are interchangeable depending on receptor signalling state (Khursigara et al., 2011) (Wu et al., 2011). Analysis of $CheW_3$ turnover in *R. sphaeroides* shows that $CheW_3$ is bound less tightly to the cluster in the presence of wild type McpB compared to variant McpB*. This supports the hypothesis that increased chemoreceptor affinity to the scaffold proteins causes tighter clustering of McpB* than wild type McpB. However, it does not rule out a change in receptor:receptor interaction and in fact, expression of McpB* in an *E. coli* strain lacking other chemoreceptors and any CheW suggests that clustering is increased for McpB* over McpB even without scaffold binding.

Chemoreceptor signalling appears to be dependent on protein flexibility

The cause of the increased affinity of the variant McpB* over the wild type McpB to form clusters appears to be due to a shift in the flexibility of McpB to become less flexible in the variant McpB* form, as shown by the MD simulations. There was very little overall structural difference between the proteins visible in the resultant structures so flexibility appears to be the only major change. Increased flexibility of the wild type form would display lower binding affinity for the scaffold proteins as the binding would prevent spatial sampling, lowering entropy in the system. In addition, increased flexibility would decrease the favourability of receptor trimerisation at the cytoplasmic tip, also due to the change in entropy required. This would account for the increased clustering at the poles seen in the fluorescence localisation studies. In a system where there is a strong interaction between these proteins already (McpB in *R. sphaeroides*, for example) this shift cannot be viewed by simple light microscopy of the cluster. Expression of McpB and McpB* in *R. sphaeroides* showed no change in fluorescence localisation and in addition, no significant change was seen for the wild type protein between rich media and minimal media in an adaptation deficient strain. However, where low, or no affinity exists between chemoreceptor and scaffold proteins (McpB in *E. coli*, for example), a change can be seen as an increased localisation of the receptors at the cell poles. It would be interesting to discover whether analysis of the binding affinity of scaffold proteins using FRAP in an adaptation deficient *R. sphaeroides* strain in various minimal and rich media results in any changes that would support the theory that signalling through a wild type chemoreceptor effects interaction with the scaffold as hypothesised here. As it has been shown here that McpB* exhibits increased kinase output, increased clustering and decreased flexibility compared to the wild type

McpB, it reasons that the increased kinase output is likely due to the increased interactions possible due to decreased flexibility.

5.Defining the specificity of the MCPs and CheWs of *R. sphaeroides*

Despite extensive study of the polar chemotaxis cluster of *R. sphaeroides*, there is still little that is known about the specificity of the multiple components both for each other and for their potential ligands (Kojadinovic et al., 2011) (Porter et al., 2008a). Phosphotransfer has been used well to determine the *in vitro* specificity for the HK and its RRs and this has shed some light on why *R. sphaeroides* retains multiple homologues of the CheYs (Porter and Armitage, 2002). However, it does not explain why *R. sphaeroides* retains multiple homologues of other chemotaxis components. In particular, knowledge of the specificity of the CheW proteins in *R. sphaeroides* is limited to $CheW_4$ and its preferential localisation to the cytoplasmic cluster and the polar localisation of $CheW_2$ and $CheW_3$ (Wadhams et al., 2003).

5.1 CheW expression in *E. coli*

UU2612 has been successful as a chassis for analysing the signalling through McpB. It is deleted for all native *E. coli* chemoreceptors and therefore allows analysis of individual MCPs by expression from plasmids (Chapter 4). Previous studies have shown that $CheW_3$ is able to recover swarming, but not chemotaxis, in an *E. coli cheW* deletion. A smooth swimming phenotype causes cells to become 'stuck' in soft agar plates, resulting in smaller swim ring sizes, and tumbling is required to swim effectively. This result suggests, therefore that CheA has become able to phosphorylate CheY. However, the lack of specific chemotaxis to an attractant suggests that the MCPs are unable to signal effectively.

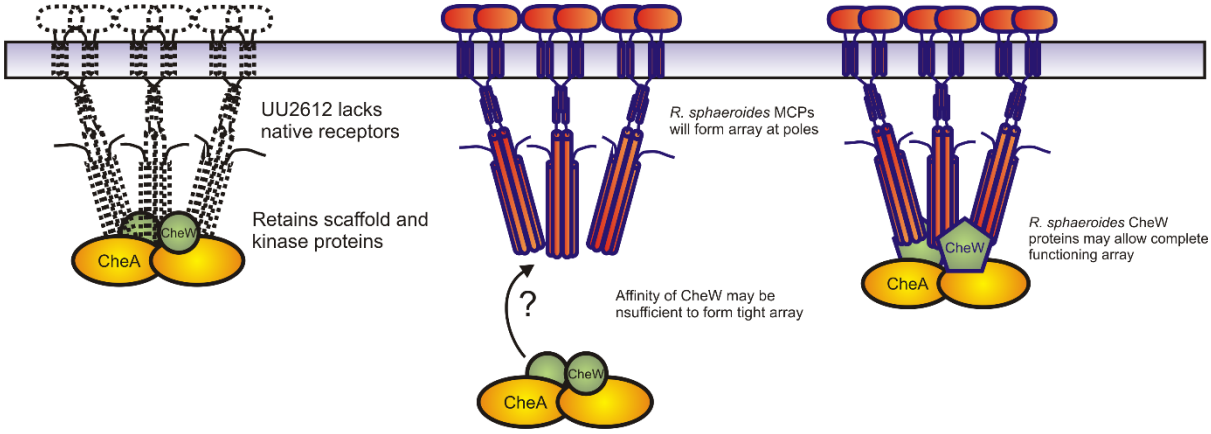

Figure 5-1 The method of *R. sphaeroides* MCP and scaffold analysis in UU2612 cells and its derivatives. On the left is shown the UU2612 polar chemotaxis array which lacks receptors and therefore does not form a functioning cluster. Addition of *R. sphaeroides* MCPs (middle) may allow a functioning array to form which will allow analysis of individual MCPs. If this is not the case, addition of the *R. sphaeroides* CheW proteins (right) should allow formation of a functioning polar chemotaxis cluster with *R. sphaeroides* MCPs. Dotted lines indicate absent MCPs, black outlines indicate native *E. coli* proteins and blue outlines indicate expression of *R. sphaeroides* proteins.

Signalling through the *E. coli* chemotaxis system should be possible when expressed in UU2612 given the redundancy previously analysed between the two species. Figure 5-1 shows that it is unknown whether the scaffold will be able to bind effectively to *R. sphaeroides* MCPs, however, expression in tandem with CheW proteins from *R. sphaeroides* should allow an effective interaction and thus enable signalling. This will enable both analysis of CheW and MCP specificities.

In order to express *R. sphaeroides* CheWs in UU2612 alongside *R. sphaeroides* MCPs, $CheW_2$ and $CheW_3$ were separately transferred to the genome into the normal *E. coli* CheW locus. This was achieved using CheW deletion strain UU2836, derived from the receptorless UU2612 strain, and the standard genome replacement technique (Chapter 3.3.12). This allowed native levels of CheW to be expressed preventing any anomalous results from differing expression levels. Expression of Tsr in these backgrounds allowed analysis of the ability of each of these systems to restore a chemotactic response.

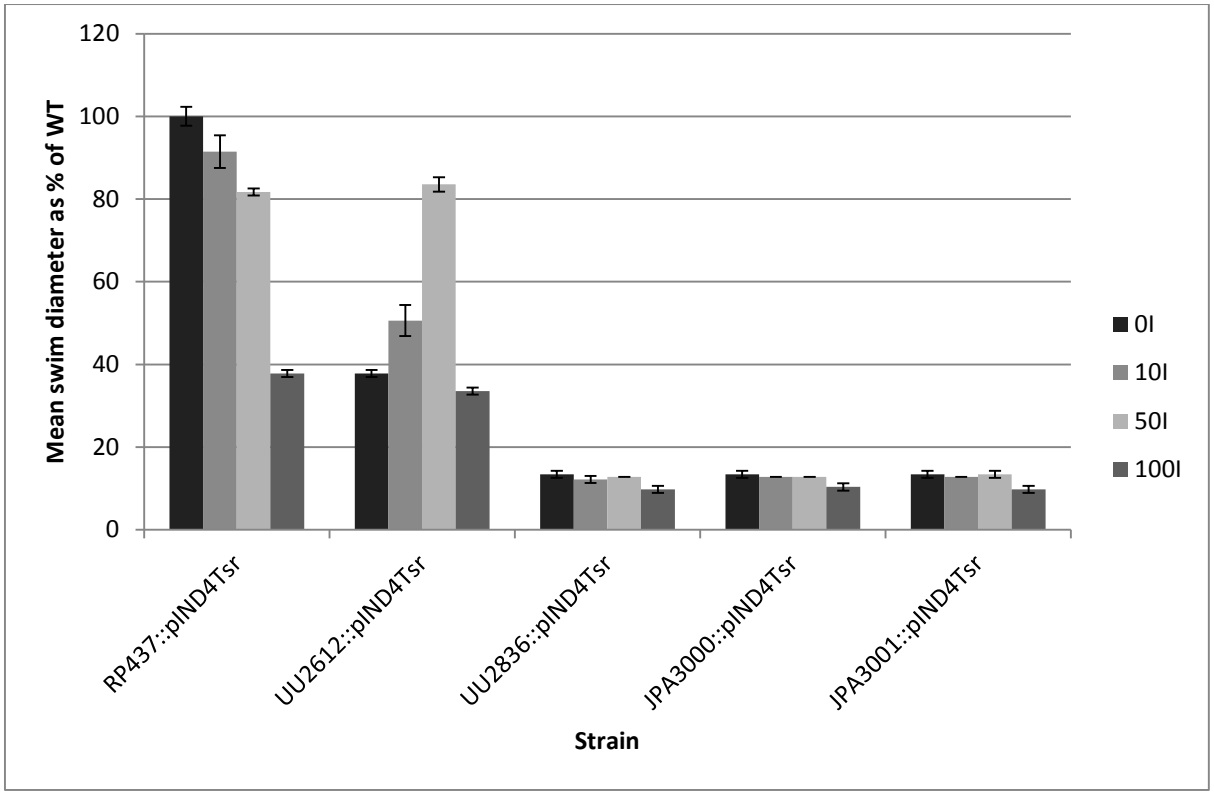

Figure 5-2 Analysis of Tsr specificity to various CheW homologues using soft-agar swim plates containing TB after 10 hours of growth at 30 °C. Tsr was expressed from the pIND4Tsr plasmid at various IPTG induction concentrations and the resultant swarm ring size plotted as a percentage of the wild type level with no Tsr induction. Wild type (RP437), receptor-less (UU2612) and receptor-less with no CheW (UU2836), with $CheW_2$ (JPA3000) and with $CheW_3$ (JPA3001) were analysed separately.

Analysis of Tsr expression in UU2612 and its derived strains show that, although expression in UU2612 recovers chemotaxis, expression in UU2836, UU2612W2 and UU2612W3 which contain either no CheW, $CheW_2$ or $CheW_3$ respectively are unable to recover a chemotactic response. This does not agree with the previous study showing that $CheW_3$ can recover some degree of swarming to an *E. coli* CheW deletion (Shah et al., 2000). The different findings in this case may be due to the levels of the CheW proteins present. A weak $CheW_3$ interaction with the *E. coli* scaffold may be overcome by over-expression from a plasmid. Whereas chromosomal expression under the native CheW promotor may result in the levels being too low to form a lasting interaction if it is of low affinity. The previous study did involve expression from the plasmid suggesting that this may account for the

discrepancy. In addition, the original study was only deleted for CheW and not the chemoreceptors and so it might be the case that the more heterogeneous array present in the wild type *E. coli* is able to better bind to *R. sphaeroides* $CheW_3$.

5.2 Creation of an *R. sphaeroides* MCP plasmid library

In order to analyse the *R. sphaeroides* MCPs in the proposed *E. coli* backgrounds, it was first necessary to create, as comprehensively as possible, a plasmid library containing *R. sphaeroides* MCPs cloned into an inducible vector. There has been much difficulty previously with cloning *R. sphaeroides* MCPs into plasmid vectors and this is believed to be due to the high GC content of *R. sphaeroides* DNA and the large size of MCP genes (Porter et al., 2011a) (Jennifer deBeyer personal communication).

MCP	Successfully cloned into pIND4	Successfully cloned with c-terminal RFP fusion
McpA	No	No
McpB	Yes	Yes
McpM	No	No
McpE	No	No
McpG	Yes	No
McpH	Yes	Yes
McpJ	Yes	No
McpR	No	No
McpV	No	No

Table 5-1 The successful clones of *R. sphaeroides* into the pIND4 inducible vector and its c-terminal fusion derivative.

Table 1 shows the success of the cloning of *R. sphaeroides* MCPs both into the pIND4 plasmid and the pIND4R C-terminal RFP fusion derivative. Some cloning was unsuccessful, however, and this is likely due to the high GC content and relatively long genes making the various stages difficult to complete.

5.3 Determining the specificity of McpH

R. sphaeroides elicits a defined and well-studied response to a chemotactic gradient of propionate (Kojadinovic et al., 2011). Deletion studies have suggested that this response may be due to binding at the receptor McpH, however, this interaction has never been directly shown (Thompson, 2005). Analysis of McpH in the UU2612 system should show a response to propionate if signalling can occur and McpH is indeed the chemoreceptor responsible for this response. As a result, McpH was expressed from the plasmid pIND4 in the same backgrounds shown for the Tsr control in Figure 5-2. Plasmid expression in *E. coli*, therefore, should allow determination of McpH response to attractants, McpH specificity to scaffold proteins, and scaffold protein specificity to the kinase.

Analysis of the swimming efficiency of McpH in various *E. coli* backgrounds shows that McpH is able to recover some swarming ability when expressed in the UU2612 background, which is lacking for all chemoreceptors but contains the native *E. coli* CheW scaffold protein and CheA kinase (Figure 5-3).

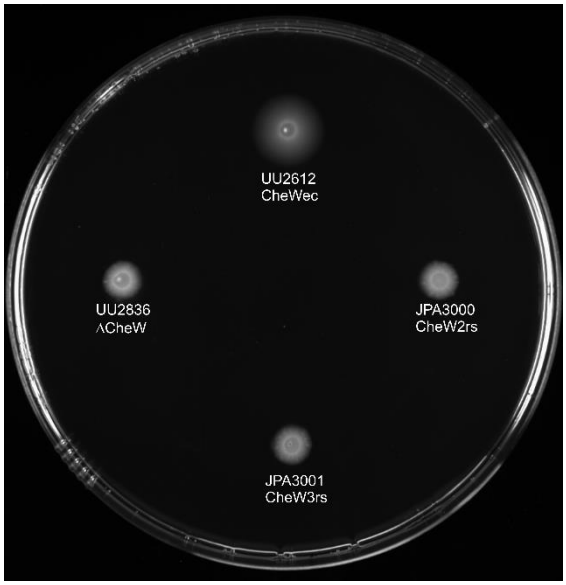

Figure 5-3 Example soft agar swim plate of McpH expression in various CheW backgrounds. UU2612 contains native *E. coli* CheW, UU2836 does not express a CheW protein, JPA3000 expresses *R. sphaeroides* $CheW_2$ and JPA3001 expresses *R. sphaeroides* $CheW_3$. Plasmid expression was induced with 50 µM IPTG.

Figure 5-4 shows that McpH expression decreases the swarming of wild type RP437 cells in rich media. This shows that either it is not as efficient at responding to components of TB or that it is disrupting wild type chemosensing. The former is unlikely as in this case the native *E. coli* receptors are present and should be responding normally. However, both conclusions require McpH to be correctly inserted into the polar array and to interact in some way with some of the wild type components. In the CheW deletion strain UU2836, swarming is not restored even after induction with 100 µM IPTG. However, expression of McpH in a receptor-less strain (UU2612) that still retains native *E. coli* CheW shows that after 10 hours growth, some, weak swarming is restored. Expression of $CheW_2$ and $CheW_3$ (JPA3000 and JPA3001 respectively) do not show any recovery of chemotaxis over the time-frame of the experiment.

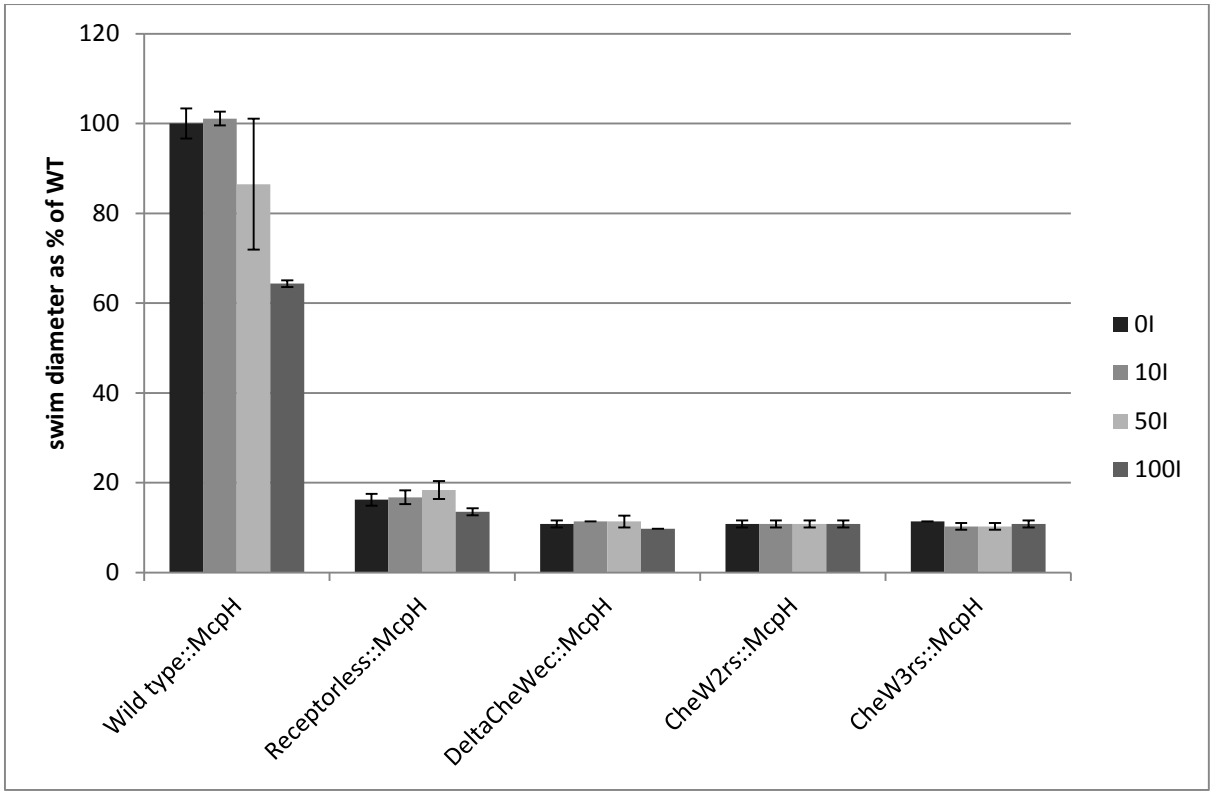

Figure 5-4 Analysis of McpH specificity to various CheW homologues using soft-agar swim plates containing TB after 10 hours of growth at 30 °C. McpH was expressed from the pIND4H plasmid at various IPTG induction concentrations and the resultant swarm ring size plotted as a percentage of the wild type level with no McpH induction. Wild type (RP437), receptor-less (UU2612) and receptor-less with no CheW (UU2836), with $CheW_2$ (UU2612W2) and with $CheW_3$ (UU2512W3) were analysed separately.

These results suggest that:

- McpH can signal and therefore bind to a component of TB
- McpH can signal albeit weakly through the *E. coli* chemosensory apparatus
- McpH requires *E. coli* CheW to signal through *E. coli* CheA
- $CheW_2$ and $CheW_3$, when expressed from the native CheW promotor, cannot facilitate a chemosensory signal from McpH to CheA.

These data supports the previous results on Tsr (chapter 5.1) and disagree with the published data and suggest that neither *R. sphaeroides* polar CheW can facilitate a chemosensory signal in *E. coli* (Shah et al., 2000).

5.4 Creation of a more native MCP analysis system

If *R. sphaeroides* McpH is able to signal through the *E. coli* system using the native CheW, but is unable to signal through *R. sphaeroides* CheW proteins, suggesting that further addition of *R. sphaeroides* chemotaxis components might be needed to create a fully functioning array and analyse the CheW specificity further. As the CheWs have been cloned into the *E. coli* genome it is possible to express the pIND4-derived plasmids in tandem with a plasmid containing a compatible origin of replication (Selzer et al., 1983). The pBAD series of plasmids are compatible with the pIND4 plasmids and allow selective arabinose induction (Guzman et al., 1995). As a result, expression of an MCP from pIND4 can be controlled with IPTG induction whilst simultaneously controlling *R. sphaeroides* $CheA_2$, or other chemotactic component, induction using arabinose.

$CheA_2$ from *R. sphaeroides* has been shown to be able to rescue a CheA deletion in *E. coli* (Shah et al., 2000). $CheA_2$, therefore, should be able to phosphorylate the *E. coli* CheY response regulator and allow a chemosensory response with an *R. sphaeroides* MCP if it is able to form functional complexes. In order to analyse this, *R. sphaeroides* McpH was expressed from the pIND4 plasmid with 50 µM IPTG and *R. sphaeroides* $CheA_2$ was expressed from the pBAD33 plasmid with 0.02% (w/v) arabinose in the same four *E. coli* backgrounds analysed previously. Co-expression of McpH and $CheA_2$ shows that a chemotactic response is still present in cells expressing an *E. coli* CheW protein. This shows that $CheA_2$ does not disrupt signalling through the *E. coli* system Figure 5-5. $CheA_2$ is also unable to elicit a chemotactic response without the presence of any CheW (UU2836 derived cells), a result which fits well with previous data showing CheW importance in

chemosensory signals. McpH and $CheA_2$ expression in cells expressing $CheW_2$ from the native CheW promoter shows a chemotactic response above the non-chemotactic UU2836 strain. The same is not the case for cells expressing $CheW_3$, which exhibits no chemotactic response above the non-chemotactic control.

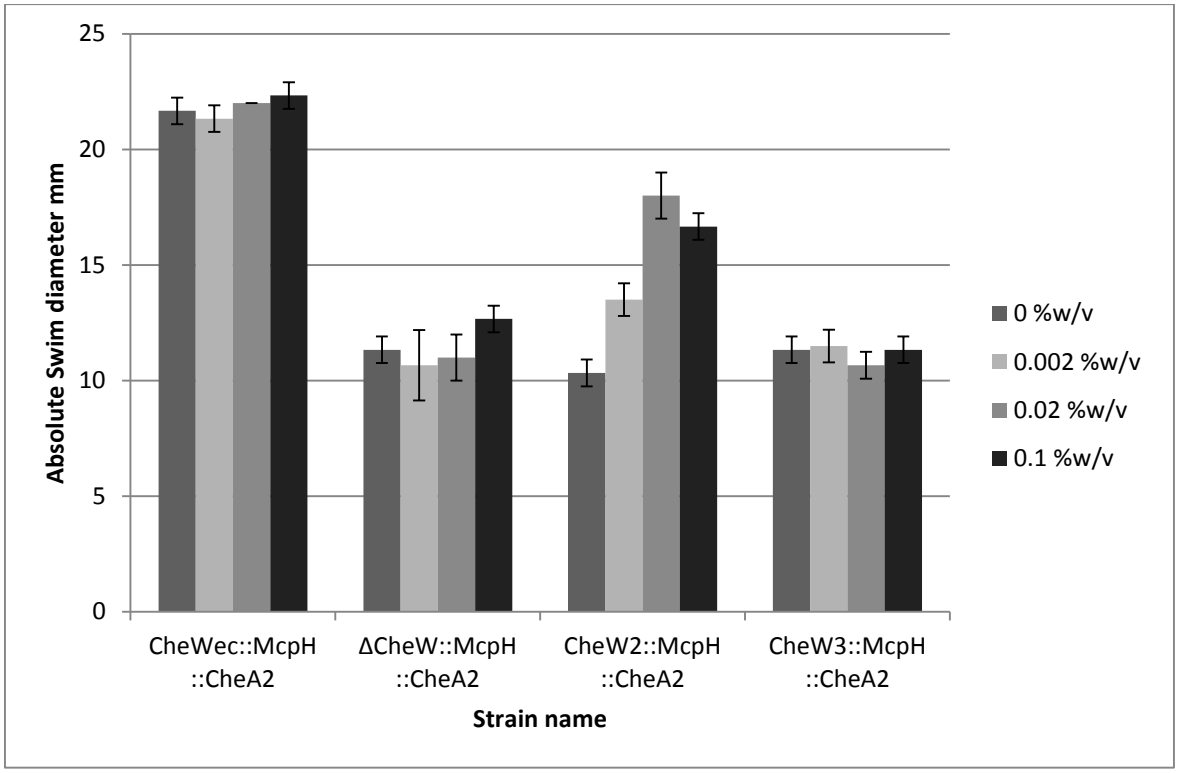

Figure 5-5 Analysis of McpH interaction with $CheW_2$ and $CheW_3$ in the presence of $CheA_2$ using soft-agar swim plates containing TB rich media. Cells were grown for 24 hours at 24 °C. McpH was induced from pIND4H using 50 µM IPTG in the presence of various arabinose induction levels of pBADA2. As a result, expression of $CheA_2$ and McpH as the sole receptor in tandem was analysed in cells expressing native *E. coli* CheW (UU2612), no CheW (UU2836) or *R. sphaeroides* $CheW_2$ (JPA3000) or $CheW_3$ (JPA3001).

The swim plate results shows that McpH does interact with $CheW_2$ and creates a chemotaxis array capable of activating the kinase effectively. Signalling must then occur through $CheA_2$ as *E. coli* CheA is unable to perform this role. This shows that $CheA_2$ can indeed signal through the *E. coli* CheY and induce motor switching. Notably, $CheW_3$ is unable to support chemotaxis as the sole CheW protein. The lack of a chemotactic response from $CheW_3$ suggests that its role is either limited to other MCPs in *R. sphaeroides*, which would describe

the need to retain homologues, or that its role is somewhat different to that of the classic CheW. The final conclusion derived from this phenotypic analysis is that McpH does indeed respond to a component of TB. This is the first time that a complete array has been reconstituted with a single *R. sphaeroides* chemoreceptor.

5.5 Fluorescence localisation of McpH

5.5.1 Localisation in *E. coli*

Determination of the localisation pattern of MCPs in *E. coli* cells has given good data on clustering for McpB and its variant McpB* (Chapter 4.7). As a result, it may be possible to determine what causes the localisation of other *R. sphaeroides* MCPs by analysing fluorescent fusions in various CheW backgrounds.

McpH-RFP was expressed as before in various CheW backgrounds to analyse whether a distinct, tight cluster was created in any case. This should determine how the signalling changes shown by the swim plate data occur.

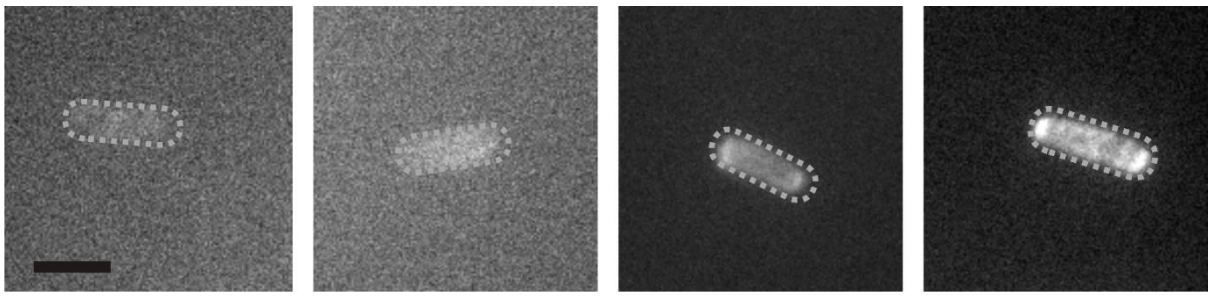

Figure 5-6 Localisation of *R. sphaeroides* McpH receptors expressed in wild type *E. coli* RP437 cells. Shown is increasing induction levels from left to right: 0 µM, 10 µM, 50 µM and 100 µM IPTG. In all images, contrast has been enhanced for maximum clarity. Cell outlines are drawn from the DIC images and shown here as a grey dotted line. Scale is consistent and bar in left image is 2 µm.

McpH does not appear to localise tightly to the poles in *E. coli* cells (Figure 5-6). At higher induction levels (50 µM and 100 µM IPTG) McpH does exhibit some bias towards polar localisation yet lateral fluorescence intensity remains high and tight clusters do not seem to form.

This may be due to over-crowding of the polar cluster as the native *E. coli* receptors are also localised to this region. In order to analyse whether this is true, McpH-RFP localisation was also analysed in *E. coli* cells lacking other chemoreceptors (UU2612).

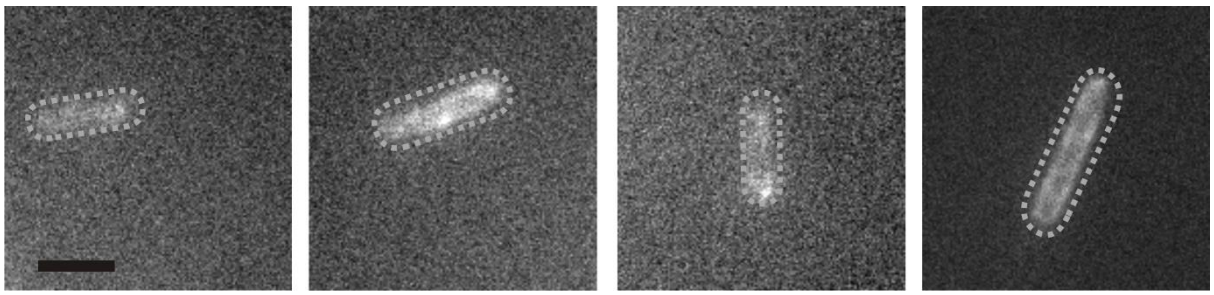

Figure 5-7 Localisation of *R. sphaeroides* McpH receptors expressed in *E. coli* cells lacking native MCPs (UU2612). Shown is increasing induction levels from left to right: 0 µM, 10 µM, 50 µM and 100 µM IPTG. In all images, contrast has been enhanced for maximum clarity. Cell outlines are drawn from the DIC images and shown here as a grey dotted line. Scale is consistent and bar in left image is 2 µm.

Array over-crowding does not appear to be responsible for the lack of tight clustering at the poles. Expression of *R. sphaeroides* McpH in *E. coli* cells lacking other MCPs shows similar amounts of lateral fluorescence intensity and although a slight bias for the polar membrane regions appears present it does not appear that McpH forms a tight chemotaxis cluster. This shows that the slight recovery of chemotaxis in this strain is not due to recovery of a tight polar cluster. This suggests that *E. coli* CheW is able to form a weak interaction with *R. sphaeroides* McpH allowing some signalling to occur but that this interaction is insufficient for full cluster formation.

McpH does not appear to localise to a tight cluster in *E. coli* and as such, replacement of the *E. coli cheW* gene with that of either *R. sphaeroides cheW*$_2$ or *cheW*$_3$ should allow analysis of which *R. sphaeroides* CheW is responsible for McpH binding and cluster formation in *R. sphaeroides*. Figure 5-8 shows the localisation pattern of McpH-RFP in *E. coli* cells lacking other chemoreceptors and expressing *R. sphaeroides* CheW$_2$. It appears that the localisation pattern is similar to that seen previously and McpH exhibits very little bias for polar localisation over lateral localisation. This suggests that even with the presence of *R. sphaeroides* CheW$_2$, tight clusters do not form.

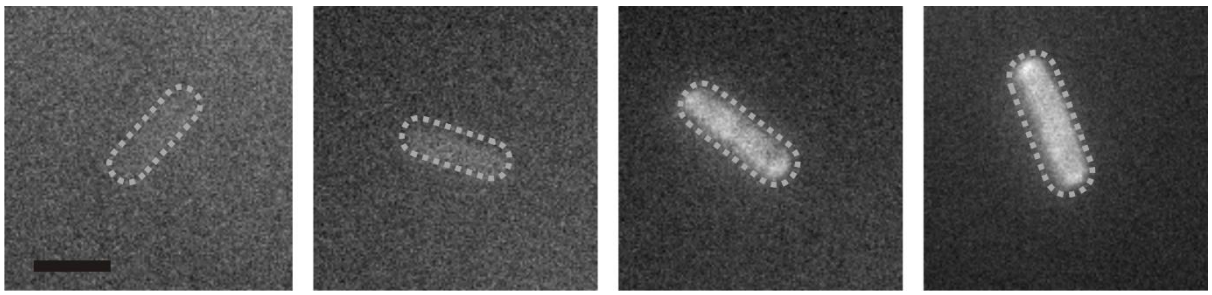

Figure 5-8 Localisation of *R. sphaeroides* McpH receptors expressed in *E. coli* cells lacking native MCPs and expressing *R. sphaeroides* CheW$_2$. Shown is increasing induction levels from left to right: 0 µM, 10 µM, 50 µM and 100 µM IPTG. In all images, contrast has been enhanced for maximum clarity. Cell outlines are drawn from the DIC images and shown here as a grey dotted line. Scale is consistent and bar in left image is 2 µm.

Analysis of McpH-RFP localisation with CheW$_3$ showed a similar pattern. In all induction levels, fluorescence intensity was largely diffuse and lacking strong bias for polar localisation. This shows that neither *R. sphaeroides* CheW$_2$ or CheW$_3$ are capable of forming tight clusters with *R. sphaeroides* McpH in *E. coli*.

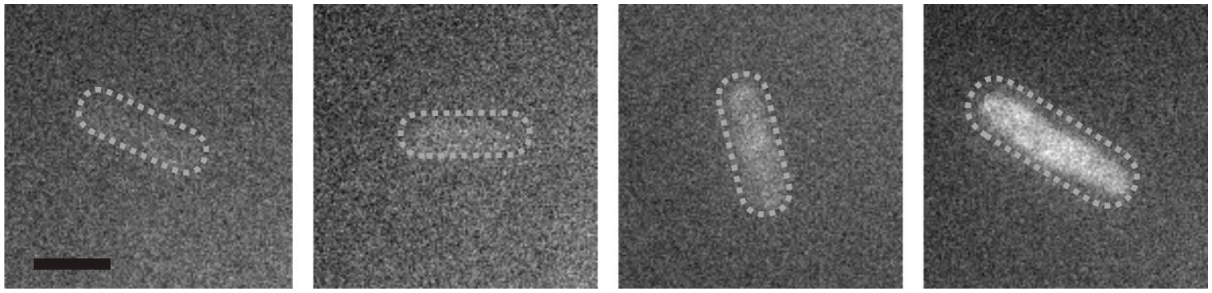

Figure 5-9 Localisation of *R. sphaeroides* McpH receptors expressed in *E. coli* cells lacking native MCPs and expressing *R. sphaeroides* $CheW_3$. Shown is increasing induction levels from left to right: 0 µM, 10 µM, 50 µM and 100 µM IPTG. In all images, contrast has been enhanced for maximum clarity. Cell outlines are drawn from the DIC images and shown here as a grey dotted line. Scale is consistent and bar in left image is 2 µm.

5.5.2 Localisation in *R. sphaeroides*

Expression of *R. sphaeroides* $CheW_2$ and $CheW_3$ in *E. coli* has given inconclusive results of how MCPs in *R. sphaeroides* are localised. Analysis of the localisation in *R. sphaeroides* may give more conclusive results as to the roles of individual CheW homologues.

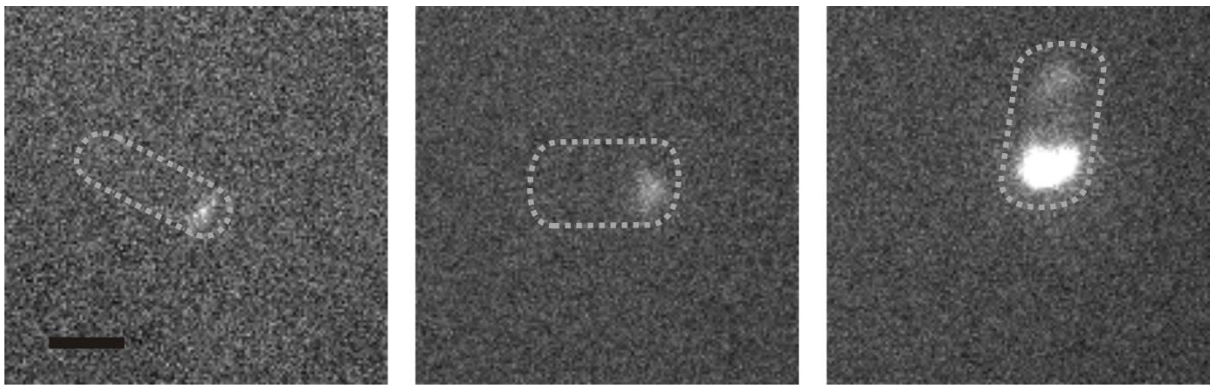

Figure 5-10 Localisation of McpH receptors expressed in wild type *R. sphaeroides* cells (WS8N). Shown is increasing induction levels from left to right: 0 µM, 10 µM and 50 µM IPTG. In all images, contrast has been enhanced for maximum clarity. Cell outlines are drawn from the DIC images and shown here as a grey dotted line. Scale is consistent and bar in left image is 1 µm.

In wild type *R. sphaeroides* cells, McpH localises to a tight polar cluster (Figure 5-10). Very little lateral fluorescence can be seen suggesting a high affinity for the polar chemotaxis array. Localisation analysis of McpH-RFP in WS8N *R. sphaeroides* cells shows that

fluorescence is indeed localised largely to one pole of the cell. Polar fluorescence in this case amounts to 49±5% of total cell fluorescence, however, 30% of this is from the single, bright pole.

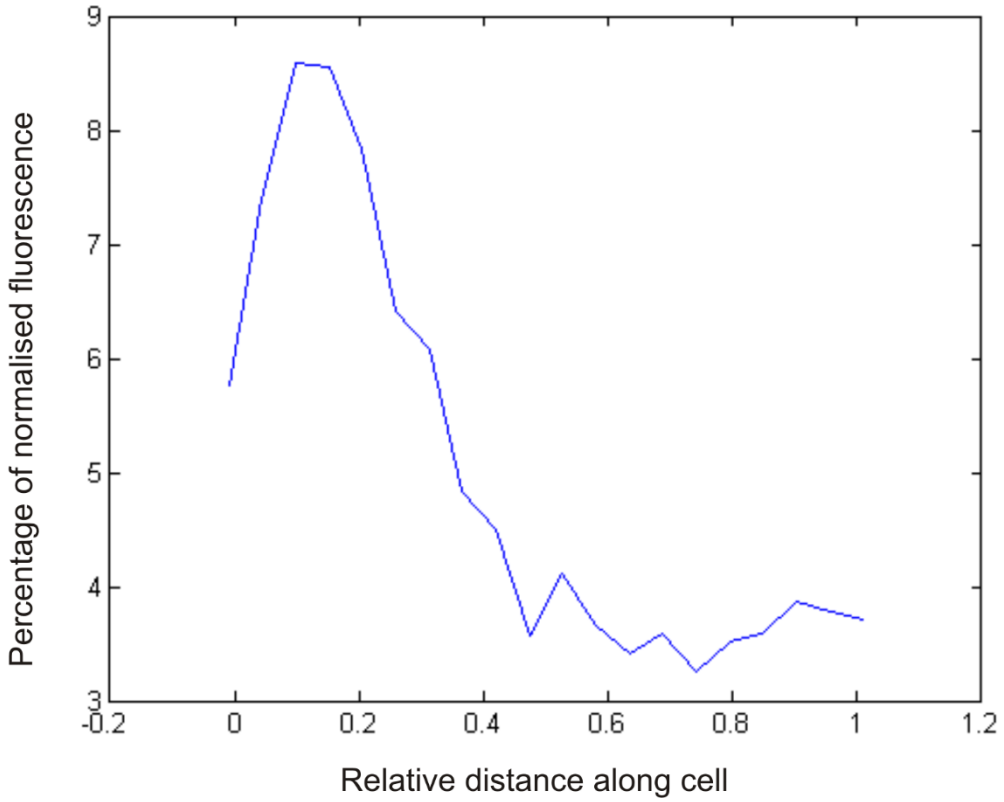

Figure 5-11 The normalised average fluorescence intensity of McpH-RFP across the length of wild type *R. sphaeroides* cells. Cells were induced with 50 µM IPTG.

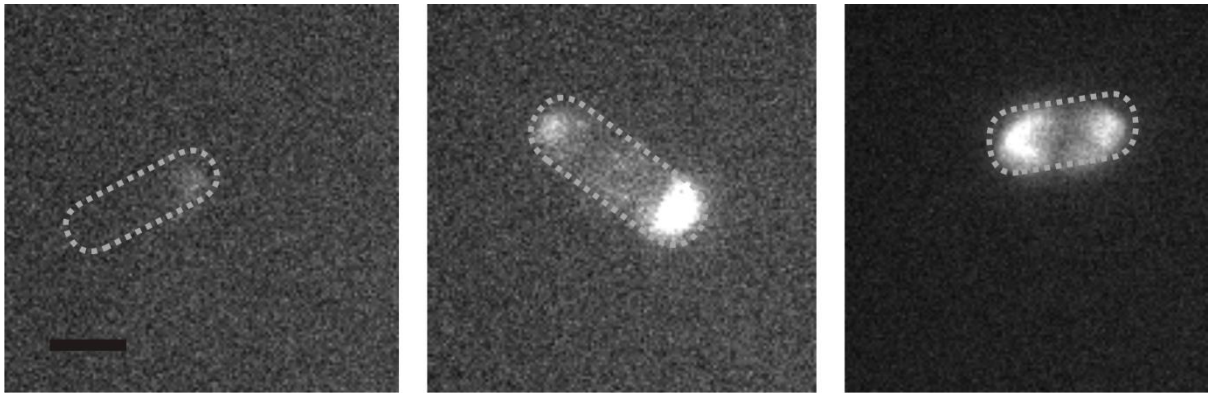

Figure 5-12 Localisation of McpH receptors expressed in *R. sphaeroides* cells deleted for the $CheW_2$ scaffold protein (JPA514). Shown is increasing induction levels from left to right: 0 µM, 10 µM and 50 µM IPTG. In all images, contrast has been enhanced for maximum clarity. Cell outlines are drawn from the DIC images and shown here as a grey dotted line.

Localisation of McpH-RFP in *R. sphaeroides* cells in which $CheW_2$ is deleted is shown in Figure 5-12. These images show that McpH-RFP predominantly localises to the polar regions of the cell in all induction levels. At the highest level of McpH-RFP expression, the amount of lateral fluorescence density increases, however, polar localisation bias is still present. This suggests that when $CheW_2$ is deleted in *R. sphaeroides* cells, McpH is still able to form a stable cluster. There may be some increased delocalisation when McpH cellular concentrations become sufficiently large which suggests that $CheW_3$ alone is not sufficient for full McpH localisation.

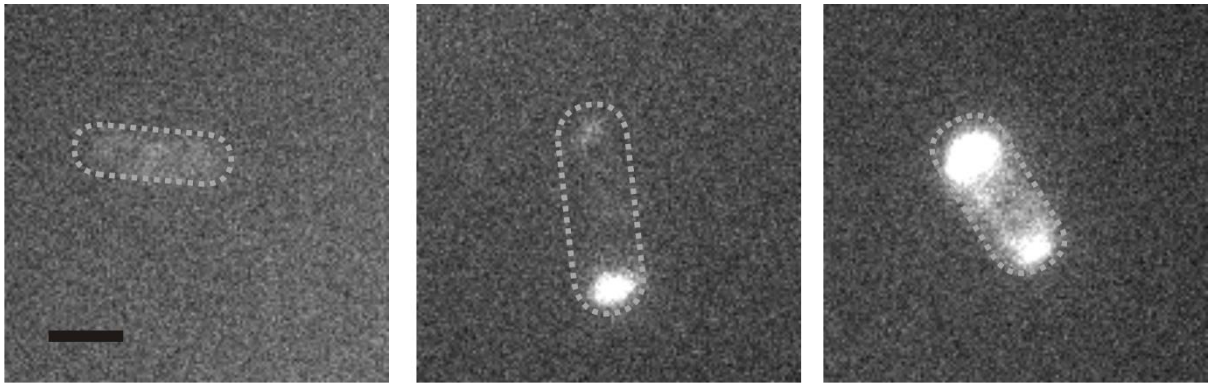

Figure 5-13 Localisation of McpH receptors expressed in *R. sphaeroides* cells deleted for the $CheW_3$ scaffold protein (JPA527). Shown is increasing induction levels from left to right: 0 µM, 10 µM and 50 µM IPTG. In all images, contrast has been enhanced for maximum clarity. Cell outlines are drawn from the DIC images and shown here as a grey dotted line.

The localisation of McpH-RFP in *R. sphaeroides* cells lacking $CheW_3$ is also strongly polar biased. At high induction levels, some lateral fluorescence density is present, however, most McpH-RFP molecules are localised to a tight cluster at the cell poles.

Plots of the average fluorescence intensity across these cells shows that there is an increase in polar localisation for JPA527 when compared with JPA514 (Figure 5-14). The former strain is deleted for $CheW_3$, whereas the latter is deleted for $CheW_2$. 46±3 (25% at major pole) of total cellular fluorescence is localised to the poles of JP514, whereas 50±4% (27% at major pole) is localised at the poles in JPA527. Also, fluorescence spots no longer appear to be localised to predominantly one pole. Two peaks are present on the profile at either ends of the cell suggesting that more cells in both deletion strains have multiple clusters than wild type cells (Figure 5-11). This suggests that deletion of $CheW_2$ has a greater effect on polar localisation of fluorescence than the deletion of $CheW_3$ and that $CheW_2$ is the major contributor to McpH localisation *R. sphaeroides*. Statistical analysis of these two data sets shows that the null hypothesis that they are the same can be rejected with a p-value of $1.05e^{-006}$. This shows that in JPA3000 ($CheW_{ec}$::$CheW_{2rs}$), there is indeed increased delocalised fluorescence to the lateral cell regions. In addition, full delocalisation is not present in either

case. This either shows that McpH is able to form clusters independently of CheW binding or that both $CheW_2$ and $CheW_3$ contribute to cluster formation.

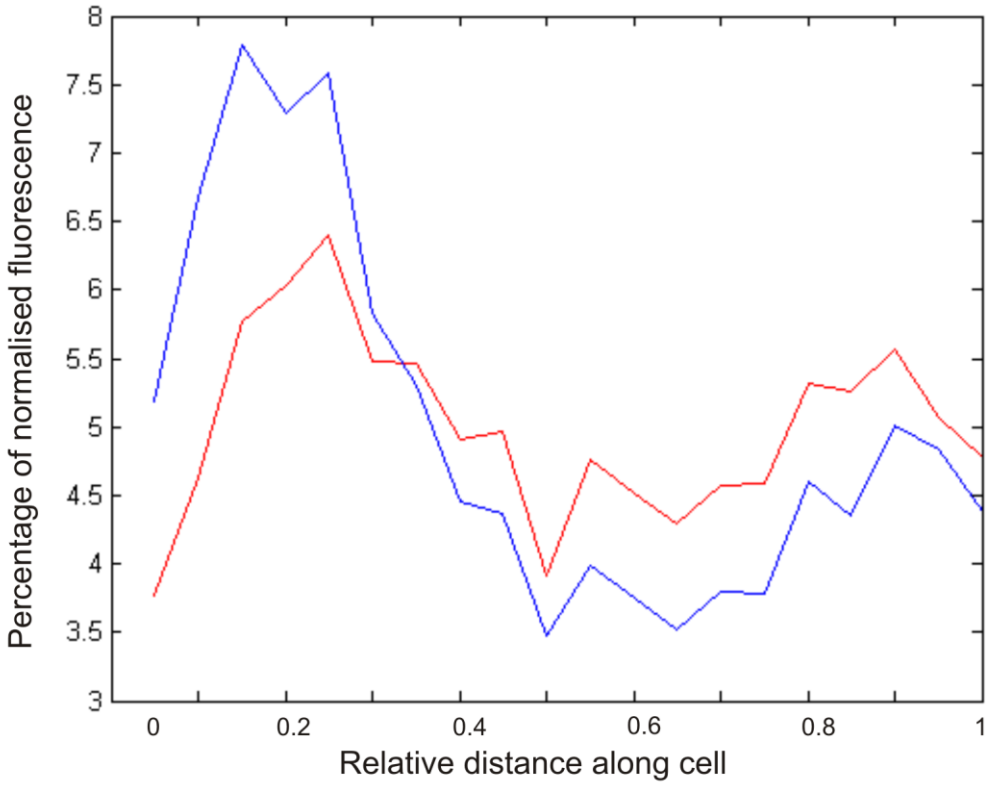

Figure 5-14 The normalised average fluorescence intensity of McpH-RFP across the length of *R. sphaeroides* cells deleted for either $CheW_2$ (red) or $CheW_3$ (blue). Cells were induced with 50 µM IPTG.

Both JPA514 and JPA527 backgrounds show decreased bias for a single pole compared with WS8N. Statistically, JPA514 shows a different localisation pattern to wild type, rejecting the null hypothesis with a p-value of 0.0015. However, JPA527 statistically has the same localisation of McpH to the poles as WS8N accepting the null hypothesis with a p-value of 0.20. The lack of any significant change to McpH-RFP localisation upon deletion, shows that $CheW_3$ does not have a significant effect on localisation of McpH to the poles of *R. sphaeroides* but $CheW_2$ does. The results also suggests that both may play some role in

the formation of a single cluster at a single pole. This may suggest a role for both CheW proteins in forming and maintaining a single cluster within the cells.

5.6 Determining the specificity of McpJ

Analysis of McpH in the *E. coli* backgrounds has shown it to be a potential method for analysing MCP-ligand specificity. As a result it may be possible to analyse other *R. sphaeroides* MCPs in this way.

McpJ was expressed from the pIND4 plasmid in the *E. coli* backgrounds used previously. This allowed analysis of McpJ signalling through the *E. coli* system as well as through individual *R. sphaeroides* CheWs.

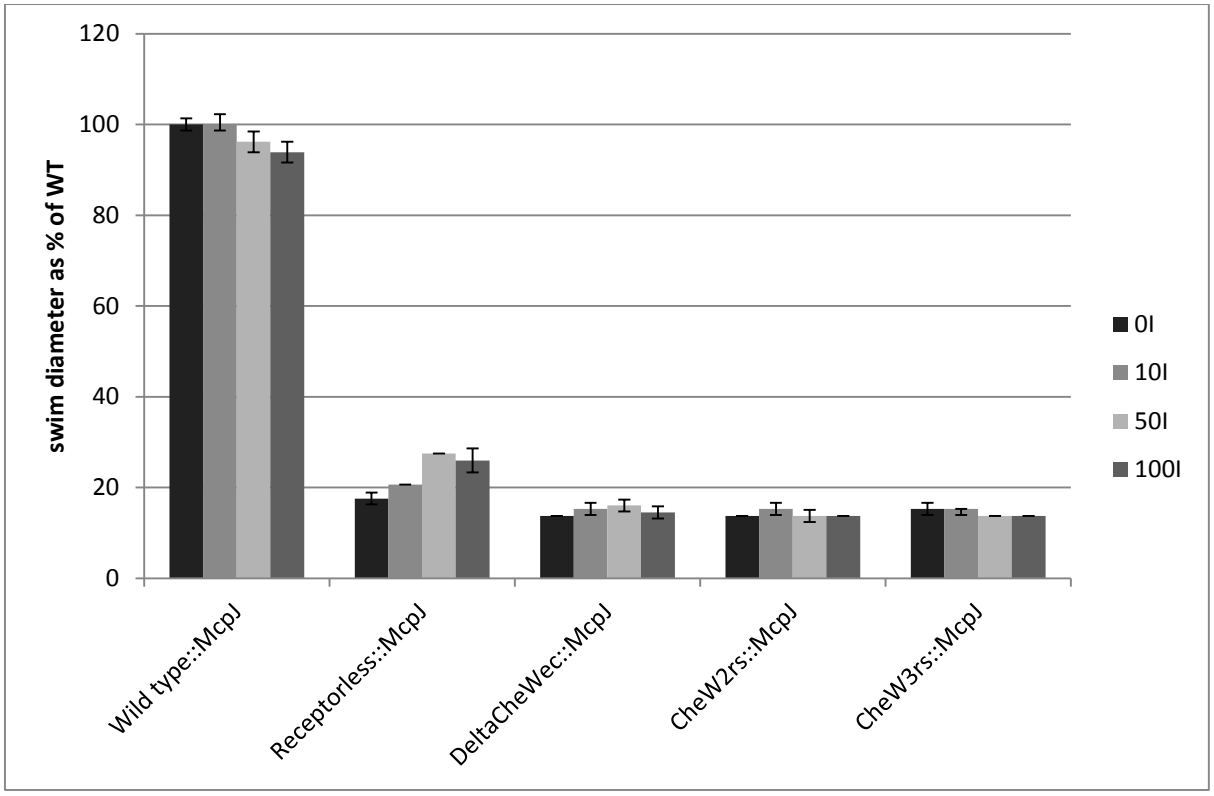

Figure 5-15 Analysis of McpJ specificity to various CheW homologues using soft-agar swim plates containing TB after 10 hours of growth at 30 °C. McpJ was expressed from the pIND4J plasmid at various IPTG induction concentrations and the resultant swarm ring size plotted as a percentage of the wild type level with no McpJ induction. Wild type (RP437), receptor-less (UU2612) and receptor-less with no CheW (UU2836), with $CheW_2$ (UU2612W2) and with $CheW_3$ (UU2512W3) were analysed separately.

Expression of McpJ in wild type *E. coli* (RP437) shows only a slight reduction in chemotaxis (Figure 5-15, first column). This shows that either McpJ does not interact well with the native *E. coli* chemoreceptor array or that its signalling in rich media does not decrease native chemosensing efficiency. McpJ can signal as the sole chemoreceptor using the native array as Figure 5-15 shows that chemosensing is slightly recovered in UU2612 by McpJ addition. As with McpH, McpJ is also unable to signal through the *E. coli* CheA when *R. sphaeroides* $CheW_2$ or $CheW_3$ are the only CheW present. This suggests that:

- McpJ also responds to a component of TB
- McpJ can signal through the *E. coli* chemosensory apparatus
- McpJ requires *E. coli* CheW to signal through *E. coli* CheA

- $CheW_2$ and $CheW_3$ cannot facilitate a chemosensory signal from McpJ to CheA when expressed from the native CheW promotor

Given that McpJ has also been shown to respond to components of TB, it should be possible, as it was for McpH to analyse the CheW specificity by expressing $CheA_2$ in tandem from plasmid pBADA2. Expression of both McpJ and CheA in *E. coli* cells shows again that $CheA_2$ does not disrupt signalling of McpJ through *E. coli* CheW and CheA (Figure 5-16). In addition, only $CheW_2$ and not $CheW_3$ supports a chemotactic response. In this case, however, the recovery of swarming is larger than the swim rings exhibited by cells expressing McpJ and *E. coli* CheW. Unlike McpH, which is assumed from deletion studies to respond to propionate, nothing is known about the potential interaction partners of McpJ. The possibility that McpJ responds to a component of TB and that it does so through $CheW_2$ and not $CheW_3$ should allow further analysis of potential ligands.

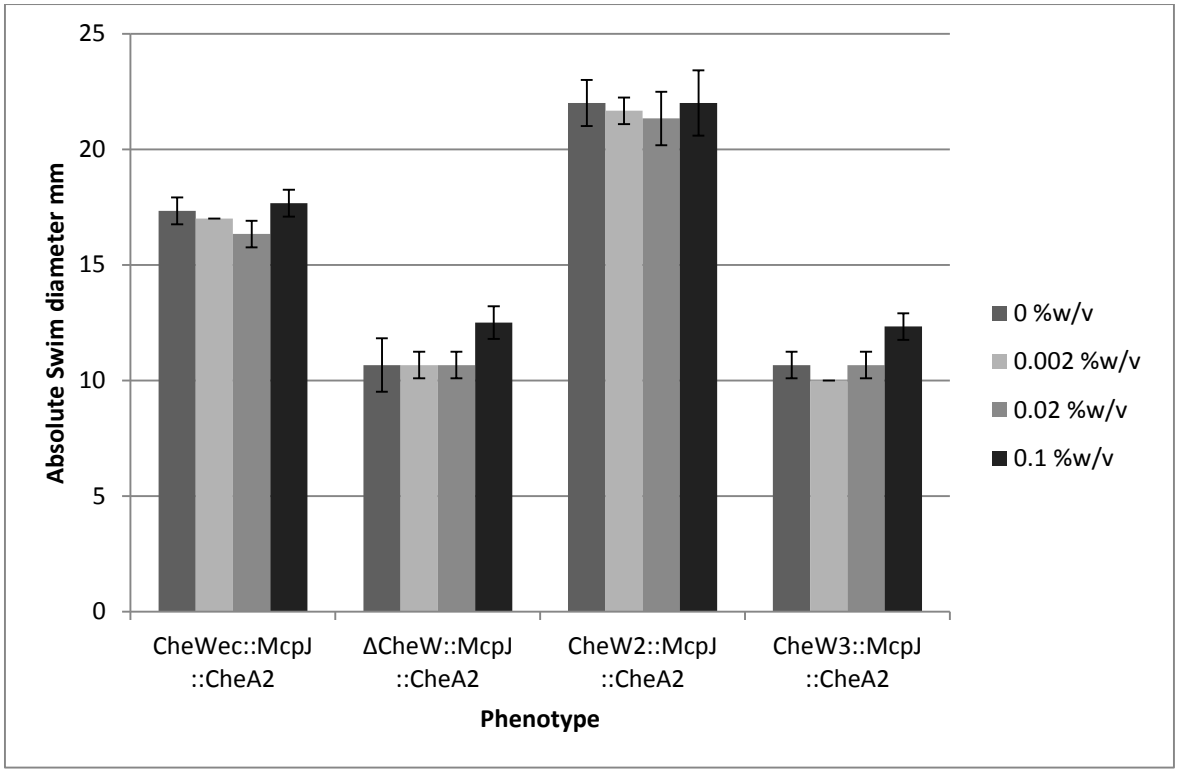

Figure 5-16 Analysis of McpJ interaction with $CheW_2$ and $CheW_3$ in the presence of $CheA_2$ using soft-agar swim plates containing TB rich media. Cells were grown for 24 hours at 24 °C. McpJ was induced from pIND4J using 50 µM IPTG in the presence of various arabinose induction levels of pBADA2. As a result, expression of $CheA_2$ and McpJ as the sole receptor in tandem was analysed in cells expressing native *E. coli* CheW (UU2612), no CheW (UU2836) or *R. sphaeroides* $CheW_2$ (UUW2) or $CheW_3$ (UUW3).

5.7 Fluorescence localisation of McpJ

Fluorescence localisation analysis of McpH in *E. coli* backgrounds proved inconclusive. However, localisation studies in *R. sphaeroides* gave some insight into the preference of $CheW_2$ and $CheW_3$ for McpH binding and cluster formation. This matched the swim plate analysis to show that $CheW_2$ appeared to play a more important role in McpH signalling. As a result, analogous *R. sphaeroides* analysis was undertaken for McpJ. McpJ was expressed from pIND4 in JPA514 and JPA527 cells to determine whether $CheW_2$ or $CheW_3$ deletions, respectively, had a greater impact on cluster localisation.

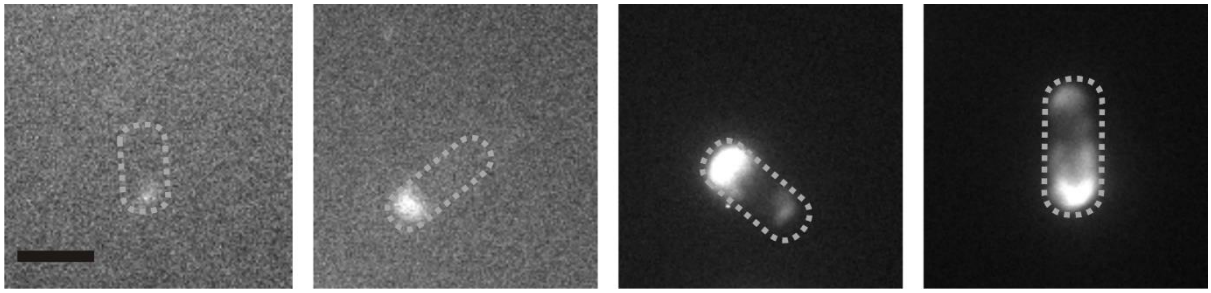

Figure 5-17 Localisation of McpJ receptors expressed in wild type *R. sphaeroides* cells (WS8N). Shown is increasing induction levels from left to right: 0 µM, 10 µM, 50 µM and 100 µM IPTG. In all images, contrast has been enhanced for maximum clarity. Cell outlines are drawn from the DIC images and shown here as a grey dotted line. Scale is consistent and bar in left image is 1 µm.

Analysis of fluorescence localisation of McpJ-RFP shows a strong polar localisation bias (Figure 5-17). This shows that McpJ does indeed localise to the polar cluster in a similar pattern seen for McpB and McpH. Some lateral fluorescence exists, which increases with increasing expression of McpJ-RFP. This increased lateral fluorescence suggests that induction with levels greater than 50 µM are less reliable as the polar cluster may become overcrowded, and the CheA and CheW scaffold proteins may become saturated with chemoreceptors, causing an increase in lateral fluorescence.

Analysis of the average normalised fluorescence profile of McpJ-RFP in WS8N cells shows strong localisation to one pole of the cell only (Figure 5-18). This suggests that the McpJ-containing polar cluster predominantly exists at one pole of the cell rather than both. 51±5% of cellular fluorescence is localised to the poles in WS8N, however, 34% of this is from a single pole with the other contributing only 17% of total cellular fluorescence.

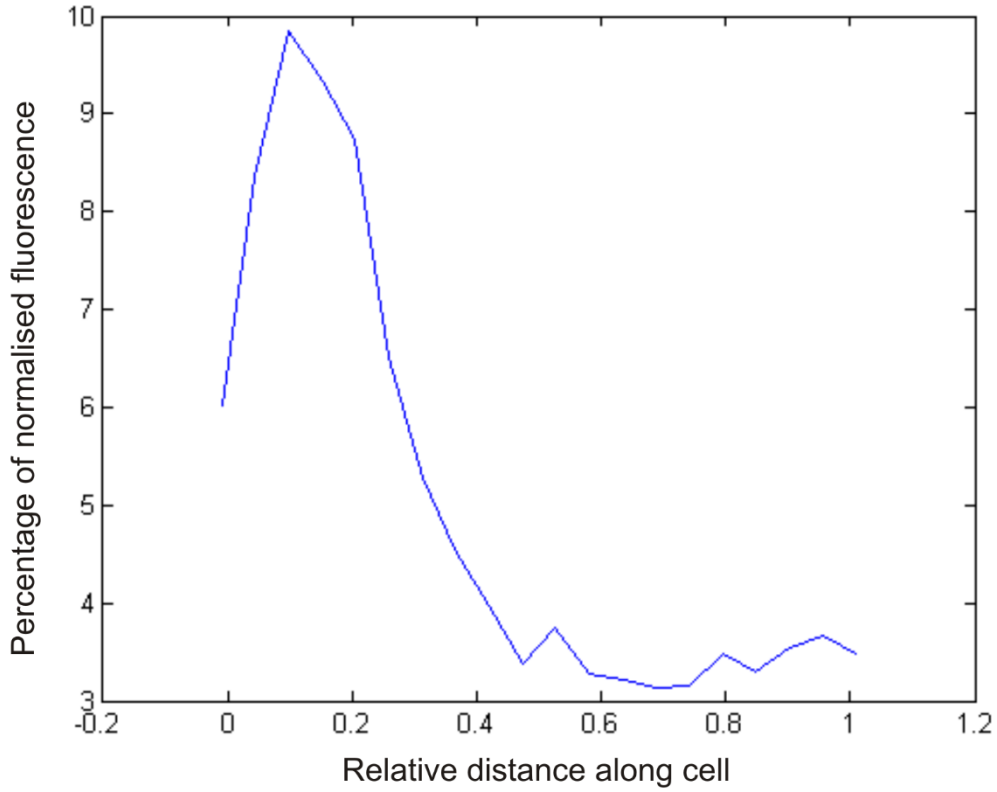

Figure 5-18 The normalised average fluorescence intensity of McpJ-RFP across the length of wild type *R. sphaeroides* cells. Cells were induced with 50 µM IPTG.

Deletion of $CheW_2$ would be expected to impact localisation of McpJ as it has been shown to enable signalling from McpJ when expressed in tandem with *R. sphaeroides* $CheA_2$ in *E. coli*.

In order to analyse this, McpJ-RFP was expressed in JPA514, an *R. sphaeroides* strain deleted for the *cheW*$_2$ gene. This showed an increase in lateral fluorescence compared to expression in wild type (WS8N) cells (Figure 5-19). McpJ-RFP retains some bias for localisation at the poles, however there is much higher fluorescence density seen in lateral regions which suggests a delocalisation from the polar cluster. This result suggests that $CheW_2$ is, as predicted, important for McpJ localisation in *R. sphaeroides*.

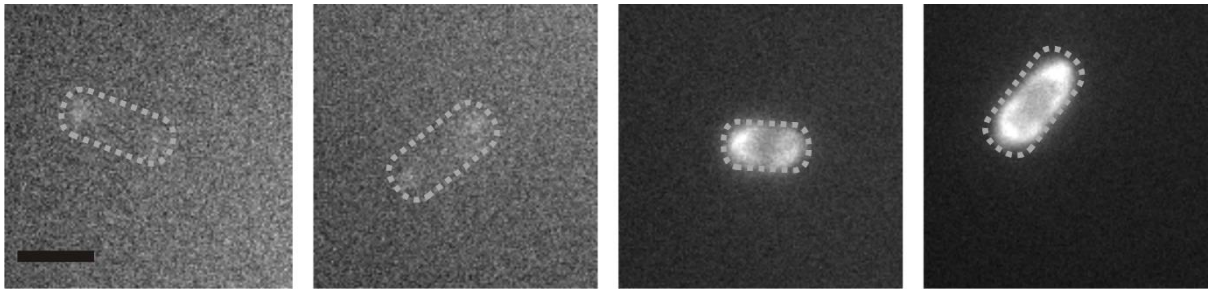

Figure 5-19 Localisation of McpJ receptors expressed in *R. sphaeroides* cells with $CheW_2$ deleted (JPA514). Shown is increasing induction levels from left to right: 0 µM, 10 µM, 50 µM and 100 µM IPTG. In all images, contrast has been enhanced for maximum clarity. Cell outlines are drawn from the DIC images and shown here as a grey dotted line. Scale is consistent and bar in left image is 1 µm.

Analysis of McpJ-RFP localisation in a $CheW_3$ deletion background was used to determine whether $CheW_3$ has a similar role in McpJ localisation to $CheW_2$. This is not predicted to be the case as $CheW_3$ is unable to restore a chemotactic response in *E. coli* cells, even with the addition of *R. sphaeroides* $CheA_2$.

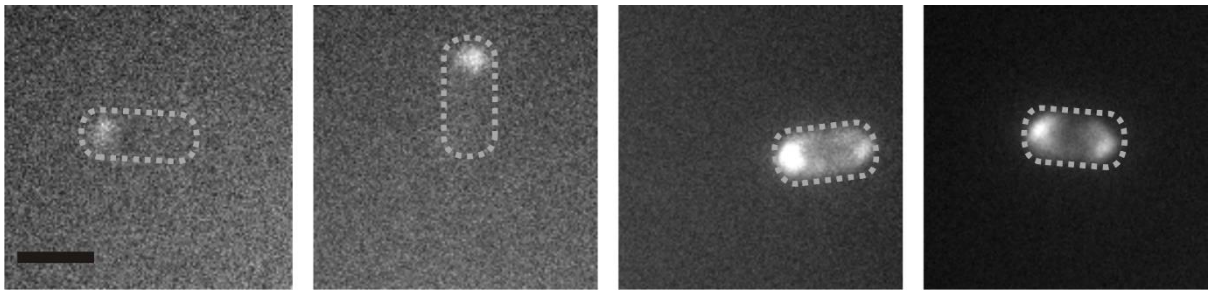

Figure 5-20 Localisation of McpJ receptors expressed in *R. sphaeroides* cells with $CheW_3$ deleted (JPA527). Shown is increasing induction levels from left to right: 0 µM, 10 µM, 50 µM and 100 µM IPTG. In all images, contrast has been enhanced for maximum clarity. Cell outlines are drawn from the DIC images and shown here as a grey dotted line. Scale is consistent and bar in left image is 1 µm.

Deletion of $CheW_3$ appears to cause an increase in lateral fluorescence density compared to wild type (Figure 5-20). The effect however, does not appear to be as large as that seen for the $CheW_2$ deletion. This suggests that $CheW_3$ does have some effect on McpJ localisation to the polar cluster but again, the effect does not seem as strong as for $CheW_2$.

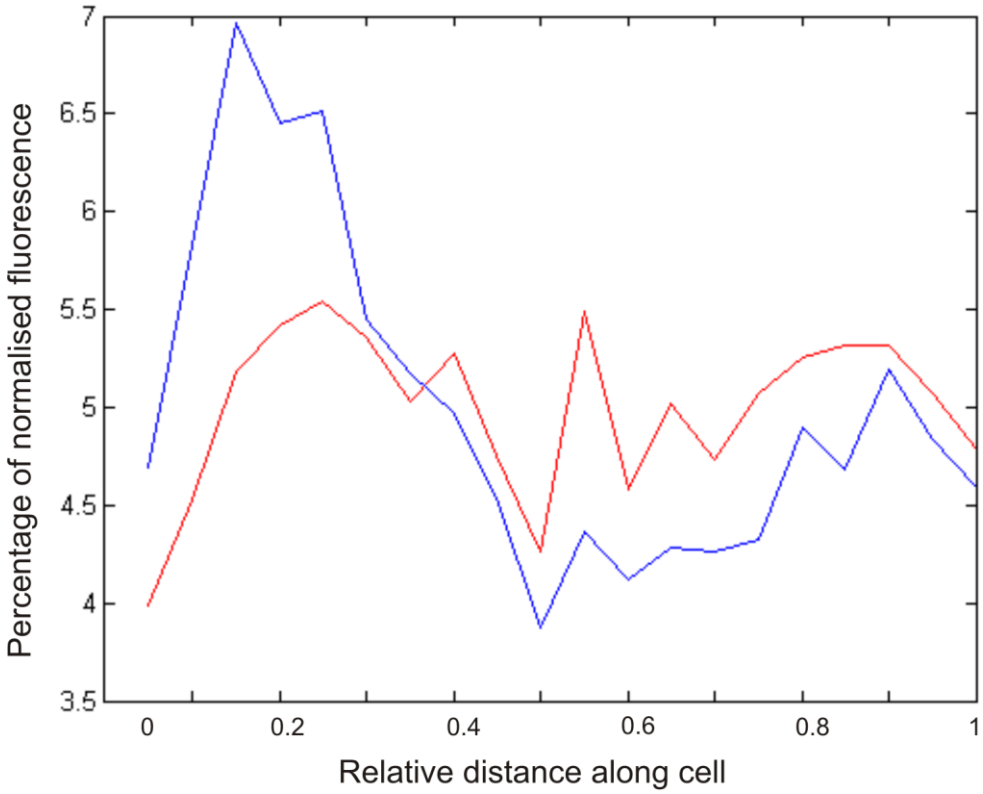

Figure 5-21 The normalised average fluorescence intensity of McpJ-RFP across the length of *R. sphaeroides* cells deleted for either $CheW_2$ (red) or $CheW_3$ (blue). Cells were induced with 50 µM IPTG.

Analysis of the average fluorescence profiles of JPA514 and JPA527 cells expressing McpJ-RFP shows that $CheW_2$ does have a greater effect on polar localisation than $CheW_3$ (Figure 5-21). A total of 44±2% (26% from the major pole) of the cells total fluorescence is localised to the poles of JPA514 cells ($CheW_2$ deletion), which shows that total polar fluorescence has decreased in this case compared to wild type cells. The graph shows that in this case, it appears that bias for one pole over the other has also been completely lost. JPA527 cells, deleted for $CheW_3$, show that 48±3% (24% of total fluorescence intensity is localised to the poles. Statistical analysis shows that the null hypothesis that JPA514 and JPA527 exhibit the same fluorescence localisation can be rejected with a p-value of $1.6e^{-007}$. This shows that $CheW_2$ affects localisation more than $CheW_3$, as has been shown for McpH. In addition, statistical analysis shows that JPA514 localisation is significantly different from WS8N

localisation, with a p-value of $4.7e^{-014}$ and JPA527 localisation is also significantly different with a p-value of $6.2e^{-004}$. This agrees with the conclusion that $CheW_3$ does affect McpJ localisation in *R. sphaeroides* but does not appear to be the major CheW responsible for this. Nor does it allow signalling to occur when expressed as the sole CheW in tandem with $CheA_2$ and McpJ in *E. coli*. Again, $CheW_2$ does appear to be responsible for localisation of McpJ and it does appear to allow a chemotaxis complex to form in *E. coli* with *R. sphaeroides* $CheA_2$. This further supports a more dominant role in localisation and signalling for $CheW_2$ than $CheW_3$.

5.8 Determining the specificity of McpG

Given the success in determining McpH and McpJ specificity in the UU2612 background and its derivatives, it should be possible to use the same mechanism for the other 7 MCPs proposed to comprise the polar cluster. The other MCP in *R. sphaeroides* that has been previously studied to some extent is McpG (Wadhams et al., 2000). As a result, this was cloned into the pIND4 vector and subjected to the same experiments as McpJ and McpH.

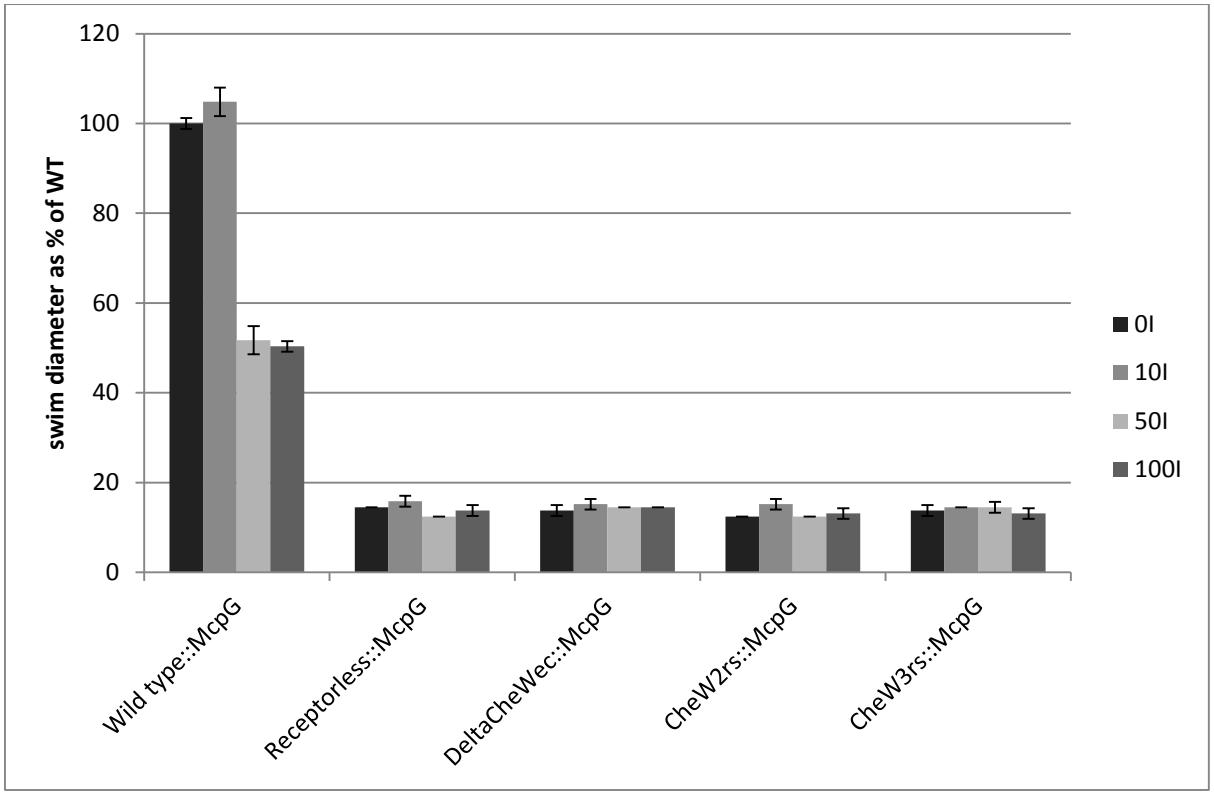

Figure 5-22 Analysis of McpG specificity to various CheW homologues using soft-agar swim plates containing TB after 10 hours of growth at 30 °C. McpG was expressed from the pIND4G plasmid at various IPTG induction concentrations and the resultant swarm ring size plotted as a percentage of the wild type level with no McpG induction. Wild type (RP437), receptor-less (UU2612) and receptor-less with no CheW (UU2836), with $CheW_2$ (UU2612W2) and with $CheW_3$ (UU2512W3) were analysed separately

Unlike McpJ and McpH, McpG shows no recovery of chemotaxis when expressed as the sole chemoreceptor. In addition it does not show chemotaxis when either of the *R. sphaeroides* CheW proteins are expressed. This could be due to many reasons, the simplest being that McpG does not respond to any component of TB. However, expression of McpG in wild type RP437 causes a large drop in chemotaxis when induced with 50 µM IPTG or more. This drop suggests that either McpG presence is disrupting cluster signalling in some way and decreasing chemotactic efficiency, or that McpG is responding to some form of repellent in TB and this is actively reducing swarming. The latter seems unlikely and repellent repsonses are less well understood and considered to be more complex. The analysis of a repellent response is much more difficult than that of an attractant as standard

soft agar swim assays all show a non-chemotactic phenotype. Furthermore, extensive taxis and free swimming assays would be needed to fully determine a repellent response through McpG. It is more likely that clustering is disrupted in some way by the presence of McpG and that this is decreasing the output of the sytem.

5.9 Direct analysis of chemoreceptor ligands

McpH has been predicted previously to be the *R. sphaeroides* MCP responsible for binding and responding to the attractant propionate (Thompson, 2005). This has not been directly shown previously, however, given that McpH and McpJ appear to respond through the *E. coli* CheW and CheA as well as the *R. sphaeroides* $CheW_2$ and $CheA_2$, it should be possible to analyse directly the response of these cells in minimal media containing a variety of attractants to determine which, if any, bind McpH and which bind McpJ.

The previous study showed that *R. sphaeroides* showed a response to propionate, pyruvate and acetate organic acids. The results from this study suggest that it is likely that McpH will respond to one, if not all, of these molecules. As a result, these were used as attractants in minimal media swim plates to determine whether McpJ or McpH responds to these. As a control, serine was used as this elicits a strong response in *E. coli* RP437 wild type cells. In addition, responses were first analysed in *E. coli* to ensure that the minimal media plates showed the expected responses.

After 24 hours incubation at 30 °C, RP437 showed almost full coverage of the plate with serine as the sole attractant. Swim ring in the organic acids swim plate was significantly smaller showing a lack of strong chemotaxis toward propionate, pyruvate and acetate in *E. coli*.

These phenotypic swim plates show that after 24 hours, *E. coli* is capable of significant swimming distance under these conditions. This shows that these minimal media plates do give the expected results and are a viable method for attractant analysis in *E. coli*.

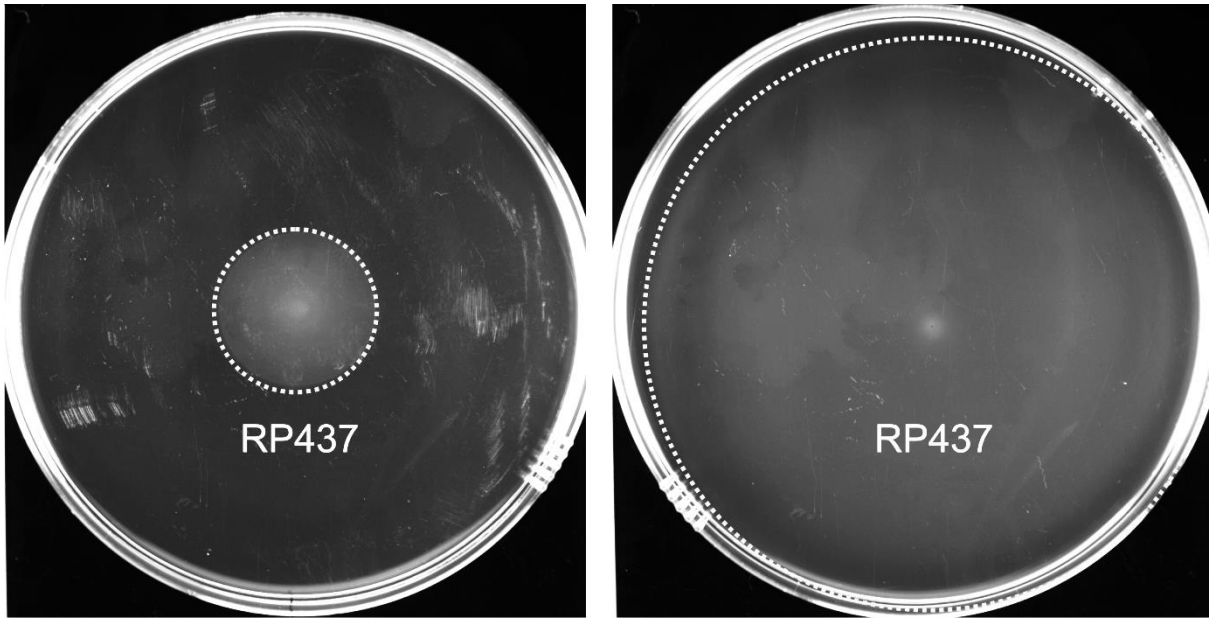

Figure 5-23 Example soft agar swim plates of RP437 in minimal media containing propionate, pyruvate and actetate (left) or serine (right) as the sole attractants. RP437 contained the empty pIND4 plasmid to provide kanamycin resistance. All attractants were present at a concentration of 100 µM. Swim rings have been outlined with grey dotted line for clarity.

In order to determine the responses of McpH and McpJ to these attractants the previously analysed CheW background strains were transformed with pIND4 plasmid expressing McpH or McpJ. In addition the same strains were also transformed with pBAD33 expressing *R. sphaeroides* $CheA_2$. These were then incubated alongside the RP437 controls and their swim ring diameter analysed compared to RP437 in the same conditions.

Without expression of $CheA_2$, only McpJ in a background expressing *E. coli* CheW shows a large increase above the non-chemotactic control strains (ΔCheW) (Figure 5-24) in response to the organic acids propionate, pyruvate and acetate. McpH, shows a small

increase above non-chemotactic as has been seen previously (chapter 5.3). Neither *R. sphaeroides* $CheW_2$ or $CheW_3$ are able to support chemotaxis in response to organic acids.

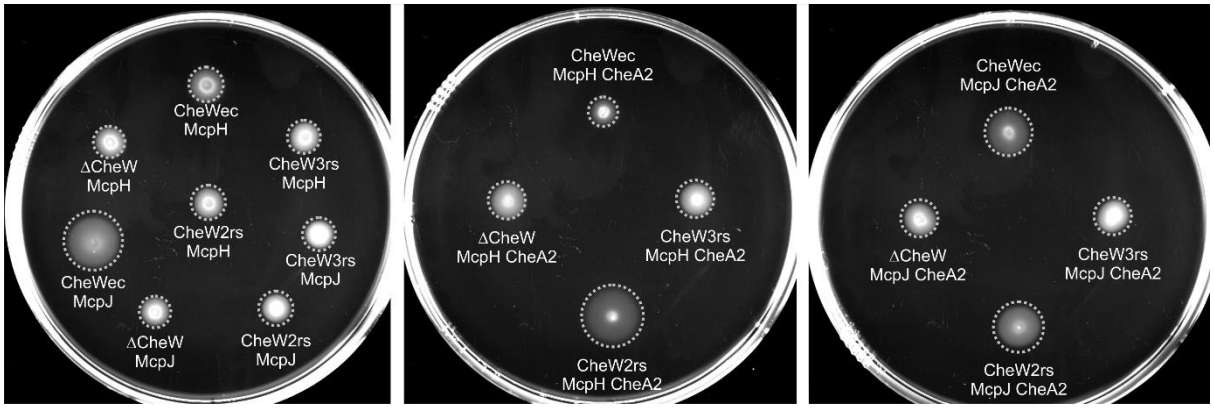

Figure 5-24 Example soft agar swim plates of *E. coli* strains expressing either McpH or McpJ and with or without *R. sphaeroides* $CheA_2$. Swim plates contained minimal media and 100 µM each of propionate, pyruvate and acetate as the only attractants. *Left* shows cells expressing as the only chemoreceptor McpH or McpJ and either *E. coli* CheW (UU2612), no CheW (UU2836), *R. sphaeroides* $CheW_2$ (JPA3000) or *R. sphaeroides* $CheW_3$ (JPA3001). *Middle* shows the same *E. coli* backgrounds expressing McpH and $CheA_2$ and *right* shows the same *E. coli* backgrounds expressing McpH and $CheA_2$.Swim rings have been outlined with grey dotted line for clarity.

Addition of *R. sphaeroides* $CheA_2$ has little effect on chemotactic ability through *E. coli* CheW by eye, however, graphical analysis shows that for both McpH and McpJ, some decrease in chemotactic efficiency is seen (Figure 5-25). Addition of $CheA_2$ to cells expressing $CheW_2$, as has been seen previously, seems to support slight increase in chemotactic ability, however, this is only around 50% (for McpH) of wild type levels of chemotaxis to organic acids. This suggests that if there is a full chemotactic response to these organic acids through this system it is occurring through both MCPs and efficiency is poor. Alternatively, neither of the MCPs is responding correctly in this system to these attractants and the recovery of some chemotactic ability seen is as a result of correct formation of a cluster resulting in non-specific signalling through CheA. The recovery of tumbling ability has allowed cells to correctly swim through the soft agar but not specifically towards an attractant signal.

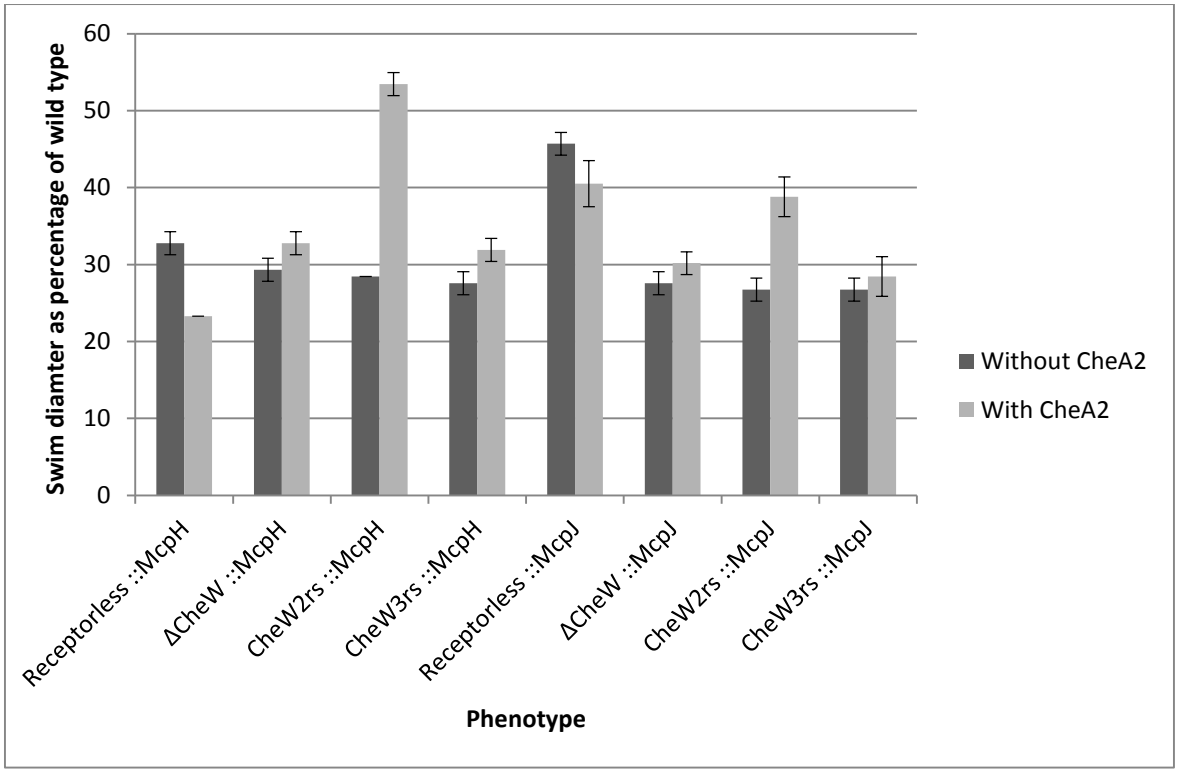

Figure 5-25 Analysis of McpH and McpJ chemotactic ability in media containing propionate, pyruvate and acetate as the only attractants after 24 hours of growth at 30 °C. McpJ and McpH were expressed from the pIND4 plasmid with 50 µM IPTG and the resultant swarm ring size plotted as a percentage of the wild type. Receptor-less (UU2612), receptor-less with no CheW (UU2836), with *R. sphaeroides* $CheW_2$ (JPA3000) or $CheW_3$ (JPA3001) were analysed separately. Show are the swim rings of cells either with or without *R. sphaeroides* $CheA_2$ expressed from the pBAD33 plasmid using 0.02% (w/v) arabinose.

R. sphaeroides does not respond well to serine as an attractant (Ingham and Armitage, 1987). As a result, it is unlikely that *R. sphaeroides* MCPs should respond well to serine when incorporated into a different chemosensory system. Therefore, similar minimal media analysis undertaken with serine as the sole attractant should help to determine whether McpH and McpJ are indeed responding to the organic acids or merely allowing passive signalling through scaffold formation.

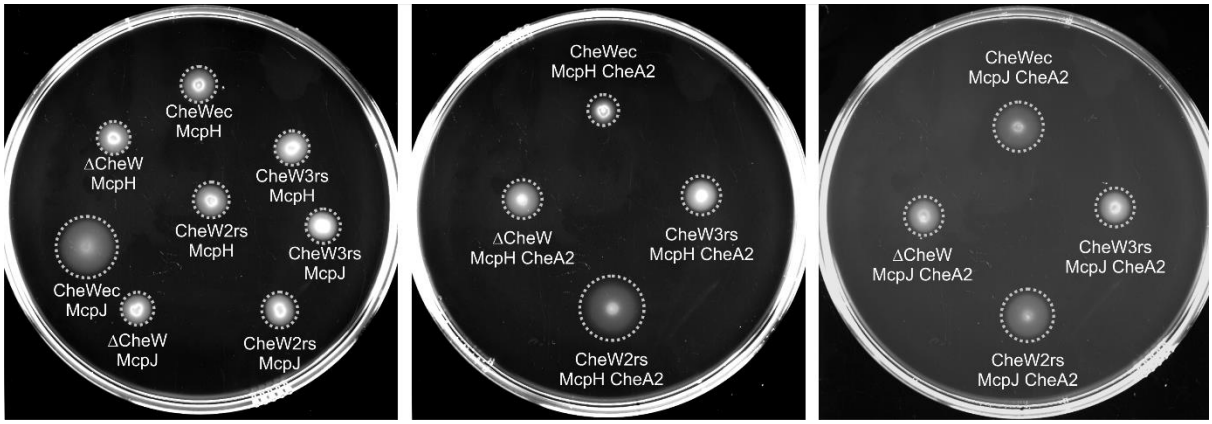

Figure 5-26 Example soft agar swim plates of *E. coli* strains expressing either McpH or McpJ and with or without *R. sphaeroides* $CheA_2$. Swim plates contained minimal media and 100 µM each of propionate, pyruvate and acetate as the only attractants. *Left* shows cells expressing as the only chemoreceptor McpH or McpJ and either *E. coli* CheW (UU2612), no CheW (UU2836), *R. sphaeroides* $CheW_2$ (JPA3000) or *R. sphaeroides* $CheW_3$ (JPA3001). *Middle* shows the same *E. coli* backgrounds expressing McpH and $CheA_2$ and *right* shows the same *E. coli* backgrounds expressing McpH and $CheA_2$. Swim rings have been outlined with grey dotted line for clarity.

McpJ again shows a recovery of chemotaxis above the non-chemotactic control (ΔCheW) (Figure 5-26). This is a similar response seen for chemotaxis towards organic acids and suggests, given that *R. sphaeroides* does not respond well to serine, that it is a non-specific response. Similar conclusions can be drawn from analysis of chemotactic ability with addition of *R. sphaeroides* $CheA_2$ (Figure 5-27). McpH is, again, shown to recover chemotactic ability and the absolute swarm sizes are similar. In this case the percentage of chemotaxis compared to wild type is much smaller as wild type *E. coli* is capable of sensing and responding to serine well. These results suggest that the recovery of a swimming phenotype has occurred in these cases and that a functioning array has been formed. It is, however, either not able to respond specifically to any of the attractants tested, meaning that the propionate sensor in *R. sphaeroides* is not McpH or McpJ, or that these MCPs are still not able to signal effectively through this system.

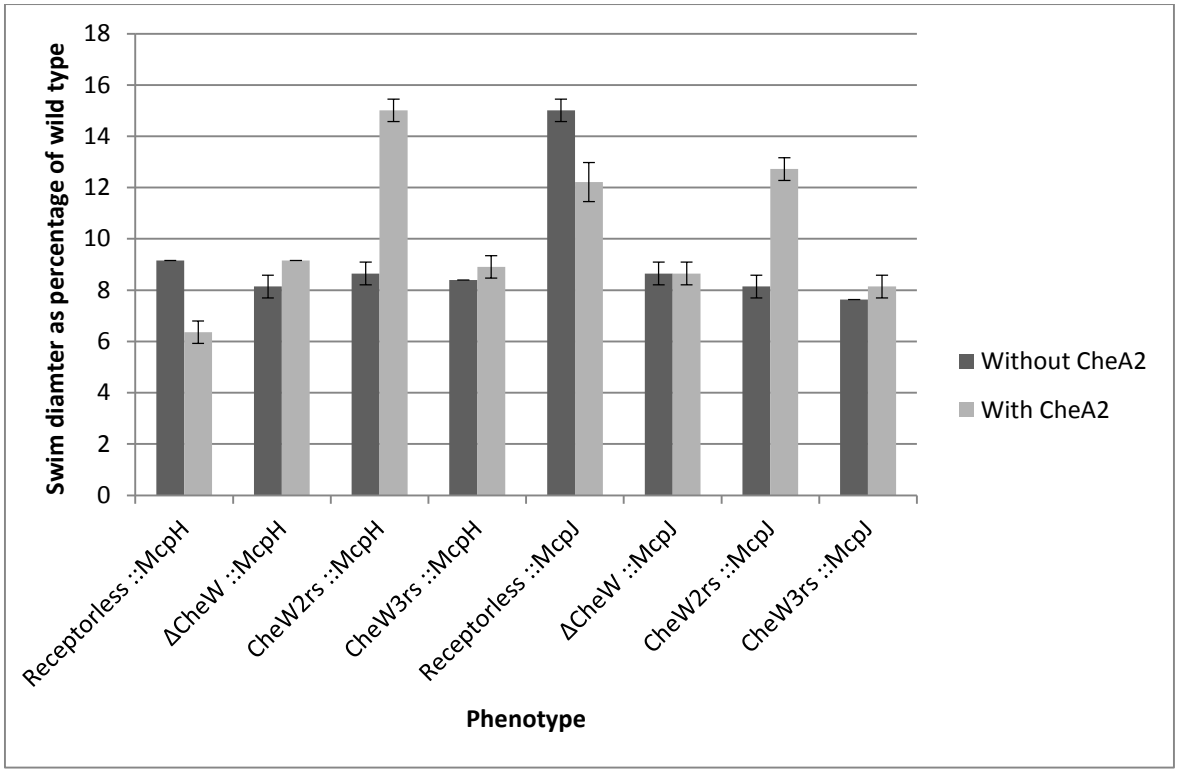

Figure 5-27 Analysis of McpH and McpJ chemotactic ability in media containing serine as the only attractant after 24 hours of growth at 30 °C. McpJ and McpH were expressed from the pIND4 plasmid with 50 µM IPTG and the resultant swarm ring size plotted as a percentage of the wild type. Receptor-less (UU2612), receptor-less with no CheW (UU2836), with *R. sphaeroides* $CheW_2$ (JPA3000) or $CheW_3$ (JPA3001) were analysed separately. Show are the swim rings of cells either with or without *R. sphaeroides* $CheA_2$ expressed from the pBAD33 plasmid using 0.02% (w/v) arabinose.

5.9.1 Free swimming analysis

The hypothesis that receptor clusters are formed and cause non-specific tumbling events can be tested by merely viewing the swimming bacteria in capillary tubes in minimal media and immediately after addition of attractant. If tumbling is recovered then it should be able to be seen in minimal media. If the cells are responding to attractant a decrease in tumbling should be visible.

Cells were grown to OD_{600nm} 0.4-0.6 and 1 ml of cells pelleted and washed in 1ml *E. coli* motility buffer before being resuspended in 1ml of the same buffer. Cells were incubated for 30 minutes at room temperature to ensure motility was recovered after centrifugation and

then taken into a capillary tube which was then sealed at both ends with silicon grease. 2 minute videos were taken immediately of the cells swimming in the sealed capillary and tumbling and running ability analysed. Attractants were added to the cells to a final concentration of 100 µM and imaged immediately to determine whether the running and tumbling phenotype altered in response to attractant presence. Strains were defined as exhibiting run and tumble events if they showed cells that had defined run and tumble events in succession through the video. If cells did not show any tumble events between runs they were defined as smooth swimming, whereas if cells did not appear to be swimming freely at all through the video they were defined as tumble cells.

Strain	Minimal media	Propionate pyruvate aspartate	Serine
Wild type	Run and tumble	Run and tumble	Smooth swimming
CheWec::McpH::$CheA_2$rs	Run and tumble*	Run and tumble*	Run and tumble*
ΔCheW::McpH::$CheA_2$rs	Smooth swimming*	Smooth swimming*	Smooth swimming*
$CheW_2$rs::McpH::$CheA_2$rs	Run and tumble*	Run and tumble*	Run and tumble*
$CheW_3$rs::McpH::$CheA_2$rs	Tumble*	Tumble*	Tumble*
$CheW_2$rs::McpJ::$CheA_2$rs	Smooth swimming	Smooth swimming	Smooth swimming

Table 5-2 The swimming phenotype of *E. coli* background strains expressing either *R. sphaeroides* McpH or McpJ, in tandem with *R. sphaeroides* $CheA_2$ and either *E. coli* CheW, no CheW, *R. sphaeroides* $CheW_2$ or *R. sphaeroides* $CheW_3$. Attractant was added to a final concentration of 100 µM. Smooth swimming cells exhibited no tumbles during the length of the video, Run and tumble cells exhibited both runs and tumble events during the video length and tumble cells exhibited no run events during the length of the video. *denotes cells with a larger fraction of cells exhibited no runs than wild type.

The analysis of free swimming of these strains shows some interesting phenotypes. As expected, wild type cells exhibited both runs and tumbles in all media with the exception of Serine addition. In this case, they showed only run events suggesting they are responding normally to the serine attractant and are not tumbling. CheW deletion strains did not exhibit any tumble events following a significant period of swimming. This is as expected as a fixed,

signalling array is not expected to form and therefore no CheY should be present. Interestingly, a large proportion of these cells exhibited poor swimming behaviour during the length of the video. Poor swimming behaviour suggests that the presence of McpH and *R. sphaeroides* $CheA_2$ may be in some way preventing a full smooth swimming phenotype. In the presence of *E. coli* CheW and *R. sphaeroides* $CheA_2$, *E. coli* cells appeared to exhibit some tumbles following periods of swimming behaviour. A large proportion of these cells also appeared to exhibit no swimming behaviour, again suggesting that the presence of McpH and $CheA_2$ is effecting swimming behaviour in some cells. Cells expressing $CheW_3$ showed no significant smooth runs throughout the length of the video, suggesting that a constant tumbling phenotype is present. The lack of any long 'run' events suggests that a chemotactic complex is able to form in these cells and that it appears to be locked active. *E. coli* cells expressing *R. sphaeroides* McpJ, $CheW_2$ and $CheA_2$ exhibited a smooth swimming phenotype in all media. This last result does not explain the larger swim rings on soft agar plates compared to the CheW deletion control. It may be that these cells do tumble but infrequently and were not seen in that state during the length of the video.

5.10 Bacterial two-hybrid to assess heterogeneity

As discussed, the reasons *R. sphaeroides* maintains multiple homologues of chemosensory proteins are unknown. The preceding sections have demonstrated that $CheW_2$ and $CheW_3$ do not have the same specificity and/or activities, suggesting that the two proteins are not redundant. However, determination of whether specificity is indeed the cause of this non-redundancy or whether CheW merely performs a different role cannot be determined from these results alone. The bacterial two-hybrid system is an *in vivo* method to analyse

interactions between proteins in bacteria (Karimova et al., 1998) (Karimova et al., 2000). Two tags are added to predicted interactors that when bound to each other form a functional enzyme that causes cAMP production. As the tags require an interaction to create this activity, if their anchors do not directly interact then the two tags will never bind, give no activity and hence not report an interaction. The presence of cAMP can be reported using a standard β-galactosidase assay, among others.

Protein	pKT25	pKNT25	pUT18	pUT18C
McpA	✓	✓	×	✓
McpB	✓	×	×	×
McpB*	✓	✓	✓	×
McpE	✓	✓	✓	✓
McpG	✓	✓	✓	×
McpH	✓	✓	✓	✓
McpJ	×	×	×	×
McpM	×	×	×	×
McpR	×	×	✓	✓
McpV	×	×	×	×
$CheW_1$	×	×	✓	✓
$CheW_2$	✓	✓	✓	×
$CheW_3$	✓	×	×	✓

Table 5-3 The successful plasmids created for bacterial two-hybrid plasmid library of *R. sphaeroides* MCPs and CheW proteins. All known *R. sphaeroides* MCPs and CheW proteins are shown in the left column. The other columns indicate the successful creation of each of the four possible plasmids required for the two-hybrid screen.

A library of the MCPs and CheWs from *R. sphaeroides* was created in order to analyse the specificity of their interactions. Two plasmids at a time were then transformed in tandem to the parental DMH1a strain and grown to stationary phase. 5 µl stationary phase culture of each interaction pair to be tested was then inoculated onto a large assay plate containing LB

with kanamycin, ampicillin, 50 µM IPTG and 40 µM 5-bromo-4-chloro-3-indolyl-β-d-galactoside (X-Gal). Plates were incubated overnight at 30 °C and then binding of each pair was analysed by determining whether each strain had turned blue. Blue colour is casued by the presence of 5,5'-dibromo-4,4'-dichloro-indigo, the product formed by β-galctosidase from X-Gal. β-galctosidase expression is cAMP controlled, and therefore in cells lacking a native cAMP system (*cya*), a close interaction of the two fusion proteins is required to produce β-galctosidase and create a blue colour. The library of chemotactic components successfully created is shown in Table 5-3. There were a number of components that could not be successfully cloned into either some or all of the background plasmids. The reason for this may be similar difficulties to those discussed earlier, the length and high GC content of *R. sphaeroides* MCP genes makes cloning more difficult and therefore more conditions must be tried in order to cause success.

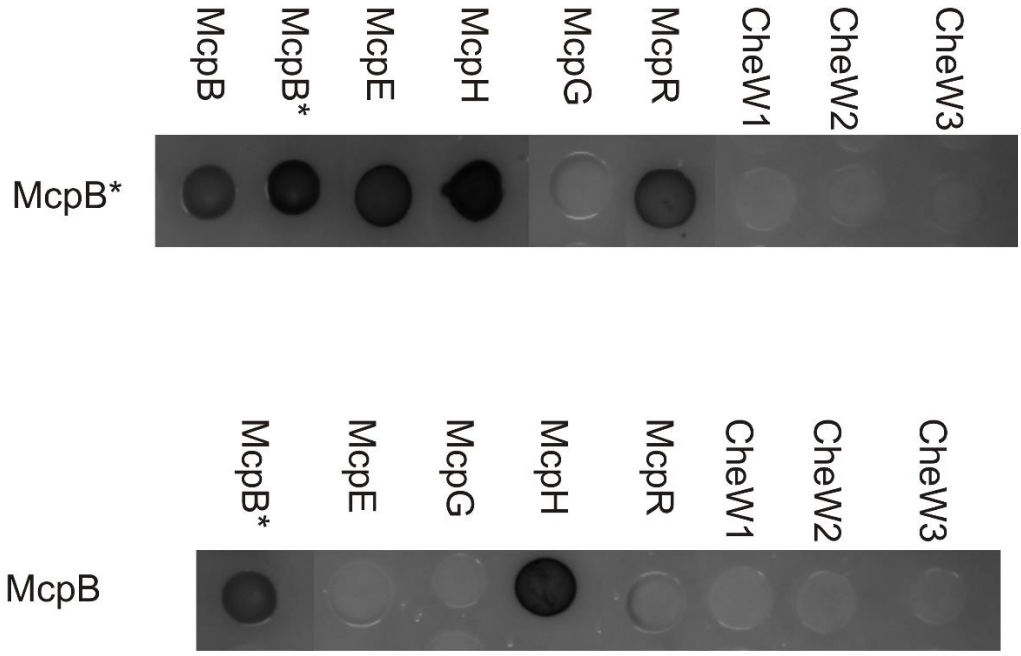

Figure 5-28 The interaction arrays of McpB and McpB*. Shown are the individual spots of the double-transformation strains on LB plates containing X-Gal. Dark colour arises from the blue product of the X-gal reaction with the β-galactosidase enzyme. Enzyme expression is under the control of cAMP created when the two fusions are significantly close together to form a full, functioning enzyme. Light colour, indicates the lack of enzyme acitivity and no close interaction between the proteins.

The results of the bacterial two-hybrid screen show multiple interactions present for many components of the polar cluster. The chemoreceptors McpB, McpB*, McpE, McpH and McpR all show interactions to other chemoreceptors (Figure 5-29). The nature of the experiment requires close contacts in order for sufficient enzyme activity to produce cAMP. As a result it can be reasoned that any proteins that successfully elicit a response must be interaction partners. In an array such as the chemotactic cluster it suggests that these proteins are at least capable of forming closely interacting signalling homotrimers, however, it is more likely from the strong responses seen that they are capable of forming mixed trimers with specific interactions between them. This is the first evidence for such mixed trimers in *R. sphaeroides*.

Very few interactions between CheW proteins and MCPs were detected. This is perhaps unsurprising given the previous results. The two-hybrid screen is performed in an *E. coli* background strain lacking its native cAMP signalling system (*cya*). The previous results suggest that $CheA_2$ may be required in order to effectively form a complex with *R. sphaeroides* CheW proteins in *E. coli* and so the lack of visible interactions here may be due to the inability of the *E. coli* CheA to facilitate this. McpH did, however, appear to show an interaction with $CheW_3$ in one case. The lack of an interaction in any other plasmid combination suggests this interaction may be weak but it does suggest $CheW_3$ is capable of binding McpH. This is in contrast with the chemotaxis phenotyping experiments previously, which show $CheW_2$ is the dominant scaffold protein responsible for signalling in *R. sphaeroides*. However, a $CheW_3$:McpH interaction does agree with the free swimming results that suggest $CheW_3$ causes a tumbling phenotype resulting from high kinase activity. These results taken together, suggest that $CheW_3$ binds strongly to McpH, potentially preventing release of the kinase and the resultant loss of kinase activity.

McpB* also appears to bind to more MCP targets than its wild type form. The lack of all plasmids for McpB means this result is preliminary, however, it suggests that McpB* has greater affinity for inter-MCP contacts. This supports the notion that the variant protein increases binding affinity for other chemoreceptors and the scaffold, shown by the fluorescence localisation and FRAP studies.

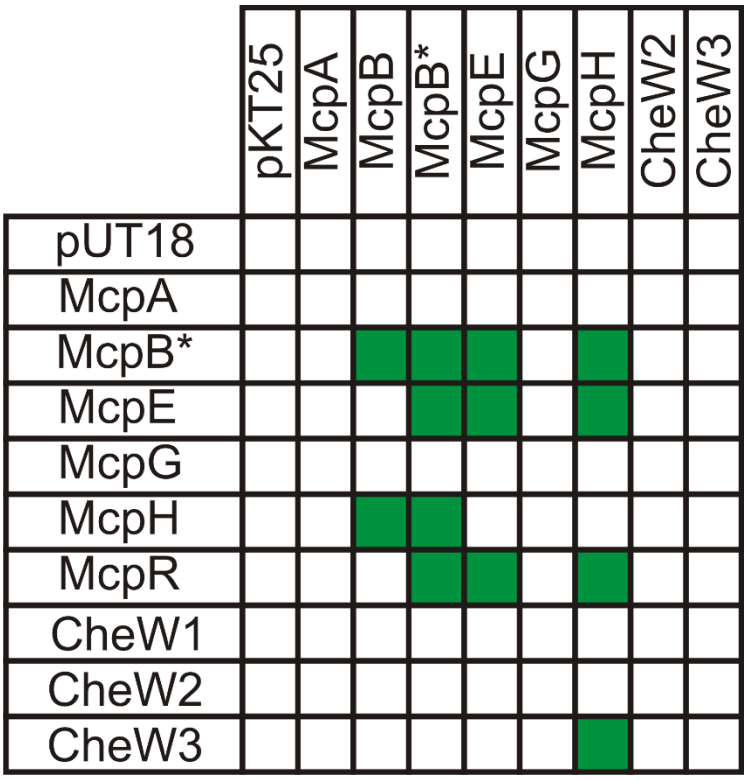

Figure 5-29 The positive results of the bacterial two-hybrid screen. Results giving a dark colour colony after 24 hours at 30 °C on LB agar containing 50 µM IPTG and 40 µM X-Gal.

5.11 Chapter Discussion

There is currently little evidence to explain why *R. sphaeroides* retains multiple homologues of proteins within its chemotactic pathway. It is not known what ligands have affinity for each receptor nor is it known why *R. sphaeroides* retains multiple CheW homologues. The aims of the studies presented here were to discover a method to screen receptor specificity,

analyse scaffold protein specificity to determine a reason for heterogeneity and propose a model for the roles of the individual protein homologues in *R. sphaeroides*. The results presented in this chapter suggest that a chemotactic array can be reconstituted in *E. coli* in order to examine the roles of individual MCPs. However, it is probable that a combination of both *R. sphaeroides cheOp2*-expressed CheW proteins and CheA2 are needed in order for full functionality to be restored. The results presented in this chapter suggest that $CheW_2$ and $CheW_3$ are not redundant in their roles and that $CheW_2$ appears to be the dominant contributor to cluster binding in *R. sphaeroides* but $CheW_3$ may play a role in 'tuning' receptor output.

Reconstitution of an *R. sphaeroides*-like chemotaxis pathway in *E. coli* should allow study of individual *R. sphaeroides* MCPs

Reconstitution of $CheW_2$ and $CheA_2$ into *E. coli* allowed recovery of kinase activity in the presence of either *R. sphaeroides* McpH or McpJ. This is shown by the recovery of swim rings in TB plates. However, it seems that neither McpH nor McpJ in this system is capable of responding specifically to a signal on minimal media plates, nor do the swim ring sizes of McpH and McpJ reconstituted pathways in rich media approach a size that matches wild type *E. coli* Tsr signalling. As a result, either a chemotaxis system capable of specific signalling has not been reconstituted or neither McpH nor McpJ can respond significantly, alone, to a component of rich media. The former conclusion is unlikely given that tumbling has been restored to some extent. If these MCPs did respond to some component tested, they should signal through the native *R. sphaeroides* chemotaxis array proteins. It therefore, seems likely that we cannot detect a response to the attractants detected by McpH or McpJ. Either the response mediated through McpH/McpJ is so small that it is undetectable by the methods used or the MCPs respond to an, as yet, unknown attractant, or that there is an

additional component required for signal transduction that is missing in these experiments. For example it may be that some tandem arrangement of MCPs in *R. sphaeroides* is required and by expressing them individually this is not created. Creation of a complete library of plasmid inducible *R. sphaeroides* MCPs should enable the screening of all *R. sphaeroides* MCPs to determine their responses to potential attractants individually. If no MCPs respond significantly to specific attractants known to affect *R. sphaeroides* then further proteins can be added. It may be the case that *R. sphaeroides* MCPs do not respond strongly to any attractants and as a result, the swim plate analyses are inconclusive. The *E. coli* chemotactic model strain RP437, was originally created by sequential enrichment of chemotactic strains on swim plates and as a result may be unnaturally enhanced for chemotactic efficiency (Parkinson, 1978). As a result, the potentially poor chemotactic efficiency of solo receptors exhibited by *R. sphaeroides* may be a more native bacterial phenotype.

Ability to form close interactions are likely important in the ability of the chemotaxis array to signal effectively

Assaying the individual interactions of each component of the array has proved possible through a two-hybrid screen. This was designed specifically for membrane-bound proteins in order to prevent the necessity for diffusion to DNA binding sites to elicit a response (Karimova et al., 2000). The results suggest that some *R. sphaeroides* MCPs are able to form mixed trimers of dimers. This should be possible within MCPs of the same heptad-class, which all of the reported interactions are. Interestingly, no interaction was seen with McpG to any other array protein tested, suggesting that it is incapable of forming close interactions with other MCPs or CheWs. This may explain the strong reduction in chemotaxis seen when expressing McpG in *E. coli* strain RP437. If McpG disrupts the array by preventing tight binding it is possible that signalling efficiency could be effected. McpB* appeared to bind

other MCPs more than McpB and in general, colour appeared during the assay earlier. This agrees with the previous data that suggest McpB* has increased interaction with other array proteins compared with the wild type form and that this may be the reason for the shift in signalling state detected.

$CheW_2$ and $CheW_3$ do not play identical roles in *R. sphaeroides* chemotaxis cluster formation.

It appears from the initial free swimming experiments on the reconstituted McpH and McpJ systems that *E. coli* cells expressing either of these MCPs and $CheW_3$ are able to create a tumbling phenotype when $CheA_2$ is also expressed Therefore these systems can activate kinase activity. In the case of McpH expression in this system, cells do not exhibit any 'run' events and the kinase activity appears to prevent exit of a tumbling event into a swim. This suggests that $CheW_3$ plays a role in forming an active kinase complex but may prevent subsequent deactivation of the $CheA_2$ kinase. The results suggest that this role may be to form a strong interaction with other cluster components that negates MCP-dependent kinase deactivation. In addition, the two hybrid screen showed that $CheW_2$ does not appear to bind strongly to any other *R. sphaeroides* MCP or CheW in *E. coli*. $CheW_3$ was shown to bind McpH, however, suggesting that $CheW_3$ binding, to McpH at least, is likely a much stronger interaction than $CheW_2$. This disagrees with the conclusion that $CheW_2$ is the dominant CheW in *R. sphaeroides* responsible for MCP cluster formation. However, it does agree with the free swimming data that suggest $CheW_3$ forms a strong interaction with McpH and McpJ. It would be interesting to analyse the differential binding affinities for the polar cluster of $CheW_2$ and $CheW_3$ using the FRAP method shown previously. These results suggest that $CheW_2$ should exhibit higher turnover than $CheW_3$. It seems from the data shown here, that a model for $CheW_2$/$CheW_3$ scaffold binding in *R. sphaeroides* could involve a 'fine tuning'

interaction in which $CheW_3$ binds strongly but also prevents cluster deactivation as a result and $CheW_2$ requires some aspect of this interaction in order to fully promote an effective MCP response to $CheA_2$. It may, therefore be possible that a combination of $CheW_2$ and $CheW_3$ is required to 'fine-tune' the response in *R. sphaeroides*, suggesting a reason for the conservation of both. An *E. coli* strain expressing $CheW_2$ and $CheW_3$ in tandem would show whether both are required in order to effectively tune a chemotactic signal.

6.Discussion

6.1 Using computational pipelines to design targeted mutations

Previous studies have used extensive mutation libraries in order to effectively analyse the roles of individual residues and/or domains within a protein. Such studies on chemoreceptors have given much of the current evidence on how signals are transferred across the membrane (Kitanovic et al., 2011), translated by the HAMP domain into a cytoplasmic signal (Zhou et al., 2009) and how binding of the scaffold proteins occurs at the cytoplasmic tip (Miller et al., 2006). Whilst, these studies are time consuming, expensive and resource intensive, they have, as stated, provided strong evidence to form the current theories of signalling through MCPs, however, this study has shown that they can now be used as a basis to populate and refine computational models potentially preventing the need for these screens in future. Chapter 4.1 has shown that computational pipelines can be designed to determine various factors resulting from TM mutagenesis without the need for extensive mutagenesis *in vivo*. The Sidekick pipeline was used to test analogous mutations with known effects on the *E. coli* chemotaxis pathway in *R. sphaeroides* McpB TM2. This was used to predict and limit the results to those with an expected outcome. The mutation with the best fit to the desired properties was chosen for further analysis. The properties desired for the mutation were an obvious, defined effect on TM z-position with either a strong bias for the same or different rotational or tilt positions within the bilayer simulation. Most mutations tested had the effect of removing much of the bias for tilt and/or position, suggesting a large change in stability of the helix, a change which may account for the signal locking effects seen in the analogous

mutations in *E. coli* (Draheim et al., 2006). Therefore, by selecting a mutation with defined, specific shifts in one of these properties it was hoped that an activity shifted mutation would be created, rather than a mutation that would completely lock the receptor cluster output. The free swimming analysis of the variant McpB* expressed in wild type *E. coli* strain RP437 suggests that basal kinase output was indeed shifted and not locked. This suggests that a mutation in the McpB protein of *R. sphaeroides* was effectively engineered to meet a specific criteria and that screening *in silico* through the Sidekick system was effective at achieving this.

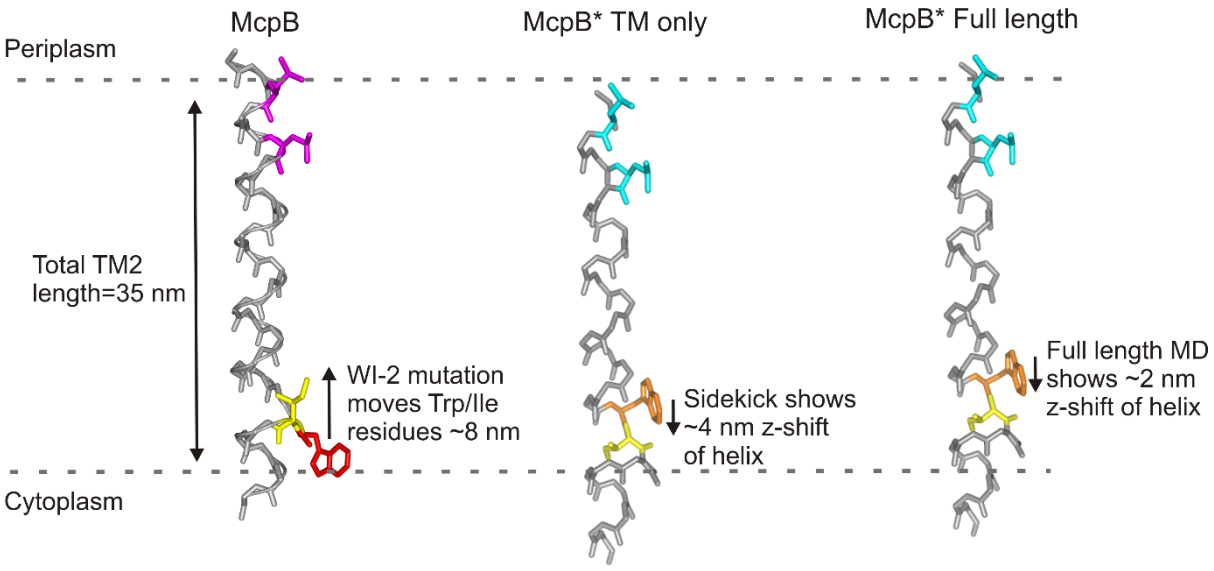

Figure 6-1 The TM2 motions predicted by the two different simulations. The dotted lines show the membrane interfacial regions and the TM2 helix of McpB is shown in all three cases as grey sticks. The cytoplasm interfacial tryptophan residue is labelled orange, the isoleucine labelled yellow and the periplasm interfacial arginines are labelled in cyan. **Left** the predicted position of wild type McpB in the membrane, which matches the simulation data. The McpB* mutation shifts the tryptophan and isoleucine residues approximately 8 nm towards the periplasm along the TM2 helix. **Middle** the predicted position of McpB* TM2 from the sidekick simulation, approximately 4 nm closer to the cytoplasm than wild type McpB TM2. **Right** the predicted position of McpB* TM2 from the full length simulation showing that the helix only shifts approximately 2 nm towards the cytoplasm

The predicted motion of the TM helix was further analysed using molecular dynamics simulations of the full length McpB*. This showed that the McpB TM2 helix, when mutated, did in fact shift towards the cytoplasm, as predicted, presumably to maintain tryptophan

contact with the bilayer interface region. However, the motion was less than that predicted by the Sidekick screen (Figure 6-1). This may explain the resultant change in activity exhibited by the variant protein, taking into account the prediction that MCP activity is dependent on cytoplasmic domain flexibility. A 2 nm shift in helix position is still larger than the 1 Å motion suggested from crystal structures that occurs when bound to ligand, which suggests that the shift upon ligand binding may be very slight (Cheung and Hendrickson, 2009). It is possible that the wild type McpB TM2 helix has inherent instability within the membrane which allows it to easily switch between active and inactive states through relatively small energetic changes upon binding. By shifting the interfacial residues of McpB*, the TM helix may be able to adopt a more stable arrangement within the bilayer and thus transmits this increased stability to the HAMP domain which then promotes the stable output helix conformation (Parkinson, 2010).

6.2 A model for signalling

It has been shown through various methods that MCPs form a large array at the polar cluster with hexagonal packing symmetry (Briegel et al., 2008) (Briegel et al., 2012) (Khursigara et al., 2008a). In addition, it has been suggested that HAMP packing is involved in the transduction of a periplasmic signal to the cytoplasmic region (Parkinson, 2010). The latter suggests that a shift between two modes of packing in HAMP switches between normal coiled-coil packing of the cytoplasmic domain and one that initiates a stutter between the helical packing which increases flexibility.

A recent study showed that upon deletion of the HAMP domain from *E. coli* Tsr receptors, the system was locked in a kinase-on state (Ames et al., 2014). This, they reasoned, showed that the kinase-on state was the native state of the receptor. This leads to the model of

signalling shown in Figure 6-2, where in the absence of any ligand binding to the receptor, there is an output of CheA kinase activity. The decreased flexibility shown by the McpB* variant protein in this computational study, suggests that this active state confirmation is the result of lower flexibility of the chemoreceptor protein cytoplasmic domain. Further analysis of the RMSD of simulations, particularly focussed around the cytoplasmic domain residues could shed further light on this conclusion. The lower flexibility exhibited by the McpB* decreases the entropic penalty caused by a tight interaction to CheA and is therefore more favourable. The formation of a MCP:CheW:CheA complex allows activation of the kinase and a kinase-on response. This decreased flexibility would also contribute to the increased localisation of variant McpB* receptors seen by the fluorescent fusion studies presented. If flexibility is decreased, MCP:MCP interaction will become more favourable as well as MCP:scaffold. If the interaction for either or both is naturally weak and thus cause naturally minimal cluster integrity (as may be the case for expression of *R. sphaeroides* components in an *E. coli* background), this increased interaction energy would favour cluster formation in such a way as to be visible as a clear increase in localisation to the polar cluster. The increase in the binding of scaffold proteins suggested from this model can be seen by the tighter binding of CheW to the variant McpB* during FRAP studies. In addition, the increase of MCP:MCP interactions by McpB* is seen in the bacterial two-hybrid analysis in which McpB* has higher affinity for other chemoreceptors than appears to be the case for the wild type McpB.

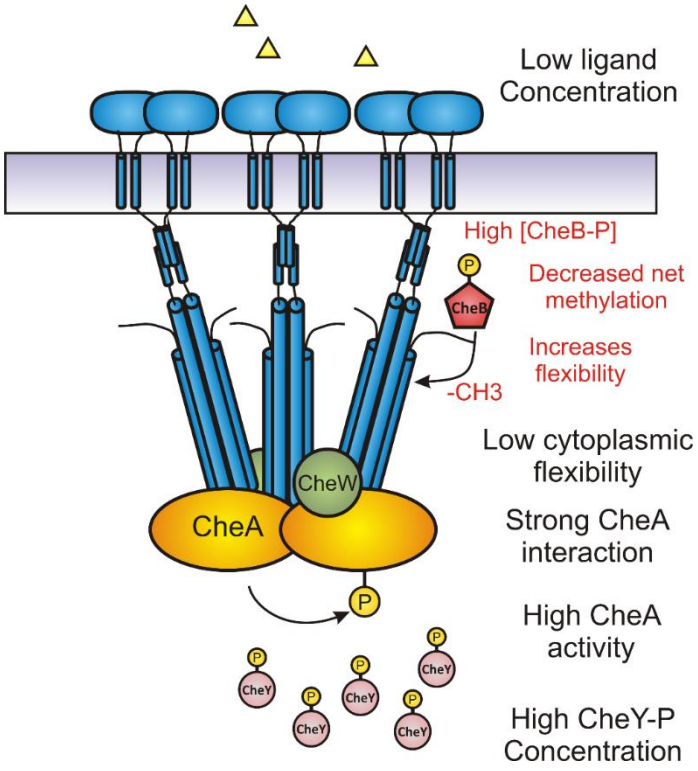

Figure 6-2 The typical polar chemotaxis array in low ligand concentration conditions. Low ligand occupancy results in the native signalling state of the receptor: a relatively stable conformation of cytoplamsmic coiled-coil packing. This stable conformation causes little entropic loss upon formation of stable array contacts both between MCP dimers and to the kinase and scaffold proteins. As a result of strong MCP binding, CheA kinase activity is increased causing a high cytoplasmic CheY-P concentration and an increase in tumbling. High CheB-P levels result in lower methylation levels to decrease stability and adapt.

In the case of high ligand occupancy, it is necessary that relatively small binding energies are utilised to cause a change significant enough to prevent CheA activity (Falke and Erbse, 2009). Therefore, it is unlikely that a specific, large structural change is caused by ligand binding. However, if HAMP packing is shifted, it is possible that large distortions in the cytoplasmic coiled-coil could merely be caused by a destabilising effect on the coiled-coil due to continuation of this shifted packing (Parkinson, 2010). One way this is proposed to occur is through differential binding of attractants to the two monomers of the ligand-binding domain (LBD) (Yeh et al., 1996). LBDs are dimeric and coupled and therefore have two ligand binding sites in each domain. It is proposed that one binding site of the LBD is a ‘strong’ site, exhibiting greater affinity for its ligand. As a result, it may be that signalling

occurs through asymmetric binding in the LBD. This would in turn cause an asymmetric shift in the TM2 helix which would presumably lead to the proposed packing shift in HAMP. This would result in the destabilisation of the cytoplasmic domain proposed here to be responsible for CheA binding and subsequent activity, however, it doesn't fully explain adaptation and its role in CheA activity. It is possible that this asymmetric TM2 shift is merely one way in which flexibility can tune the cytoplasmic domain, as demonstrated by the studies shown here on the McpB* variant and other mutagenesis studies on the TM2 helix (Draheim et al., 2006). All previous studies have shifted the activity of the chemoreceptor by mutating both monomers of the dimer. This would presumably not result in the asymmetric shift proposed above to result in a change in cytoplasmic domain flexibility. However, it is possible that mutation of both monomers merely shifts the state of the protein to a more flexible mode through coupling of some other form, such as interaction with the bilayer. Such a direct shift of flexibility state without an asymmetric motion, may also be the case for the role of methylation in adaptation and would go some way to explaining how some chemoreceptors contain methylation sites that activate the kinase and others that deactivate (Zimmer et al., 2000). Any mutation, or adaptation, that stabilises the cytoplasmic domain and results in lower flexibility is likely to increase the interaction with other MCP dimers and the CheA kinase. Whereas, any mutation, or adaptation that decreases cytoplasmic packing stability should cause some destabilisation of the cytoplasmic domain as a whole. Such increased local destabilisation may result in increased flexibility, which would cause a higher entropic penalty to tight cluster formation and a lower affinity for other MCP dimers and the CheA kinase, resulting in lower kinase activity. This model for the lack of CheA kinase activity in the presence of attractant stimulus is shown in Figure 6-3.

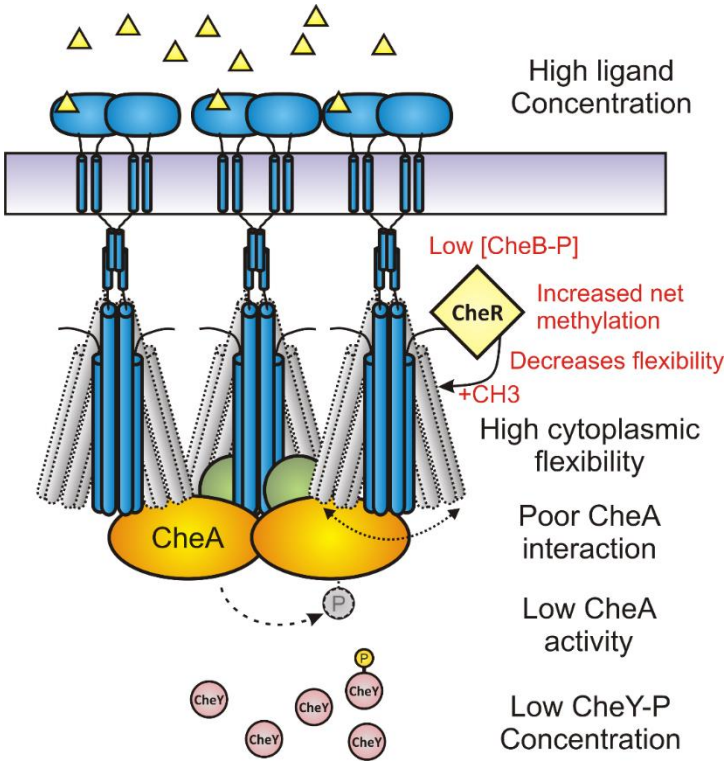

Figure 6-3 The typical polar chemotaxis array in high ligand conditions. High ligand occupancy results in a non-native, high energy receptor state: a less stable conformation of cytoplamsmic coiled-coil packing. This unstable conformation is inherently flexible and so causes a high entropic loss upon formation of stable array contacts both between MCP dimers and to the kinase and scaffold proteins. As a result binding is weak, CheA kinase activity is low and CheY-P concentration is low, resulting in a low chance of tumbling. Low CheB-P levels result in high net methylation levels which increases cytoplasmic domain stability and adapts the receptor.

This mechanism allows for rapid changes in activity and requires very little energy to achieve. In addition, it goes someway to describing the cooperativity of chemotactic signalling. CheA and CheW proteins form an array at the base of the polar cluster and anchor the receptor trimer of dimers into the hexagonal packing seen. If stability of one such trimeric unit is disrupted, local disorder would increase. This would decrease the average enthalpic contribution of the bonds present between cluster components, making the order necessary for array binding less favourable. The result is that forming a fixed and rigid structure surrounding local disorder becomes less favourable and hence the surrounding receptors will also be less likely to strongly bind and activate the CheA kinase. Such a

'melting and freezing' state of receptors has been proposed and computed to be likely previously and evidence shown here supports this mechanism (Bray and Williams, 2008).

6.3 *R. sphaeroides* chemotaxis protein specificity

R. sphaeroides contains multiple homologues of chemotaxis proteins. The roles of some, homologues is known, such as those involved in the cytoplasmic cluster (Wadhams et al., 2002). $CheW_2$ and $CheW_3$ are known to localise predominantly at the polar cluster, however, little is known other than this and their specificity for individual MCPs is not known. In addition, ligand partners of *R. sphaeroides* MCPs have not been determined directly. The results presented here show that *R. sphaeroides* $CheW_2$ and $CheW_3$ are not redundant proteins. Only $CheW_2$ supports output from the kinase when present as the only CheW, when expressed in tandem with $CheA_2$ and McpH or McpJ in the receptor-less *E. coli* system. $CheW_3$ does not support such a phenotype in swim plates but does appear to constitute a tumbling phenotype in free swimming. This suggests it can form a functioning complex with $CheA_2$ in order to allow tumbling to occur, but is not able to signal efficiently in order to terminate the tumbling event, and as a result its full function remains unknown. The lack of prolonged swimming events in strains expressing $CheW_3$ in tandem with $CheA_2$ and McpH suggests that $CheW_3$ causes constitutive kinase activity. If reasoned with the bacterial two-hybrid data and the model of kinase activity presented here, it may be that $CheW_3$ has a high affinity for complex formation and is part of a mechanism of fine tuning of the *R. sphaeroides* chemotaxis cluster. High affinity of $CheW_3$ cluster binding would continue to overcome entropic penalties from MCP binding that may stem from increased adaptation

or lack of signal. Both $CheW_2$ and $CheW_3$ may be required to create a complex effectively tuned to accurately respond to stimuli.

Reconstitution of $CheW_2$ and $CheA_2$ into an *E. coli* background allowed the recreation of a chemotactic complex able to activate kinase activity. However, it appears from analysis on minimal media plates and the subsequent free swimming analysis that neither McpH nor McpJ is able to respond specifically to any component of rich media in this background. In addition, both showed the same chemotactic response to all attractants tested in minimal media swim plates. There are several conclusions one could draw from this, however, in the context of the other results contained here it is likely that $CheW_3$ is also needed to tune the chemotactic array in order to effectively signal specifically to known attractants. A strain that expresses both $CheW_2$ and $CheW_3$ from the genome would allow this conclusion to be analysed further.

$CheW_3$ appears from both free swimming and bacterial two-hybrid analysis to have a stronger interaction for the chemoreceptors than $CheW_2$. This would explain the lack of a swimming phenotype if taken together with the previous model for signalling. If $CheW_3$ is able to bind tightly to the receptors, the flexible state will not be favoured and $CheA_2$ will always be able to form stable contacts. As a result, $CheA_2$ would remain active and cellular CheY-P would remain sufficiently high to continue tumbling. This indeed suggests that in *R. sphaeroides*, a combination of $CheW_2$ and $CheW_3$ is used to ‘fine-tune’ an appropriate chemotaxis signal from the receptor array.

7.Bibliography

Aiba, H., Nakasai, F., Mizushima, S., and Mizuno, T. (1989). Phosphorylation of a bacterial activator protein, OmpR, by a protein kinase, EnvZ, results in stimulation of its DNA-binding ability. J. Biochem. *106*, 5–7.

Airola, M. V., Watts, K.J., Bilwes, A.M., and Crane, B.R. (2010). Structure of concatenated HAMP domains provides a mechanism for signal transduction. Structure *18*, 436–448.

Airola, M. V., Sukomon, N., Samanta, D., Borbat, P.P., Freed, J.H., Watts, K.J., and Crane, B.R. (2013). HAMP domain conformers that propagate opposite signals in bacterial chemoreceptors. PLoS Biol. *11*, e1001479.

Alex, L.A., and Simon, M.I. (1994). Protein histidine kinases and signal tranduction in prokaryotes and eukaryotes. Trends Genet. *10*, 133–138.

Alexander, R.P., and Zhulin, I.B. (2007). Evolutionary genomics reveals conserved structural determinants of signaling and adaptation in microbial chemoreceptors. Proc. Natl. Acad. Sci. U. S. A. *104*, 2885–2890.

Alexander, R.P., Lowenthal, A.C., Harshey, R.M., and Ottemann, K.M. (2010). CheV: CheW-like coupling proteins at the core of the chemotaxis signaling network. Trends Microbiol. *18*, 494–503.

Alexandre, G., and Zhulin, I.B. (2003). Different evolutionary constraints on chemotaxis proteins cheW and cheY revealed by heterologous expression studies and protein sequence analysis. J. Bacteriol. *185*, 544–552.

Alt, W. (1980). Biased random walk models for chemotaxis and related diffusion approximations. J. Math. Biol. *9*, 147–177.

Ames, P., Studdert, C.A., Reiser, R.H., and Parkinson, J.S. (2002). Collaborative signaling by mixed chemoreceptor teams in Escherichia coli. Proc. Natl. Acad. Sci. U. S. A. *99*, 7060–7065.

Ames, P., Zhou, Q., and Parkinson, J.S. (2014). HAMP domain structural determinants for signalling and sensory adaptation in Tsr, the Escherichia coli serine chemoreceptor. Mol. Microbiol. *91*, 875–886.

Amin, D.N., and Hazelbauer, G.L. (2010). The chemoreceptor dimer is the unit of conformational coupling and transmembrane signaling. J. Bacteriol. *192*, 1193–1200.

Anand, G.S., and Stock, A.M. (2002). Kinetic basis for the stimulatory effect of phosphorylation on the methylesterase activity of CheB. Biochemistry *41*, 6752–6760.

Anand, G.S., Goudreau, P.N., Lewis, J.K., and Stoc, A.M. (2000). Evidence for phosphorylation-dependent conformational changes in methylesterase CheB. Protein Sci. *9*, 898–906.

Appleby, J.L., and Bourret, R.B. (1998). Proposed signal transduction role for conserved CheY residue Thr87, a member of the response regulator active-site quintet. J. Bacteriol. *180*, 3563–3569.

Ban, C., Junop, M., and Yang, W. (1999). Transformation of MutL by ATP binding and hydrolysis: a switch in DNA mismatch repair. Cell *97*, 85–97.

Barkai, N., and Leibler, S. (1997). Robustness in simple biochemical networks. Nature *387*, 913–917.

Barnakov, A., Altenbach, C., Barnakova, L., Hubbell, W.L., and Hazelbauer, G.L. (2002). Site-directed spin labeling of a bacterial chemoreceptor reveals a dynamic, loosely packed transmembrane domain. Protein Sci. *11*, 1472–1481.

Bartelli, N.L., and Hazelbauer, G.L. (2011). Direct evidence that the carboxyl-terminal sequence of a bacterial chemoreceptor is an unstructured linker and enzyme tether. Protein Sci. *20*, 1856–1866.

Baumgartner, J.W., and Hazelbauer, G.L. (1996). Mutational analysis of a transmembrane segment in a bacterial chemoreceptor. J. Bacteriol. *178*, 4651–4660.

Bell, C.H., Porter, S.L., Strawson, A., Stuart, D.I., and Armitage, J.P. (2010). Using structural information to change the phosphotransfer specificity of a two-component chemotaxis signalling complex. PLoS Biol. *8*, e1000306.

Berg, H.C. (2003). The rotary motor of bacterial flagella. Annu. Rev. Biochem. *72*, 19–54.

Berleman, J.E., and Bauer, C.E. (2005a). Involvement of a Che-like signal transduction cascade in regulating cyst cell development in Rhodospirillum centenum. Mol. Microbiol. *56*, 1457–1466.

Berleman, J.E., and Bauer, C.E. (2005b). A che-like signal transduction cascade involved in controlling flagella biosynthesis in Rhodospirillum centenum. Mol. Microbiol. *55*, 1390–1402.

Bi, S., Yu, D., Si, G., Luo, C., Li, T., Ouyang, Q., Jakovljevic, V., Sourjik, V., Tu, Y., and Lai, L. (2013). Discovery of novel chemoeffectors and rational design of Escherichia coli chemoreceptor specificity. Proc. Natl. Acad. Sci. U. S. A. *110*, 16814–16819.

Bilwes, A.M., Alex, L.A., Crane, B.R., and Simon, M.I. (1999). Structure of CheA, a signal-transducing histidine kinase. Cell *96*, 131–141.

Boldog, T., Grimme, S., Li, M., Sligar, S.G., and Hazelbauer, G.L. (2006). Nanodiscs separate chemoreceptor oligomeric states and reveal their signaling properties. Proc. Natl. Acad. Sci. U. S. A. *103*, 11509–11514.

Borkovich, K.A., and Simon, M.I. (1990). The dynamics of protein phosphorylation in bacterial chemotaxis. Cell *63*, 1339–1348.

Borkovich, K.A., Alex, L.A., and Simon, M.I. (1992). Attenuation of sensory receptor signaling by covalent modification. Proc. Natl. Acad. Sci. *89*, 6756–6760.

Boukhvalova, M.S., Dahlquist, F.W., and Stewart, R.C. (2002). CheW binding interactions with CheA and Tar. Importance for chemotaxis signaling in Escherichia coli. J. Biol. Chem. *277*, 22251–22259.

Bourret, R.B., Borkovich, K.A., and Simon, M.I. (1991). Signal transduction pathways involving protein phosphorylation in prokaryotes. Annu. Rev. Biochem. *60*, 401–441.

Bowie, J.U., Pakula, a a, and Simon, M.I. (1995). The three-dimensional structure of the aspartate receptor from Escherichia coli. Acta Crystallogr. D. Biol. Crystallogr. *51*, 145–154.

Bray, D., and Williams, D. (2008). How the "melting" and "freezing" of protein molecules may be used in cell signaling. ACS Chem. Biol. *3*, 89–91.

Briegel, A., Ding, H.J., Li, Z., Werner, J., Gitai, Z., Dias, D.P., Jensen, R.B., and Jensen, G.J. (2008). Location and architecture of the Caulobacter crescentus chemoreceptor array. Mol. Microbiol. *69*, 30–41.

Briegel, A., Li, X., Bilwes, A.M., Hughes, K.T., Jensen, G.J., and Crane, B.R. (2012). Bacterial chemoreceptor arrays are hexagonally packed trimers of receptor dimers networked by rings of kinase and coupling proteins. Proc. Natl. Acad. Sci. U. S. A. *109*, 3766–3771.

Burbulys, D., Trach, K.A., and Hoch, J.A. (1991). Initiation of sporulation in B. subtilis is controlled by a multicomponent phosphorelay. Cell *64*, 545–552.

Burrows, L.L. (2012). Pseudomonas aeruginosa twitching motility: type IV pili in action. Annu. Rev. Microbiol. *66*, 493–520.

Del Campo, A.M., Ballado, T., de la Mora, J., Poggio, S., Camarena, L., and Dreyfus, G. (2007). Chemotactic control of the two flagellar systems of Rhodobacter sphaeroides is mediated by different sets of CheY and FliM proteins. J. Bacteriol. *189*, 8397–8401.

Capra, E.J., and Laub, M.T. (2012). Evolution of two-component signal transduction systems. Annu. Rev. Microbiol. *66*, 325–347.

Cardozo, M.J., Massazza, D.A., Parkinson, J.S., and Studdert, C.A. (2010). Disruption of chemoreceptor signalling arrays by high levels of CheW, the receptor-kinase coupling protein. Mol. Microbiol. *75*, 1171–1181.

Cashman, D.J., Ortega, D.R., Zhulin, I.B., and Baudry, J. (2013). Homology modeling of the CheW coupling protein of the chemotaxis signaling complex. PLoS One *8*, e70705.

Chervitz, S.A., and Falke, J.J. (1996). Molecular mechanism of transmembrane signaling by the aspartate receptor: a model. Proc. Natl. Acad. Sci. U. S. A. *93*, 2545–2550.

Cheung, J., and Hendrickson, W.A. (2009). Structural analysis of ligand stimulation of the histidine kinase NarX. Structure *17*, 190–201.

Cheung, J., Bingman, C.A., Reyngold, M., Hendrickson, W.A., and Waldburger, C.D. (2008). Crystal structure of a functional dimer of the PhoQ sensor domain. J. Biol. Chem. *283*, 13762–13770.

Cho, H.S., Lee, S.Y., Yan, D., Pan, X., Parkinson, J.S., Kustu, S., Wemmer, D.E., and Pelton, J.G. (2000). NMR structure of activated CheY. J. Mol. Biol. *297*, 543–551.

Cluzel, P., Surette, M., and Leibler, S. (2000). An ultrasensitive bacterial motor revealed by monitoring signaling proteins in single cells. Science *287*, 1652–1655.

DeBeyer, J. (2013). Roles of the two chemotaxis clusters in Rhodobacter sphaeroides. University of Oxford.

Djordjevic, S., and Stock, A.M. (1997). Crystal structure of the chemotaxis receptor methyltransferase CheR suggests a conserved structural motif for binding S-adenosylmethionine. Structure *5*, 545–558.

Djordjevic, S., Goudreau, P.N., Xu, Q., Stock, A.M., and West, A.H. (1998). Structural basis for methylesterase CheB regulation by a phosphorylation-activated domain. Proc. Natl. Acad. Sci. U. S. A. *95*, 1381–1386.

Draheim, R.R., Bormans, A.F., Lai, R., and Manson, M.D. (2005). Tryptophan residues flanking the second transmembrane helix (TM2) set the signaling state of the Tar chemoreceptor. Biochemistry *44*, 1268–1277.

Draheim, R.R., Bormans, A.F., Lai, R.-Z., and Manson, M.D. (2006). Tuning a bacterial chemoreceptor with protein-membrane interactions. Biochemistry *45*, 14655–14664.

Dyer, C.M., and Dahlquist, F.W. (2006). Switched or not?: the structure of unphosphorylated CheY bound to the N terminus of FliM. J. Bacteriol. *188*, 7354–7363.

Dyer, C.M., Vartanian, A.S., Zhou, H., and Dahlquist, F.W. (2009). A molecular mechanism of bacterial flagellar motor switching. J. Mol. Biol. *388*, 71–84.

Endres, R.G. (2009). Polar chemoreceptor clustering by coupled trimers of dimers. Biophys. J. *96*, 453–463.

Endres, R.G., and Wingreen, N.S. (2006). Precise adaptation in bacterial chemotaxis through "assistance neighborhoods". Proc. Natl. Acad. Sci. U. S. A. *103*, 13040–13044.

Engström, P., and Hazelbauer, G.L. (1980). Multiple methylation of methyl-accepting chemotaxis proteins during adaptation of E. coli to chemical stimuli. Cell *20*, 165–171.

Falke, J.J., and Erbse, A.H. (2009). The piston rises again. Structure *17*, 1149–1151.

Falke, J.J., and Hazelbauer, G.L. (2001). Transmembrane signaling in bacterial chemoreceptors. Trends Biochem. Sci. *26*, 257–265.

Falke, J.J., Bass, R.B., Butler, S.L., Chervitz, S.A., and Danielson, M.A. (1997). The two-component signaling pathway of bacterial chemotaxis: a molecular view of signal transduction by receptors, kinases, and adaptation enzymes. Annu. Rev. Cell Dev. Biol. *13*, 457–512.

Feher, V.A., Zapf, J.W., Hoch, J.A., Whiteley, J.M., McIntosh, L.P., Rance, M., Skelton, N.J., Dahlquist, F.W., and Cavanagh, J. (1997). High-resolution NMR structure and backbone dynamics of the Bacillus subtilis response regulator, Spo0F: implications for phosphorylation and molecular recognition. Biochemistry *36*, 10015–10025.

Ferré, A., De La Mora, J., Ballado, T., Camarena, L., and Dreyfus, G. (2004). Biochemical study of multiple CheY response regulators of the chemotactic pathway of Rhodobacter sphaeroides. J. Bacteriol. *186*, 5172–5177.

Ferris, H.U., Dunin-Horkawicz, S., Mondéjar, L.G., Hulko, M., Hantke, K., Martin, J., Schultz, J.E., Zeth, K., Lupas, A.N., and Coles, M. (2011). The mechanisms of HAMP-mediated signaling in transmembrane receptors. Structure *19*, 378–385.

Ferris, H.U., Dunin-Horkawicz, S., Hornig, N., Hulko, M., Martin, J., Schultz, J.E., Zeth, K., Lupas, A.N., and Coles, M. (2012). Mechanism of regulation of receptor histidine kinases. Structure *20*, 56–66.

Fiedler, U., and Weiss, V. (1995). A common switch in activation of the response regulators NtrC and PhoB: phosphorylation induces dimerization of the receiver modules. EMBO J. *14*, 3696–3705.

Francis, N.R., Levit, M.N., Shaikh, T.R., Melanson, L.A., Stock, J.B., and DeRosier, D.J. (2002). Subunit organization in a soluble complex of tar, CheW, and CheA by electron microscopy. J. Biol. Chem. *277*, 36755–36759.

Francis, N.R., Wolanin, P.M., Stock, J.B., Derosier, D.J., and Thomas, D.R. (2004). Three-dimensional structure and organization of a receptor/signaling complex. Proc. Natl. Acad. Sci. U. S. A. *101*, 17480–17485.

Gegner, J.A., Graham, D.R., Roth, A.F., and Dahlquist, F.W. (1992). Assembly of an MCP receptor, CheW, and kinase CheA complex in the bacterial chemotaxis signal transduction pathway. Cell *70*, 975–982.

Greenfield, D., McEvoy, A.L., Shroff, H., Crooks, G.E., Wingreen, N.S., Betzig, E., and Liphardt, J. (2009). Self-organization of the Escherichia coli chemotaxis network imaged with super-resolution light microscopy. PLoS Biol. *7*, e1000137.

Grimsley, J.K., Tjalkens, R.B., Strauch, M.A., Bird, T.H., Spiegelman, G.B., Hostomsky, Z., Whiteley, J.M., and Hoch, J.A. (1994). Subunit composition and domain structure of the Spo0A sporulation transcription factor of Bacillus subtilis. J. Biol. Chem. *269*, 16977–16982.

Griswold, I.J., Zhou, H., Matison, M., Swanson, R. V, McIntosh, L.P., Simon, M.I., and Dahlquist, F.W. (2002). The solution structure and interactions of CheW from Thermotoga maritima. Nat. Struct. Biol. *9*, 121–125.

Guzman, L.M., Belin, D., Carson, M.J., and Beckwith, J. (1995). Tight regulation, modulation, and high-level expression by vectors containing the arabinose PBAD promoter. J. Bacteriol. *177*, 4121–4130.

Haldimann, A., and Wanner, B.L. (2001). Conditional-replication, integration, excision, and retrieval plasmid-host systems for gene structure-function studies of bacteria. J. Bacteriol. *183*, 6384–6393.

Hall, B.A., Armitage, J.P., and Sansom, M.S.P. (2011). Transmembrane helix dynamics of bacterial chemoreceptors supports a piston model of signalling. PLoS Comput. Biol. *7*, e1002204.

Hall, B.A., Armitage, J.P., and Sansom, M.S.P. (2012). Mechanism of bacterial signal transduction revealed by molecular dynamics of Tsr dimers and trimers of dimers in lipid vesicles. PLoS Comput. Biol. *8*, e1002685.

Hall, B.A., Halim, K.B.A., Buyan, A., Emmanouil, B., and Sansom, M.S.P. (2014). Sidekick for Membrane Simulations: Automated Ensemble Molecular Dynamics Simulations of Transmembrane Helices. J. Chem. Theory Comput. *10*, 2165–2175.

Hamblin, P.A., Bourne, N.A., and Armitage, J.P. (1997). Characterization of the chemotaxis protein CheW from Rhodobacter sphaeroides and its effect on the behaviour of Escherichia coli. Mol. Microbiol. *24*, 41–51.

Hamer, R., Chen, P.-Y., Armitage, J.P., Reinert, G., and Deane, C.M. (2010). Deciphering chemotaxis pathways using cross species comparisons. BMC Syst. Biol. *4*, 3.

Hazelbauer, G.L., Falke, J.J., and Parkinson, J.S. (2008). Bacterial chemoreceptors: high-performance signaling in networked arrays. Trends Biochem. Sci. *33*, 9–19.

Herrera Seitz, M.K., Frank, V., Massazza, D. a, Vaknin, A., and Studdert, C. a (2014). Bacterial chemoreceptors of different length classes signal independently. Mol. Microbiol.

Hess, J.F., Oosawa, K., Kaplan, N., and Simon, M.I. (1988). Phosphorylation of three proteins in the signaling pathway of bacterial chemotaxis. Cell *53*, 79–87.

Hu, J., Xin, Z., Shugang, L., Zhicao, L., Feng, P., and Songlin, C. (2011). Image processing method for laser damage probability measurement by single-shot of laser pulse. Opt. Express *19*, 10625–10631.

Huala, E., Stigter, J., and Ausubel, F.M. (1992). The central domain of Rhizobium leguminosarum DctD functions independently to activate transcription. J. Bacteriol. *174*, 1428–1431.

Hughson, A.G., and Hazelbauer, G.L. (1996). Detecting the conformational change of transmembrane signaling in a bacterial chemoreceptor by measuring effects on disulfide cross-linking in vivo. Proc. Natl. Acad. Sci. U. S. A. *93*, 11546–11551.

Hulko, M., Berndt, F., Gruber, M., Linder, J.U., Truffault, V., Schultz, A., Martin, J., Schultz, J.E., Lupas, A.N., and Coles, M. (2006). The HAMP domain structure implies helix rotation in transmembrane signaling. Cell *126*, 929–940.

Ind, A.C., Porter, S.L., Brown, M.T., Byles, E.D., de Beyer, J.A., Godfrey, S.A., and Armitage, J.P. (2009). Inducible-expression plasmid for Rhodobacter sphaeroides and Paracoccus denitrificans. Appl. Environ. Microbiol. *75*, 6613–6615.

Ingham, C.J., and Armitage, J.P. (1987). Involvement of transport in Rhodobacter sphaeroides chemotaxis. J. Bacteriol. *169*, 5801–5807.

Isaac, B., Gallagher, G.J., Balazs, Y.S., and Thompson, L.K. (2002). Site-directed rotational resonance solid-state NMR distance measurements probe structure and mechanism in the transmembrane domain of the serine bacterial chemoreceptor. Biochemistry *41*, 3025–3036.

Island, M.D., Wei, B.Y., and Kadner, R.J. (1992). Structure and function of the uhp genes for the sugar phosphate transport system in Escherichia coli and Salmonella typhimurium. J. Bacteriol. *174*, 2754–2762.

Jeffery, C.J., and Koshland, D.E. (1993). Three-dimensional structural model of the serine receptor ligand-binding domain. Protein Sci. *2*, 559–566.

Jiang, M., Bourret, R.B., Simon, M.I., and Volz, K. (1997). Uncoupled phosphorylation and activation in bacterial chemotaxis. The 2.3 A structure of an aspartate to lysine mutant at position 13 of CheY. J. Biol. Chem. *272*, 11850–11855.

Karimova, G., Pidoux, J., Ullmann, A., and Ladant, D. (1998). A bacterial two-hybrid system based on a reconstituted signal transduction pathway. Proc. Natl. Acad. Sci. U. S. A. *95*, 5752–5756.

Karimova, G., Ullmann, A., and Ladant, D. (2000). A bacterial two-hybrid system that exploits a cAMP signaling cascade in Escherichia coli. Methods Enzymol. *328*, 59–73.

Karimova, G., Dautin, N., and Ladant, D. (2005). Interaction network among Escherichia coli membrane proteins involved in cell division as revealed by bacterial two-hybrid analysis. J. Bacteriol. *187*, 2233–2243.

Kearns, D.B. (2010). A field guide to bacterial swarming motility. Nat. Rev. Microbiol. *8*, 634–644.

Kentner, D., and Sourjik, V. (2009). Dynamic map of protein interactions in the Escherichia coli chemotaxis pathway. Mol. Syst. Biol. *5*, 238.

Khursigara, C.M., Wu, X., and Subramaniam, S. (2008a). Chemoreceptors in Caulobacter crescentus: trimers of receptor dimers in a partially ordered hexagonally packed array. J. Bacteriol. *190*, 6805–6810.

Khursigara, C.M., Wu, X., Zhang, P., Lefman, J., and Subramaniam, S. (2008b). Role of HAMP domains in chemotaxis signaling by bacterial chemoreceptors. Proc. Natl. Acad. Sci. U. S. A. *105*, 16555–16560.

Khursigara, C.M., Lan, G., Neumann, S., Wu, X., Ravindran, S., Borgnia, M.J., Sourjik, V., Milne, J., Tu, Y., and Subramaniam, S. (2011). Lateral density of receptor arrays in the membrane plane influences sensitivity of the E. coli chemotaxis response. EMBO J. *30*, 1719–1729.

Kim, K.K., Yokota, H., and Kim, S.H. (1999). Four-helical-bundle structure of the cytoplasmic domain of a serine chemotaxis receptor. Nature *400*, 787–792.

Kirby, J.R., and Zusman, D.R. (2003). Chemosensory regulation of developmental gene expression in Myxococcus xanthus. Proc. Natl. Acad. Sci. U. S. A. *100*, 2008–2013.

Kirby, J.R., Saulmon, M.M., Kristich, C.J., and Ordal, G.W. (1999). CheY-dependent methylation of the asparagine receptor, McpB, during chemotaxis in Bacillus subtilis. J. Biol. Chem. *274*, 11092–11100.

Kirby, J.R., Kristich, C.J., Saulmon, M.M., Zimmer, M.A., Garrity, L.F., Zhulin, I.B., and Ordal, G.W. (2001). CheC is related to the family of flagellar switch proteins and acts independently from CheD to control chemotaxis in Bacillus subtilis. Mol. Microbiol. *42*, 573–585.

Kitanovic, S., Ames, P., and Parkinson, J.S. (2011). Mutational analysis of the control cable that mediates transmembrane signaling in the Escherichia coli serine chemoreceptor. J. Bacteriol. *193*, 5062–5072.

Kojadinovic, M., Sirinelli, A., Wadhams, G.H., and Armitage, J.P. (2011). New motion analysis system for characterization of the chemosensory response kinetics of Rhodobacter sphaeroides under different growth conditions. Appl. Environ. Microbiol. *77*, 4082–4088.

Kondo, H., Nakagawa, A., Nishihira, J., Nishimura, Y., Mizuno, T., and Tanaka, I. (1997). Escherichia coli positive regulator OmpR has a large loop structure at the putative RNA polymerase interaction site. Nat. Struct. Biol. *4*, 28–31.

Larkin, M.A., Blackshields, G., Brown, N.P., Chenna, R., McGettigan, P.A., McWilliam, H., Valentin, F., Wallace, I.M., Wilm, A., Lopez, R., et al. (2007). Clustal W and Clustal X version 2.0. Bioinformatics *23*, 2947–2948.

Leake, M.C., Chandler, J.H., Wadhams, G.H., Bai, F., Berry, R.M., and Armitage, J.P. (2006). Stoichiometry and turnover in single, functioning membrane protein complexes. Nature *443*, 355–358.

Lee, S.Y., Cho, H.S., Pelton, J.G., Yan, D., Berry, E.A., and Wemmer, D.E. (2001). Crystal structure of activated CheY. Comparison with other activated receiver domains. J. Biol. Chem. *276*, 16425–16431.

Levit, M.N., and Stock, J.B. (2002). Receptor methylation controls the magnitude of stimulus-response coupling in bacterial chemotaxis. J. Biol. Chem. *277*, 36760–36765.

Li, G., and Weis, R.M. (2000). Covalent modification regulates ligand binding to receptor complexes in the chemosensory system of Escherichia coli. Cell *100*, 357–365.

Li, M., and Hazelbauer, G.L. (2004). Cellular stoichiometry of the components of the chemotaxis signaling complex. J. Bacteriol. *186*, 3687–3694.

Li, X., Fleetwood, A.D., Bayas, C., Bilwes, A.M., Ortega, D.R., Falke, J.J., Zhulin, I.B., and Crane, B.R. (2013). The 3.2 Å resolution structure of a receptor: CheA:CheW signaling complex defines overlapping binding sites and key residue interactions within bacterial chemosensory arrays. Biochemistry *52*, 3852–3865.

Li, Y., Hu, Y., Fu, W., Xia, B., and Jin, C. (2007). Solution structure of the bacterial chemotaxis adaptor protein CheW from Escherichia coli. Biochem. Biophys. Res. Commun. *360*, 863–867.

Lim, S.-K., Kim, S.J., Cha, S.H., Oh, Y.-K., Rhee, H.-J., Kim, M.-S., and Lee, J.K. (2009). Complete genome sequence of Rhodobacter sphaeroides KD131. J. Bacteriol. *191*, 1118–1119.

Lindahl, E., Hess, B., and van der Spoel, D. (2001). GROMACS 3.0: A package for molecular simulation and trajectory analysis. J. Mol. Model. *7*, 306–317.

Lipkow, K., Andrews, S.S., and Bray, D. (2005). Simulated diffusion of phosphorylated CheY through the cytoplasm of Escherichia coli. J. Bacteriol. *187*, 45–53.

Lowry, D.F., Roth, A.F., Rupert, P.B., Dahlquist, F.W., Moy, F.J., Domaille, P.J., and Matsumura, P. (1994). Signal transduction in chemotaxis. A propagating conformation change upon phosphorylation of CheY. J. Biol. Chem. *269*, 26358–26362.

Lukat, G.S., Stock, A.M., and Stock, J.B. (1990). Divalent metal ion binding to the CheY protein and its significance to phosphotransfer in bacterial chemotaxis. Biochemistry *29*, 5436–5442.

Lukat, G.S., Lee, B.H., Mottonen, J.M., Stock, A.M., and Stock, J.B. (1991). Roles of the highly conserved aspartate and lysine residues in the response regulator of bacterial chemotaxis. J. Biol. Chem. *266*, 8348–8354.

Lukat-Rodgers, G.S., and Rodgers, K.R. (1997). Characterization of ferrous FixL-nitric oxide adducts by resonance Raman spectroscopy. Biochemistry *36*, 4178–4187.

MacFarlane, S.A., and Merrick, M. (1985). The nucleotide sequence of the nitrogen regulation gene ntrB and the glnA-ntrBC intergenic region of Klebsiella pneumoniae. Nucleic Acids Res. *13*, 7591–7606.

Mackenzie, C., Choudhary, M., Larimer, F.W., Predki, P.F., Stilwagen, S., Armitage, J.P., Barber, R.D., Donohue, T.J., Hosler, J.P., Newman, J.E., et al. (2001). The home stretch, a first analysis of the nearly completed genome of Rhodobacter sphaeroides 2.4.1. Photosynth. Res. *70*, 19–41.

Macnab, R., and Koshland, D.E. (1974). Bacterial motility and chemotaxis: light-induced tumbling response and visualization of individual flagella. J. Mol. Biol. *84*, 399–406.

Makino, K., Amemura, M., Kim, S.K., Nakata, A., and Shinagawa, H. (1993). Role of the sigma 70 subunit of RNA polymerase in transcriptional activation by activator protein PhoB in Escherichia coli. Genes Dev. *7*, 149–160.

Mao, H., Cremer, P.S., and Manson, M.D. (2003). A sensitive, versatile microfluidic assay for bacterial chemotaxis. Proc. Natl. Acad. Sci. U. S. A. *100*, 5449–5454.

Martin, A.C., Wadhams, G.H., Shah, D.S., Porter, S.L., Mantotta, J.C., Craig, T.J., Verdult, P.H., Jones, H., and Armitage, J.P. (2001). CheR- and CheB-dependent chemosensory adaptation system of Rhodobacter sphaeroides. J. Bacteriol. *183*, 7135–7144.

Martin, A.C., Gould, M., Byles, E., Roberts, M.A.J., and Armitage, J.P. (2006). Two chemosensory operons of Rhodobacter sphaeroides are regulated independently by sigma 28 and sigma 54. J. Bacteriol. *188*, 7932–7940.

Martínez, A., Torello, S., and Kolter, R. (1999). Sliding motility in mycobacteria. J. Bacteriol. *181*, 7331–7338.

Martínez-del Campo, A., Ballado, T., Camarena, L., and Dreyfus, G. (2011). In Rhodobacter sphaeroides, chemotactic operon 1 regulates rotation of the flagellar system 2. J. Bacteriol. *193*, 6781–6786.

Mattick, J.S. (2002). Type IV pili and twitching motility. Annu. Rev. Microbiol. *56*, 289–314.

McCarter, L.L. (2006). Regulation of flagella. Curr. Opin. Microbiol. *9*, 180–186.

McCleary, W.R. (1996). The activation of PhoB by acetylphosphate. Mol. Microbiol. *20*, 1155–1163.

McEvoy, M.M., Muhandiram, D.R., Kay, L.E., and Dahlquist, F.W. (1996). Structure and dynamics of a CheY-binding domain of the chemotaxis kinase CheA determined by nuclear magnetic resonance spectroscopy. Biochemistry *35*, 5633–5640.

Mignot, T., Shaevitz, J.W., Hartzell, P.L., and Zusman, D.R. (2007). Evidence that focal adhesion complexes power bacterial gliding motility. Science *315*, 853–856.

Milburn, M. V, Privé, G.G., Milligan, D.L., Scott, W.G., Yeh, J., Jancarik, J., Koshland, D.E., and Kim, S.H. (1991). Three-dimensional structures of the ligand-binding domain of the bacterial aspartate receptor with and without a ligand. Science *254*, 1342–1347.

Miller, A.S., and Falke, J.J. (2004). Side chains at the membrane-water interface modulate the signaling state of a transmembrane receptor. Biochemistry *43*, 1763–1770.

Miller, A.S., Kohout, S.C., Gilman, K.A., and Falke, J.J. (2006). CheA Kinase of bacterial chemotaxis: chemical mapping of four essential docking sites. Biochemistry *45*, 8699–8711.

Miller, L.D., Yost, C.K., Hynes, M.F., and Alexandre, G. (2007). The major chemotaxis gene cluster of Rhizobium leguminosarum bv. viciae is essential for competitive nodulation. Mol. Microbiol. *63*, 348–362.

Miyata, M. (2010). Unique centipede mechanism of Mycoplasma gliding. Annu. Rev. Microbiol. *64*, 519–537.

Mizuno, T. (1997). Compilation of all genes encoding two-component phosphotransfer signal transducers in the genome of Escherichia coli. DNA Res. *4*, 161–168.

Mizuno, T. (1998). His-Asp phosphotransfer signal transduction. J. Biochem. *123*, 555–563.

Monticelli, L., Kandasamy, S.K., Periole, X., Larson, R.G., Tieleman, D.P., and Marrink, S.-J. (2008). The MARTINI Coarse-Grained Force Field: Extension to Proteins. J. Chem. Theory Comput. *4*, 819–834.

Le Moual, H., and Koshland, D.E. (1996). Molecular evolution of the C-terminal cytoplasmic domain of a superfamily of bacterial receptors involved in taxis. J. Mol. Biol. *261*, 568–585.

Van Niel, C.B. (1944). The culture, general physiology, morphology and classification of the non-sulfur purple and brown bacteria. Bacteriol. Rev. *8*, 1–118.

Nixon, B.T., Ronson, C.W., and Ausubel, F.M. (1986). Two-component regulatory systems responsive to environmental stimuli share strongly conserved domains with the nitrogen assimilation regulatory genes ntrB and ntrC. Proc. Natl. Acad. Sci. U. S. A. *83*, 7850–7854.

Ortega, D.R., Mo, G., Lee, K., Zhou, H., Baudry, J., Dahlquist, F.W., and Zhulin, I.B. (2013a). Conformational coupling between receptor and kinase binding sites through a conserved salt bridge in a signaling complex scaffold protein. PLoS Comput. Biol. *9*, e1003337.

Ortega, D.R., Yang, C., Ames, P., Baudry, J., Parkinson, J.S., and Zhulin, I.B. (2013b). A phenylalanine rotameric switch for signal-state control in bacterial chemoreceptors. Nat. Commun. *4*, 2881.

Park, H., and Inouye, M. (1997). Mutational analysis of the linker region of EnvZ, an osmosensor in Escherichia coli. J. Bacteriol. *179*, 4382–4390.

Park, S.-Y., Borbat, P.P., Gonzalez-Bonet, G., Bhatnagar, J., Pollard, A.M., Freed, J.H., Bilwes, A.M., and Crane, B.R. (2006). Reconstruction of the chemotaxis receptor-kinase assembly. Nat. Struct. Mol. Biol. *13*, 400–407.

Parkinson, J.S. (1978). Complementation analysis and deletion mapping of Escherichia coli mutants defective in chemotaxis. J. Bacteriol. *135*, 45–53.

Parkinson, J.S. (2010). Signaling mechanisms of HAMP domains in chemoreceptors and sensor kinases. Annu. Rev. Microbiol. *64*, 101–122.

Pedetta, A., Parkinson, J.S., and Studdert, C.A. (2014). Signalling-dependent interactions between the kinase-coupling protein CheW and chemoreceptors in living cells. Mol. Microbiol. *93*, 1144–1155.

Perez, E., and Stock, A.M. (2007). Characterization of the Thermotoga maritima chemotaxis methylation system that lacks pentapeptide-dependent methyltransferase CheR:MCP tethering. Mol. Microbiol. *63*, 363–378.

Perez, E., West, A.H., Stock, A.M., and Djordjevic, S. (2004). Discrimination between different methylation states of chemotaxis receptor Tar by receptor methyltransferase CheR. Biochemistry *43*, 953–961.

Philippe, N., Alcaraz, J.-P., Coursange, E., Geiselmann, J., and Schneider, D. (2004). Improvement of pCVD442, a suicide plasmid for gene allele exchange in bacteria. Plasmid *51*, 246–255.

Piasta, K.N., Ulliman, C.J., Slivka, P.F., Crane, B.R., and Falke, J.J. (2013). Defining a key receptor-CheA kinase contact and elucidating its function in the membrane-bound bacterial chemosensory array: a disulfide mapping and TAM-IDS Study. Biochemistry *52*, 3866–3880.

Pilizota, T., Brown, M.T., Leake, M.C., Branch, R.W., Berry, R.M., and Armitage, J.P. (2009). A molecular brake, not a clutch, stops the Rhodobacter sphaeroides flagellar motor. Proc. Natl. Acad. Sci. U. S. A. *106*, 11582–11587.

Plank, M., Wadhams, G.H., and Leake, M.C. (2009). Millisecond timescale slimfield imaging and automated quantification of single fluorescent protein molecules for use in probing complex biological processes. Integr. Biol. (Camb). *1*, 602–612.

Porter, S.L., and Armitage, J.P. (2002). Phosphotransfer in Rhodobacter sphaeroides chemotaxis. J. Mol. Biol. *324*, 35–45.

Porter, S., Wadhams, G.H., and Armitage, J.P. (2008a). Rhodobacter sphaeroides: complexity in chemotactic signalling. Trends Microbiol. *16*, 251–260.

Porter, S.L., Warren, A. V., Martin, A.C., and Armitage, J.P. (2002). The third chemotaxis locus of Rhodobacter sphaeroides is essential for chemotaxis. Mol. Microbiol. *46*, 1081–1094.

Porter, S.L., Wadhams, G.H., Martin, A.C., Byles, E.D., Lancaster, D.E., and Armitage, J.P. (2006). The CheYs of Rhodobacter sphaeroides. J. Biol. Chem. *281*, 32694–32704.

Porter, S.L., Wadhams, G.H., and Armitage, J.P. (2007). In vivo and in vitro analysis of the Rhodobacter sphaeroides chemotaxis signaling complexes. Methods Enzymol. *423*, 392–413.

Porter, S.L., Roberts, M.A.J., Manning, C.S., and Armitage, J.P. (2008b). A bifunctional kinase-phosphatase in bacterial chemotaxis. Proc. Natl. Acad. Sci. U. S. A. *105*, 18531–18536.

Porter, S.L., Wilkinson, D.A., Byles, E.D., Wadhams, G.H., Taylor, S., Saunders, N.J., and Armitage, J.P. (2011a). Genome sequence of Rhodobacter sphaeroides Strain WS8N. J. Bacteriol. *193*, 4027–4028.

Porter, S.L., Wadhams, G.H., and Armitage, J.P. (2011b). Signal processing in complex chemotaxis pathways. Nat. Rev. Microbiol. *9*, 153–165.

Purcell, E.M. (1976). Life at low Reynolds number. In AIP Conference Proceedings, (AIP), pp. 49–64.

Rao, C. V., Glekas, G.D., and Ordal, G.W. (2008). The three adaptation systems of Bacillus subtilis chemotaxis. Trends Microbiol. *16*, 480–487.

Rapsomaniki, M.A., Kotsantis, P., Symeonidou, I.-E., Giakoumakis, N.-N., Taraviras, S., and Lygerou, Z. (2012). easyFRAP: an interactive, easy-to-use tool for qualitative and quantitative analysis of FRAP data. Bioinformatics *28*, 1800–1801.

Reader, R.W., Tso, W.W., Springer, M.S., Goy, M.F., and Adler, J. (1979). Pleiotropic aspartate taxis and serine taxis mutants of Escherichia coli. J. Gen. Microbiol. *111*, 363–374.

Rebbapragada, A., Johnson, M.S., Harding, G.P., Zuccarelli, A.J., Fletcher, H.M., Zhulin, I.B., and Taylor, B.L. (1997). The Aer protein and the serine chemoreceptor Tsr independently sense intracellular energy levels and transduce oxygen, redox, and energy signals for Escherichia coli behavior. Proc. Natl. Acad. Sci. U. S. A. *94*, 10541–10546.

Robinson, V.L., and Stock, A.M. (1999). High energy exchange: proteins that make or break phosphoramidate bonds. Structure *7*, R47–R53.

Rosser, G., Fletcher, A.G., Wilkinson, D.A., de Beyer, J.A., Yates, C.A., Armitage, J.P., Maini, P.K., and Baker, R.E. (2013). Novel methods for analysing bacterial tracks reveal persistence in Rhodobacter sphaeroides. PLoS Comput. Biol. *9*, e1003276.

Rudner, D.Z., and Losick, R. (2010). Protein subcellular localization in bacteria. Cold Spring Harb. Perspect. Biol. *2*, a000307.

Sali, A., and Blundell, T.L. (1993). Comparative protein modelling by satisfaction of spatial restraints. J. Mol. Biol. *234*, 779–815.

Sambrook, J., and W Russell, D. (2001). Molecular Cloning: A Laboratory Manual. Cold Spring Harb. Lab. Press. Cold Spring Harb. NY 999.

Sanders, D.A., Gillece-Castro, B.L., Stock, A.M., Burlingame, A.L., and Koshland, D.E. (1989). Identification of the site of phosphorylation of the chemotaxis response regulator protein, CheY. J. Biol. Chem. *264*, 21770–21778.

Sarkar, M.K., Paul, K., and Blair, D. (2010). Chemotaxis signaling protein CheY binds to the rotor protein FliN to control the direction of flagellar rotation in Escherichia coli. Proc. Natl. Acad. Sci. U. S. A. *107*, 9370–9375.

Schulmeister, S., Ruttorf, M., Thiem, S., Kentner, D., Lebiedz, D., and Sourjik, V. (2008). Protein exchange dynamics at chemoreceptor clusters in Escherichia coli. Proc. Natl. Acad. Sci. U. S. A. *105*, 6403–6408.

Scott, W.G., Milligan, D.L., Milburn, M. V, Privé, G.G., Yeh, J., Koshland, D.E., and Kim, S.H. (1993). Refined structures of the ligand-binding domain of the aspartate receptor from Salmonella typhimurium. J. Mol. Biol. *232*, 555–573.

Segall, J.E., Ishihara, A., and Berg, H.C. (1985). Chemotactic signaling in filamentous cells of Escherichia coli. J. Bacteriol. *161*, 51–59.

Selzer, G., Som, T., Itoh, T., and Tomizawa, J. (1983). The origin of replication of plasmid p15A and comparative studies on the nucleotide sequences around the origin of related plasmids. Cell *32*, 119–129.

Shah, D.S., Porter, S.L., Harris, D.C., Wadhams, G.H., Hamblin, P.A., and Armitage, J.P. (2000). Identification of a fourth cheY gene in Rhodobacter sphaeroides and interspecies interaction within the bacterial chemotaxis signal transduction pathway. Mol. Microbiol. *35*, 101–112.

Shapiro, M.J., Panomitros, D., and Koshland, D.E. (1995). Interactions between the methylation sites of the Escherichia coli aspartate receptor mediated by the methyltransferase. J. Biol. Chem. *270*, 751–755.

Shi, X., Wegener-Feldbrügge, S., Huntley, S., Hamann, N., Hedderich, R., and Søgaard-Andersen, L. (2008). Bioinformatics and experimental analysis of proteins of two-component systems in Myxococcus xanthus. J. Bacteriol. *190*, 613–624.

Shiomi, D., Zhulin, I.B., Homma, M., and Kawagishi, I. (2002). Dual recognition of the bacterial chemoreceptor by chemotaxis-specific domains of the CheR methyltransferase. J. Biol. Chem. *277*, 42325–42333.

Silversmith, R.E., Levin, M.D., Schilling, E., and Bourret, R.B. (2008). Kinetic characterization of catalysis by the chemotaxis phosphatase CheZ. Modulation of activity by the phosphorylated CheY substrate. J. Biol. Chem. *283*, 756–765.

Simms, S.A., Keane, M.G., and Stock, J. (1985). Multiple forms of the CheB methylesterase in bacterial chemosensing. J. Biol. Chem. *260*, 10161–10168.

Simon, R., Priefer, U., and Pühler, A. (1983). A Broad Host Range Mobilization System for In Vivo Genetic Engineering: Transposon Mutagenesis in Gram Negative Bacteria. Bio/Technology *1*, 784–791.

Singh, M., Berger, B., Kim, P.S., Berger, J.M., and Cochran, A.G. (1998). Computational learning reveals coiled coil-like motifs in histidine kinase linker domains. Proc. Natl. Acad. Sci. U. S. A. *95*, 2738–2743.

Sistrom, W.R. (1977). Transfer of chromosomal genes mediated by plasmid r68.45 in Rhodopseudomonas sphaeroides. J. Bacteriol. *131*, 526–532.

Skidmore, J.M., Ellefson, D.D., McNamara, B.P., Couto, M.M., Wolfe, A.J., and Maddock, J.R. (2000). Polar clustering of the chemoreceptor complex in Escherichia coli occurs in the absence of complete CheA function. J. Bacteriol. *182*, 967–973.

Sockett, R.E., Foster, J.C.A., and Armitage, J.P. (1990). Molecular Biology of the Rhodobacter Sphaeroides Flagellum. FEMS Symp. 473–479.

Sourjik, V. (2004). Receptor clustering and signal processing in E. coli chemotaxis. Trends Microbiol. *12*, 569–576.

Sourjik, V., and Berg, H.C. (2002a). Binding of the Escherichia coli response regulator CheY to its target measured in vivo by fluorescence resonance energy transfer. Proc. Natl. Acad. Sci. U. S. A. *99*, 12669–12674.

Sourjik, V., and Berg, H.C. (2002b). Receptor sensitivity in bacterial chemotaxis. Proc. Natl. Acad. Sci. U. S. A. *99*, 123–127.

Sourjik, V., and Berg, H.C. (2004). Functional interactions between receptors in bacterial chemotaxis. Nature *428*, 437–441.

Van Der Spoel, D., Lindahl, E., Hess, B., Groenhof, G., Mark, A.E., and Berendsen, H.J.C. (2005). GROMACS: fast, flexible, and free. J. Comput. Chem. *26*, 1701–1718.

Springer, M.S., Goy, M.F., and Adler, J. (1979). Protein methylation in behavioural control mechanisms and in signal transduction. Nature *280*, 279–284.

Stewart, V., and Chen, L.-L. (2010). The S helix mediates signal transmission as a HAMP domain coiled-coil extension in the NarX nitrate sensor from Escherichia coli K-12. J. Bacteriol. *192*, 734–745.

Stock, J. (1999). Signal transduction: Gyrating protein kinases. Curr. Biol. *9*, R364–R367.

Stock, A., Chen, T., Welsh, D., and Stock, J. (1988). CheA protein, a central regulator of bacterial chemotaxis, belongs to a family of proteins that control gene expression in response to changing environmental conditions. Proc. Natl. Acad. Sci. U. S. A. *85*, 1403–1407.

Stock, A.M., Mottonen, J.M., Stock, J.B., and Schutt, C.E. (1989). Three-dimensional structure of CheY, the response regulator of bacterial chemotaxis. Nature *337*, 745–749.

Stock, A.M., Martinez-Hackert, E., Rasmussen, B.F., West, A.H., Stock, J.B., Ringe, D., and Petsko, G.A. (1993). Structure of the magnesium-bound form of CheY and mechanism of phosphoryl transfer in bacterial chemotaxis. Biochemistry *32*, 13375–13380.

Stock, A.M., Robinson, V.L., and Goudreau, P.N. (2000). Two-component signal transduction. Annu. Rev. Biochem. *69*, 183–215.

Swain, K.E., Gonzalez, M.A., and Falke, J.J. (2009). Engineered socket study of signaling through a four-helix bundle: evidence for a yin-yang mechanism in the kinase control module of the aspartate receptor. Biochemistry *48*, 9266–9277.

Szurmant, H., Bunn, M.W., Cho, S.H., and Ordal, G.W. (2004a). Ligand-induced conformational changes in the Bacillus subtilis chemoreceptor McpB determined by disulfide crosslinking in vivo. J. Mol. Biol. *344*, 919–928.

Szurmant, H., Muff, T.J., and Ordal, G.W. (2004b). Bacillus subtilis CheC and FliY are members of a novel class of CheY-P-hydrolyzing proteins in the chemotactic signal transduction cascade. J. Biol. Chem. *279*, 21787–21792.

Tanaka, T., Saha, S.K., Tomomori, C., Ishima, R., Liu, D., Tong, K.I., Park, H., Dutta, R., Qin, L., Swindells, M.B., et al. (1998). NMR structure of the histidine kinase domain of the E. coli osmosensor EnvZ. Nature *396*, 88–92.

Terasawa, S., Fukuoka, H., Inoue, Y., Sagawa, T., Takahashi, H., and Ishijima, A. (2011). Coordinated reversal of flagellar motors on a single Escherichia coli cell. Biophys. J. *100*, 2193–2200.

Terwilliger, T.C., Wang, J.Y., and Koshland, D.E. (1986a). Surface structure recognized for covalent modification of the aspartate receptor in chemotaxis. Proc. Natl. Acad. Sci. U. S. A. *83*, 6707–6710.

Terwilliger, T.C., Wang, J.Y., and Koshland, D.E. (1986b). Kinetics of receptor modification. The multiply methylated aspartate receptors involved in bacterial chemotaxis. J. Biol. Chem. *261*, 10814–10820.

Thiem, S., and Sourjik, V. (2008). Stochastic assembly of chemoreceptor clusters in Escherichia coli. Mol. Microbiol. *68*, 1228–1236.

Thompson, S.R. (2005). A study of multiple chemosensory gene homologues in Rhodobacter sphaeroides. University of Oxford.

Toker, A.S., and Macnab, R.M. (1997). Distinct regions of bacterial flagellar switch protein FliM interact with FliG, FliN and CheY. J. Mol. Biol. *273*, 623–634.

Tomomori, C., Tanaka, T., Dutta, R., Park, H., Saha, S.K., Zhu, Y., Ishima, R., Liu, D., Tong, K.I., Kurokawa, H., et al. (1999). Solution structure of the homodimeric core domain of Escherichia coli histidine kinase EnvZ. Nat. Struct. Biol. *6*, 729–734.

Vaknin, A., and Berg, H.C. (2007). Physical responses of bacterial chemoreceptors. J. Mol. Biol. *366*, 1416–1423.

Vaknin, A., and Berg, H.C. (2008). Direct evidence for coupling between bacterial chemoreceptors. J. Mol. Biol. *382*, 573–577.

Vladimirov, N., and Sourjik, V. (2009). Chemotaxis: how bacteria use memory. Biol. Chem. *390*, 1097–1104.

Volz, K. (1993). Structural conservation in the CheY superfamily. Biochemistry *32*, 11741–11753.

Volz, K., and Matsumura, P. (1991). Crystal structure of Escherichia coli CheY refined at 1.7-A resolution. J. Biol. Chem. *266*, 15511–15519.

Vu, A., Wang, X., Zhou, H., and Dahlquist, F.W. (2012). The receptor-CheW binding interface in bacterial chemotaxis. J. Mol. Biol. *415*, 759–767.

Wadhams, G.H., and Armitage, J.P. (2004). Making sense of it all: bacterial chemotaxis. Nat. Rev. Mol. Cell Biol. *5*, 1024–1037.

Wadhams, G.H., Martin, a C., and Armitage, J.P. (2000). Identification and localization of a methyl-accepting chemotaxis protein in Rhodobacter sphaeroides. Mol. Microbiol. *36*, 1222–1233.

Wadhams, G.H., Martin, A.C., Porter, S.L., Maddock, J.R., Mantotta, J.C., King, H.M., and Armitage, J.P. (2002). TlpC, a novel chemotaxis protein in Rhodobacter sphaeroides, localizes to a discrete region in the cytoplasm. Mol. Microbiol. *46*, 1211–1221.

Wadhams, G.H., Warren, A. V., Martin, A.C., and Armitage, J.P. (2003). Targeting of two signal transduction pathways to different regions of the bacterial cell. Mol. Microbiol. *50*, 763–770.

Wadhams, G.H., Martin, A.C., Warren, A. V., and Armitage, J.P. (2005). Requirements for chemotaxis protein localization in Rhodobacter sphaeroides. Mol. Microbiol. *58*, 895–902.

Wang, X., Vu, A., Lee, K., and Dahlquist, F.W. (2012). CheA-receptor interaction sites in bacterial chemotaxis. J. Mol. Biol. *422*, 282–290.

Weis, R.M., Hirai, T., Chalah, A., Kessel, M., Peters, P.J., and Subramaniam, S. (2003). Electron microscopic analysis of membrane assemblies formed by the bacterial chemotaxis receptor Tsr. J. Bacteriol. *185*, 3636–3643.

Welch, M., Oosawa, K., Aizawa, S., and Eisenbach, M. (1993). Phosphorylation-dependent binding of a signal molecule to the flagellar switch of bacteria. Proc. Natl. Acad. Sci. U. S. A. *90*, 8787–8791.

West, A.H., Martinez-Hackert, E., and Stock, A.M. (1995). Crystal structure of the catalytic domain of the chemotaxis receptor methylesterase, CheB. J. Mol. Biol. *250*, 276–290.

Wood, T.M., Yates, C.A., Wilkinson, D.A., and Rosser, G. (2012). Simplified Multitarget Tracking Using the PHD Filter for Microscopic Video Data. IEEE Trans. Circuits Syst. Video Technol. *22*, 702–713.

Wu, J., Li, J., Li, G., Long, D.G., and Weis, R.M. (1996). The receptor binding site for the methyltransferase of bacterial chemotaxis is distinct from the sites of methylation. Biochemistry *35*, 4984–4993.

Wu, K., Walukiewicz, H.E., Glekas, G.D., Ordal, G.W., and Rao, C. V (2011). Attractant binding induces distinct structural changes to the polar and lateral signaling clusters in Bacillus subtilis chemotaxis. J. Biol. Chem. *286*, 2587–2595.

Wylie, D., Stock, A., Wong, C.Y., and Stock, J. (1988). Sensory transduction in bacterial chemotaxis involves phosphotransfer between Che proteins. Biochem. Biophys. Res. Commun. *151*, 891–896.

Xie, Z., Ulrich, L.E., Zhulin, I.B., and Alexandre, G. (2010). PAS domain containing chemoreceptor couples dynamic changes in metabolism with chemotaxis. Proc. Natl. Acad. Sci. U. S. A. *107*, 2235–2240.

Yeh, J.I., Biemann, H.P., Pandit, J., Koshland, D.E., and Kim, S.H. (1993). The three-dimensional structure of the ligand-binding domain of a wild-type bacterial chemotaxis receptor. Structural comparison to the cross-linked mutant forms and conformational changes upon ligand binding. J. Biol. Chem. *268*, 9787–9792.

Yeh, J.I., Biemann, H.P., Privé, G.G., Pandit, J., Koshland, D.E., and Kim, S.H. (1996). High-resolution structures of the ligand binding domain of the wild-type bacterial aspartate receptor. J. Mol. Biol. *262*, 186–201.

Yu, E.W., and Koshland, D.E. (2001). Propagating conformational changes over long (and short) distances in proteins. Proc. Natl. Acad. Sci. U. S. A. *98*, 9517–9520.

Zhang, P., Khursigara, C.M., Hartnell, L.M., and Subramaniam, S. (2007). Direct visualization of Escherichia coli chemotaxis receptor arrays using cryo-electron microscopy. Proc. Natl. Acad. Sci. U. S. A. *104*, 3777–3781.

Zhao, R., Collins, E.J., Bourret, R.B., and Silversmith, R.E. (2002). Structure and catalytic mechanism of the E. coli chemotaxis phosphatase CheZ. Nat. Struct. Biol. *9*, 570–575.

Zhou, Q., Ames, P., and Parkinson, J.S. (2009). Mutational analyses of HAMP helices suggest a dynamic bundle model of input-output signalling in chemoreceptors. Mol. Microbiol. *73*, 801–814.

Zhou, Q., Ames, P., and Parkinson, J.S. (2011). Biphasic control logic of HAMP domain signalling in the Escherichia coli serine chemoreceptor. Mol. Microbiol. *80*, 596–611.

Zhu, X., Rebello, J., Matsumura, P., and Volz, K. (1997). Crystal structures of CheY mutants Y106W and T87I/Y106W. CheY activation correlates with movement of residue 106. J. Biol. Chem. *272*, 5000–5006.

Zimmer, M.A., Tiu, J., Collins, M.A., and Ordal, G.W. (2000). Selective methylation changes on the Bacillus subtilis chemotaxis receptor McpB promote adaptation. J. Biol. Chem. *275*, 24264–24272.

Appendix A

Primers

Primers for MCP expression and localisation

Primer name	Sequence
CheABAD_f	GCAGGTACCAGGAGGATTCATCATGATGGACGACGACATGATGG
CheABAD_r	GATTCTCTGCAGTGCCGCGGCTCCTCGACGGTCTTC
RFP_f	ATCTTGAGATCTGTGTCTAAGGGCGAAGAG
RFP_r	ATCTGCAAGCTTTCAATTAAGTTTGTGCCCC
McpB_f	ATCTCGTCATGAGACTGTCCATCAAGCTG
McpB_r	ATCTCGGGATCCGGCCGCATGGTCGGTGG
McpBstar_F	GCCGCAGCCTGGATCGGCAGCGTGGTAACC
McpBstar_R	GGTTACCACGCTGCCGATCCAGGCTGCGGC
McpG_f	GGACTGTCATGAGACTCTCGATCCGCAAC
McpG_r	TTAGTTTGATCACGCGACGCGCGCTCGCGCGAAG
McpH_f	ATTGGCTCATGATGAAGGCCTCCATG
McpH_r	AATCATAGATCTGCGGGTGCCCGCGC
McpJ_f	GGCTAGACATGTCGATCAAGCTCAAGCTCGCC
McpJ_r	GTCTAGGGATCCGCGGCCCTGACGCTGGAAG
Tsr_f	GGTCGCCCATGGATGTTAAAACGTATCAAAATTGTGACC
Tsr_r	GGTCGGAGATCTTTAAAATGTTTCCCAGTTC

Table 0-1 The primers used in the making of MCP expression plasmids along with other plasmids used in the localisation study.

Primers for R. sphaeroides CheW gene transfer into *E. coli*

Primer name	Sequence
CheWdel_1	TGAGATGCATGCGTACGCGTTGCGGATGAAG
CheWdel_4	GATCAGCCTGCAGGGAGGGAAATGATGTGCCTCAC
CheW2coli_ex_5	GATCAATGATGTTGCTCATATTGTTACCTTTTTACTC
CheW2coli_ex_6	GTGTGGCCGTCGCCTGATTCTCCCGATTTCCTC
CheW2coli_ex_7	GAGTAAAAAGGTAACAATATGAGCAACATCATTGATC
CheW2coli_ex_8	GAGGAAATCGGGAGAATCAGGCGACGGCCACAC
CheW3coli_ex_5	CGTCATCGAGATCATATTGTTACCTTTTTACTC
CheW3coli_ex_6	CAGGGCGAGCTGCAATGATTCTCCCGATTTCCTC
CheW3coli_ex_7	GAGTAAAAAGGTAACAATATGATCTCGATGACG
CheW3coli_ex_8	GAGGAAATCGGGAGAATCATTGCAGCTCGCCCTG

Table 0-2 The primers used in the making of constructs for gene transfer of *R. sphaeroides* CheWs into *E. coli*.

Primers for bacterial two-hybrid study

Primer name	Sequence
CheW1b2h_f	ATCTCGTCTAGAAATGGCGGCCGTGAGCCTGGAC
CheW1b2h_r	ATCTCGGGTACCGACATCATCCGCCTGACGTTC
CheW2b2h_f	ATCTCGTCTAGAAATGAGCAACATCATTGATCTC
CheW2b2h_r	ATCTCGGGTACCGAGGCGACGGCCACAC
CheW3b2h_f	ATCTCGTCTAGAAATGATCTCGATGACGGCATCC
CheW3b2h_r	ATCTCGGGTACCGATTGCAGCTCGCCCTG
McpBb2h_f	ATCTCGTCTAGAAATGAGACTGTCCATCAAGCTG
McpBb2h_r	ATCTCGGGTACCGAGGCCGCATGGTCGGTC
McpEb2h_f	ATCTCGTCTAGAAATGAAGGTGACGATCAGAAG
McpEb2h_r	ATCTCGGGTACCGAGGCCACGGCGCGCCAGTC
McpGb2h_f	ATCTCGTCTAGAAATGAGACTCTCGATCCGCAAC
McpGb2h_r	ATCTCGGGTACCGACGCGACGCGCGCTCGCGCGAAG
McpHb2h_f	ATCTCGTCTAGAAATGATGAAGGCCTCCATG
McpHb2h_r	ATCTCGGGTACCGAGCGGGTGCCCGCGC
McpRb2h_f	ATCTCGTCTAGAAATGTCCATCAAGTTGAAGC
McpRb2h_r	ATCTCGGGTACCGAGGCCGCATCATGACGCCGGAAC
McpVb2h_f	ATCTCGTCTAGAAATGATGCTCTCCCTTAAGGC
McpVb2h_r	ATCTCGGGTACCGATGCTGCCGCGGCCTGCAG

Table 0-3 The primers used in the making of the bacterial two-hybrid library of *R. sphaeroides* MCPs and CheWs.

Appendix B

Media and reagents

Lysogeny Broth

Ingredient	Quantity per litre
Bacto-tryptone	10 g
NaCl	5 g
Yeast extract	5 g

LB Agar

Ingredient	Quantity per litre
Agar	20 g
Bacto-tryptone	10 g
NaCl	5 g
Yeast extract	5 g

Succinate (Sux) media

Ingredient	Quantity per litre
Casamino acids	1 g
Concentrated base	2% (v/v)
Growth factors	0.2% (v/v)
NaCl	0.5 g
(NH4)2SO4	0.5 g
Phosphate buffer 1 M pH 7.0	2% (v/v)
Sodium succinate	2.0 g
Adjust to pH 7.2 with KOH	

1M Phosphate buffer

Ingredient	Quantity per litre
K_2HPO_4	174.18 g
KH_2PO_4	136.09 g
Adjust to pH 7.0 with KOH	

Concentrated base

Ingredient	Quantity per litre
Ammonium molybdate(.4H_2O)	4.6 mg
$CaCl_2.6H_2O$	2.5 g
$FeSO_4.7H_2O$	50 mg
Metals 44 solution	2.5% (v/v)
$MgSO_4.7H_2O$	14.5 g
Nitrilotriaccetic acid (Na salt)	5.94 g
Adjust to pH 6.8	

Metals 44 solution

Ingredient	Quantity per litre
Tetrasodium versenate (EDTA) 178	2.5 g
$CoCl_2.6H_2O$	200 mg
$CuSO_4.5H_2O$	390 mg
$FeSO_4.7H_2O$	5 g
H_3BO_3	120 mg
$MnSO_4.7H_2O$	2 g
Sulphuric acid 3 M	0.15% (v/v)
$ZnSO_4.7H_2O$	11 g

Growth factors

Ingredient	Quantity per litre
Biotin	20 mg
$NaHCO_3$	500 mg
Niacin (Nicotinic acid)	1 g
Thiamine HCl	500 mg

M22

Ingredient	Quantity
Concentrated base	2% (v/v)
Growth factors	0.2% (v/v)

10x M9

Ingredient	Quantity per litre
$NaHPO_4.2H_2O$	75.2 g
$KHPO_4$	30 g
NaCl	5 g
NH_4Cl	10 g

SOC Media

Ingredient	Quantity
Glucose	20 mM
MgCl	10 mM
$MgSO_4$	10 mM
NaCl	10 mM
Tryptone	20 g/l
Yeast extract	5 g/l

5x DNA loading dye

Ingredient	Quantity
Bromophenol blue	0.25 % (w/v)
Glycerol	70 % (w/v)
TRIS base	30 % (w/v)
Xylene cyanol	0.25 % (w/v)

10x TBE

Ingredient	Quantity per litre
Boric acid	55 g
TRIS base	108 g
EDTA	7.4 g
pH 8.3	

TFB I

Ingredient	Quantity
$CaCl_2.2H_2O$	10 mM
Glycerol	15 % (v/v)
KCH_3COO	30 mM
$MnCl2.4H_2O$	50 mM
RbCl	100 mM
Adjust to pH 5.8 with acetic acid	

TFB II

Ingredient	Quantity
$CaCl_2.2H_2O$	75 mM
Glycerol	15 % (v/v)
PIPES	10 mM
$RbCl_2$	10 mM
Adjust to pH 6.8 with HCl	

Reagents and media, unless stated otherwise are all made up to 1 litre with MilliQ water